



<https://theses.gla.ac.uk/>

Theses Digitisation:

<https://www.gla.ac.uk/myglasgow/research/enlighten/theses/digitisation/>

This is a digitised version of the original print thesis.

Copyright and moral rights for this work are retained by the author

A copy can be downloaded for personal non-commercial research or study, without prior permission or charge

This work cannot be reproduced or quoted extensively from without first obtaining permission in writing from the author

The content must not be changed in any way or sold commercially in any format or medium without the formal permission of the author

When referring to this work, full bibliographic details including the author, title, awarding institution and date of the thesis must be given

Enlighten: Theses

<https://theses.gla.ac.uk/>
research-enlighten@glasgow.ac.uk



UNIVERSITY
of
GLASGOW

Inhibition of Cracking in Pulsed Laser Welding of Aluminium Alloys

**A thesis submitted to
the Department of Mechanical Engineering
University of Glasgow**

**in fulfilment of the requirement for
the Degree : Master of Science**

by

Seog-Yoon Jeong , 1998

Laser and Optical Systems Engineering Centre

© Seog-Yoon Jeong , May , 1998

ProQuest Number: 10391140

All rights reserved

INFORMATION TO ALL USERS

The quality of this reproduction is dependent upon the quality of the copy submitted.

In the unlikely event that the author did not send a complete manuscript and there are missing pages, these will be noted. Also, if material had to be removed, a note will indicate the deletion.



ProQuest 10391140

Published by ProQuest LLC (2017). Copyright of the Dissertation is held by the Author.

All rights reserved.

This work is protected against unauthorized copying under Title 17, United States Code
Microform Edition © ProQuest LLC.

ProQuest LLC.
789 East Eisenhower Parkway
P.O. Box 1346
Ann Arbor, MI 48106 – 1346

GLASGOW
UNIVERSITY
LIBRARY

11429 (copy 2)

Abstract

Pulsed laser welding of Aluminium Silicon alloys has been investigated experimentally to discover the causes of welding cracking which affect these alloys and a means for its prevention. Cracking was observed in conduction and non-conduction limited modes of welding, being more severe in the latter because of higher quenching rates induced in the fused material.

The specimen alloys chosen were a heat-treatable type-6082-T6 and a non-heat-treatable type-5251-H24. Welds were generated with a high pulse repetition frequency ND34:YAG laser, capable of operating with a mean power of 500W. The power intensity in the weld was selected by variation of the pulse parameters to achieve the desired welding modes.

Control was exercised over the degree of overlap present between successive weld spots by appropriate variations of the pulse repetition frequency and the velocity of translation of the incident beam. Cross sections of weld were examined microscopically; a scanning electron microscope was employed to analyse variations in the concentrations of the alloying elements in the fused zone.

With these results, cracking was attributed to tensile failure in the last alloy to freeze which was weakened by the segregation of silicon consequent upon non-equilibrium freezing of the volatile components was another caused factor.

A complete solution was found by the inclusion of a high silicon content wire in the weld preparation. By this means, the silicon content in the last metal was raised, in the conduction limited mode, and spatial gradients of the temperature were reduced.

Acknowledgement

By staying in research field for an year and half, I found out lots of things which I felt always curious before challenge the Master. Unlimited challenges and enthusiasm in order to achieve the aim... Now I'm here with a result to solve the problems in aluminum welding. In the way of doing this, there were big and small reputational matters both my country and myself which was shameful but possibly can happen in entire human life. These are, I believe, because no one can predict the happening, even for tomorrow. No matter how, one and half year of research period in Glasgow will be the best time in my life.

I would like to thank my supervisor, professor B.F.Scott, for his outstanding guidance and supervision all throughout the research work and Caroline Adam (secretary) for her kindly help, Jimmy Wilson who have given me a splendid technical advice and supports from first to the end, Ian pedan of his optical supports, George Folconer for his helpful technical arrangements and Donald.N.B. Ouyang for his friendly advise as a fellow as well as all of research colleagues in the department.

I also thank to Mr./ Mrs. Han, who are my landlord and landlady, for their endless encouragement and endurance everyday as being Christians.

I really appreciate to my parent for the financial support and great thank to University of Glasgow for supporting the Asian Economy Hardship fund at the end of the research. Finally, thanks to the God for giving me a health to study. I wish the God blessed all the people above and same to the people who I haven't mentioned in this page.

Contents

Abstract	i
Acknowledgment	ii
Contents	iii
Chapter 1. Introduction	
1.1. Objectives	1
1.2. Hypothesis	2
1.3. Achievements	3
Chapter 2. Literature Review	
2.1. Characteristics of Pulse Laser Welding	4
2.1.1. Solid State Lasers for Welding	
2.1.2. Solid state laser (ND ³⁺ : YAG laser)	
2.2. Aluminum Alloys	7
2.2.1. Phase Diagrams	
2.2.2. Strengthening Processes and phase changes	
2.2.3. Significance for welding	
2.2.3.1. Welding Cracking	
2.2.3.2. Evaporation	
2.2.3.3. Porosity	
2.2.3.4. Rapid Quenching	
2.3. Solidification cracking in Laser welding	17
2.4. Non-Equilibrium Alloy Solidification	19
2.5. Prevention of cracking	21
Chapter 3. Experiment Arrangements	
3.1. Introduction	22
3.2. Welding Apparatus	22
3.2.1. Variation of Beam Pulse and Welding Parameters	
3.2.1.1. The incident Laser pulse energy	
3.2.1.2. Pulse Duration	
3.2.1.3. Pulse Repetition Frequency	
3.2.2. Welding traveling speed	
3.2.3. Laser beam diameter	

3.2.4. Calculation of the power intensity and the overlapping ratio	
3.2.4.1. Power Intensity	
3.2.4.2. Overlapping Ratio	
3.2.5. Gas shielding	
3.3. Beam delivery system and Optical fiber	31
3.3.1. Time sharing and Energy sharing system	
3.3.2. Optical Fibers	
3.4. Experiment Procedures	34
3.4.1. Preparing the specimens	
3.4.1.1. Laser parameters	
3.4.1.2. Etching Solution	
3.4.2. Property test and their procedures	
3.4.2.1. Macro/Microscopic Inspections(Non-destructive test)	
3.4.2.2. Tensile strength test (Destructive test)	
3.4.2.3. Micro Hardness test (Destructive test)	
3.4.2.4. SEM and EPMA	

Chapter 4. Experiments and Analyses

4.1. Introduction	44
4.2. Relationship of welding variables to the Fusion Size	45
4.2.1. Relationship of Power Intensity to the fusion size	
4.2.1.1. Fusion size varying with Pulse Energies	
4.2.1.2. Fusion size varying with Pulse Duration	
4.2.2. Relationship of Welding Overlap to the fusion size	
4.2.2.1. Fusion size varying with P.R.F.	
4.2.2.2. Fusion size varying with Welding Velocity	
4.2.3. Surface Treatment	
4.2.3.1. Pulse Energy	
4.2.3.2. Pulse Duration	
4.3. Prevention of cracking in the fusion	55
4.3.1. Addition of Filler Wire	
4.3.2. Result of chemical Analysis (EPMA)	
4.3.2.1. Square Butt joint without filler metal	
4.3.2.2. Groove Butt joint with ER4043	
4.3.2.3. Groove Butt joint with ER4047	
4.3.3. Tensile Strength Test	64
4.3.3.1. 6082-T6 alloy	
4.3.3.2. 5251-H24 alloy	
4.3.4. Micro Hardness Test	67
4.3.4.1. Square Butt joint without filler metal	

4.3.4.2. Groove Butt joint with ER4043

4.3.4.3. Groove Butt joint with ER4047

Chapter 5. Discussion of Results

5.1. Crack Formations	71
5.2. Heat Affected Zone	73
5.3. Fusion Zone	74
5.4. Other Welding Defaults	77
5.4.1. Porosity	
5.4.2. Misalignment	

Chapter 6. Conclusions	79
-------------------------------	-----------

Chapter 7. Future Work	80
-------------------------------	-----------

References	81
-------------------	-----------

Appendix

Appendix i.1. Experiment Lists	1
Appendix i.2. Image Libraries	7
Appendix i.3. Laser Head Assembly and sharing system drawings (Lumonics)	50
Appendix i.4. Physical & Mechanical properties/chemical compositions of Aluminium alloys 6082-T6, 5251-H24 and Filler Wire ER4043, ER4047 (AALCO Ltd. MUREX Ltd.)	77

Chapter 1 Introduction

1.1. Objectives

The aim is to advance laser welding of Aluminum alloys through an understanding of the thermodynamics of the process. The objective is to investigate pulsed laser welding of thin sections using an Nd³⁺:YAG laser combined with a fiber optic delivery system that can be manipulated by a robot.

Drop through and, otherwise, loss of material from the front of the weld affect pulsed welds made in Aluminum. Primary concern is longitudinal cracking, propagating along the center line of the welding and caused by rapid post weld quenching of the melted zone. This latter is severe in Aluminum, because of its very high thermal diffusivity and large coefficient of thermal expansion. The interest is in alloys with Silicon, Magnesium and etc. in which phase changes and segregation of the alloying component greatly affect the mechanical properties and integrity of welds.

Weld control is exerted, in the main by variation of the beam waist character and pulse energy, which alter the weld size and the peak power intensity, and of the pulse length which is chosen to achieve the required penetration. However, the interaction of these parameter is complex and, particularly, two modes of welding occur. Conduction limited welding at lower intensities generates large shallow welds; high intensity welds involve strong convection currents, affecting energy transport in the fused region, and are characteristically deep and narrow. This second mode is particularly subject to cracking.

The experimental work has sought to discover the boundary conditions of the several physical and mechanical effects which have been described. Analysis has been by metallurgical inspection of weld cross-sections and, quantitatively by electron beam microscopy and chemical analysis.

The avoidance of cracking is the major issue and remains unresolved in deep penetration welding.

The research work is based on experiment and has as its objectives the following:

- A. to investigate crack formation in Aluminum Alloys and its relationship with the laser characteristics.
- B. The use of different filler wires with silicon contents chosen to reduce the propensity for weld cracking.

1.2. Hypothesis

Non-conduction limited welding of Aluminum Alloys accompanied by the risk of :

- Loss of material in the surface because of explosive non-equilibrium evaporations.
- Drop-through of the fused material caused by the high vapour pressure exerted on the irradiated surface.
- Cracking along the central plane of the fused zone caused by tensile stress consequent upon rapid quenching of the weld.
- Associated with the above, variations across the weld of concentrations of alloying elements, e.g. gradients of the silicon concentration in Aluminum-Silicon alloys.
- Loss by evaporation of the more volatile alloying elements, e.g. Magnesium in Aluminum.
- Porosity caused by evaporation
- Deleterious changes the base metal structure in the Heat Affected Zone.

It was postulated that the inclusion in the weld preparation of a filler wire having a high silicon content would prevent cracking by raising the silicon content of the final alloy freezing on the mid-plane of the weld and, thereby, shifting the composition out of the critical range for cracking.

The tensile strength of the weld would also be raised. It was also expected that the loss of material by explosive disruption of the surface would be compensated by the added mass of material and reduced energy gradients in the superficial volume of the bead which, being continuous, can sustain higher energy fluxes.

These improvements have been realized and the volume of the heat affected zone has been reduced because it has been possible to raise the power intensity incident on the weld.

Therefore, there are three theoretical approaches that have been accomplished ;

- (1) Increase the Silicon impurity in the alloy to reduce the cooling speed : rapid quenching , by the result, remove the welding cracking.
- (2) Increase the tensile strength by the addition of alloying element to the fusion zone.
- (3) Minimize the HAZ by choosing the pulse operating parameters correctly.

1.3. Achievements

The advantages of pulse laser operations and sufficient amount of Silicon to overcome the solidification cracking has improved the welding qualities.

- Deep penetration welding from laser welding variables on Aluminum Alloy investigates both high efficiency welding parameters and crack danger zone.
- Pulse Laser operation has reduced the size of HAZ, which normally proceeds over aging and annealing effect on Aluminum alloys.
- Additional Silicon has inhibited the weld cracking as well as strengthened the welding fusion zone.

Enrichment of the silicon content in the centre of the fused zone by including an silicon filler wire in the weld preparation has prevented weld cracking on solidification which would otherwise occur. Not only is cracking avoided, but the tensile strength of the weld is substantially raised. Cracking has been avoided in the more critical deep penetration mode of welding with the advantage that the heat-affected zone (HAZ) is substantially reduced.

Chapter 2. Literature review

2.1. Characteristics of Pulsed Laser Welding

2.1.1. Solid State Lasers for Welding

Electrons in the atoms of the transmission or rare earth element can be selectively excited to higher levels upon their exposure to intense incoherent optical radiation. Coherent emission during laser action is described in a reference [ref.1]. Once excited, the electrons return to their normal energy state in one or more steps, each involving loss of a quantum of energy. Lasing occurs if one of these energy losses results in the emission of a quantum of electro-magnetic radiation (Photon). The wavelength of all solid-state lasers is determined by the fluorescence spectrum of the dopant element.

There are several reasons the laser is of potential interest for fusion welding:

- (1) High intensity : 10^9 to 10^{11} W/m², which can be achieved by optically focusing a laser beam, By contrast the power intensity in arc welding is two or three orders less than these levels.
- (2) The laser delivers its energy in the form of light, it can be operated in air, vacuum, inert gas, liquid, transparent windows and any transparent environment.
- (3) There is no mechanical contact with the work piece and no requirement that the material being worked be a conductor of electricity.
- (4) Laser beam can be transferable through an optic system, which can be bent.
- (5) Long term cost effective.

2.1.2. Solid state laser (Nd³⁺:YAG laser)

Solid state lasers are based on single crystals or a glass doped with small concentrations of a transition element or rare earth; e.g. neodymium in glass or Yttrium Aluminum Garnet (YAG). Glass or these systems offer low values of threshold and high values of gain; moreover, the thermal conductivity of YAG is over ten times greater than that of glass which making it superior at high mean

power levels. ND:YAG lasers emit near infra-red radiation with a short wavelength of $1.064\mu\text{m}$ which is better absorbed by metal than is the longer wavelength of $10.64\mu\text{m}$ generated by CO_2 lasers (Figure 2.1, 2.2). Therefore, the YAG laser has a distinct advantage compared with the CO_2 Laser when welding high diffusivity high surface reflectivity materials, such as aluminum and copper or their alloys.

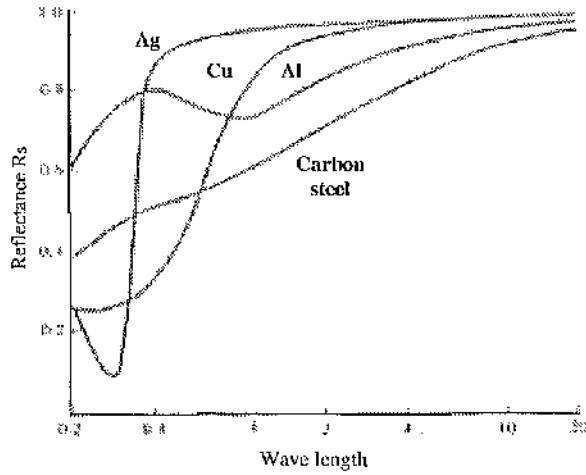


Figure 2.1. Reflectance versus wavelength for various polished metal surfaces at room temperature.

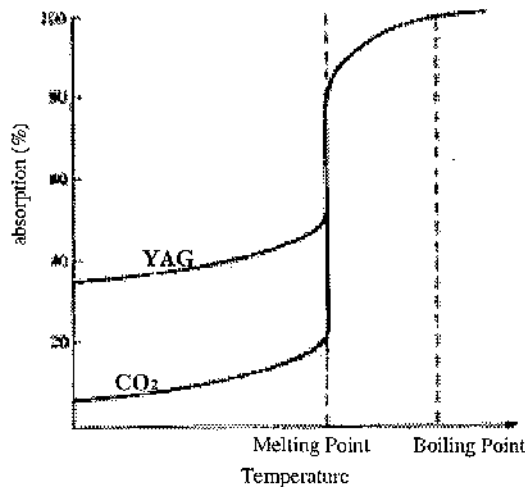


Fig. 2.2 Schematic variation of absorption with temperature for a typical metal surface for both the YAG and CO_2 laser wavelengths (J.Wilson et al[ref.1] 5.1Theoretical Analysis, p.167)

The interaction between laser and material has studied by numerical and experimental means [ref.30,37,40,49]. At high intensities are caused deleterious metal vapour and plasma formation [ref.38,43,44,45]. With the high power intensities available from pulsed solid state lasers the absorption of radiation in aluminum is still high. The comparison is high mean power with CO₂ system which is affected by the high reflectivity and high thermal diffusivity of aluminum. Surface treatment has been employed to alleviate this difficulty. Mechanical scratching of the surface with emery paper [ref.44,45] has improved welding with higher wave length lasers. This research has included a set of experiments compare roughened surface at various power intensities (Chapter 4.)

2.2. Aluminum Alloys

Aluminum is known for its light weight and excellent corrosion resistance and is widely employed in commercial products [ref.4]. Its density is about 0.1 (lb/in³), being approximately one third that of steel [ref.3]. The tenacious refractory oxide film on its surface has good electrical, thermal conductivity & high reflectivity to both heat and light without sparking and magnetic effect. These properties make welding difficult. Aluminum alloys melt at 755 to 933K depending upon the alloying present [ref.14]. Structural applications of Aluminum alloys have been chosen in their specific requirements such as automobile, building, aerospace and transport. The most widely used Aluminum wrought alloys are the binary and ternary alloy systems 5XXX and 6XXX¹⁾.

The conventional aluminum alloys can be divided into 8 groups depending upon their major alloying element²⁾. Series 1,3,4,5XXX are usually called work hardening alloys. Silicon is the major alloying component; Iron is also present. In the 5XXX series alloys (Al-Mg system), the addition of Magnesium and Copper accommodates special purpose applications. The maximum Magnesium content in the Aluminum is 37.3% in the equilibrium (Figure 2.4 (b)).

Series 2,4,6,7XXX alloys are precipitation-hardening alloys, which are strengthened by increasing the solid solubility in Aluminum with increasing temperature. The most famous alloys are the series 6XXX (Al-Mg-Si system) which the compound Mg₂Si is used at the ratio of Mg: Si=1.73 (Figure 2.4(a)).

¹⁾ Introduction of Aluminum Alloys : Seminar from Aluminum Federation.

2.2.1. Phase Diagrams

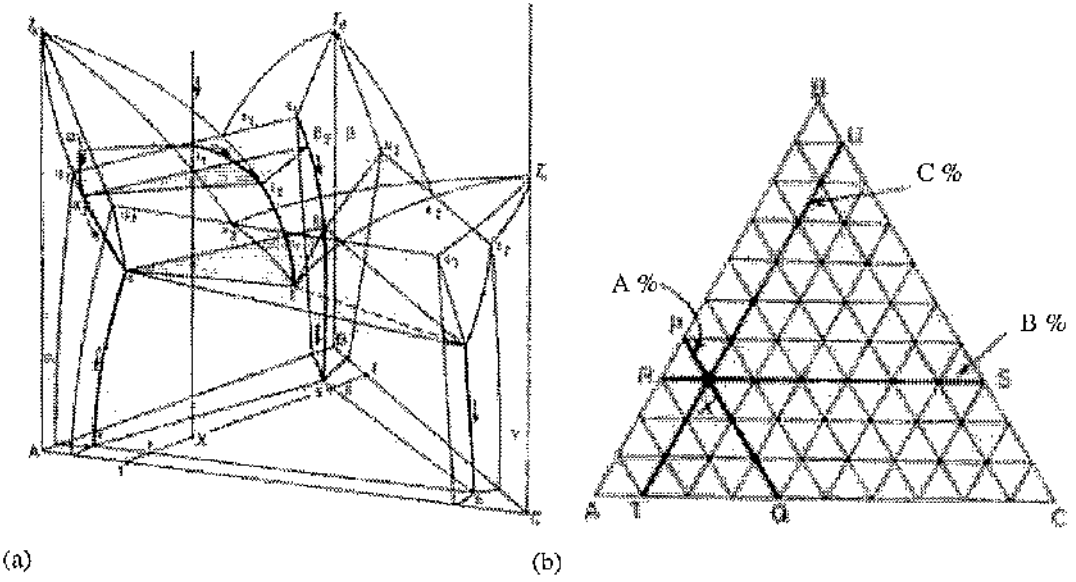


Figure 2.3. Schematics: (a) equilibrium solidification of Ternary Alloy X and (b) the Gibbs triangle (After A.Prince, Alloy Phase Equilibria, Elsevier, Amsterdam, 1966. [ref.12, p53])

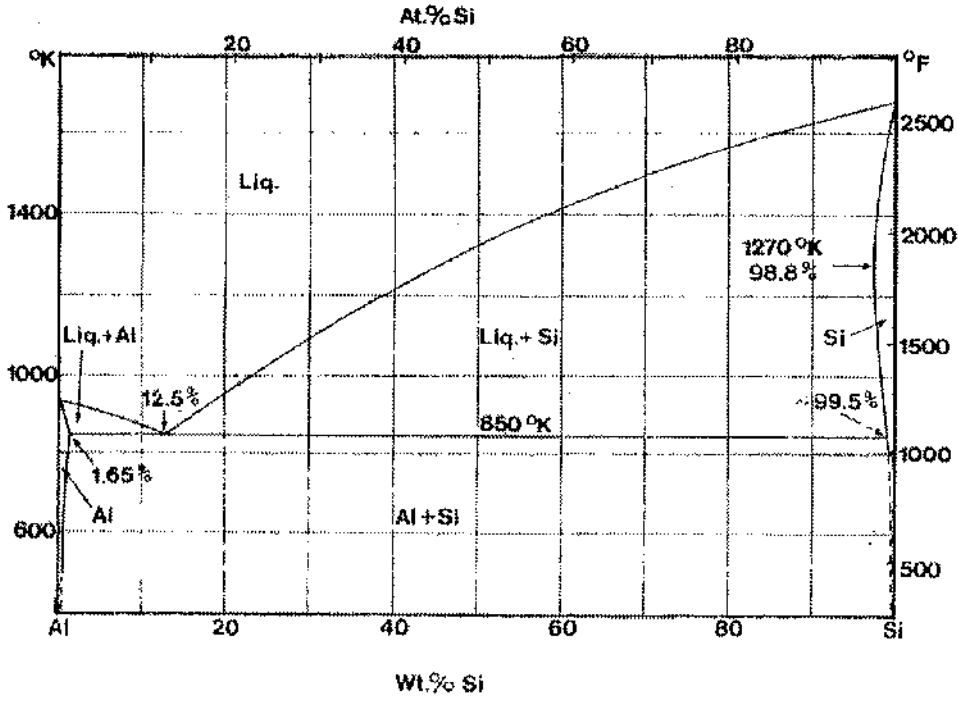


Figure 2.4 (a) Phase diagram of Al-Si binary alloy

²⁾ Metal hand book [ref.3], Light alloys Metallurgy of the Light metals [ref.14]

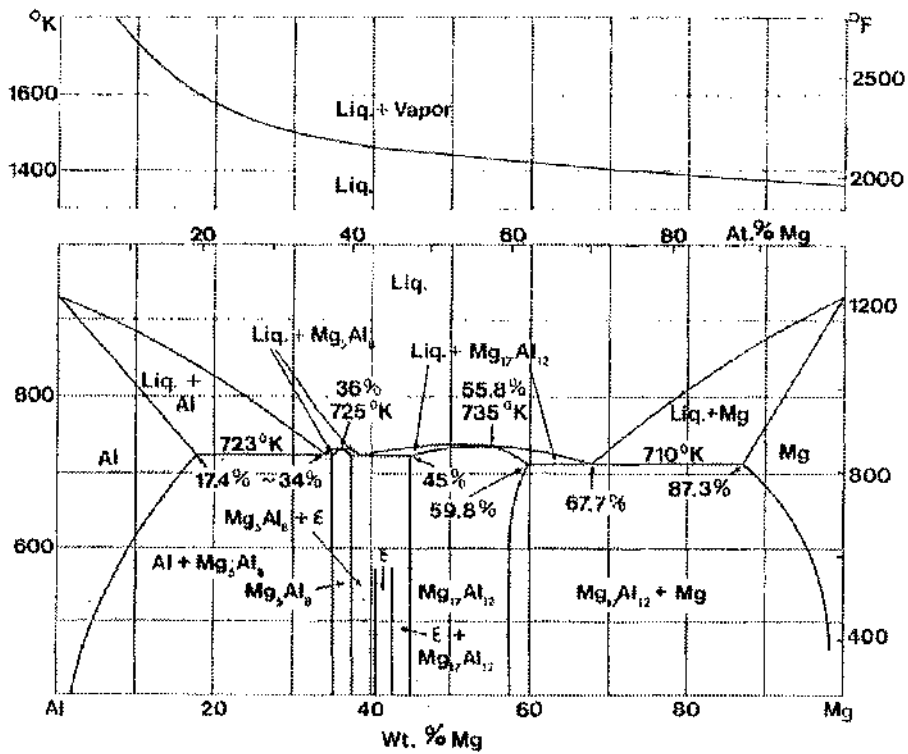


Figure 2.4 (b) Phase diagrams of Binary Al-Mg Alloys

2.2.2. Strengthening Process and Phase Changes

The strengthening mechanisms increase mechanical properties for their specific purpose. Two different temper-hardening effect can be categorized which are strain hardening of non-heat-treatable alloys and solid solution hardening of heat-treatable alloys¹⁾. Figure 2.5(a) and 2.6 show the increase of strength associated with the hardening effect; the elongation decreases simultaneously. Strain hardening is denoted by the symbol "H" and is categorized in three groups: H1: Strain hardened only, H2: Strain hardened and partially annealed, H3: Strain hardened and stabilized [ref.4]

Precipitation hardening includes a solution heat treatment at high temperature²⁾ to maximize the solubility of elements that participate in subsequent ageing treatments. The high strength is produced by the finely dispersed precipitates during ageing heat treatment. The symbol of the treatment "T" denotes a temper which has 10 different levels in various applications. Ageing time can affect to the properties (fig.2.3(b))

¹⁾ Strengthening mechanisms of Aluminum and their alloys have fully explained in Metal Handbook [ref.3, p.37.]

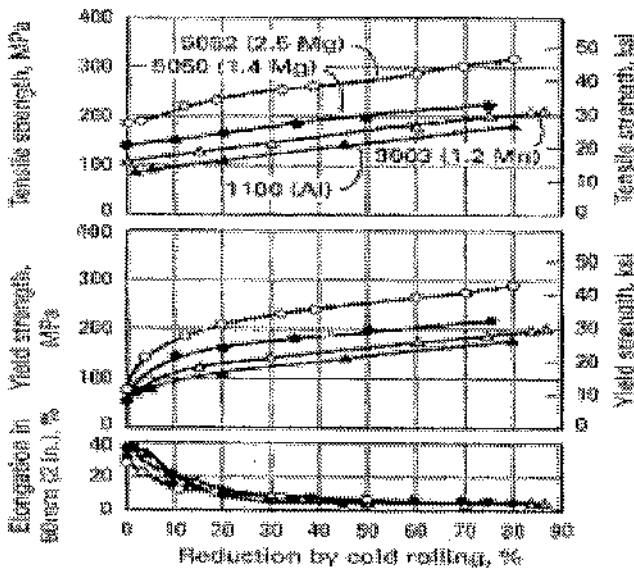


Figure 2.5(a). Mechanical properties related to the strain hardening. Metals Handbook Vol.2, Aluminum and Engineered Wrought products, p.39

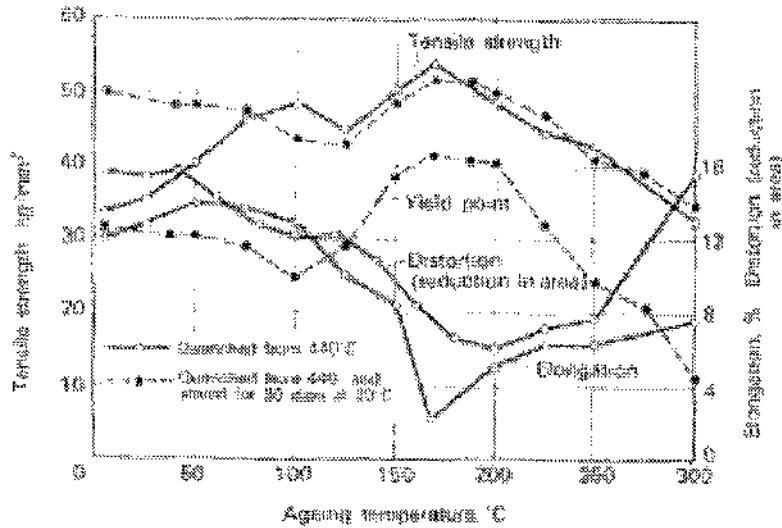


Figure 2.5 (b). Mechanical properties in various ageing temperatures. Alloy quenched at 440°C and subsequently stored at 20°C for 30 days. J.W.Martin, Precipitation hardening, Section II, II.2 reversion, p113.[ref.18].

²⁾ Normally the temperature range is below the solidus temperature.

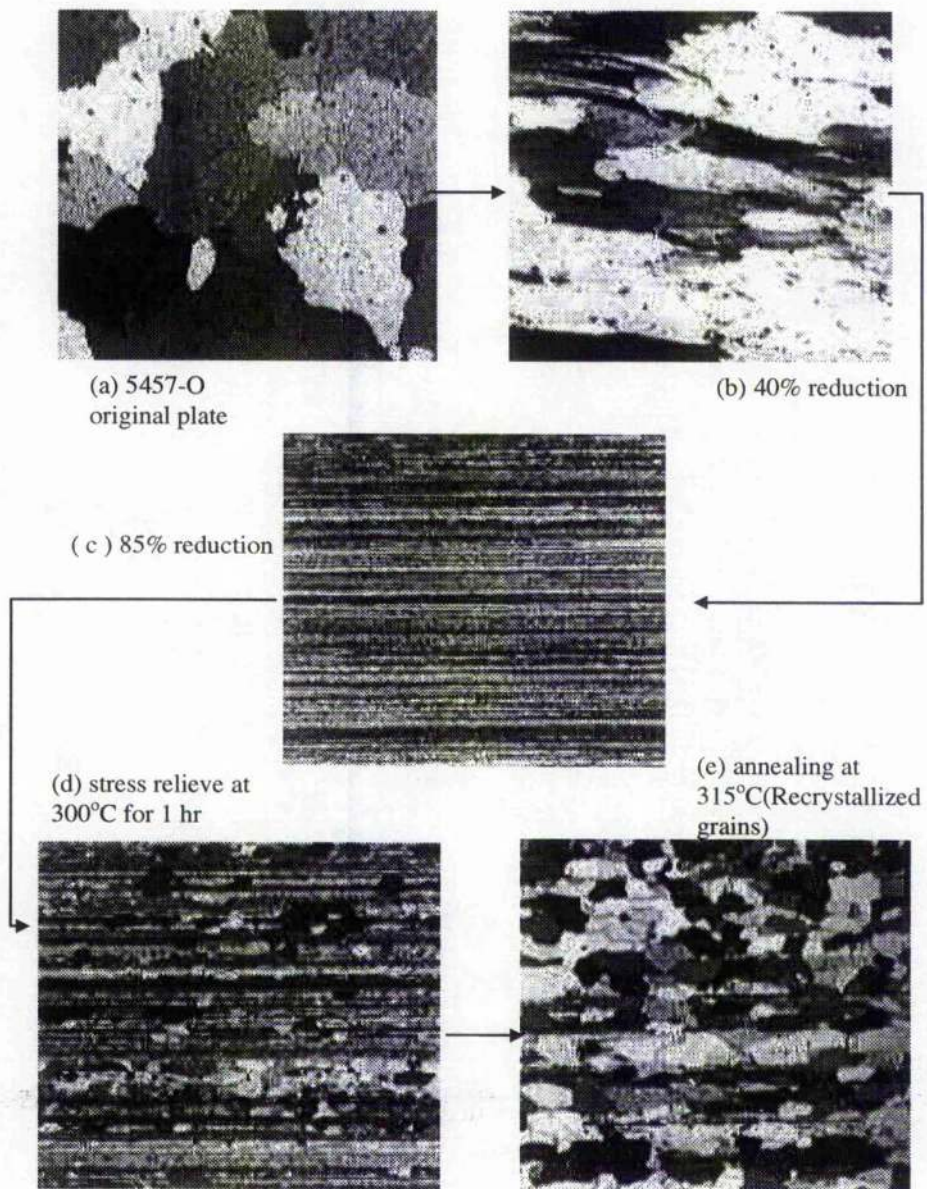


Figure 2.6. 5XXX series structural differences from alloy strengthening process
Barker's reagent(X100) Metals handbook, 9th edition, Vol.9, Metallurgy and Microstructures,
American Society for Metals, Aluminum Alloys, p361~362.[ref.42]

2.2.3. Significance for welding

2.2.3.1. Welding cracking

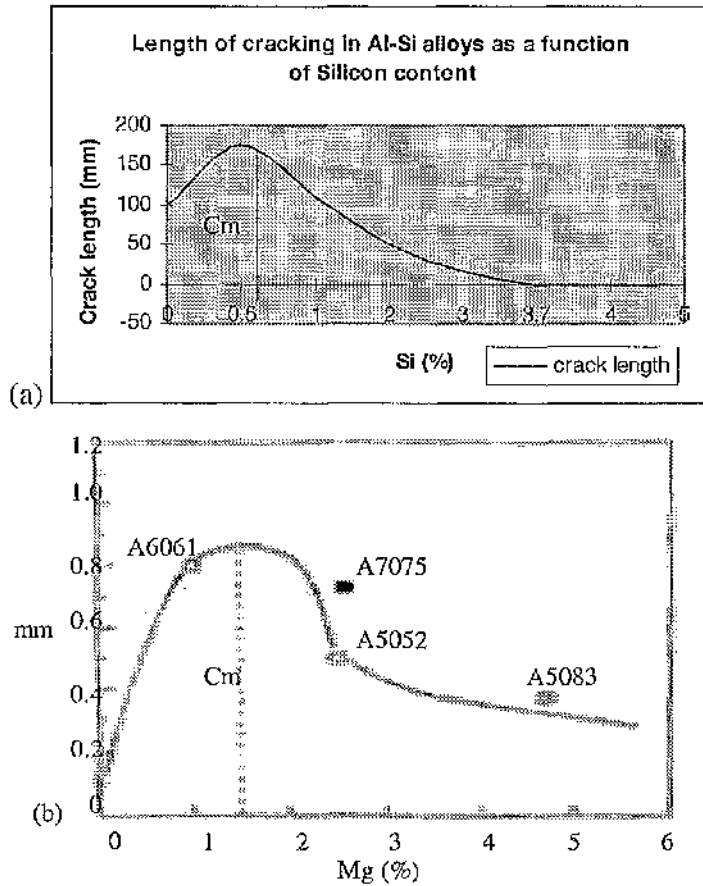


Figure 2.7 Length of cracking in restrained (a) casting Al-Si alloys : J.B.Lancaster *et al* [ref.8] and (b) wrought Al-Mg alloys : Muneharu Kutsuna *et al* [ref.39]

Figure 2.7 (a) and (b) show the relationship with cracking of the constitution of the alloys with Si and Mg. These demonstrate the crack sensitivity in casting and indicative of the performance in conduction limited welding. The sensitivity to cracking rises to a maximum (C_m) at about 0.5% Silicon (a) and 1.5% Magnesium (b), then decrease rapidly as the alloying content increases.

Figure 2.8 shows the typical welding cracking on aluminum alloy. Cracks which form above the solidus temperature are known as super-solidus cracks; those forming below the solidus are subsolidus cracks. The metallurgical distinction between these two cracking modes is significant for crack formation in welding.

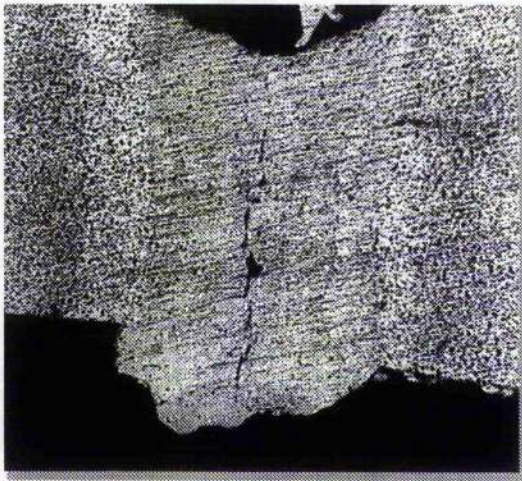


Figure 2.8
 Typical experimental example of welding cracking of Aluminum Alloy(AA5251-H24) by pulse ND³⁺:YAG laser
 Welding parameter :
 E=45J,PRF=7Hz,P.D=6.2msec,V=4.0mm/sec

(1) Super-solidus cracking (Hot Cracking)

There are two preconditions for cracking during welding. Figure 2.9 shows the propensity for the cracking of two alloys. The difference between the coherence and nil-ductility temperature is known as the brittle range. Generally alloys which possess a long brittle range are sensitive to welding cracking, while crack-resistant alloys have a short brittle range. In the case of aluminum alloys, cracking is promoted by variation of the alloy elements. The longer brittle range, the greater possibility that harmfully high contraction stress will set up. In addition, there is a correlation between the tensile strength within the brittle range and the tendency towards welding cracking in a crack-sensitive metal.

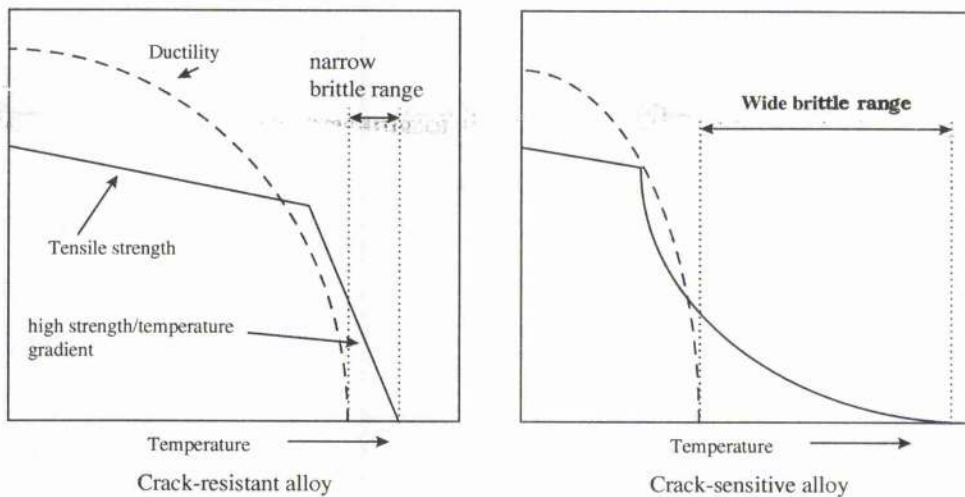


Figure. 2.9. Mechanical properties contrast of crack resistant and sensitive alloys [ref.8]

(2) Sub-solidus cracking (Cold Cracking)

Sub-solidus cracking occurs below the melting temperature. Failure is caused by brittleness on the application of a tensile stress. Embrittlement develops in time so that cracking may occur several months after solidification.

In some cases it is difficult to decide whether cracking is caused in the super-solidus or sub-solidus regions. Crack sensitive alloys are subject to both forms of defect.

2.2.3.2. Evaporation

Alloying elements of low melting temperature, such as magnesium may evaporate preferentially during welding, leaving a reduced alloying composition. Porosity in the weld is an associated result [ref.8]. The boiling point of Mg is 1380K compared with 2727K for Aluminum. The loss of the alloying element, e.g. of Magnesium, is greatest on the top and at the center of the fusion zone (Chapter 4.3.1.2).

2.2.3.3. Porosity

Porosity reduces the strength of the weld metal. Porosity in Aluminum welding is due to either grimy surfaces, rejection of hydrogen, or evaporation of alloying components [ref.4,8]. The sensitivity of Aluminum to hydrogen porosity is associated with two factors: The high ratio between the volume of hydrogen which can be absorbed in the weld and the solubility of this gas in the region of the melting point. Secondly, The presence of hydrogen in the laser exposure. The oxide film is a potential source of hydrogen in Aluminum welding. Absorbed films of moisture or impurities on the Aluminum surface are invariably present when the metal is exposed to the atmosphere.

2.2.3.4. Rapid Quenching

The high thermal diffusivity of aluminum has two effects in welding. As shown in figure 2.8, high thermal diffusivity causes the HAZ to be larger in aluminum. The structure of the fusion region is affected by the very rapid cooling. The convection of energy in the fusion zone of a non-conduction-limited weld is not readily modeled, yet it is the dominant mechanism determining the rate at which the fused material is quenched.

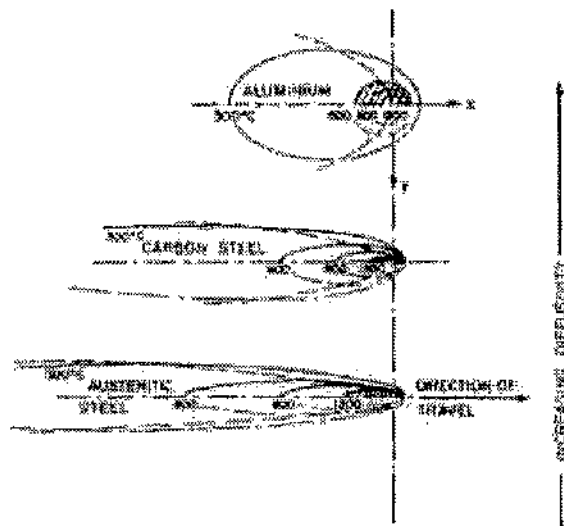


Figure 2.10. Effect of changes in thermal conductivity (K_s) from different materials. (After T.G.Gray, J.Spence and T.H. North, Rational Welding Design, NewnesButterworth, London, 1975) Further readings: ref.48,15

Neither is the non-equilibrium processes causing phase changes in the alloy at high temporal rates of temperature change understood. It is for these reasons that the investigation is essentially experimental.

A parallel project has however measured the temporal rate of change at the surface of the weld [ref.23]. An adaptation of the two colour method of temperature measurement has yielded the result given in figure 2.11. A correlation of such temperature measurements with the phase found in the weld cross-section is being attempted. Process at the surface of welds and the fusion zone have been investigated using e.g. fast CCD cameras. [ref.44, 45,46,47]

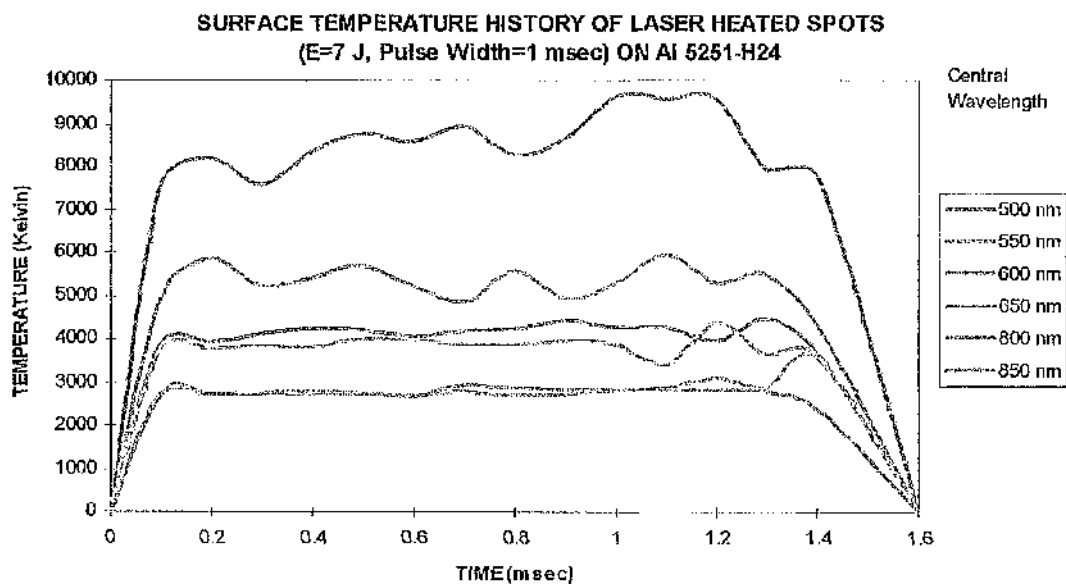


Figure 2.11. Surface Temperature profile of pulse Nd^{3+} : YAG laser irradiated aluminum (5251-H24 alloy). Pulse duration (τ) = 1msec, cooling was after the pulse from 1msec to 1.6msec [ref.23]

2.3. Solidification cracking in Laser Welding

L.A. Guierrez et al.[ref.32] have compared Tungsten Gas Arc Welding (GTAW) and continuous wave (cw) CO₂ Laser Beam Weld (LBW) on the basis of metallurgical and mechanical property tests using AA6013-T6 Alloy with AA4043 as a filler metal. From this research, it is concluded that solidification cracking is caused by the fast solidification speed, which favors a columnar structure. The maximum hot tearing susceptibility of Aluminum Alloy is at 1% Si (wt%) in the fusion zone. GTAW and CO₂LBW were 1.2 and 2.4 % on AA6013, so that a higher Si content filler metal was used in order to remove the cracking. The sizes of the HAZ and the fusion zone of both welds were estimated from the hardness profile. The HAZ and fusion zones of GTAW were about 30 mm and 5mm, while those of CO₂ LBW were 6 mm and 2 mm. In both of results, the hardness was decreased compare to that of the base metal. The related tensile properties decreased on GTAW by 40 % and on CO₂ LBW by 35 % when compared to the base metal with failures in the HAZ in the case of GTAW and in the fusion center in the case of CO₂ LBW.

S.Venkat et al. [ref.34] employed a 3kW CO₂ LBW to weld AA5754-O and AA6111-T4 alloys in tailored blanks for automotive applications. The most significant concerns were: vaporization of low boiling point, strengthening elements due to the high power intensity of laser beam; over ageing in heat-treatable and annealing in non-heat-treatable alloys; HAZ liquitation and solidification cracking.

This experimental based research has found the total elongation was 80 to 110% of base metal with ductile rupture on AA5754-O and the related micro hardness on HAZ had increased, while that of 6111-T4 was 30 to 70% that of the base metal, with both brittle inter-dendritic and ductile rupture failure. The micro hardness was slightly decreased due to the over-ageing and annealing effect. The result of Electron Probe Micro Analysis (EPMA) measuring the Al and Mg elements show that the weight percent of Magnesium had decreased in the fusion zone. The loss in the 5754-O alloy was very large.

The phenomenon of evaporation was also investigated by CW Nd: YAG laser [ref.44] that the Mg evaporation was greatest on the top and centre of the fusion zone.

A.Blake et al [ref. 43] investigated the control of the Magnesium loss by Plasma Suppression CW CO₂ Laser autogeneous welding on AA5083 alloy. The minimum loss was 0.9% and that of a well penetrated welding sample increased from 1.2 to 11% by 7kW CO₂ Laser. Reduced porosity was evident from radiographic examination of the microstructure in the fusion region.

Muneharu Kutsuna et al.[ref. 39] investigated the metallurgical aspects of Aluminum Alloys, Carbon Steels and Stainless steels welded with CO₂ and YAG Lasers. The crack susceptibility of the Aluminum alloy with Magnesium (figure 2.3) was a maximum at 1.5% in the alloy. The experimental result correlated hydrogen porosity formation in three categories: small spherical porosities (type A) in the fusion, large polygonal(type B) and spherical porosities (type C). Spherical shape porosity (type C) was associated with element loss due to evaporation.

The relationship between solidification cracking and alloy composition was explained by J.F.Lancaster et al [ref.8] that the maximum cracking length in binary Al-Si alloy was at 0.5% of Si and it decreased when the Si content was increased.

These references works suggest that cracking is caused by:

- 1) Comparatively poor brittle structure, because of rapid solidification speed due to the high thermal diffusivity.
- 2) Loss of strengthening elements, e.g. magnesium evaporation and spatter production in the high power intensity welding and silicon segregation in the fusion center area.
- 3) The silicon concentration on the centre line falls and leads high crack formability in Al-Silicon non-eutectic alloys.

This latter is explained by non-equilibrium solidification of the alloy from the fused material.

2.4. Non-Equilibrium Alloy Solidification

There were three categories have explained in the reference¹⁾ to explain the alloy solidifications which are;

- (1) Infinity slow (equilibrium) solidification
- (2) Solidification with no diffusion in the solid but perfect mixing in the liquid.
- (3) Solidification with no diffusion in the solid and only diffusional mixing in the liquid.

According to the theory, the molten metal during the welding process keeps bouncing because of the buoyancy-driven flow [ref.10] or convection flow [ref.48] so that the solidification on the welding can be explained by applying second case in the categories.

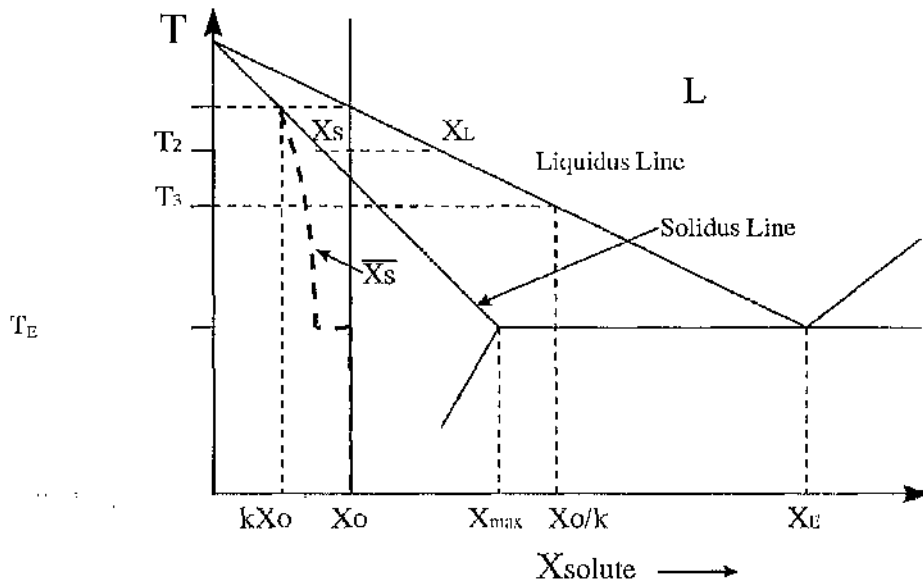


Figure 2.12. Planar front solidification of alloy X_0 . $K=X_S/X_L$ is constant. \bar{X}_S indicates the non-equilibrium cooling of X_0 alloy.

Chapter 4. Solidification, figure 20 David A. Porter et al., 1981, [ref.12.]

¹⁾ Phase Transformations in Metals and Alloys, 4.3 Alloy Solidification, p208~215. [Ref.12]

Assuming that there is no diffusion in the solid metal but the liquid composition is homogeneous during unidirectional solidification. When it starts solidification, a solid wall appears at temperature T_1 . The solid containing kX_0 mol of solute forms (fig.2.13(a)). The first solid will be purer than the liquid metal so that the solute is rejected into the liquid, therefore it raises the composition concentration higher than X_0 (fig.2.13(b)). When it keeps on the cooling, temperature is lower than T_1 and solute in next layer of solid is somewhat richer than the first layer. This non-equilibrium cooling mechanism can be applied in the welding process with X_0 being the silicon concentration.

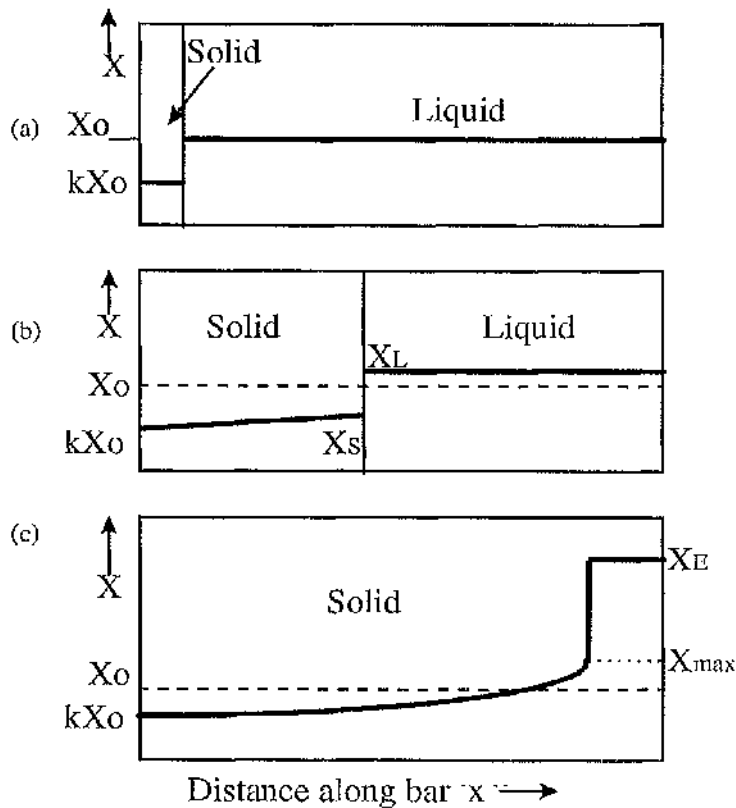


Figure 2.13. Solidification of alloy X_0 . (a) solidification starts (b) composition profile just under T_1 , (c) composition profile at T_2 , (c) composition profile at the T_E and below T_E

2.5. Prevention of cracking

In this research, two experimental approach have been considered in combination to prevent welding cracking;

- (1) Precise laser parameter control
- (2) Additional alloying element

In laser parameter control, solidification crack inhibitions have investigated by controlling the precise laser parameters. Laser parameters have chosen by the laser control panel in all range variables. The result of the method has shown in chapter 4.3. Relationship of laser parameter control to the fusion size.

According to the reference investigations, Mg and Si are the main components affecting cracking (Chapter 2.3.) The solution was to enhance the si content of the last metal to solidify by incorporating a high silicon content wire in the weld preparation. Two alloys were investigated: ER4043 having 5% silicon and ER4047 having 12% of silicon.

Chapter 3. Experimental Arrangements

3.1. Introduction

In laser welding, a quality weld is achieved by properly choosing the laser operating parameters such a pulse energy, pulse duration, Pulse Repetition Frequency (PRF) and welding focus. Each target material has its properties, which influence laser processing. [ref.5] ;

- (1) The volume of fusion zone or Heat Affected Zone (HAZ)
- (2) Material removal or evaporation
- (3) Embrittlement of welding zone
- (4) Limited temperature and limited time of contact between liquid and solid
- (5) Sufficient depth of penetration
- (6) Prevention of oxidation by protected surrounding

All of those subject can be changed by controlling the Laser welding variables to obtain an effective weld as a prior consideration.

3.2. Welding Apparatus

3.2.1. Changeable operating parameters on Nd³⁺:YAG laser

3.2.1.1. The incident laser Pulse Energy

The pulse energy influences the total amount of heat transfer to the effected zone and some parameters of radiation, therefore, it is varied by means of filters or diagrams. The range of pulse energies was available from 1 to maximum 50 joules in the pulsed ND³⁺YAG laser on the workpiece. The average laser power incident is the product of pulse energy (E) and pulse repetition frequency (PRF).

3.2.1.2. Pulse duration (Pulse Width)

The optimum pulse duration range can be decided for each material and the depth of the molten zone, and within this range of welding is obtained without excessive removal of the material from the heated zone [ref.2]. Pulse duration(τ) determines the mean

power of the pulse with pulse energy in the power calculation. Most of the laser parameter was valid on the frequency range of 1Hz to 20Hz so as to get a sufficient penetration from pulse energy. Pulse width can be changed in different pulse energy.

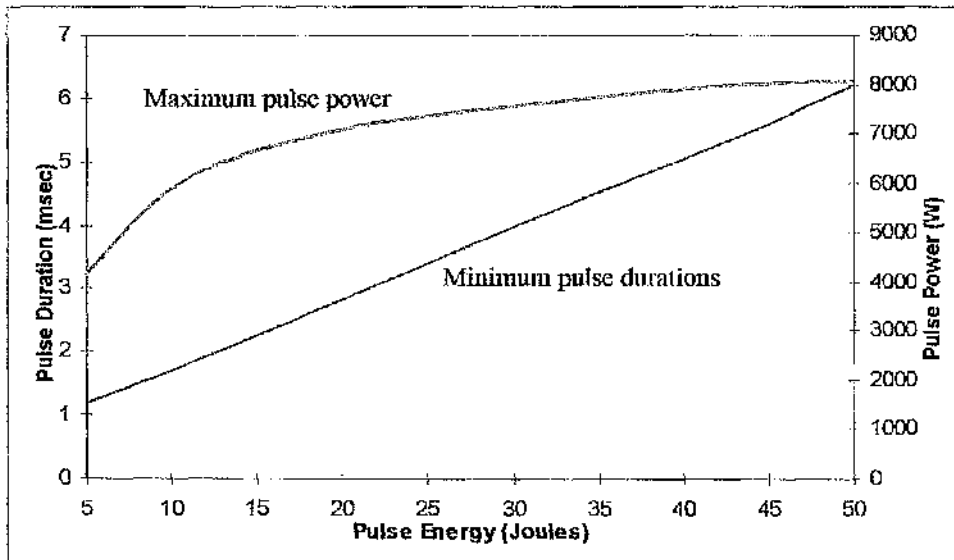


Figure 3.1. The Laser Power Limitations on different Pulse Energies and Pulse Durations :
Graph shows that maximum pulse power obtained from the minimum pulse duration with certain pulse energies

3.2.1.3. Pulse Repetition Frequency (P.R.F.)

The limitation on pulse repetition frequency (PRF) is the mean power at which the laser can be operated. The PRF can change the overlap ratio of the welding result from 1 to 100 Hz and by altering the transitional speed of the workpiece. Mean power of the laser takes into account of PRF with pulse Energy. In the experiments, deep penetration welding has restricted the range from 1 to 20 Hz by the need to operate the laser at sufficiently high pulse energies. The laser operating parameters are shown in figure3.2, which defines the maximum pulse energy at different frequencies, which Lumonics ND³⁺: YAG Laser can develop. Non-conduction limited welding can be achieved in the range 1 to 10Hz to increase the power intensity.

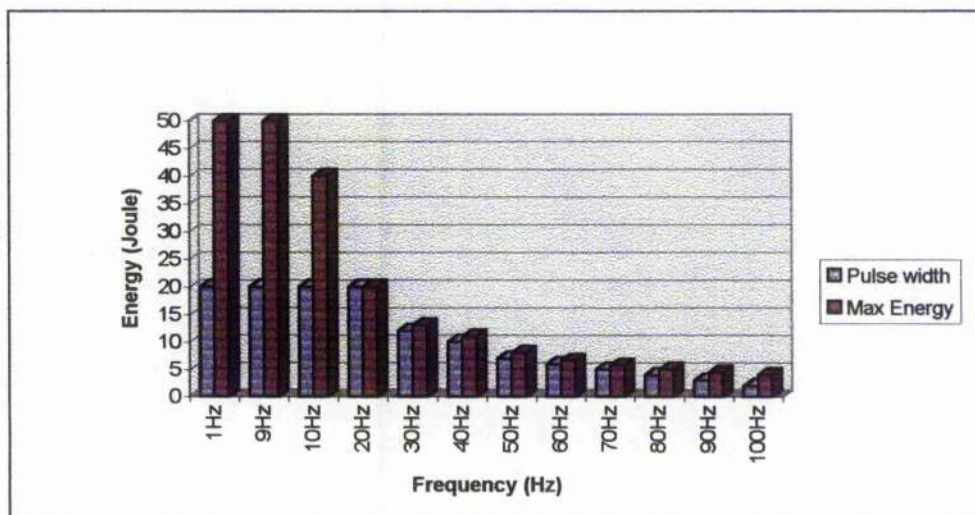


Figure 3.2. Relationship of pulse energy and Frequency (PRF) under average power 400W.

3.2.2. Weld traveling speed

Welding velocity is another factor to change the welding overlap. The workpiece is stationary, the optical fiber beam delivery system is released by an IBM 7540 SCARA robot. A linear point-moving program called “pweld.exe” controls the robot. Three different traveling speeds of welding have been investigated; namely: 2.9 / 4.0 / 5.8 mm/sec. Welding speed has increased by decreasing the coordinate point in the program.

3.2.3. Laser Beam diameter

Beam diameter is, from the simple Optics, one of the most important variables to determine the power intensity. From a Gaussian beam profile, the diameter is defined as being that at the $1/e^2$ point of the intensity profile and containing 80% of the total power [ref.5].

In the fixed optical aperture, the simplest technique of beam diameter determination is direct laser beam exposing on the negative photographic film to decide the near-field zone (the Fresnel zone), which would be the focal distance on the focusing head assembly.

The spot size has been minimized by an experiment in a vertical angle of laser beam as a function of focal length and the result of the spot size reading; the minimum spot size was 1.5 mm diameter.

Other important parameter to decide the spot size is the pulse input power (W) because of the beam divergency in each power is altered. From the experiment, size of the spot was constantly increased when increase the pulse power (Table 3.2 and 3.3). The values from the size reading have used for the calculations for the power intensity.

No.	focal distance (mm)	Spot diameter d (mm)
1	68	7.3
2	70	6.5
3	72	5
4	74	4
5	76	2.9
6	78	1.52
7(F)	80	1.5
8	82	1.53
9	84	3
10	86	4.5
11	88	6
12	90	7
13	92	8.2

Table 3.1. Determination of focal distance and focal size measurement. F is focal distance.



Figure 3.3. Spot size reading from negative photographic film

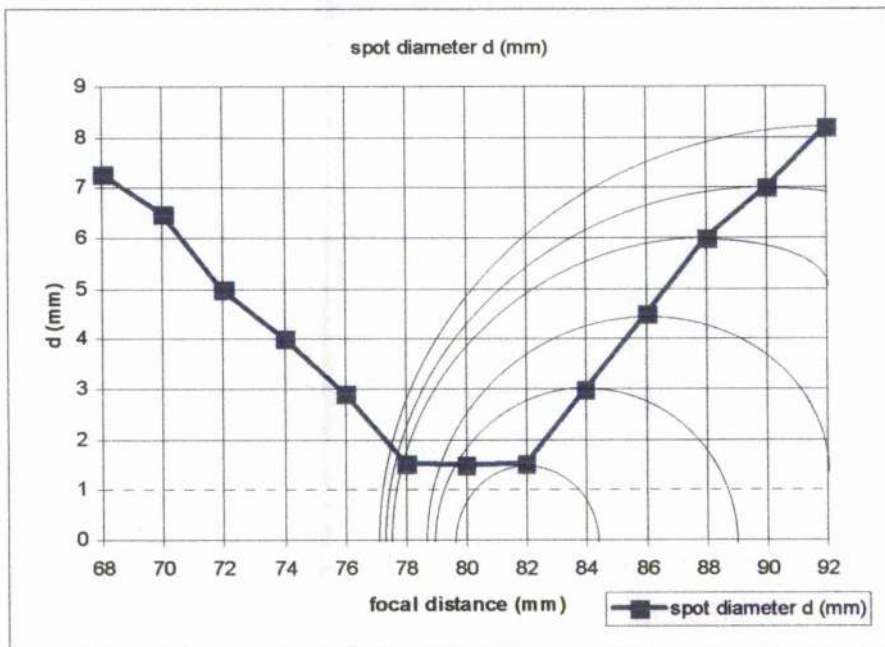


Figure 3.4. Size reading of laser single spot in different focal distance
Laser parameter: $E=10J$ / $PRF=10Hz$ / $\tau=10msec$

E (Joules)	5	10	15	20	25	30	35	40	45	50
d (mm)	1.5	1.55	1.6	1.65	1.7	1.75	1.8	1.85	1.9	1.95

Table 3.2. Size reading of laser single spot in altered pulse energy

Other parameters: PRF = 8Hz / τ = 7msec / focal distance (80mm)

τ (msec)	5	6.2	7.5	8.8	10	12.5	15	17.5	19.9
d (mm)	1.74	1.71	1.68	1.65	1.62	1.59	1.56	1.53	1.5

Table 3.3. Size reading of laser single spot in altered pulse duration

Other parameters: E = 30J / τ = 7 msec / focal distance (80mm)

3.2.4. Calculations of the power intensity and the overlapping ratio

3.2.4.1 Power Intensity

The mean pulse power can be obtained from the relationship between pulse energy and pulse duration (Chapter 3.2.1.1 and 3.2.1.2). The power intensity can calculate when derive the measurement of exact the focal spot size. (Table 3.2.)

(1) The relationship between the Pulse energy and the pulse duration is;

$$PulsePower(P) = \frac{PulseEnergy(J)}{PulseDuration(msec)} (W)$$

$$PowerIntensity(I) = \frac{P(W)}{\frac{\pi r^2}{4}} (W / m^2)$$

where r = half diameter of the spot size (mm).

For Instance, The relationship between pulse duration to the pulse power is¹⁾,

$$Mean\ pulse\ power\ (P) = \frac{E(J)}{\tau(sec)} (W) \text{ where, } E : \text{ pulse energy, } \tau : \text{ pulse width}$$

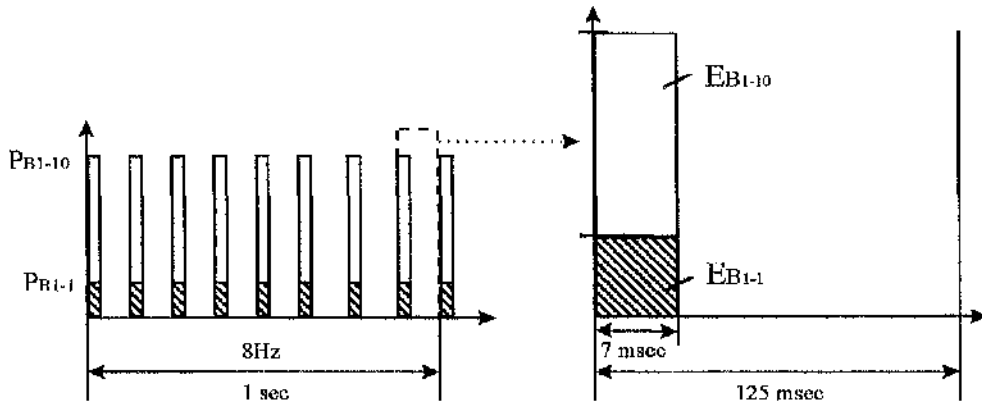


Figure 3.5. Laser Power calculation from different Laser out put energy- 5J and 50J
 (Other operating parameters: PRF=8Hz, $\tau=7\text{msec}$, $V=2.9\text{mm/sec}$)

From the experiment list¹⁾,

$$P_{B-1-1-1} = \frac{5J}{7\text{msec}} = 714.29 \text{ W}$$

$$P_{B-1-1-10} = \frac{50J}{7\text{msec}} = 7142.9 \text{ W}$$

Measured spot size can be applied from table 3.2. So that the power intensities (I) are;

$$I_{B-1-1-1} = 714.29\text{W}/[\pi(1.5)^2 \times 10^{-6}] = 1.01 \times 10^8 (\text{W/m}^2)$$

$$I_{B-1-7-10} = 7142.9\text{W}/[\pi(1.95)^2 \times 10^{-6}] = 1.01 \times 10^9 (\text{W/m}^2)$$

(2) The relationship between pulse duration to the pulse power are²⁾;

$$\text{Mean pulse power} = \frac{E(J)}{\tau(\text{sec})} \text{ where, } E : \text{ pulse energy, } \tau : \text{ pulse width (see table 4.)}$$

¹⁾ Appendix i.1. Experiment lists, table 1. Experiment list of pulse energy changes to the weld fusion sizes.

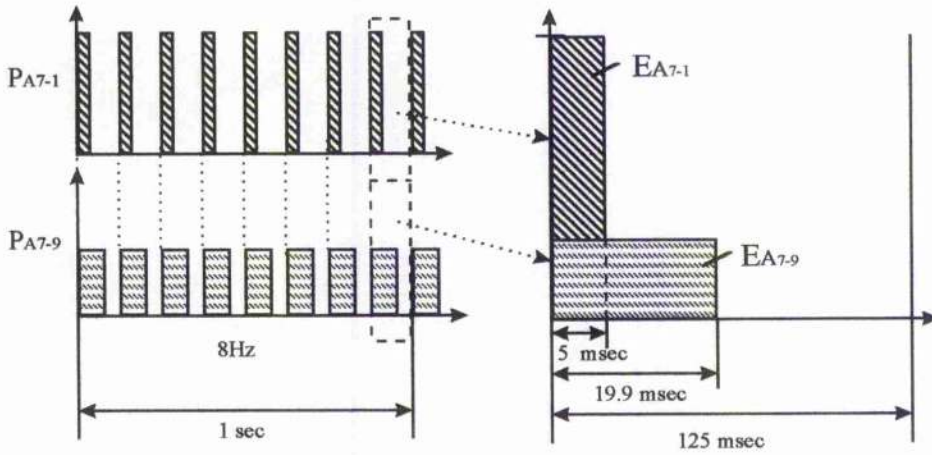


Figure 3.6. A Schematic of Pulse shape for the pulse power calculation

From the experiment list²⁾,

$$P_{A-1-7-1} = \frac{30J}{5 \times 10^{-3} \text{ sec}} = \underline{6000 \text{ W}},$$

$$P_{A-1-7-9} = \frac{30J}{19.9 \times 10^{-3} \text{ sec}} = \underline{1507.5 \text{ W}}$$

Measured spot size can be applied from table 3.3. So that the power intensities are;

$$I_{A-1-7-1} = 6000\text{W}/[\pi(1.74)^2 \times 10^{-6}] = 1.88 \times 10^{10} \text{ (W/m}^2\text{)}$$

$$I_{A-1-7-9} = 1507.5\text{W}/[\pi(1.5)^2 \times 10^{-6}] = 4.73 \times 10^9 \text{ (W/m}^2\text{)}$$

3.2.4.2. Overlapping Ratio

Overlap defines a percentage of the diameter, which has overlapped in certain welding velocity so that the size of the diameter and spot distance is the main factor to decide the welding overlap. In order to calculate the welding overlap, assume that shape of the resolidified molten metal is spherical,

$$r(\%) = \frac{D - d}{D} \times 100$$

where, D = surface diameter of laser irradiated spot,

d = distance between spots which relate as;

²⁾ Appendix i.1. Experiment lists, table 2. Experiment list of pulse duration changes to the weld fusion sizes.

$$d = \frac{V}{PRF}$$

where, V: welding velocity (mm/sec),

PRF: Pulse Repetition Frequency (Hz)

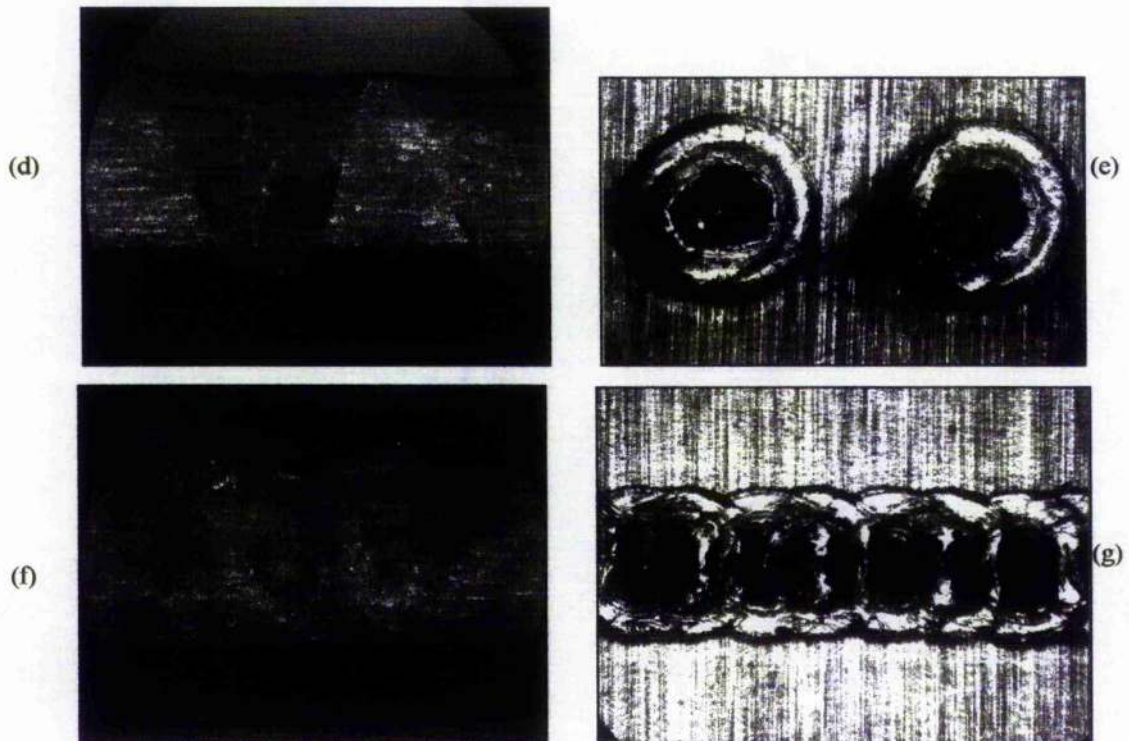
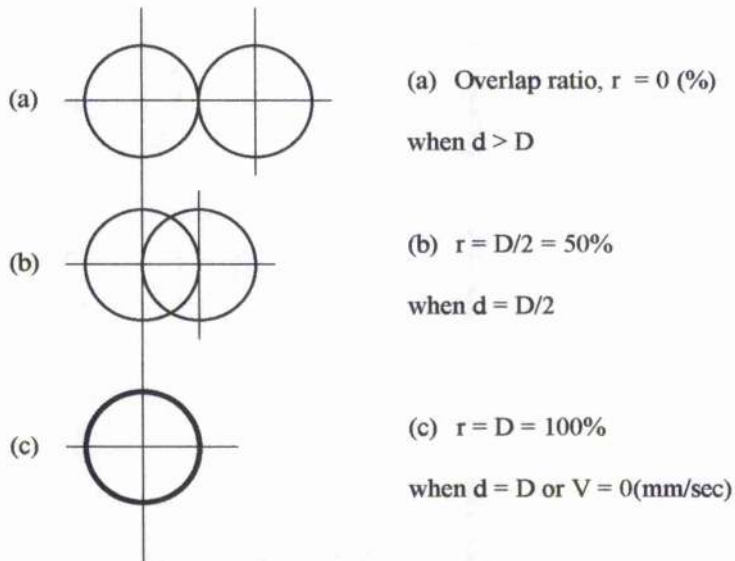


Figure 3.7. Calculations of welding overlapping ratio and their examples.

(a),(d),(e) : overlap ratio = 0(%) , (b),(f),(g) : overlap ratio = 50(%)

(d),(f) : Welding transverse section , (e), (g) : Top view of welding surface

3.2.5. Gas shielding

Applying proper shielding can reduce the prevention of both plasma block and material surface oxidation. Choices for the shielding gas are Helium, CO₂ and Argon, which are essentially inert during the welding process. Helium may be used at high powers and for deep penetrating welding applications. However, being economical and commonly Argon gas is used as welding surroundings. This experiment Argon shielding method have selected and 1 to 1.5 bar of gas pressure inclined at 45° of the weld surface was used (Figure.3.8).

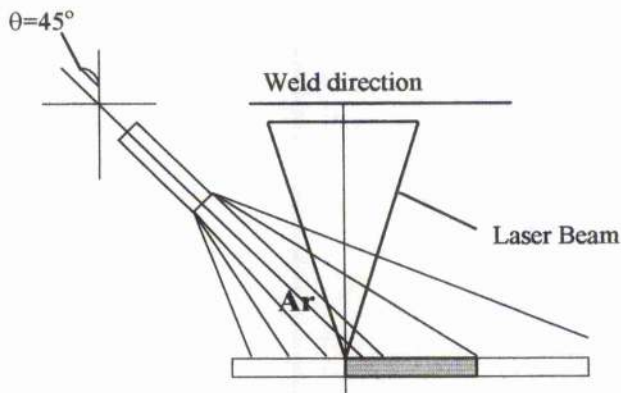


Figure 3.8. Schematic picture of shielding gas delivery (impact type, Ar gas shielding)

3.3. Beam Delivery System and Optical fiber

3.3.1 Time sharing and Energy sharing system

The principal of fiber optic has been explained in many places [ref.1,2,7,35,36,37]. ND:YAG laser systems are available with beam sharing systems to increase the productivity in a cost-effective manner using optical guiding mirrors and fibers. The time sharing system delivers the same laser energy as output by a shutter switch that is possible to obtain a sequential weld.

The energy-sharing device divides the laser output energy between several fibers as shown in Figure 3.9. However, practical application of energy sharing devices causes an energy loss so that one optical fiber was used during the experiments to increase the welding depth in welding experiments.

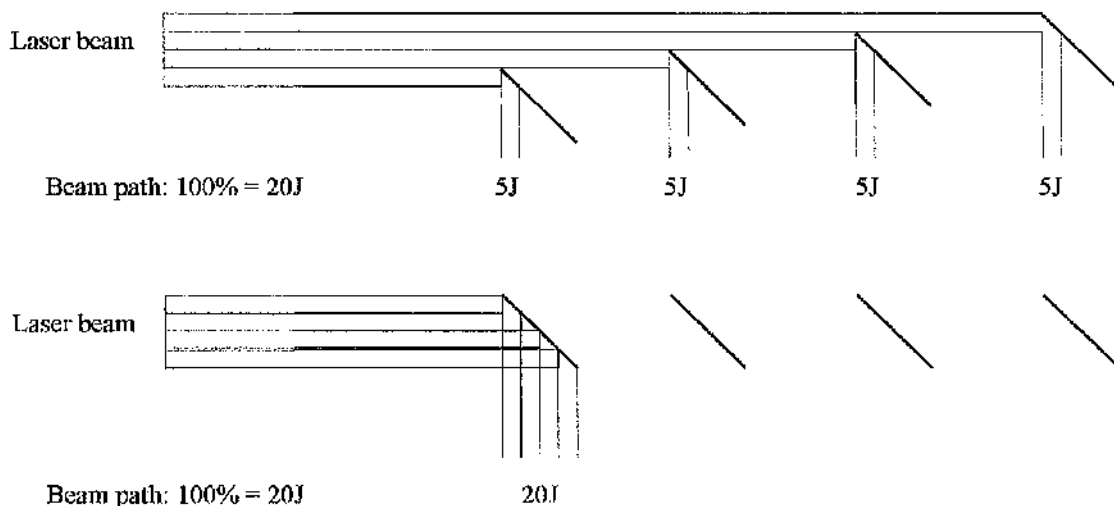


Figure 3.9. A Schematic of (a) Energy sharing system and (b) experiment set up.

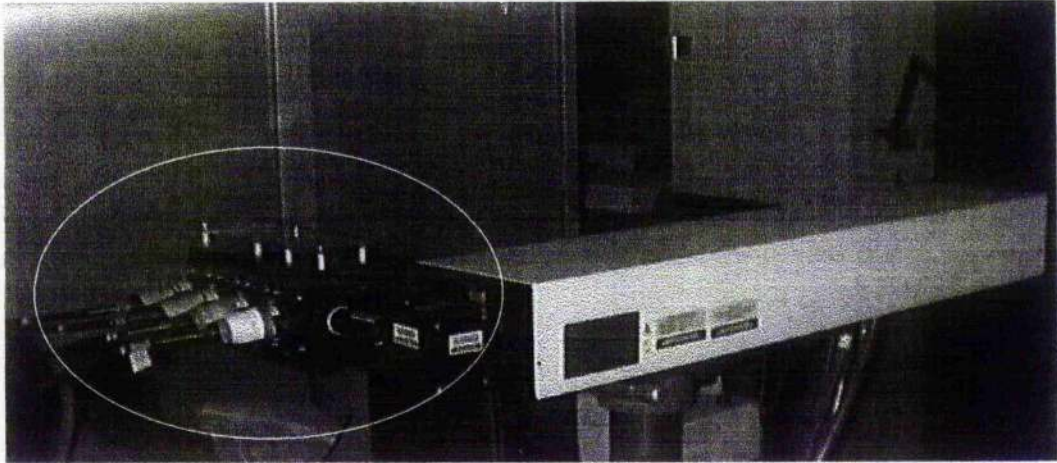


Figure 3.10. Fiber optical multi-flex beam delivery system (Energy sharing system) and Lumonics ND³⁺: YAG Laser

3.3.2 Optical fiber

Most commonly used industrial laser in present is CO₂ laser and ND:Lasers. Beam delivery system has generally two different systems for each of them. Flexible beam delivery system for CO₂ laser use guiding mirrors, while ND: laser has the possibility to use optical fibers to guide the radiation to the focusing lens as an advantage of smaller wave length. Recently there is optical fiber for CO₂ laser in the commercial market is available in special applications.

The principle of fiber optic is to guide the laser radiation beam through the centre of fiber core. The cladding surrounds the core, which is totally reflective if the incidental angle is sufficiently large (Figure 3.11).

Figure 3.11. The ray path theory and internal fiber core reflection of laser beam⁹

Recent development, there are two different fibers which produce distinctive characteristics to be, finally, determined weld penetration.

Graded Index (GI) fibers have a output characteristic of Gaussian beam distribution, such as a smaller diameter and higher intensity beam profile that the most of high intensity laser-material processing commonly used. Stepped Index (SI) fibers produce a “top hat” energy distribution and larger beam diameter. Figure 3.12 shows the major output characteristic of GI and SI fibers.

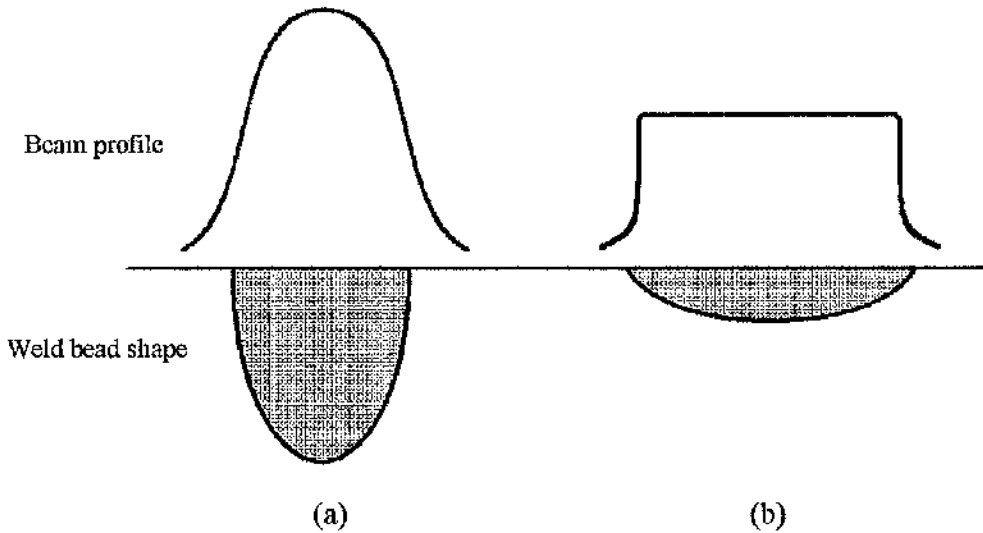
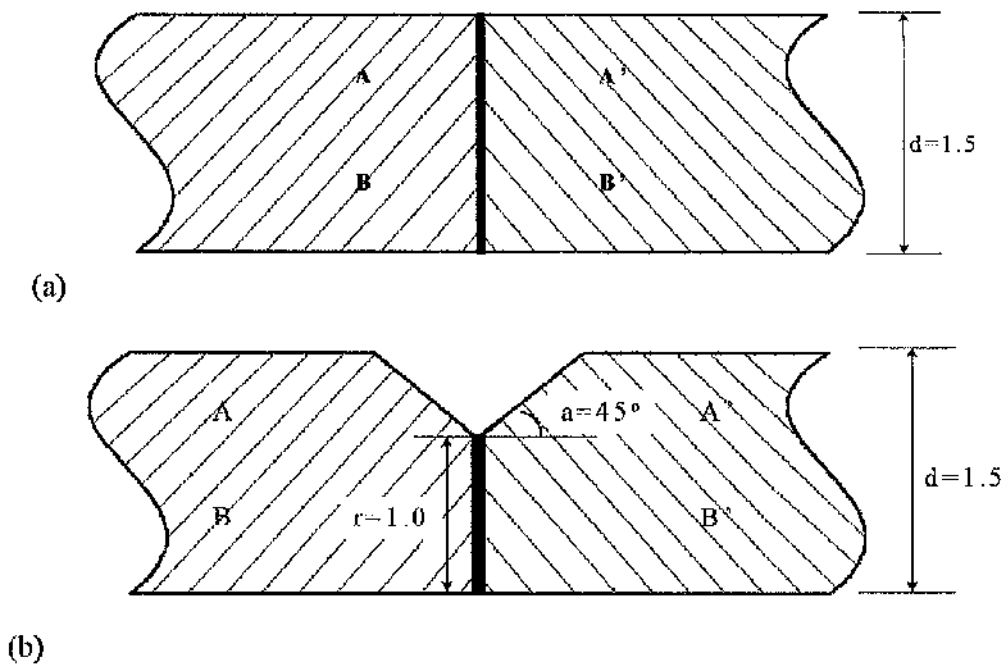


Figure 3.12. Beam profile and weld bead shape of (a) Graded Index fiber and (b) Stepped Index fiber

3.4. Experiment procedure

3.4.1 Preparing the specimens

Aluminum has been supplied from AALCO.UK.Ltd. With thickness of 1.5mm on specimens 5251-H24 and 6082-T6. All samples ((a), (b)) have been cut to a size of 45X80X1.5mm and (b) has been grooved by a milling machine in preparation for welding experiment with intermediate component. Selected filler metals were ER4043 and ER4047. Before the welding procedure, each specimen was cleaned using Methanol to prevent the oil, protein effect on the welding.



A = A': AA6082-T6 Aluminum B = B': AA5251-H24 alloy
 which represent LBW of similar material a: groove angle, r : root face

Figure 3.13 Preparation of welding specimens



Figure 3.14. A Schematic of welding intermediate component (Grooved butt joint)

Base \ Filler Metal	No filler metal	ER 4043	ER4047
AA6082-T6	A-1	A-2	A-3
AA5251-H24	B-1	B-2	B-3

Table 3.4. Preparation of welding specimens

In the experiment list, the symbol “A” and “B” indicates each of AA6082-T6, AA5251-H24 Aluminum Alloys and the numbers which follows the symbol is a specimen number at variance experiments. For instance, B-2 represents the base metal of 6082-T6¹⁾ Aluminum Alloy (ISO) welds with filler wire of ER4043²⁾. In order to compare the results, welding variables has fixed as $E=50\text{J}$ / $\text{PRF}=8\text{Hz}$ / $\tau=7\text{msec}$ / $V=2.9\text{mm/sec}$.

3.4.1.1 Welding procedure

Welding variables	Min. to Max. range (unit)
Pulse Energy (E)	5 ~ 50 (J)
Pulse Repetition Frequency (PRF)	1 ~ 100 (Hz)
Pulse Duration (τ)	1 ~ 20 (msec)
Welding Velocity (V)	2.9 ~ 5.8 (mm/sec)

Table 3.5. Welding variable ranges for the experiment

The welding variables, pulse power and welding overlap, have changed laser parameters and preparation of samples were same condition in A-1 and B-1, which mentioned in table 3.4. The acceptable parameters for welding with filler metals were; $E=50\text{J}$, $\text{PRF}=8\text{Hz}$, $\tau=7\text{msec}$ and $V=2.9\text{mm/sec}$, so that fixed laser parameters in all experiments for filler metal welding.

¹⁾ Internationally agreed four-digit system that changes with major alloy elements. 6082 is equivalent to the old British designation of H30, 5251 is equal to N4. Normally write “AA” for Aluminum Alloy T6,H24 are the alternative alloy temper system. T6(old British standard:TF) describes Solution Heat-treated and then artificially aged. H24(old British:H4) indicates Half hard.



Figure 3.15 Welding set up : fixture and welding Focusing head manipulated by the Scara type robot which control the welding speed

3.4.1.2 Etching solution

Welded samples has been mounted by epoxy or Bakelite [ref.42] and polished from #100 ~ 1500 to γ -Alumina ($d=0.5\mu\text{m}$). Polished samples has been cleaned by ultra sonic cleaner and etched.

Etching solution for the Aluminum Alloys have two choices which were Keller's etch [ref.42] and 10ml HF, 15ml HCl, 25ml HNO_3 , 50ml H_2O . The later etchant has been mentioned by L.A.Guitterez et al [ref.32]. In a comparison microstructure of the etching result on the welded Aluminum specimens, the structures etched with HF, HCl, HNO_3 and H_2O were observed to be clearer than the Keller's etch. Etching time was approximately 5minutes and 2 minutes.

²⁾ ER represents ElectRode and 4043 is the same system as ¹⁾ that 5% of Silicon added rode and 4047 added 12% of Silicon. The shape of filler metal was shown in 3.1.2.

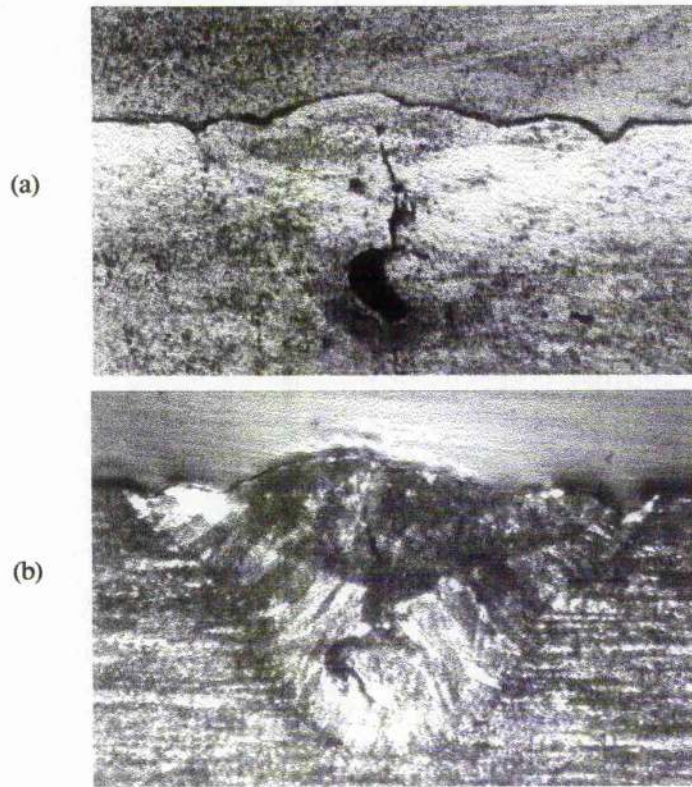


Figure 3.16 Comparing the microstructure of etching results.
(a) Keller's etch , (b) HF 10ml, HCl 15ml, HNO₃ 25ml, H₂O 50ml

3.4.2 Property test and their procedures

Material test on the welded Aluminum Alloy was performed to establish and compare the phenomena of selected additional Silicon effect on the intermediate component.

3.4.2.1. Macro / Microscopic inspections (non-destructive test)

Macro picture inspections

The geometry of the fusion zone and HAZ were found from macro pictures of welded samples. The image has been captured by the Optima software via a CCD camera through the microscope. Each of the welding geometry was saved as images and plotted to measure both the fusion size (the penetration depth and weld bead size) and to inspect the crack formation.

3.4.2.2. Microscopy

The optical microscope was used to observe and capture images of the microstructures (magnification: $\times 50$ and $\times 100$). The captured images are plotted in appendix i.2. The Scanning Electron Microscope has been used because of its large depth of focus.

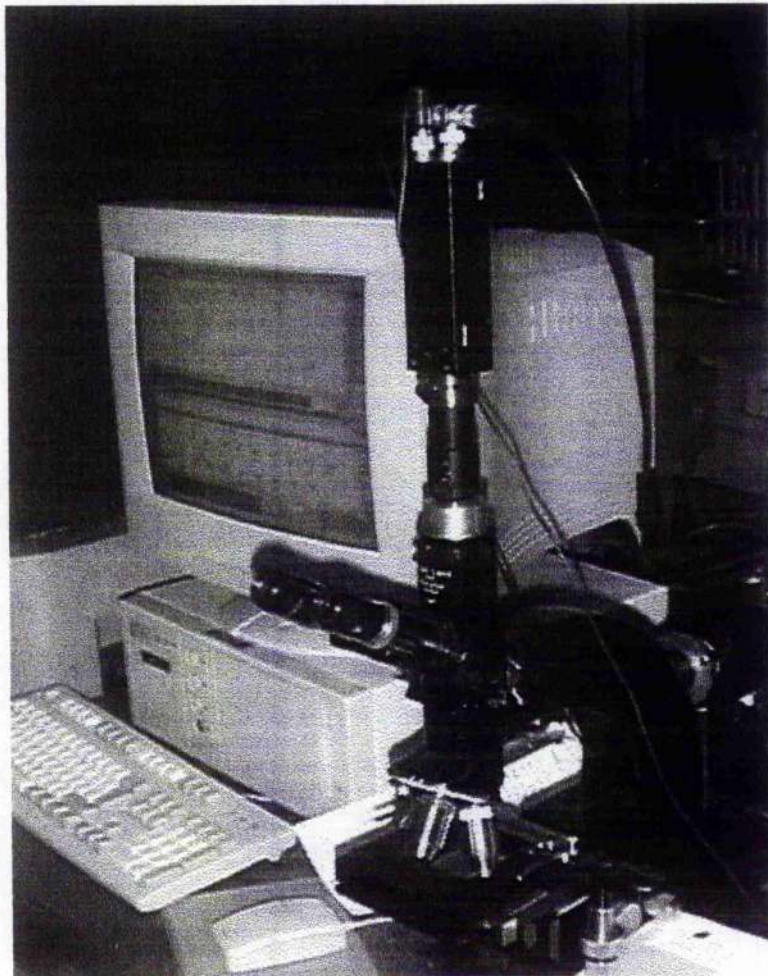


Figure 3.17. Optimas image processing system for the macro / microscopic observation

Optical microscope connect to the Pentium computer via CCD camera.

The magnification of use : $\times 5$ Macro inspection / $\times 50$, $\times 100$: Micro inspection

3.4.2.3. Tensile strength test (Destructive)

The evaluation of the maximum tensile load on the laser-welded Aluminum Alloys with or without filler metal determined the Ultimate Tensile Strength (UTS). The fully penetrated welding specimens were processed under the altered laser parameter (specimen size : 90X26X1.5) by a ND³⁺:YAG laser cutting machine with operating parameter of pulse energy of 33J at 11Hz frequency, pulse duration of 5msec, and polished by emery paper to reduce the stress concentration. Specimens were tested in the as-welded condition.

Samples welded with filler materials (ER4043 and ER4047) were processed to remove the welding beads and to identify the before-weld thickness of 1.5mm. Specimen size was 90 X 25 X 1.5.

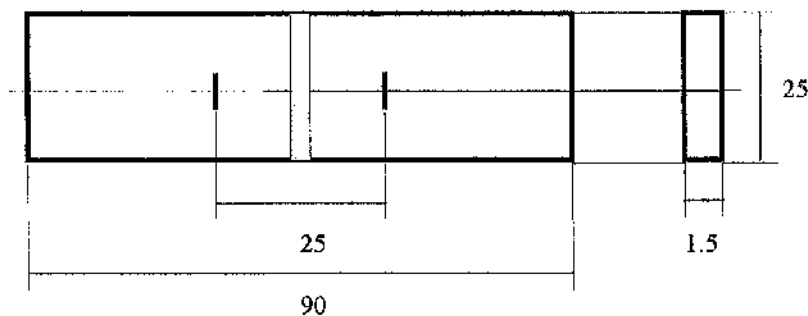


Figure 3.18 Size of the Tensile test specimen

The equation for the tensile test is [ref.22] ;

$$\sigma_t = \frac{F_{\max}}{A_o} \text{ kN/mm}^2(\text{MN/m}^2)$$

where, F_{\max} = maximum tensile load (kN)

A_o = original cross-sectional area (mm)

The average tensile strength for base metal samples of 6082-T6 were $\sigma_t = 210 \text{ MN/m}^2$ and for samples 5251-H24 were $\sigma_t = 297.6 \text{ MN/m}^2$. The tensile strength profiles are shown in figure 3.19 and 3.20, where U is the maximum tensile load used and F the point of failure.

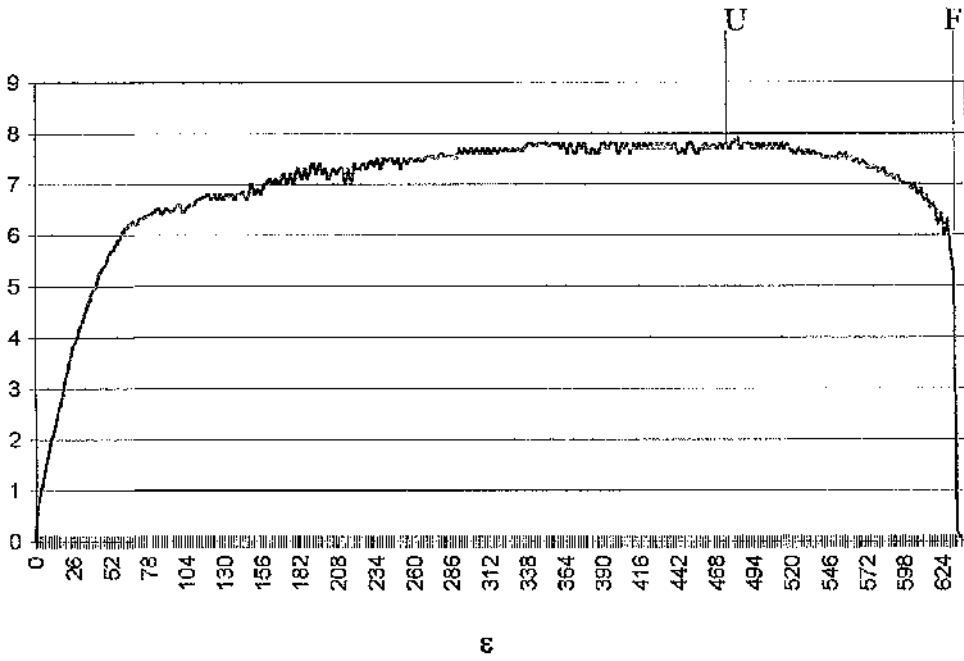


Figure 3.19. Tensile strength test history of solid 6082-T6 Aluminum Alloy ($Y = F$ (kN))

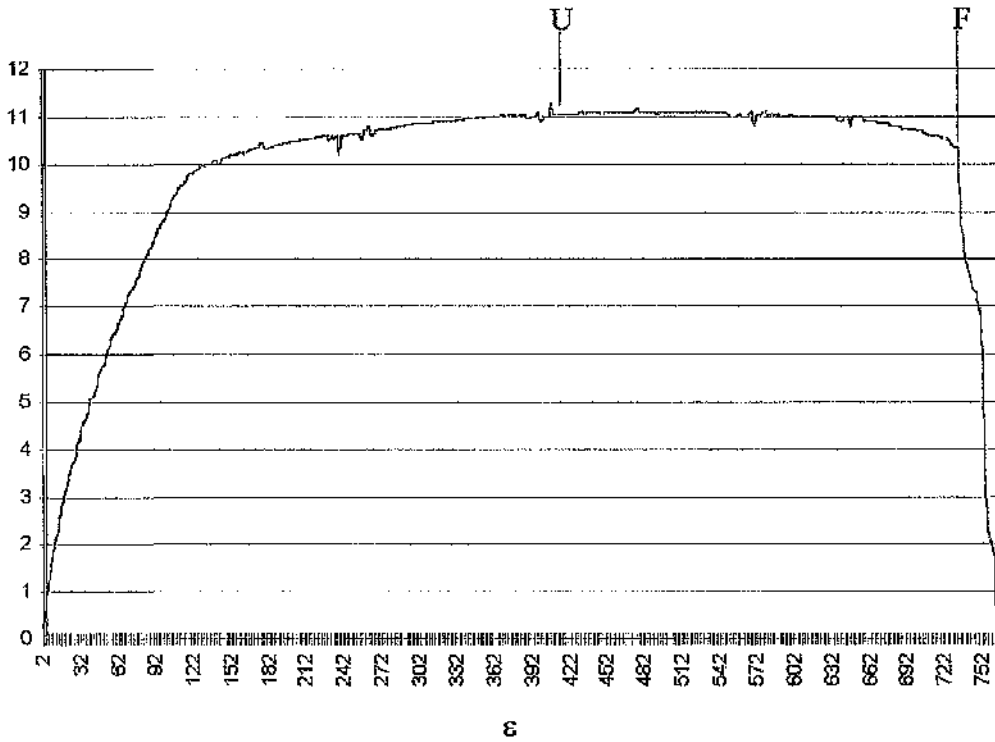


Figure 3.20 Tensile strength test history of solid 5251-H24 Aluminum Alloy ($Y = F$ (kN))

3.4.2.4. Micro hardness test

Hardness profile testing on the welding geometry of both the 6082-T6 and 5251-H24 Aluminum Alloys to determine the size of the Heat Affected Zone and the changing hardness profiles. After the weight and length calibrations, the test length was 3mm from the fusion center to base metal with an indentation interval of 200 μ m along the weld geometry [ref.22].

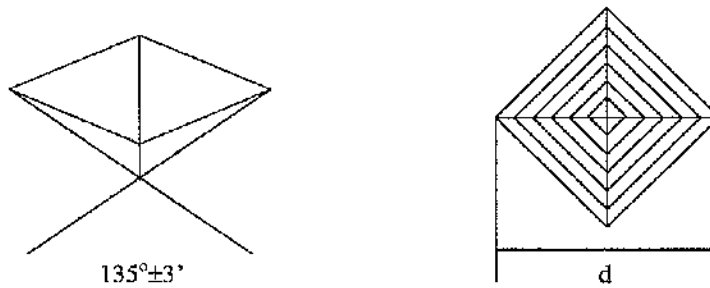


Figure 3.21 Diamond shape on the hardness test machine and size measuring

Substantial equation for the Vickers hardness test is

$$H_d = \frac{F}{S} = \frac{2F \sin \theta}{d^2} = 1854.4 \frac{P}{d^2} \quad (\text{kgf/mm}^2)$$

where, $P = 0.1 \text{ kgf}$

The hardness profiles across the fusion zone were measured on identifying the welding conditions of the test specimens with 400W of laser power and a welding translation speed of 2.9 mm/sec. 30 indentations on each specimen were performed at 100 μ m intervals over 6mm of the distance. The Vicker's microhardness, $H_{d0.1}$, profiles are shown in Chapter 4.

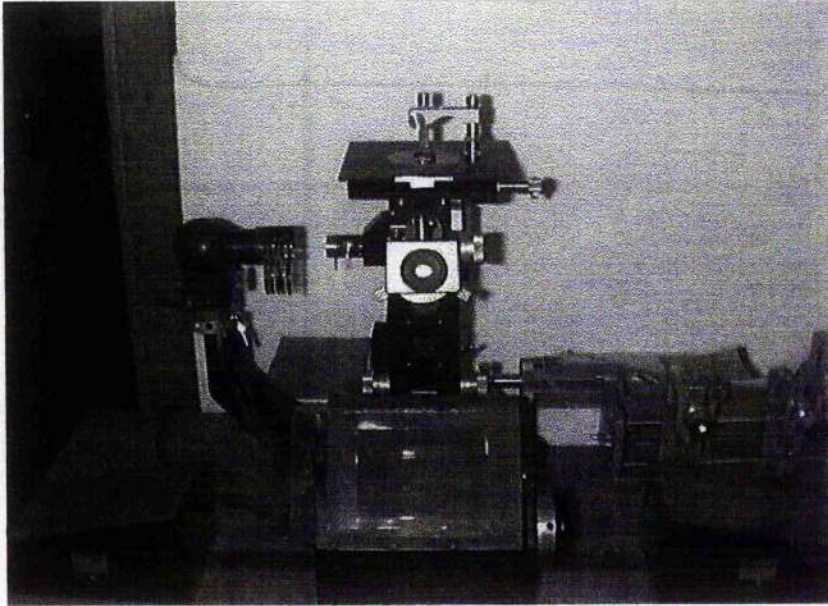


Figure 3.22 Vicker's micro hardness test machine

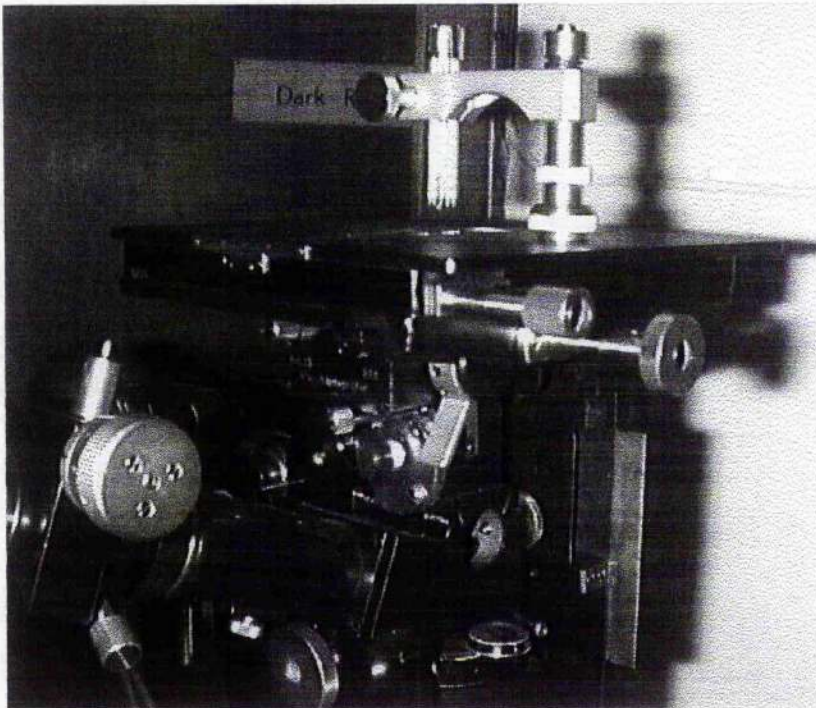


Figure 3.23 Close picture of Test flat form

3.4.2.5. Scanning Electron microscopy and Electro Probe Micro Analysis(EPMA)

The quantitative investigation through a Scanning Electro Microscope has been done in both the microscopic and chemical analyses.

(1) Microscopy

The wavelength of visible light is difficult to resolve an object of a smaller size than about $1\mu\text{m}$, with magnification in excess of $\times 2000$, from the optical microscope [ref.22]. In an electron microscope, a beam of electrons is produced by an electron gun of magnetic lens. The electrons pass through an evacuated tube and is focused on to the specimen. The scattered electron beams are then picked up by a collector and modulated in the cathode ray tube, which produces a picture of the surface area.

(2) Electron Probe Micro Analysis(EPMA)

A fine electron beam is directed at a specific area of the specimen. An X-ray emission which follows the excitation is characteristic of the chemical element, when a material is excited in the scanned area. From the analysis of the emission, spot areas of the chemical composition can be obtained both qualitatively and quantitatively [ref.16].

The facility used in this experiment was Leo Electron Microscope (Stereo Scan 360) with integrated with AN10855 energy dispersive x-ray micro analyzer. Specimens are carbon-coated in a vacuum condition two days before the experiment for both microscopy and EPMA.

Chapter 4. Analysis of Experiments

4.1. Introduction

Though the generation of a fused zone depends upon complex interactions of the contributing physical process, the thresholds at which these various processes can be determined by the power intensity in the irradiated spot. Two modes of welding are observed: Intensities in the region of 10^9W/m^2 are insufficient to generate vapor to a significant degree and the fusion region, being not greatly disturbed, grows by conduction in the solid and the liquid. Significant vapor generation ensues at 10^{11}W/m^2 and the liquid phase is unstable; convection is the dominant mode of heat transfer and the fusion zone penetrates the weld joint effectively.

The first of these is described as being the conduction limited mode weld. The weld takes the form of a hemispherical bowl, its width being greater than its penetration and the surface disturbance is small. There is a wide heat affected zone in the solid phase and the evidence of fast, but not rapid, quenching in the metallurgical structure of the fused zone. In contrast, the non-conduction limited mode weld has a penetration depth which characteristically exceeds the weld width sometimes by five to ten times, depending upon the physical properties of the weld metal. The heat affected zone is narrow, whilst the fused material exhibits very small grains ordered along column, being the evidence of very rapid quenching. A poorly controlled weld will have suffered loss of material from its upper surface. In aluminum alloys, particularly, super-solidus cracking is prevalent with the last freezing alloy being susceptible to failure in tension. The ranges of experiments include both of these regimes of welding.

Cracking on the central plane of the weld upon solidification of the last to freeze alloy is the major defect occurring in pulsed laser welding of alloys. In the experimental work the susceptibility to cracking of two alloys were mapped by systematic variation of the parameters characterizing the laser pulse. The amelioration of weld defects by the inclusion of a high alloy filler wire was examined following the same experimental scheme.

4.2. Relationship of Laser Parameter Control to the Fusion Size

4.2.1. Relationship of Power Intensity to the Fusion Size

4.2.1.1. Fusion size varying with pulse energies

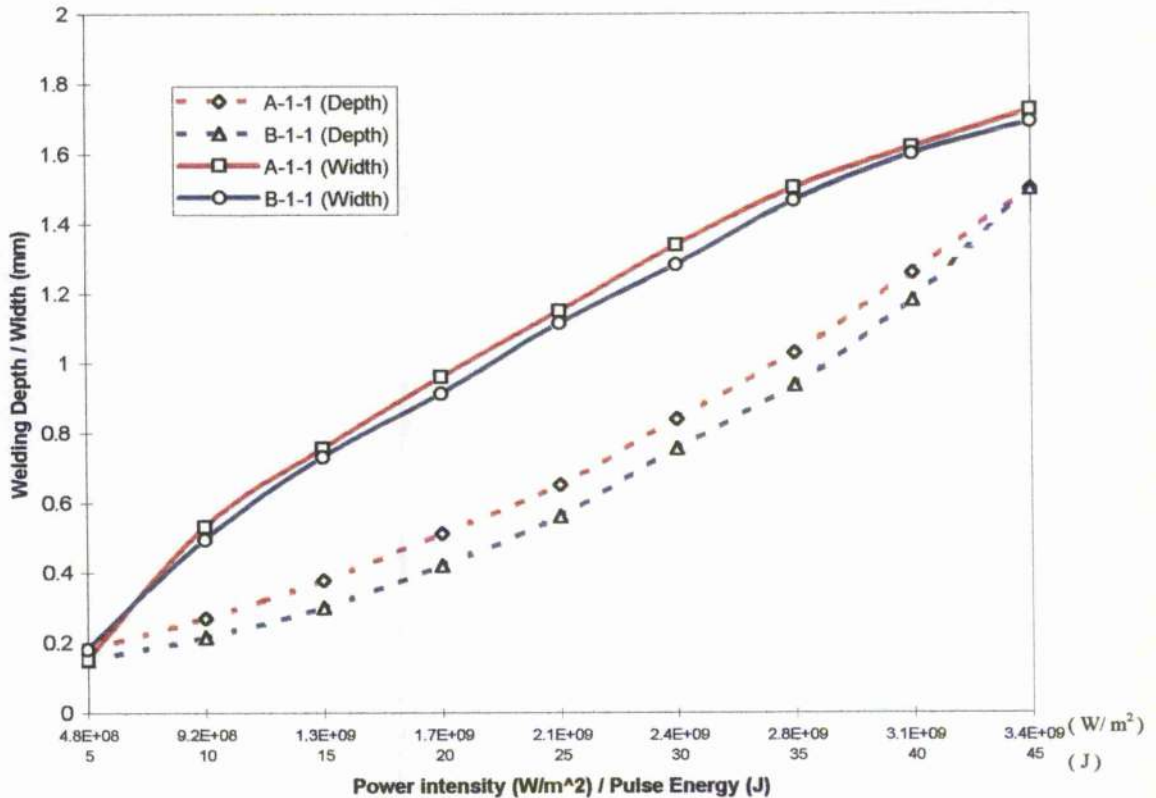


Figure 4.1 Fusion size alterations from the pulse energy¹⁾

PRF, Pulse duration (τ) and Welding velocity (V) was constant (PRF=8Hz / τ =7msec / V =2.9mm/sec)

Figure 4.1 shows the exact relationship between pulse energy and fusion size that welding depth and the weld bead size were directly proportional to the pulse energy. Power intensity varied from 5×10^8 to 3.5×10^9 W/m² and welding depth has altered from 0.2 to 1.7 which 8.5 times increased. Figure 4.2 shows that the fusion size changes from laser power intensity. First specimens were fusion sizes in the transverse section and top view of low power intensity irradiated material, second sample are the high

¹⁾ A and B in the graph indicate AA6082-T6 and AA5251-H24 alloys. Experiment list refer to appendix i.1. table 1. Experiment lists of the fusion size variation with Pulse Energy (A-1-1 and B-1-1). Microstructure refer to the Appendix i.2 Image Libraries.

power intensity irradiated material of same cutting position with ten times increased the pulse energy. From these pictures, pulse energy was found that the most important factor to decide the fusion sizes and related welding default. When increased the pulse energy, the crack tendency has increased in the centre of fusion. There was no substantial differences of size changing have found in 6082-T6 (A) and 5251-H24 (B) alloys.

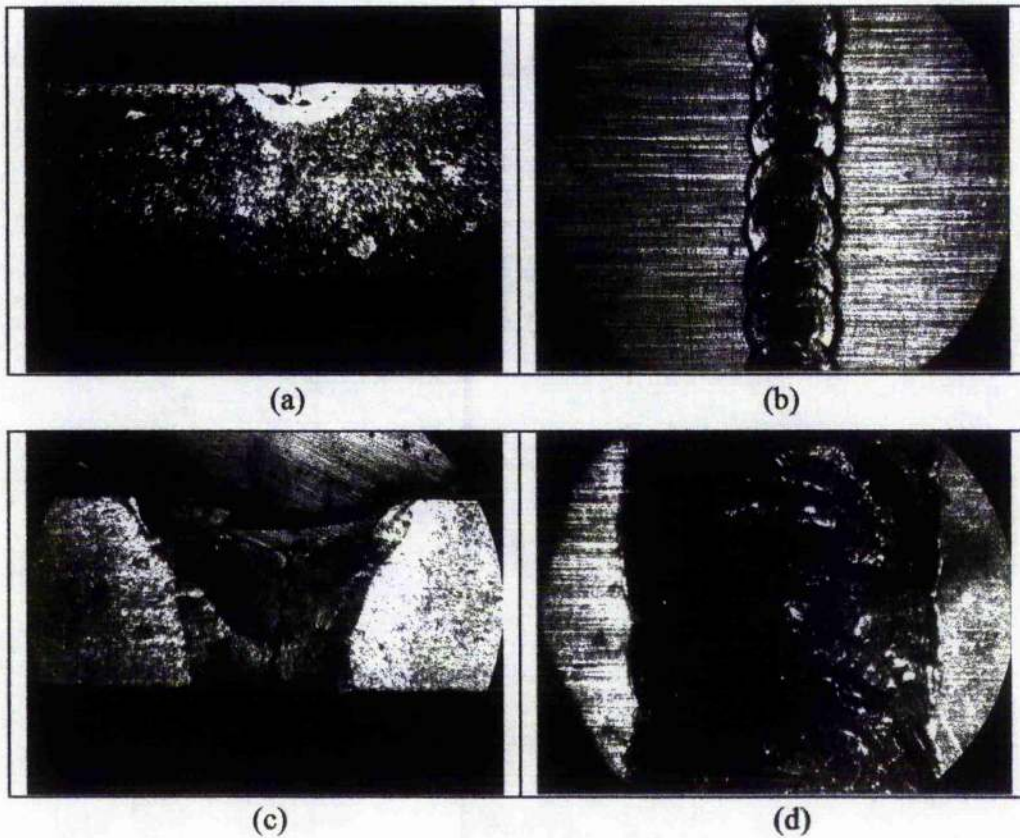


Figure 4.2. Welding result: macro pictures of altered pulse energies. (a),(b): $E=10J$, (c),(d): $E=45J$. Other constant welding variables: $PRF=8Hz/\tau=7msec/V=2.9mm/sec$. Additional macro pictures see in Appendix.i.1, A-1-1, B-1-1. (a),(b): Welding depth / Width = 0.24 / 0.525 mm , (c),(d) = 1.5 / 1.65 mm

4.2.1.2. Fusion size varying with pulse duration (Pulse width)

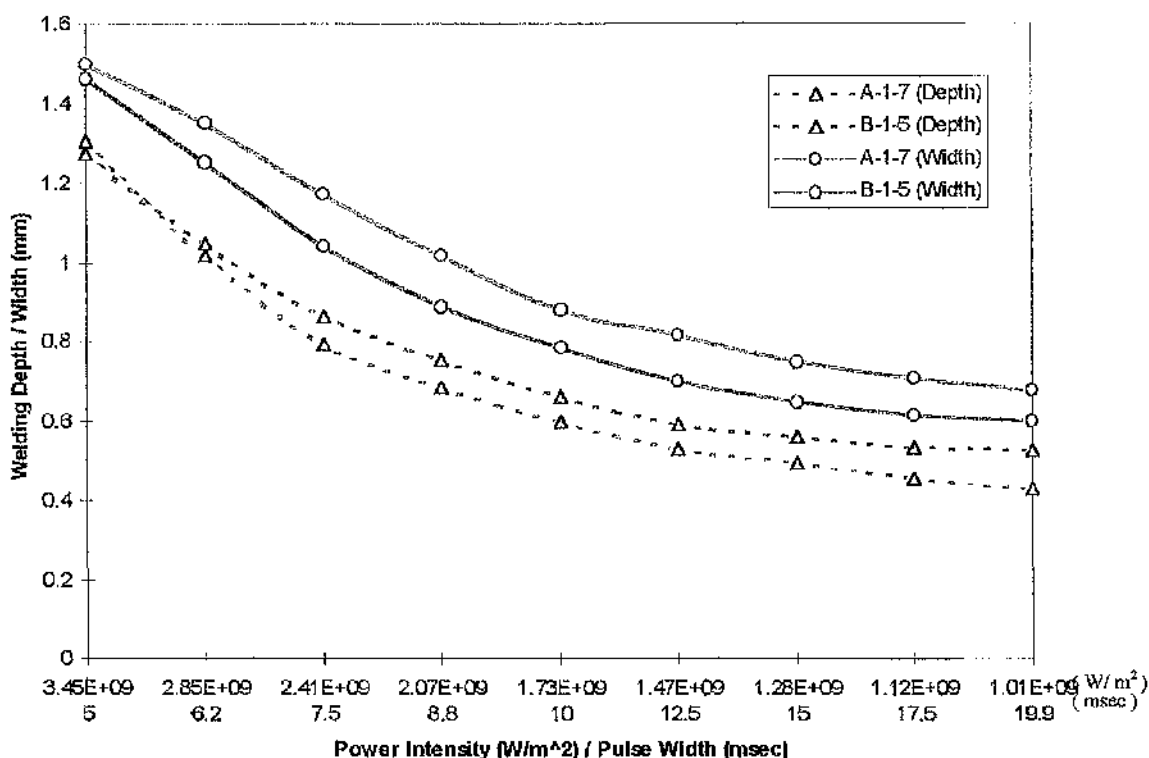


Figure 4.3. The weld fusion sizes variation with pulse duration changes.¹⁾

Pulse energy (E), PRF and Welding velocity (V) was constant ($E=30\text{J}$ / $\text{PRF}=8\text{Hz}$ / $V=2.9\text{mm/sec}$)

Size of focal spot (d) measurement for the power intensity calculation: constantly increased from 1.5 to 1.74mm

As shown in the figure 4.3, experiment have clearly explained that size of fusion had big differences in pulse duration alterations. The surface condition which the different oxide film layer from the strengthening process might be caused slightly different result of fusion sizes in a comparison of 6082-T6 (A) and 5251-H24 (B) alloys. The fusion size has decreased as increase the pulse duration, which related reverse proportion as can see in figure 4.4.

¹⁾ A and B in the graph indicate AA6082-T6 and AA5251-H24 alloys. Experiment list refer to table 2 in Appendix i.1. Experiment lists of the fusion size variation with Pulse Energy (A-1-5 and B-1-5). Microstructures refer to the Appendix i.2 Image Libraries. Size of irradiated spot refers to chapter 3. Size reading of laser single spot in altered pulse duration (Table 3.3).

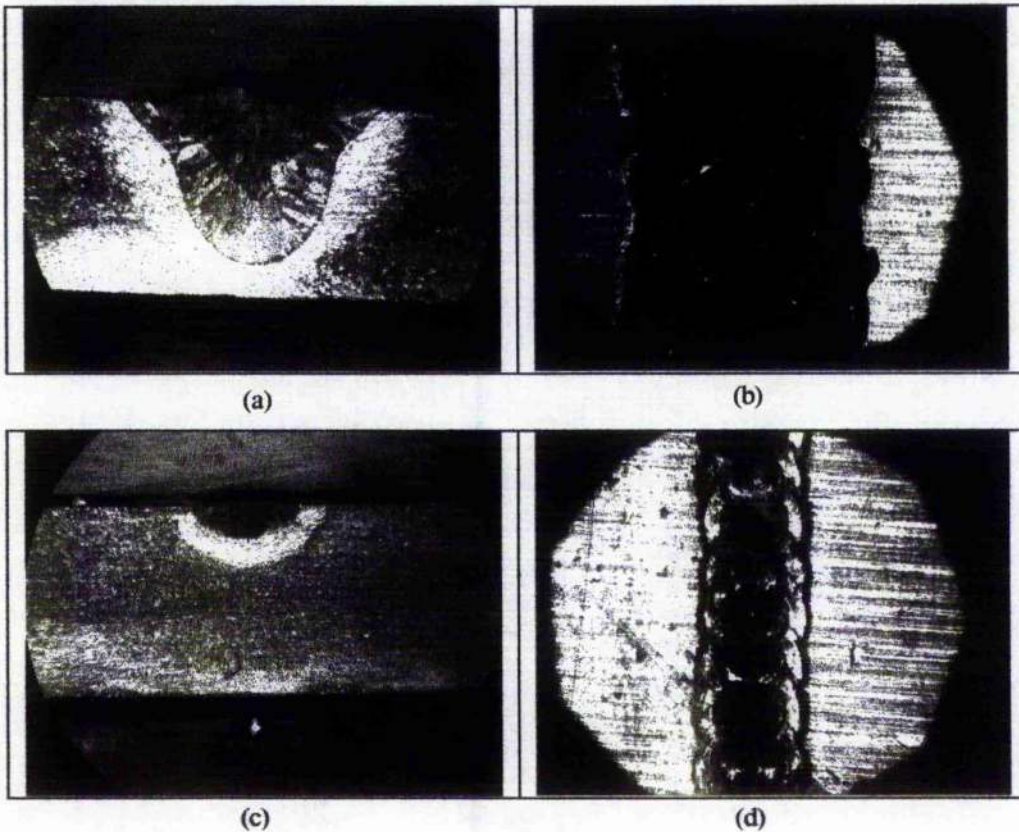


Figure 4.4. Welding result: macro pictures in transverse section (welding depth) and top view(welding width) of altered pulse duration times. (a),(b): $\tau=5\text{msec}$, (c),(d): $\tau=19.9\text{msec}$. Other constant welding variables: $E=30\text{J/ PRF}8\text{Hz/ V}=2.9\text{mm/sec}$. Additional macro pictures see in Appendix.i.1, A-1-7,B-1-5. (a),(b): Welding depth / Width = 1.275 / 1.35 mm , (c),(d) = 0.525 / 0.6 mm

Pulse duration effect in terms of welding result can be explained by three cases, firstly, from the power differences in the pulsed Nd^{3+} : YAG laser, which decrease the power intensity as increasing the pulse duration, secondly, that is also the specific material thermal property, for instance, steel requires longer pulse duration, while aluminum needs shorter pulse width to increase the melting efficiency [ref.2]. For a given pulse energy, there is a pulse duration at which the depth of the molten pool is the largest for shorter pulse duration. The increased power intensity can cause instabilities in the fused material and for longer duration the pulse power density is insufficient to cause penetration.

4.2.2. Relationship of weld overlap to the fusion size

4.2.2.1. Fusion size varying with Pulse Repetition Frequency (P.R.F.)

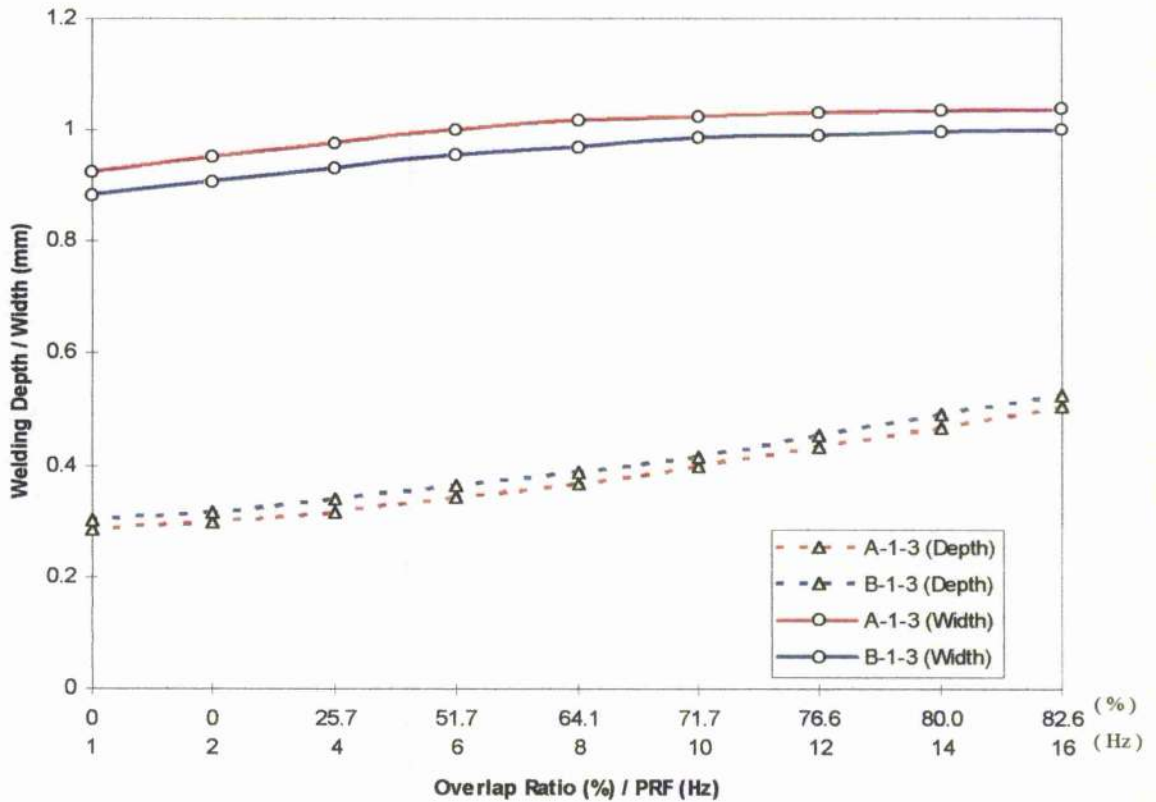


Figure 4.5. Frequency (PRF) alteration to the fusion size¹⁾

The constant variables: $E=25\text{J} / \tau=7\text{msec}$ ($I = 3.93 \times 10^8 \text{W/m}^2$) / $V=2.9\text{mm/sec}$

From the constant pulse power and welding velocity, Frequency did not effected dramatically to the fusion size. Welding depth of single pulse (1Hz) was about 0.25mm and 16Hz was approximately 0.5mm observed, which about 2 times of a penetration depth increase in all range of experiment.

¹⁾ X axis is overlap ratio calculated from PRF alteration with the welding width. Frequencies and the width values refer to table 3. in chapter 3.2. Pulse power=3571.4W and spot size $d=1.7\text{mm}$. Power intensity was constant as $3.93 \times 10^8 \text{ (W/m}^2)$. "A" and "B" indicate the AA6082-T6 and 5251-H24 and A-1-3 and B-1-3 refer to experiment lists in the table 3. Micro structure refer to appendix i.2.

The frequency was the most important operating parameter to change the overlap ratio which may reduce the mechanical property by the Magnesium evaporation in Aluminum Alloys with welding speed or the factor can change the welding discontinuity.

4.2.2.2. Fusion size varying with welding velocities

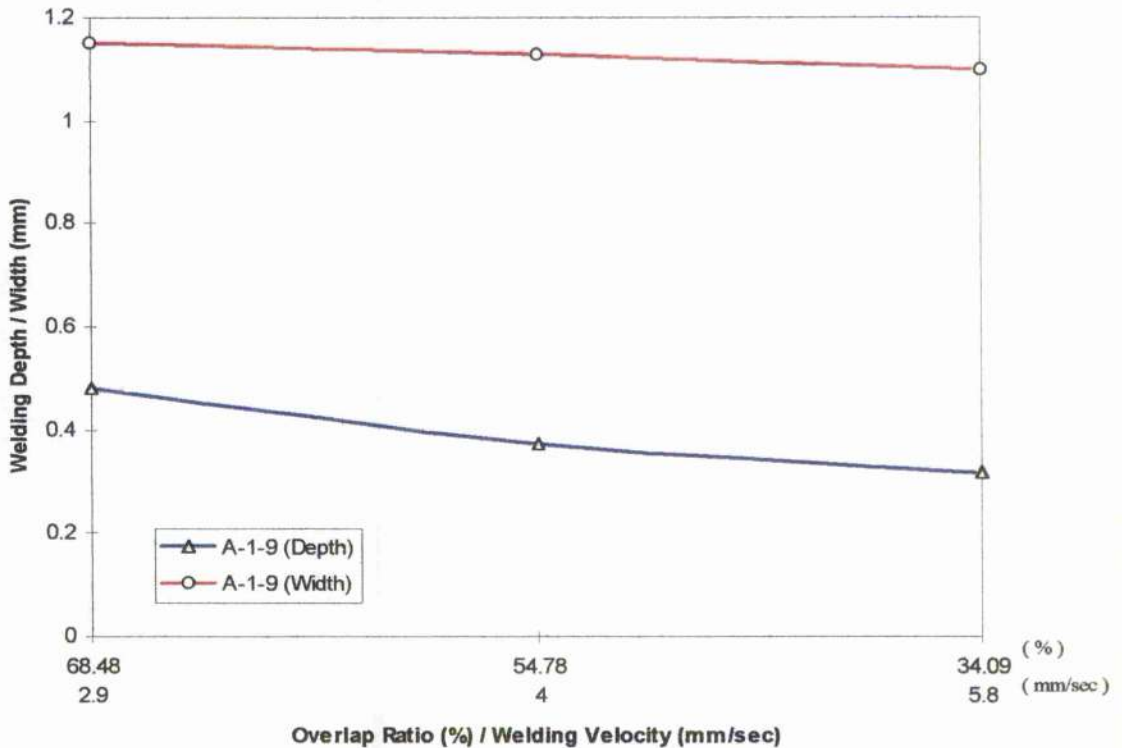


Figure 4.6. Fusion size varying with welding velocities : 2.9mm/sec,4.0mm/sec,5.8mm/sec¹⁾.

The constants: $E=25J$ / $\tau=7msec$ ($I=2.23 \times 10^9 W/m^2$) / PRF=8Hz / spot diameter (d)=1.6mm

Welding velocity alteration in the frequency range of 8Hz did not have big differences in the size of fusion, which slightly decreased when increased the velocities. The result was nearly same as P.R.F. alterations that overlapping ratio was decreased when increase the welding velocity. These were the typical operating process differences between continuous laser and pulse laser that fusion size did not increased because of rapid cooling during pulse off period.

Overlapping ratio was approximately 68% on 2.9mm/sec, 54% on 4.0mm/sec, 34% on 5.8mm/sec have found. Overlap ratio was decreased when increase the velocity.

Welding overlap was not highly related to the changing of fusion size, because of, again, the characteristic of pulse laser operation and competitively high thermal properties of aluminum alloys²⁾. Figure 4.7 Shows that the overlap ratio changes in different Frequencies and welding velocities in a longitudinal section view.

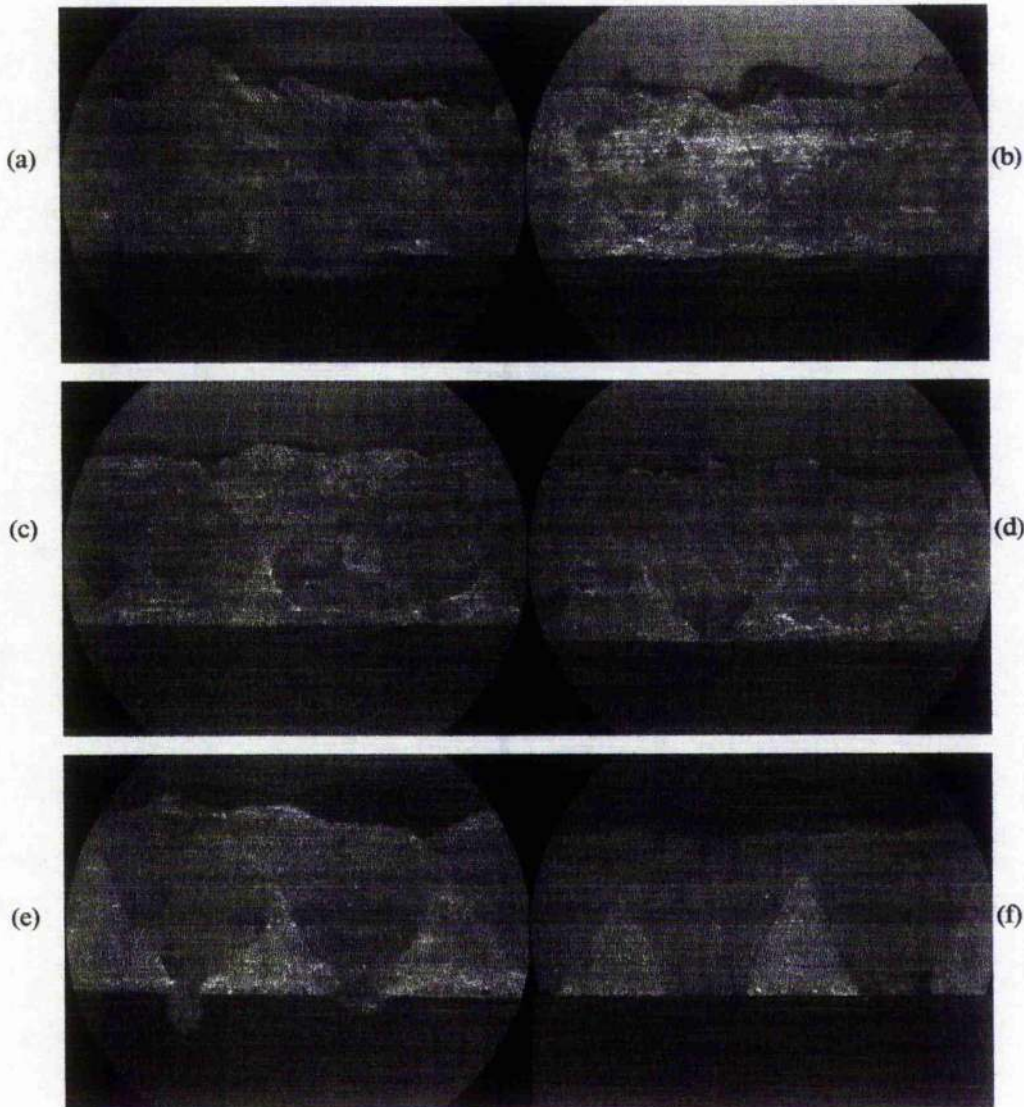


Figure 4.7. Overlapping ratio varied with PRF and welding velocity (welding longitudinal section: fusion centre $\pm 50\mu\text{m}$). (a) 87.5%, (b) 68.3%, (c) 50.5%, (d) 42.7%, (e) 33.3%, (f) 18.2%.

¹⁾ A-1-9-1 refer to the experiment list in chapter 3, table 4. Pulse power = 3571.4W, $d=1.6\text{mm}$ (constant) so that power intensity was constant ($I=2.23\times 10^9\text{W/m}^2$) Microstructures refer to the Appendix i.1. Image Library

4.2.3. Surface Treatment

A set of experiment has carried out in order to investigate the reduction of reflectivity on the surface. Mechanical treatment, surface had roughened by emery paper #400 before the welding process.

4.3.4.1. Pulse energy

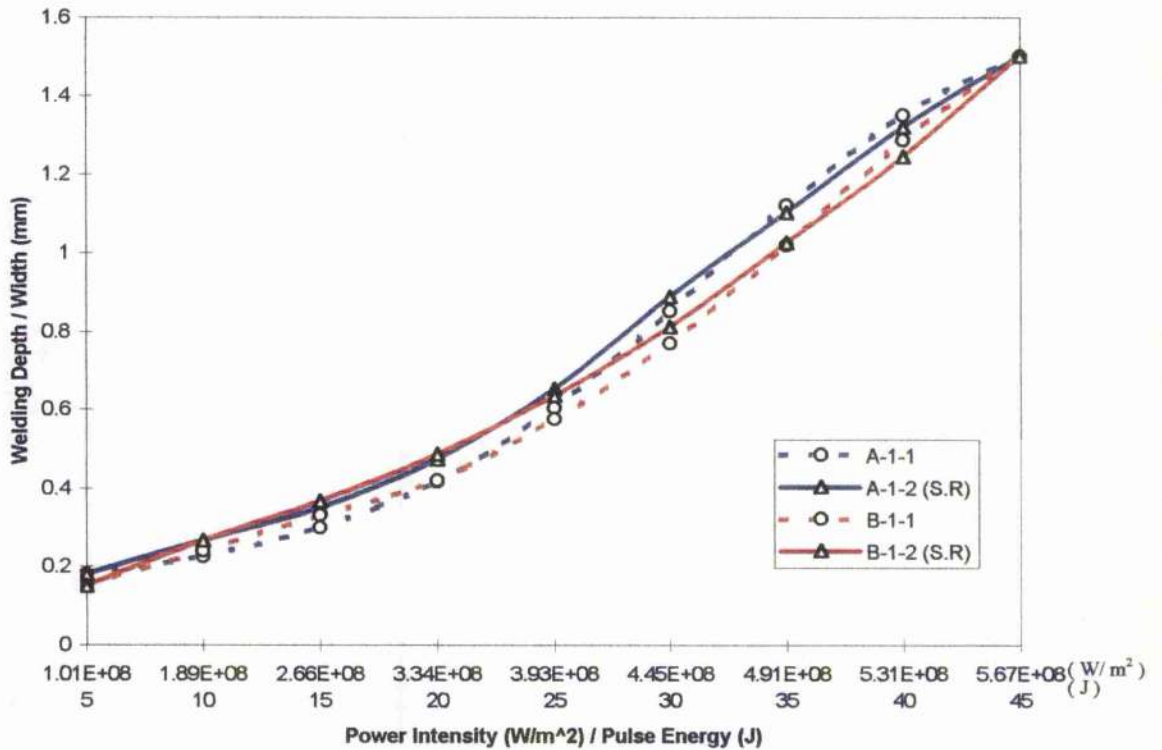


Figure 4.8. Surface Roughness effect of pulse Energy alteration to Welding Depth

²⁾ Chapter 2.1.3, (4) Rapid quenching.

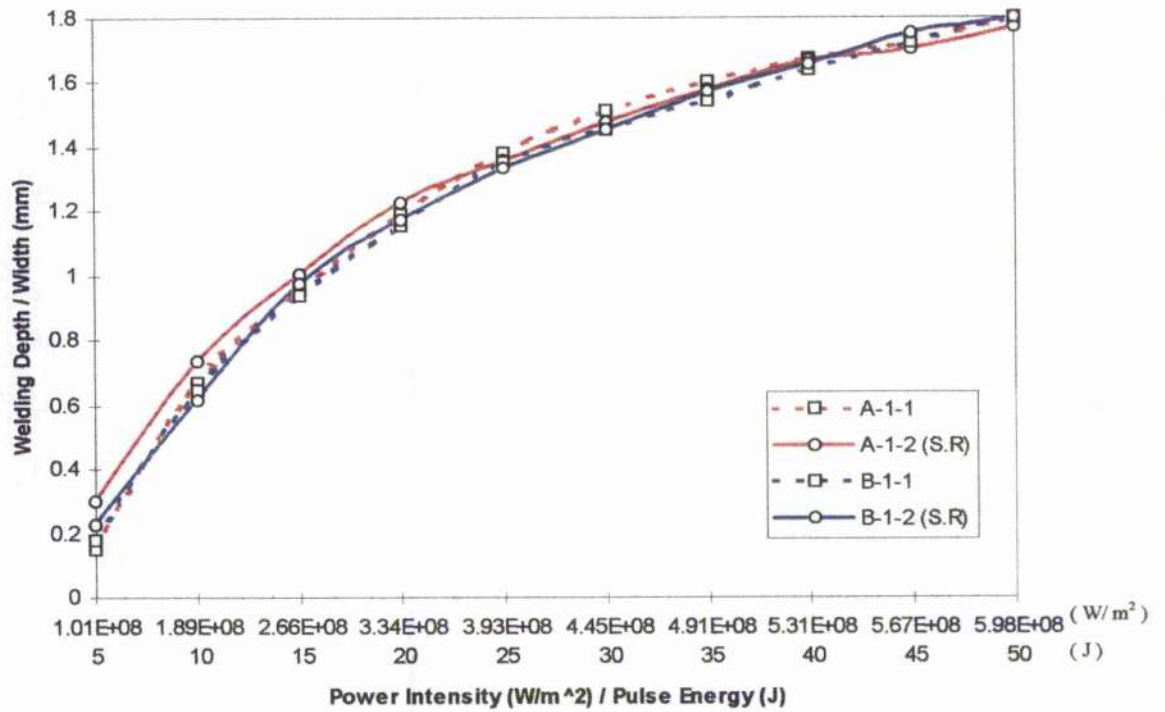


Figure 4.9. Surface Roughness effect of pulse energy alteration to welding width¹⁾.

4.3.4.2. Surface roughness effect varying with Pulse duration

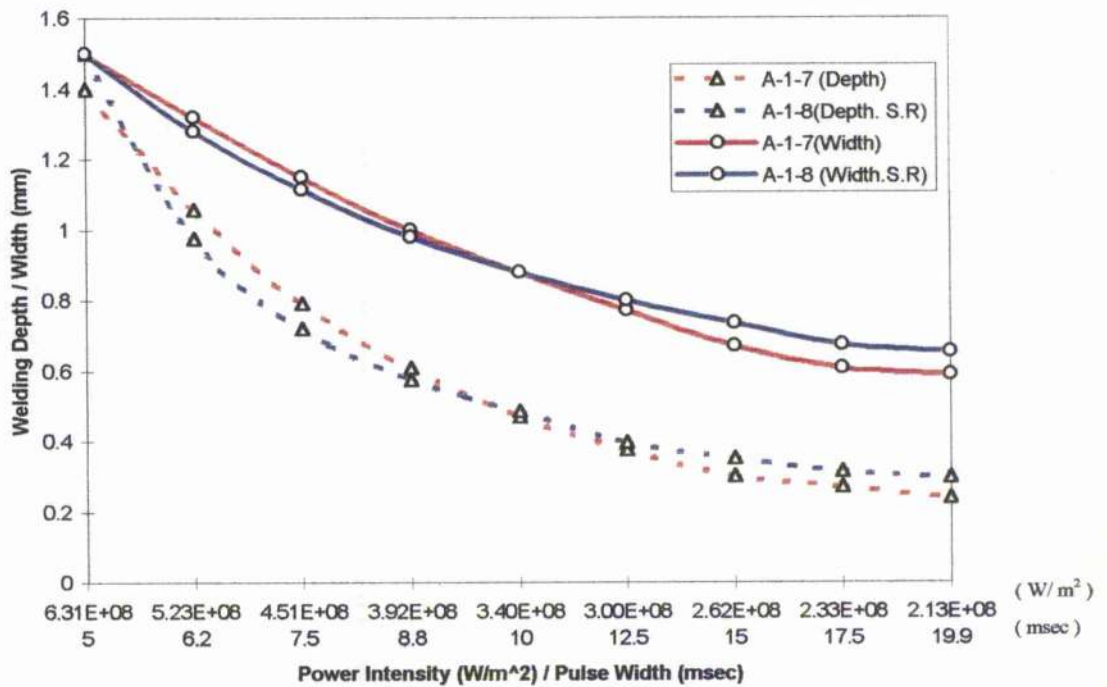


Figure 4.10. Surface roughness effect on different Pulse Duration to the fusion size

¹⁾ Surfaces have roughened by the emery paper (#400). A,B indicate 6082-T6,5251-H24. A1,B1 and A2,B2 refer to the experiment list A-1-1 and A-1-2 in the table 1 and 6.

As shown in the results of the welding depth and width, there were little welding depth has increased on 6082-T6 alloy in low power intensity, because of removing the surface oxide coating, which may come from the T6 heat treatment. In high intensity welding, however, there were no substantial differences found in all range of experiments.

At low power intensities, the surface stays and does not get evaporated. While, in high intensity welding, the reflectivity on the surface disappears, because of oxide film layer get evaporated and it produces a plasma block which interrupt the material processing as well as laser beam absorbed into it. When material is in the interaction with the laser, energy transfer to the target material rapidly and the plasma blows away from the shielding gas during pulse-off period. In this phenomena, surface reflectivity is less important, therefore, welding depths and width are more rely upon the material thermal property than the surface reflectivity in, high intensity, deep penetration welding.

4.3. Prevention of Cracking in the fusion zone

4.3.1. Addition of a Filler Wire

As mentioned in chapter 2.5, another way of experiment to remove a weld crack has carried out with filler metal which added Si were used. The result has compared both qualitative and quantitative measurements from the existences of filler metals. The preparations of samples were plotted in table 3.3 (Chapter 3.4).

4.3.2. Results of Chemical Analysis

Results of Electron Probe Micro Analysis (EPMA) from Scanning Electro Microscope (SEM) on 6082-T6 and 5251-H24 alloys are shown with occurrences of filler metal. Samples of operating parameter were identified as $E = 50J / PRF = 8Hz / \tau = 7msec / V = 2.9 mm/sec$. The distributions of chemical analysis have been selected in 11 areas under the SEM spot mode detection on the welding geometry of 6082-T6 and 5251-H24 alloys. Seven different locations on the fusion have been examined and plotted on the graphs.

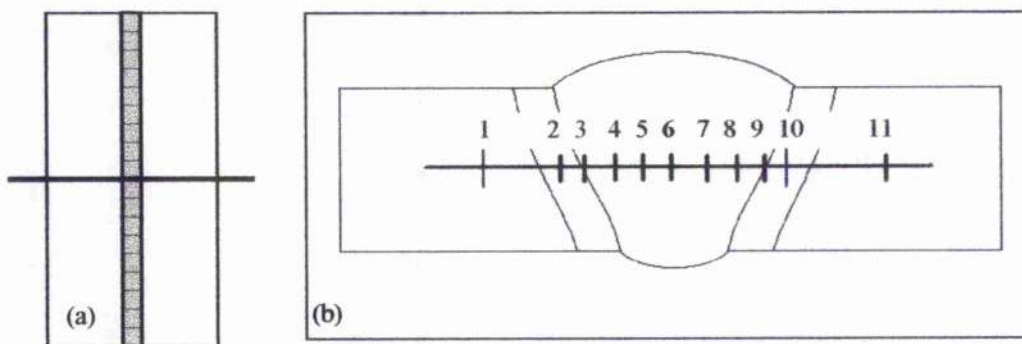


Figure 4.11 Chemical Analysis distributions on the welding geometry
(a) top view of weld sample cutting area, (b) welding cross section and detection areas

A - 1

Area	Fe	Cr	Mn	Cu	Mg	Si	Al
1	0.351	0.015	0.322	0.02	0.961	0.736	97.595
2	0.538	0.025	0.396	0	0.923	0.701	98.051
4	0.653	0.02	0.4	0.04	0.073	0.701	98.113
6	0.549	0.011	0.423	0.045	0	1.003	97.869
8	0.605	0.02	0.4	0.04	0.097	0.701	98.137
10	0.529	0.025	0.449	0	0.906	0.653	97.965
11	0.232	0.015	0.322	0.02	0.961	0.736	97.714

Table 4.9. EPMA result of 6082-T6 alloy without filler metal (A-1 in table 3.2).
Area 6 represents the fusion centre.

B - 1

Area	Fe	Cr	Mn	Cu	Mg	Si	Al
1	0.351	0.015	0.322	0.02	1.268	0.613	97.595
2	0.44	0.025	0.396	0	1.216	0.699	98.051
4	0.382	0.051	0.44	0.071	0.177	0.714	98.113
6	0.37	0.011	0.423	0.098	0.032	0.944	97.869
8	0.382	0.02	0.4	0.064	0.269	0.726	98.137
10	0.369	0.051	0.391	0	1.094	0.7	97.965
11	0.232	0.015	0.322	0.02	1.171	0.58	97.714

Table 4.10. EPMA result of 5251-H24 alloy without filler metal (B-1 in table 3.2).

A - 2

Area	Fe	Cr	Mn	Cu	Mg	Si	Al
1	0.56	0.01	0.32	0.02	0.75	1.25	96.98
2	0.57	0.05	0.39	0.03	0.74	1.2	97.47
4	0.5	0.04	0.34	0	0.67	1.82	97.24
5	0.52	0.07	0.42	0.04	0.56	3.09	96.13
6	0.5	0.05	0.46	0.08	0.26	3.86	95.05
7	0.54	0.05	0.4	0.01	0.59	2.49	96.86
8	0.56	0.04	0.35	0	0.83	1.86	96.25
10	0.54	0.04	0.3	0.03	0.71	1.16	97.21
11	0.63	0.01	0.32	0.06	0.8	1.04	97.7

Table 4.11 EPMA result of 6082-T6 alloy with ER4043 filler metal (A-2 in table 3.2).

B - 2

Area	Fe	Cr	Mn	Cu	Mg	Si	Al
1	0.07	0.02	0	0.07	1.13	0.78	91.82
2	0.23	0.06	0	0.03	1.2	1	95.39
4	0.33	0.03	0.07	0.08	1.11	3.8	92.52
5	0.08	0.03	0	0.06	0.89	6.48	94.39
6	0.25	0.04	0	0.09	0.44	7.07	89.29
7	0.26	0.04	0	0.1	0.44	5.89	92.66
8	0.35	0.05	0	0	1	3.45	92.74
10	0.01	0.08	0	0.01	1.14	0.95	96.67
11	0.05	0	0.06	0	1	0.85	97.56

Table 4.12. EPMA result of 5251-H24 alloy with ER4043 filler metal (A-1 in table 3.2).

A - 3

Area	Fe	Cr	Mn	Cu	Si	Mg	Al
1	0.04	0.05	0	0.03	1.18	1.31	97.28
2	0.02	0	0	0.03	1.64	1.33	97.45
4	0.18	0.02	0	0	7.6	0.55	90.95
5	0.23	0.04	0	0	10.21	0.25	88.77
6	0.34	0.05	0.04	0.04	10.61	0.38	88.31
7	0.14	0.05	0.04	0.05	9.6	0.3	94.28
8	0.29	0.01	0.04	0.01	7.11	0.83	91.3
10	0.01	0.03	0.04	0.04	1.44	0.95	91.89
11	0.1	0.01	0.04	0.06	1.04	0.91	97.7

Table 4.13 EPMA result of 6082-T6 alloy with ER4047 filler metal (A-3 in table 3.2).

B - 3

Area	Fe	Cr	Mn	Cu	Si	Mg	Al
1	0.05	0	0.06	0	1.33	1.45	97.56
2	0.02	0.06	0	0.05	1.54	1.25	97.85
4	0.17	0.03	0	0.01	11	0.73	87.68
5	0.2	0	0.02	0.02	12.44	0.66	86.79
6	0.22	0	0	0	12.63	0.4	87.79
7	0.17	0	0	0.01	11.86	0.73	89.01
8	0.25	0.01	0.03	0.05	8.8	1.12	92.28
10	0.25	0.02	0.01	0.04	1.81	1.39	89.5
11	0.01	0.04	0	0.03	1.03	1.2	87.87

Table 4.14. EPMA result of 6082-T6 alloy with ER4047 filler metal (B-3 in table 3.2).

4.3.2.1. Conventional square butt joint without filler metals

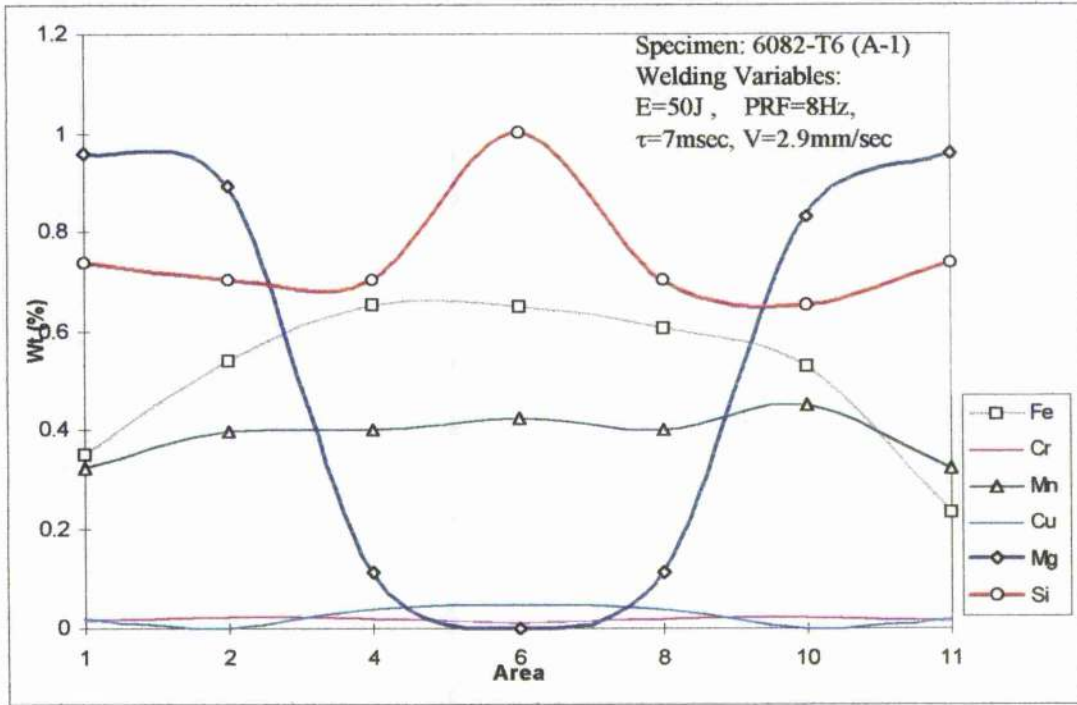


Figure 4.12 EPMA result of the welding sample (A-1). Detection area see in fig.4.10.

Experiment list refers to table 4.9.

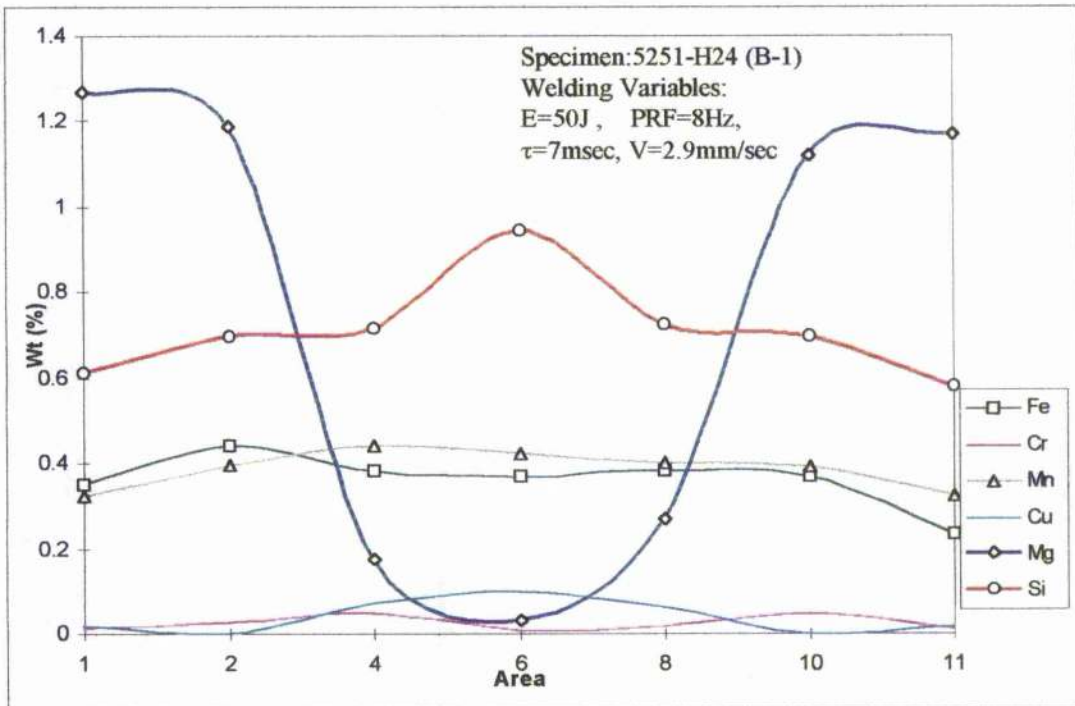


Figure 4.13 EPMA result of the welding sample (B-1). Detection area see in fig.4.10.

Experiment list refers to table 4.10.

A – 1 (6082 alloy without filler metal)

The figure 4.12 shows that there is an average decrease in Mg concentration which due to high energy density keyhole welding which causes evaporation. The average weight percent of Magnesium in the base metal was 0.961%, HAZ was 0.914%, while in the fusion zone value was 0.085% and fusion centre was the minimum 0% has been detected.

The average weight percent of Si in the base metal was 0.737%, HAZ was 0.677%, while in the fusion zone was 0.801% and fusion centre value was the maximum 1.003%. Centre line Si component concentration might cause hot cracking. Other special purpose elements are rarely altered in the welding fusion.

B – 1 (5251 alloy without filler metal)

The average Mg weight percent of base metal was about 1.22%, HAZ was 1.11% and that of fusion zone was 0.159%, fusion centre was the minimum 0.032% has been found. The average Silicon weight percent on base metal was about 0.596%, HAZ was about 0.7%. The average weight percent of fusion zone was 0.794%, fusion centre was 0.944% detected.

Both of aluminium alloys (A,B) were very sensitive to Laser beam welding as well as Magnesium loss was significant.

4.3.2.2. Grooved butt joint with 5% Si added filler metal (ER4043)

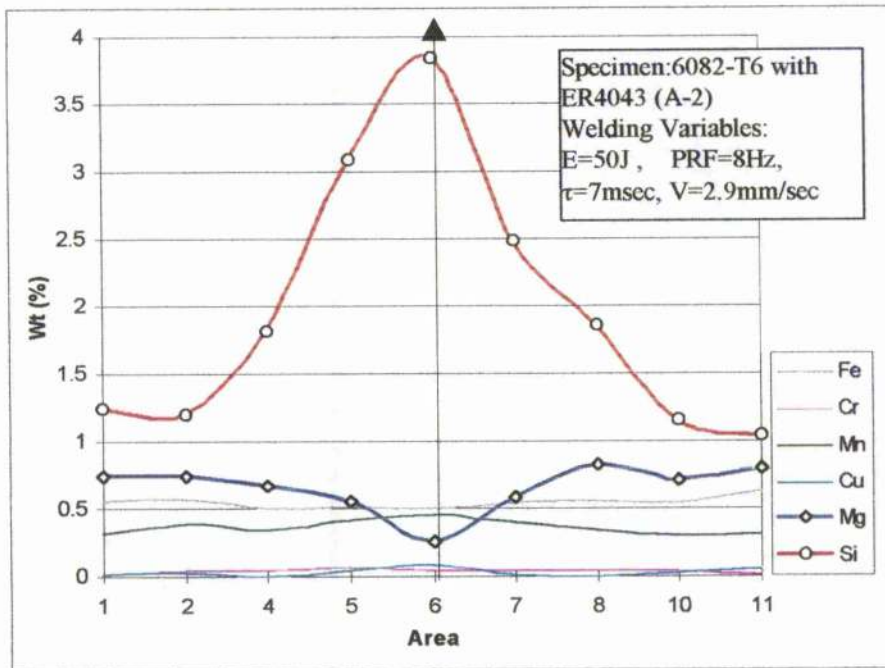


Figure 4.14 EPMA result of LBW on AA6082-T6 with ER4043 (5% Si)
 Experiment list refer to table 4.11.

A - 2 (6082 alloy with 5% Si filler metal)

The average weight percent of Magnesium in the base metal was 0.775%, HAZ was 0.73%, while in the fusion zone average was about 0.73% and fusion centre was the minimum 0.26%. The average weight percent of Si in the base metal was 1.145%, HAZ was 1.18%, while the average fusion weight percent was 2.62% and fusion centre was the maximum 3.85% observed. Silicon content on the fusion centre was exceeding the crack danger region¹⁾.

¹⁾ Chapter 2.2.3.1. Welding cracking. Fig.2.7 (a)

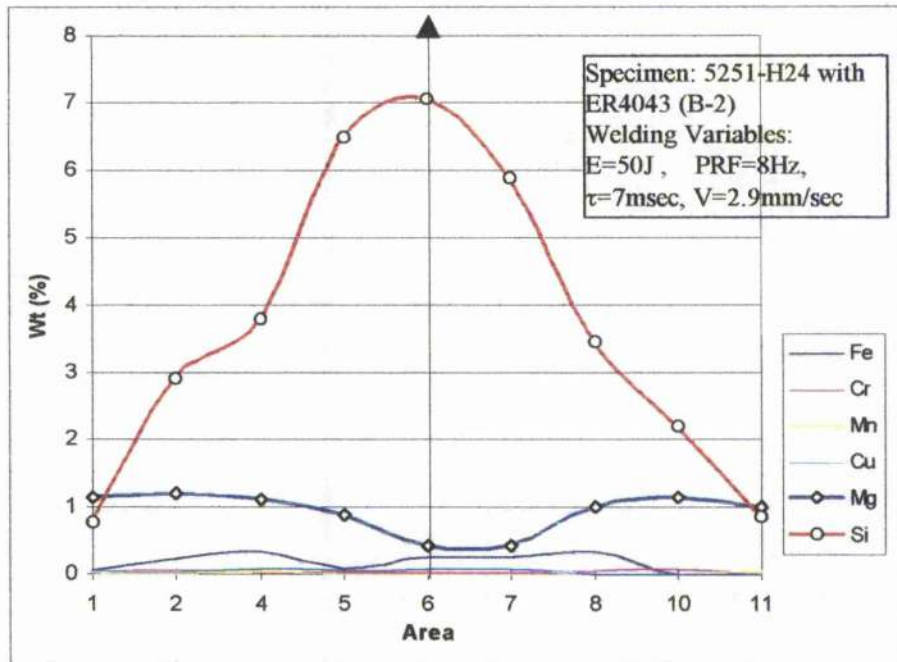


Figure 4.15 EPMA result of LBW on AA5251-H24 with ER4043 (5% Si)

Experiment list refers to table 4.12.

B – 2 (5251 alloy with 5% Si filler metal)

Magnesium loss on fusion centre can still be detected. Magnesium content in the fusion zone was 0.8 ~1.2 % and 0.8 % along the fusion centre has been found.

The fusion zone average Wt (%) of Mg was about 0.776% and fusion centre was the minimum 0.44%. The average weight percent of Si in the base metal was 0.815%, while the average fusion weight percent was 5.338% and fusion centre was the maximum 7.07% observed.

4.3.2.3. Grooved butt joint with 12% Si added filler metal (ER4047)

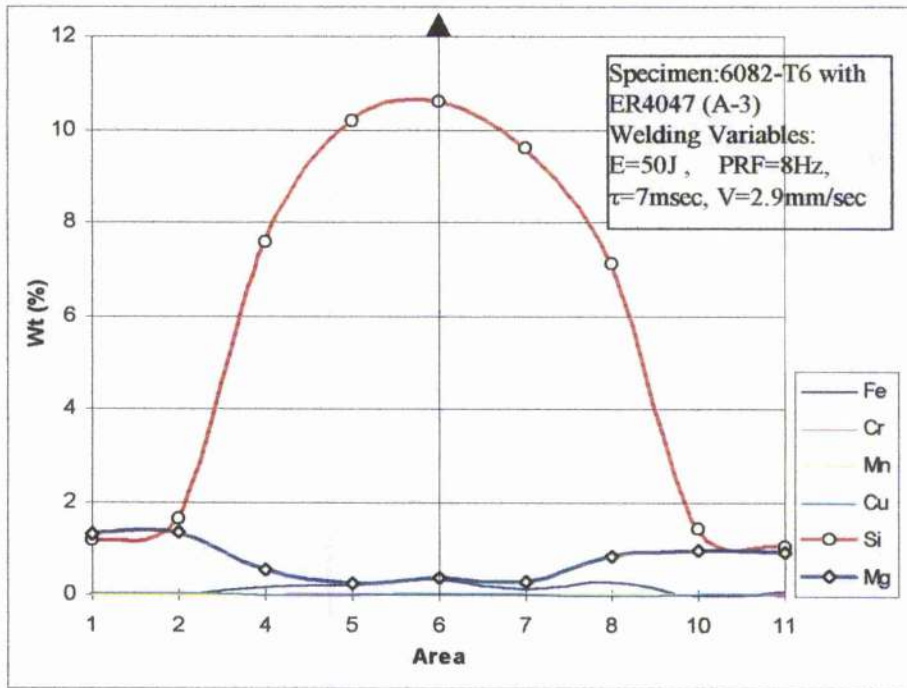


Figure 4.16. EPMA result of LBW on AA6082-T6 with ER4047 (12% Si)
 Experiment list refers to table 4.13.

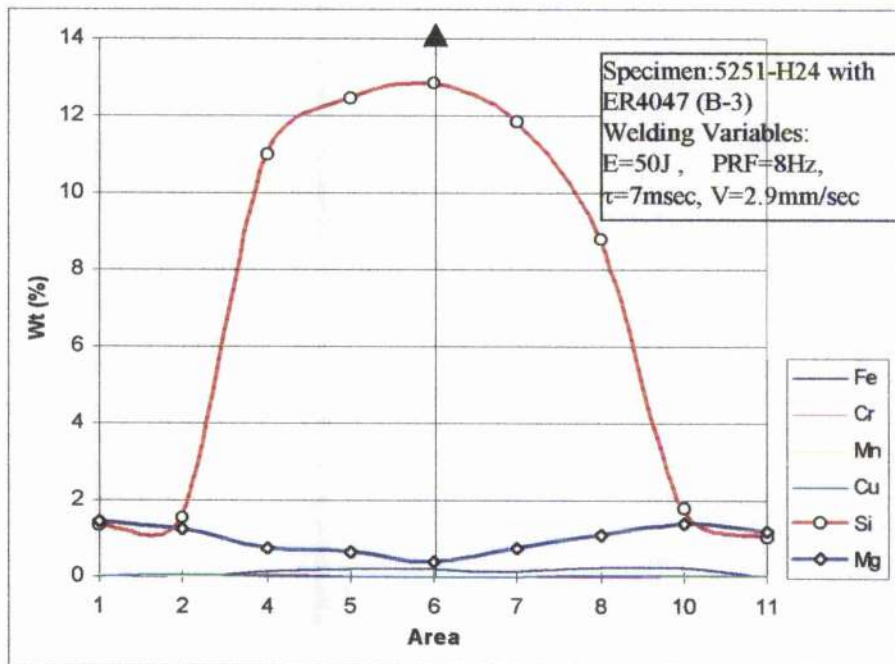


Figure 4.17. EPMA result of LBW on AA5251-H24 with ER4047 (12% Si)
 Experiment list in table 4.14.

A – 3 (6082 alloy with 12% Si filler metal)

The average fusion zone Silicon weight percent was 9.026% and 10.612% in the fusion centre found, while Mg Wt (%) of average fusion zone was 0.462% and 0.38% in the fusion centre observed.

B – 3 (5251 alloy with 12% Si filler metal)

The average weight percent of Magnesium on fusion zone was 0.728% and 0.4% in the fusion centre detected. The average weight percent of Si on the fusion zone was 11.38% and 12.83% in the fusion centre in 5251-H24 alloy. Mg loss in the fusion has been observed on both of aluminium alloys.

4.3.3. Tensile strength test

Symbol : E=Pulse energy / τ =pulse width / PRF=Frequency / V = velocity

6082-T6	No \ unit	E	τ	PRF	V	UTS	note
		J	msec	Hz	mm/sec	MN/m ²	
A - 1	1	35	5	8	2.9	6.67	
	2	35	6.2	8	2.9	33.3	
	3	35	7	8	2.9	18.6	
	4	40	7	8	2.9	6.67	
	5	45	7	6	2.9	6.67	
	6	45	7	6	2.9	19.46	Surface Roughened
	7	45	7	8	4	13.3	
	8	45	7	8	5.8	2.87	Surface Roughened
	9	50	7	8	2.9	2.66	
	10	50	7	8	2.9	6.67	Surface Roughened
	11	50	7	8	4	6.67	
	12	50	7	8	5.8	13.3	
A - 2	1	50	7	8	2.9	144	
	2	50	7	8	4	149.3	ER4043
	3	50	7	8	5.8	141.33	
A - 3	1	50	7	8	4	202.67	
	2	50	7	8	2.9	194.67	ER4047
	3	50	7	8	5.8	210.67	

5251-H24	No \ unit	E	τ	PRF	V	UTS	note
		J	msec	Hz	mm/sec	MN/m ²	
B - 1	1	35	5	8	2.9	6.67	
	2	35	6.2	8	2.9	13.33	
	3	35	7	8	2.9	10.66	
	4	40	7	8	2.9	29.33	
	5	45	7	6	2.9	69.33	
	6	45	7	6	2.9	80	Surface Roughened
	7	45	7	8	4	54	
	8	45	7	8	5.8	33.3	Surface Roughened
	9	50	7	8	2.9	24	
	10	50	7	8	2.9	6.67	Surface roughened
	11	50	7	8	4	37.33	
	12	50	7	8	5.8	24	
B - 2	1	50	7	8	2.9	216	
	2	50	7	8	4	208	ER4043
	3	50	7	8	5.8	181.33	
B - 3	1	50	7	8	4	254.66	
	2	50	7	8	2.9	254.93	ER4047
	3	50	7	8	5.8	224	

Table 4.15 Tensile strength test results in different specimen preparations.

The symbols used represent different combinations of the laser operating parameters (A-1,2,3 , B-1,2,3 refer to table 3.4 Preparation of welding specimens in chapter 3.)

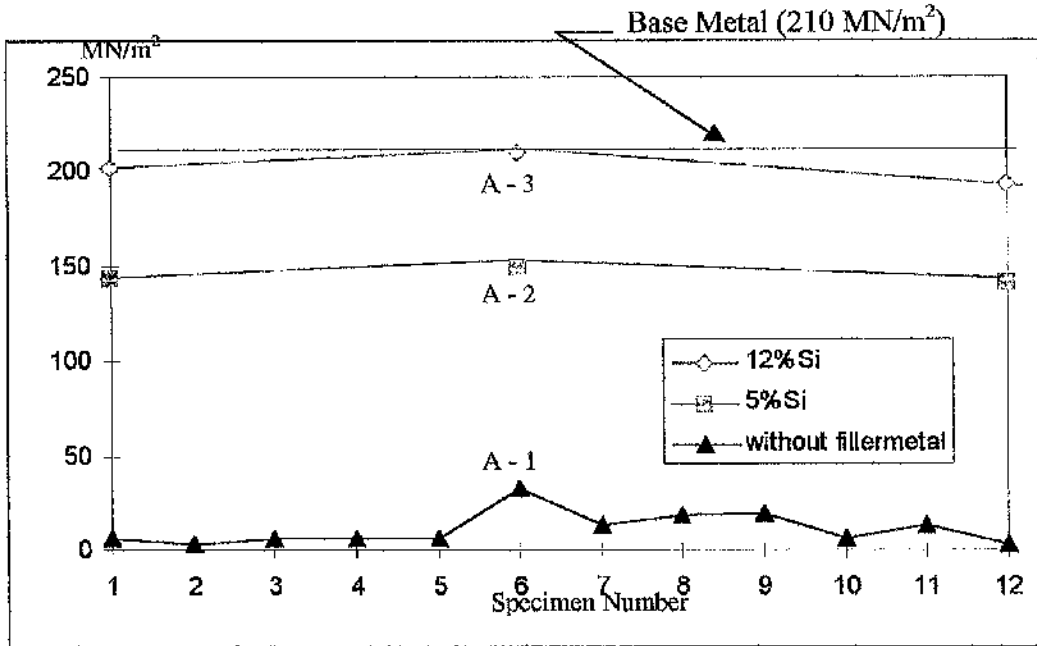


Figure 4.18. 6082-T6 Tensile Test Results on additional Silicon. A-1,2,3 refer to table 3.4.

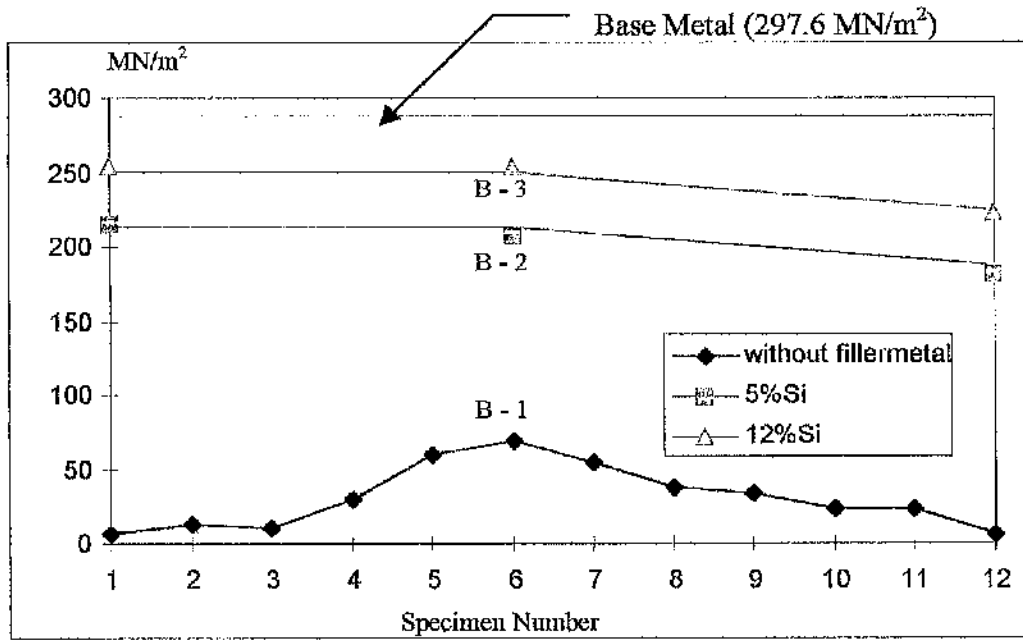


Figure 4.19. 5251-H24 Tensile Test Results with or without filler metals. B-1,2,3 refer to table 3.4.

4.3.3.1. 6082-T6 (A-1, A-2, A-3)

According to the tensile test result, specimen group1 in 6082-T6 alloy (A-1) has massive strength decrease found in welding without filler metal (Fig.4.18). The maximum tensile strength test result was 33 MN/m² which 94.6% of strength decreased compared to the base metal respectively. Specimen group 2 of 1 to 3 (A-2-1,2,3), welding with 5% of Silicon intermediate alloy (ER4043) found the strength improvement, where the specimen A-2-3 was 11 times stronger than the average A-1 group result. The fracture area of specimens 1 and 3 (A-2-1 and A-2-3) were in the fusion zone and specimen 2 (A-2-2) was in the HAZ.

In specimen group A-3, welding with 12% silicon added filler metal (ER4047), tensile test result of sample 3 (A-3-3) was 210.67 MN/m², which slightly over the base metal strength so that the fracture point was on the base metal with the Lüder's line. The tensile strength increased about 17 times compared to the specimens in A-1 group and 28.5% of the improvement compared to the A-2 group (ER4043) has been observed.

4.3.3.2. 5251-H24 (B-1, B-2, B-3)

The Tensile test result on the AA5251-H24 was substantially higher than AA6082-T6 alloys (figure 4.19). The specimen group1 (B-1) has found that the maximum 69.33 MN/m² which the strength reduction was approximately 90% observed. The group 2 (B-2) observed higher test result than same condition of AA6082-T6 alloys which approximately 201MN/m². The specimen 1 and 2 found that the fracture point was on the Heat Affected Zone.

The group 3 (B-3) has found the strongest tensile strength, 254.93MN/m², (B-3-2), whilst base metal is 297.6MN/m² so that 85.6% of strength compare to base metal been observed and approximately 700% of strength improved compare to the without filler metal (B-1). In B-3 condition, fracture area was on the HAZ in all the samples.

4.3.4. Micro hardness test

Vicker's Hardness test result (Kg/mm²)

Distance (mm)	A-3	A-2	A-1	B-1	B-2	B-3
0	76.01	76.00	82.00	57.57	57.00	61.00
0.1	75.48	76.42	80.00	57.84	56.00	57.31
0.2	76.00	80.20	80.00	61.40	55.00	55.27
0.3	74.94	76.70	79.30	60.59	60.00	58.20
0.4	74.00	76.01	80.20	60.59	63.50	55.70
0.5	75.34	76.00	78.00	61.16	62.30	60.59
0.6	75.00	74.60	79.70	60.00	62.80	63.84
0.7	71.60	74.40	79.10	59.00	60.60	63.50
0.8	65.38	75.40	79.30	61.80	64.00	69.41
0.9	65.38	68.00	77.10	62.20	68.70	70.83
1	64.20	62.00	77.50	69.20	68.80	71.60
1.1	62.60	64.60	77.70	70.40	68.80	69.60
1.2	59.40	62.00	73.50	71.60	69.20	83.44
1.3	88.00	71.70	73.50	52.00	72.90	107.80
1.4	90.30	72.50	63.00	53.00	81.50	109.80
1.5	94.31	71.70	64.60	43.98	82.70	111.51
1.6	95.40	75.60	53.50	50.40	84.40	107.00
1.7	92.90	73.40	63.40	50.80	77.80	102.50
1.8	92.00	72.30	61.50	70.00	69.20	79.50
1.9	88.30	71.70	70.00	69.20	68.80	70.80
2	61.10	63.40	70.30	70.00	69.20	71.60
2.1	61.50	64.60	71.10	60.60	70.00	70.80
2.2	60.00	64.60	78.50	59.80	63.10	70.83
2.3	61.10	75.34	77.00	60.00	61.80	62.30
2.4	64.20	75.34	78.50	58.40	58.20	62.30
2.5	74.50	75.08	76.00	59.46	62.00	64.30
2.6	74.30	76.69	78.50	59.19	65.10	62.33
2.7	76.00	71.70	81.30	60.59	62.30	62.03
2.8	75.08	76.00	79.30	64.30	60.00	63.10
2.9	76.42	74.00	81.00	56.79	60.00	61.40
3	76.00	76.00	80.20	55.77	57.80	61.80

Indentation	60.00	div.	Length Constant	0.26	μm
weight	100.00	gram	Indent interval	100.00	μm

Table 4.16. Experiment results of Micro hardness test.
Welding variables: E=50J / PRF=8Hz / τ =7msec / V=2.9mm/sec.
A,B-1,2,3 refer to table 3.4 in chapter 3.
Equation for the test refers to chapter 3. Micro hardness test.

6082-T6 alloy in different specimen preparations (A-1, A-2, A-3)

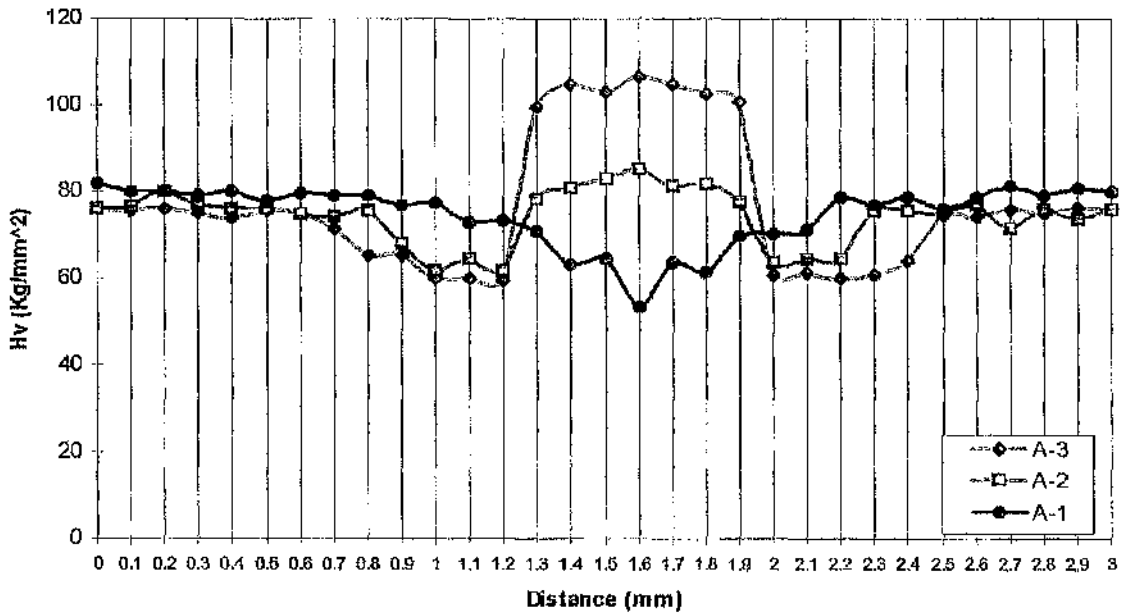


Figure 4.20. Micro hardness profiles of 6082-T6 alloy in different specimen preparations. A-1, A-2, A-3 refer to table 3.4 preparation of welding specimens (Chapter 3.)

5251-H24 alloy in different specimen preparations (B-1, B-2, B-3)

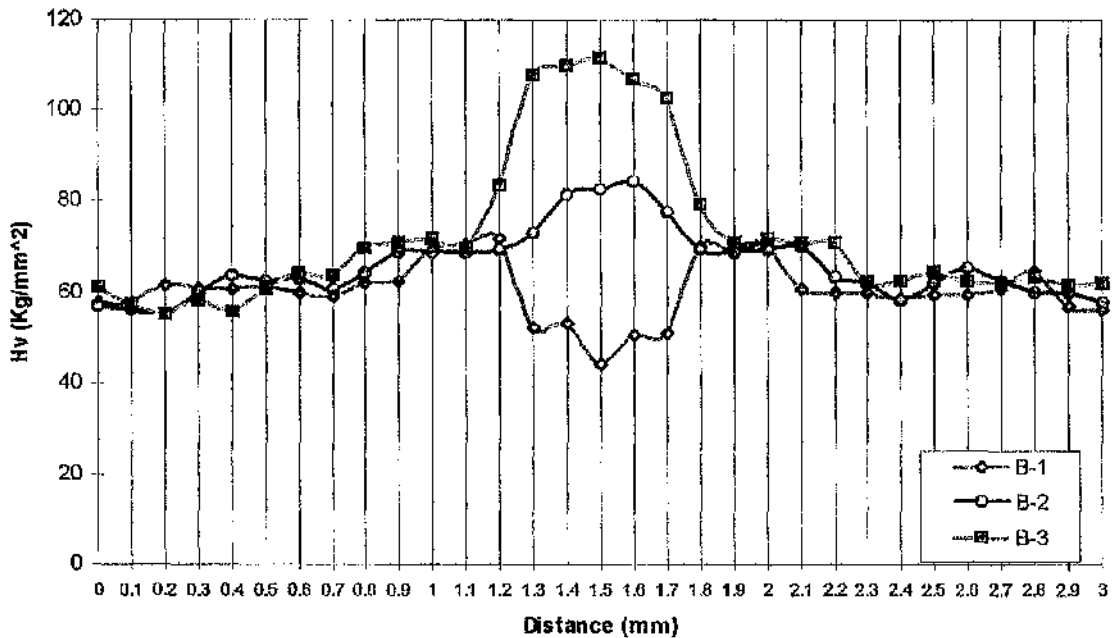


Figure 4.21. Micro hardness profiles of 5251-H24 alloy in different specimen preparations. B-1, B-2, B-3 refer to table 3.4 preparation of welding specimens (Chapter 3.)

4.3.4.1. Square butt joint without filler metal LBW (A-1, B-1)

A – 1 (6082 alloy without filler metal)

The average hardness on the 6082-T6 base metal was 79.16 kg/mm^2 and hardness has decreased on the HAZ and fusion zone. The average hardness on the HAZ was about 71 kg/mm^2 and minimum hardness was 53.5 kg/mm^2 along the welding center (Figure 4.20 A-1). A dramatic hardness decrease on the centre was due to the testing on the welding crack. The size of HAZ was approximately 0.4mm observed.

B – 1 (5251 alloy without filler metal)

The hardness profile of welded 5251-H24 alloy was about 60.21 kg/mm^2 on base metal and fusion centre was about 44 kg/mm^2 (fig.4.21 B-1). one difference was the increased hardness on HAZ compare to 6082 alloy. Hardness on the HAZ was about 70.4 kg/mm^2 . This result may caused by the aging effect on non-heat treatable Aluminum Alloy. The size of HAZ was about 0.4mm found from the profile.

4.3.4.2. ER 4043(5% Silicon) with grooved-butt joint LBW (A-2, B -2)

A – 2 (6082 alloy with 5% Si filler metal)

The hardness profile along the HAZ was approximately 63 kg/mm^2 and the fusion centre was the maximum of 75.6 kg/mm^2 (figure 4.20 A-2). The center area of hardness increasing was the silicon affect. The maximum hardness on the fusion zone was slightly higher than the hardness of base metal where the different profile of welding without filler wire which about 0.2mm observed.

B – 2 (5251 alloy with 5% Si filler metal)

The average hardness on the fusion was 77.86kg/mm^2 where centre was the greatest (87.7kg/mm^2). That of HAZ was 68.88kg/mm^2 which was higher than hardness of A-1 specimen condition and the size of HAZ was about 0.2mm found.

4.3.4.3. ER 4047(12% Silicon) with grooved-butt joint LBW (A-3, B-3)

A – 3 (6082 alloy with 12% Si filler metal)

The hardness profile of 6082-T6 with 12% Si added filler metal (Figure 4.20 A-3) was similar to that of welding with 5% Si filler metal. The hardness profile of the average fusion zone was 91.6kg/mm^2 , compare to that of A-2 was 72.7kg/mm^2 , and the maximum was 95.40kg/mm^2 on the fusion centre. The size of HAZ was slightly bigger than welding on 6082-T6 alloy with ER4043 filler metal.

B – 3 (5251 alloy with 12% Si filler metal)

5251-H24 (Figure 4.21 B-3) has a different profile as 6082-T6 alloy, the average hardness on the fusion zone was 91.6kg/mm^2 where fusion centre was the maximum 95.4kg/mm^2 . Due to the aging effect on the HAZ, size of HAZ was 0.4mm which hardness was higher than base metal.

From the Vicker's hardness test result or profiles, size of HAZ was clear in different specimen preparations. Fusion size of 6082 alloy in A-1 condition was 1.4 to 1.8mm where 0.4mm, HAZ was approximately 0.1mm. In A-2 condition, fusion size was about 0.6mm, HAZ was 0.2mm on each side found. In A-3 condition, fusion size was 0.6mm and HAZ was 0.4mm on each side. The size of fusion and HAZ on 5251 alloy was almost same as 6082 alloy, but the profile of HAZ was different because of strengthening process, which mentioned on chapter 2.

Chapter 5. Discussion of results

5.1. Crack Formations on the welding variables

In experimental results, fusion size differences from the pulse energy alteration have obvious increase have been found and cracking has formed mainly in the higher energy (table 5.1,2).

That of the pulse duration alterations have an opposite result as pulse energy alterations that welding depth decreased dramatically according to the pulse power calculations, which might be caused from power intensity decrease on longer laser pulse.

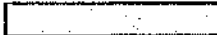
Welding cracking easily formed in the welding in shorter pulse duration (table 5.2).

There were no big differences of fusion size from the weld overlap changes, but slight welding depth increases have been found when increase the overlapping ratio. Welding cracking can be seen easily from high overlapping ratios, in other word, high frequencies and low welding velocity have high possibilities of welding crack (table 5.3,4).

The comparative result of differences between continuous and pulse laser operations are the welding speed variations which were not directly related to change the welding depth because of the fast cooling during the inter-pulse period.

O : Weld Crack in the fusionzone

X : No weld crack

 : Crack Danger Zone

Specimen \ E(J)	5	10	15	20	25	30	35	40	45	50
A-1-1	X	X	X	O	X	X	O	O	O	O
A-1-2	X	X	X	O	X	O	O	O	O	O
B-1-1	X	O	X	O	O	O	O	X	O	O
B-1-2	X	O	X	X	O	X	O	O	O	O

Table 5.1. The crack formation alteration from Pulse Energy

(The constant parameters: $\tau=7\text{msec}$ / PRF=8Hz/ V=2.9mm/sec. The experiment lists refer to the table 1 in the chapter 4.2. Related macro picture refer to the Appendix i. Image Libraries, i.1)

Specimen \ T(msec)	5	6.2	7.5	8.8	10	12.5	15	17.5	19.9
A-1-5	O	O	O	O	X	X	X	X	X
A-1-7	O	O	O	O	X	O	O	O	X
B-1-4	O	O	O	O	O	X	O	O	O
B-1-5	O	O	X	X	O	O	O	X	X

Table 5.2. The crack formation alteration to the Pulse Width. "T" in the table indicates Pulse duration (τ) (The constant parameters: 35J(A-1-5, B-1-4) or 30J(A-1-7, B-1-5)/ PRF=8Hz/ $\tau=7\text{msec}$ / V=2.9mm/sec. The experiment lists refer to the table 2 in the chapter 4.2. Related macro picture refer to the Appendix i.2 Image Libraries)

Specimen \ PRF(Hz)	1	2	4	6	8	12	16
A-1-3	X	X	X	X	X	O	O
A-1-4	X	X	X	X	O	O	O
B-1-3	X	X	X	X	O	O	O

Table 5.3. The crack formation alteration from the Pulse Repetition Frequency (PRF)

The constant parameters: E=25J/ $\tau=7\text{msec}$ / V=2.9mm/sec. The experiment lists refer to the table 3 and table 6 (A-1-4) in the chapter 4.2. Related macro picture refer to the Appendix i. Image Libraries, i.1)

Specimen \ V(mm/sec)	2.9	4	5.8
A-1-9-1	X	X	X
A-1-9-2	O	O	O
A-1-9-3	O	O	O
A-1-10-1	O	O	X
A-1-10-2	O	O	O
A-1-10-3	O	O	O

Table 5.4. The crack formation alterations from the welding speed

(The other constant parameters: E=30J(A-1-9-1, A-1-10-1), 40J(A-1-9-2, A-1-10-2), 50J(A-1-9-3, A-1-10-3) / PRF=8Hz/ $\tau=7\text{msec}$. The experiment lists refer to the table 4 and table 7 in Appendix i.1.

Related macro picture refer to the Appendix i.2 Image Libraries)

5.2. Heat Affected Zone

There were different micro hardness profile have been found from strengthening processes on work-hardening alloy and heat-treatable alloy. The hardness increase on the HAZ compare to the base metal on AA5251-H24 alloy have found due to the age hardening effect when welded in high overlapping, While 6082-T6 alloy has decreased the hardness, because of the softening effect from precipitation (figure 5.1). According to the reference, subsequent heat treatment could not solve the over aging effect, except may have to employ the full reheat-treatment [ref.15]. One specifically need to be considered is the size of HAZ (approximately 1mm) which were much smaller than other commercially used fusion welding method such as GTAW or CW CO₂ Laser Beam Welding [ref.32]. From the advantages of pulse laser operation, there was no evidences of age hardened region have found. The microstructures from SEM have found that the size of grain in HAZ was coarser than base metal.

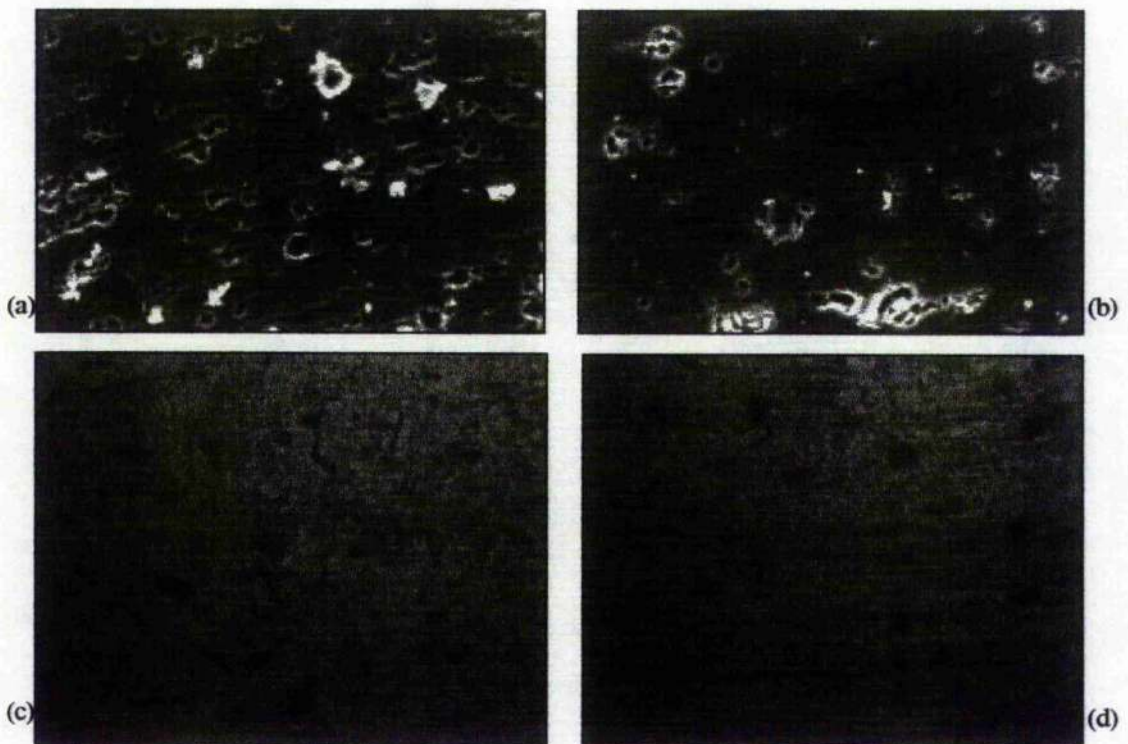


Figure 5.1. Microstructure comparison of HAZ in Laser welded Aluminum Alloy (AA6082-T6)

Microstructures have taken by SEM ($\times 1000$) (a),(b) and optical microscope (c),(d)

(a),(c): HAZ (coarsened grain) (b),(d): Base metal of 6082-T6 alloy

The hardness results of welding with filler metals on HAZ have slightly bigger than that of without filler metal were observed which may be caused from lower melting temperature range due to the higher Silicon contents.

5.3. Fusion Zone

From the microstructure, fusion zone could separate in two regions, which were equiaxed zone and columnar zone. Columnar zone was near the fusion line which the cooling speed was rapid, while equiaxed zone near fusion center which cooling speed was slower than columnar zone.

Since laser beam interacts with Aluminum, the alloy composition keeps changing and bouncing. When molten metal is on the cooling, it try to freeze along the amount of base metal Si content, however, the non-equilibrium cooling reject and raise the silicon concentration¹⁾ as well as rapid quenching²⁾ makes Aluminum frozen out of the last melt. So that Silicon ends up with depleted and low silicon lead the region where crack formability is greatest³⁾.

One single laser pulse interacting on the Aluminum Alloy were shown in figure 5.2.(a) that columnar zone was almost dominated in fusion zone, because of fast resolidification speed[ref.6.23.32] and the solidification cracks were formed toward the fusion center. Microstructure of multi spots have same results; columnar structure been found, however, welding cross section have slightly different because of overlapping area. Figure5.2 (b) have shown that the welding overlapping effect. After the solidification of previous spot, second welding spot produced with certain distance from welding velocity in unit area. When the welding velocity is slow or frequencies is high, overlapping ratio under the unit area is higher so that higher possibilities of evaporation loss and shrinkage. Therefore, higher welding velocity or low frequencies in order to minimize the overlap welding could reduce the problems in welding without filler wire. Welding variables could reduce the problems, however, other mechanical property was still unacceptable. Hardness has decreased compare to the base metal, especially fusion center was greatest, due to the longitudinal crack. After the tensile test, all the welding failure was on the fusion center and very low elongation observed.

¹⁾ Chapter 2.4. Non-equilibrium alloy solidification

²⁾ Chapter 2.2.3. (4) Rapid Quenching.

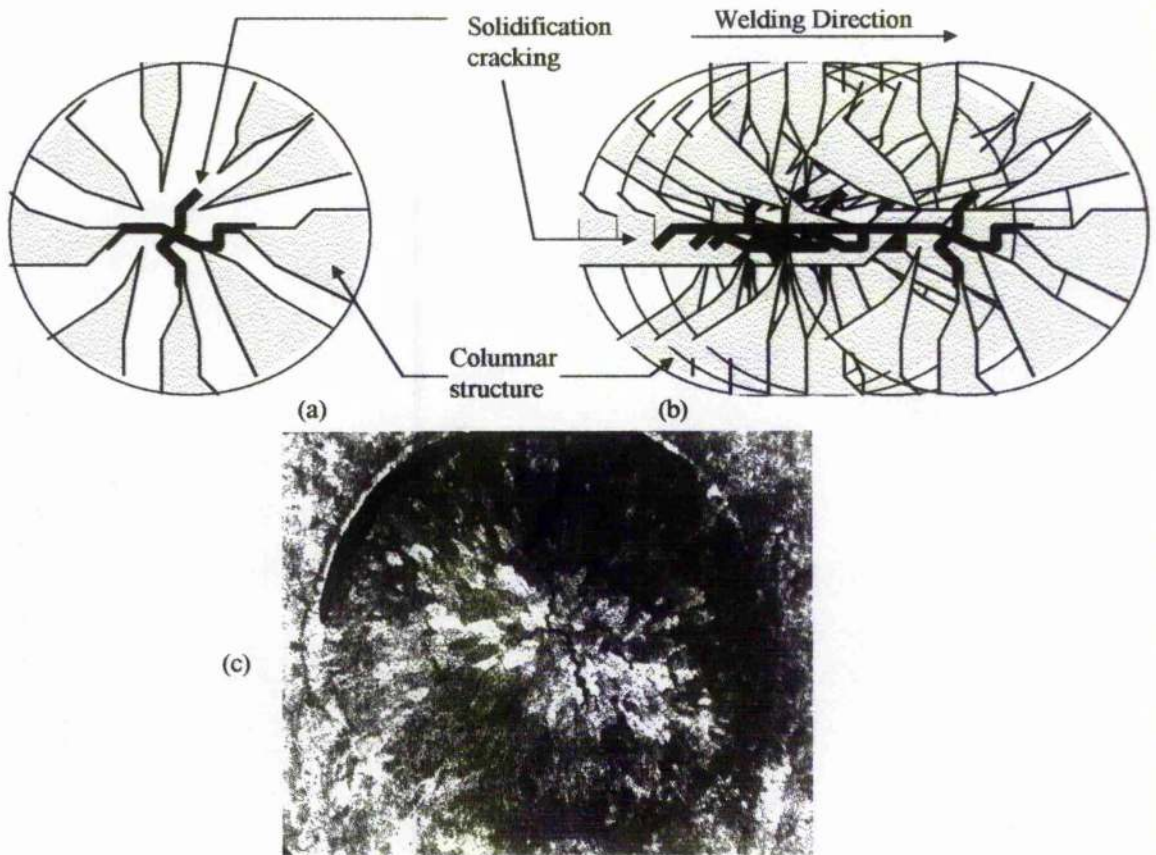


Figure 5.2. (a) Single pulse interacting on the Aluminum Alloy surface (b) multi pulse interacting on Aluminum Alloy surface (c) typical example of solidification cracking on single pulsed aluminum alloy. (Microstructures refer to the Appendix i.2.)

Welding with silicon added filler metals have found the smaller columnar structure when welded with higher silicon filler metals than without filler metals (Figure 5.3). That may be caused from slower resolidification speed.

From the reading of Vicker's hardness test, hardness have increased in the welding fusion zone and fusion center was greatest when increased an amount of Silicon, according to the hardness profile. This was a natural effect according to the mechanical property changes of Al-Si Binary Alloy⁴⁾. The maximum hardness was on the fusion center, which may be caused from Silicon segregation. The tensile property has tremendously increased compare to the base metal and almost same strength has obtained from 12% silicon filler metal (ER4047).

³⁾ Chapter 2.2.3. (1) Welding cracking figure.2.5 and J.F. Lancaster, 9.1.3. Cracking, figure.9.1, [ref.8].

⁴⁾ Mechanical properties of aluminum-silicon alloys, as function of silicon content, figure.2.55, [ref.13].

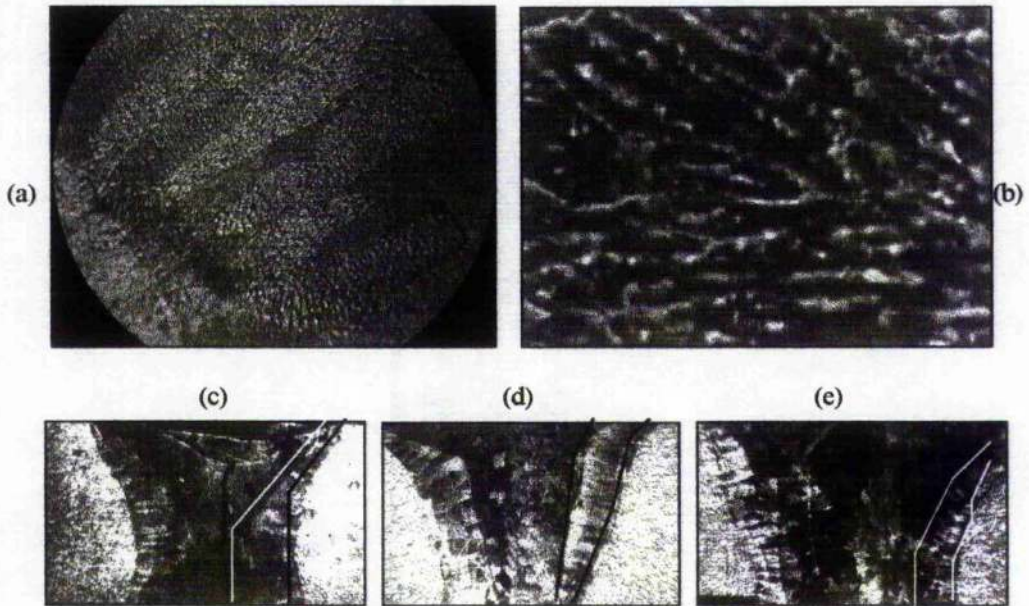


Figure 5.3. Size of Columnar structures changes on different Silicon contents (indicated in black and white lines) Typical Columnar structures near fusion line (a) optical microscope, (b) SEM, (c) without Silicon, (d) welding with filler wire ER4043 (5% Si), (e) welding with filler wire ER4047 (12% Si) The constant welding parameters: $E=50\text{J}$ / $\text{PRF}=8\text{Hz}$ / $\tau=7\text{msec}$ / $V=2.9\text{mm/sec}$

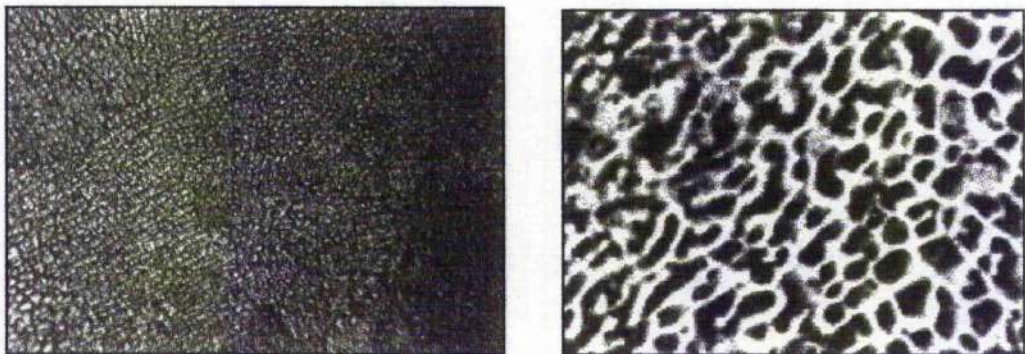


Figure 5.4. Equiaxed Structures¹⁾ (a) optical Microscope (X100) (b) SEM (X1000)²⁾

Welding Parameter: $E=45\text{J}$ / $\text{PRF}=9\text{Hz}$ / $\tau=5.8\text{ msec}$ / $V=2.9\text{ mm/sec}$

¹⁾ The size of Equiaxed structure differences can be seen in figure 5.3 (c),(d),(e) which adjacent to the columnar structure in the fusion zone.

²⁾ The microstructure from SEM was negative images so those white lines were the Equiaxed structure which same as black lines in optical microscope.

5.4. Other welding defaults

5.4.1. Porosity

Porosity was still unsolved welding default in Aluminum Alloys because very high intensity of Nd^{3+} :YAG laser operation and low boiling temperature of alloy elements may lead the porosities. The type of porosities were mainly type B: spherical shape, type C: angular shape porosity been found according to the experiment result from Muneharu Kutsuna[ref.39]. They were caused from the evaporation. Methanol Cleaning process before the welding process was not sufficiently prevent the porosities; remove the Oil, paint, rust on the base metal and filler wire. Another possibility can estimate from the air gap between the welding joint, because of round shape of filler wire and 90° grooved base metal. Reference [ref.9] has shown the case solution for porosities so that the avoidance of porosities are: chemical treatment to remove the surface oxide film; reduce the air gap between base metal and filler metal are required. Evaporation of low temperature alloying components is a feature of high intensity laser welding which results in weld porosity. Type B, spherical porosity was seen in microstructure in figure 5.5. The collapse of the set-up gap and of gaps surrounding the filler wire were also the causes of voids and porosity in the fused zone. There latter can and should be controlled. In particular, the filler wire should be formed to accommodate the weld penetration geometry.

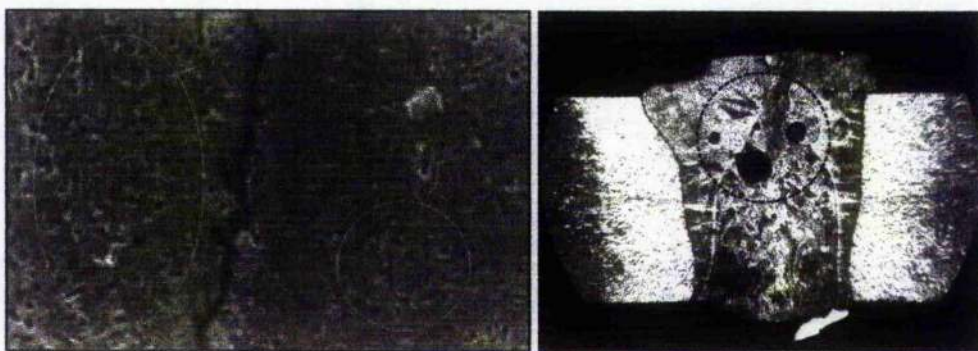


Figure 5.5. Porosities (a) micro porosity (SEM $\times 1000$) (b) Macro porosity (Optical microscope $\times 5$)
Welding conditions: (a) $E=35\text{J}$ / $\text{PRF}=8\text{Hz}$ / $\tau=7\text{msec}$ / $V=4.0\text{mm/sec}$ welding without filler wire , (b) $E=50\text{J}$ / $\text{PRF}=8\text{Hz}$ / $\tau=7\text{msec}$ / $V=2.9\text{mm/sec}$ welding with 12% silicon included filler wire(ER4047)

5.4.2. Misalignment

The low welding power and wrong joint design caused welding defaults such as ① incomplete fusion, ② under cut which are well known as misalignment. Incomplete fusion describes the failure of adjacent base and weld metal to fuse together completely. Under cut is left unfilled weld metal. Main both defaults are the stress concentrations [ref.15], which the figure 5.6 has shown that a typical example of misalignment defaults.

① Incomplete fusion was mainly come from the filler wire quantity and conduction limited type welding process, because available size of commercial purpose electrodes only diameter of 1.6mm. So that mechanical treatment or higher power welding was required.

② Under cut was mainly came from mismatches of base metal. Usually size of fusion was less than 1mm on back bead so that very accurate welding position was essentially required.

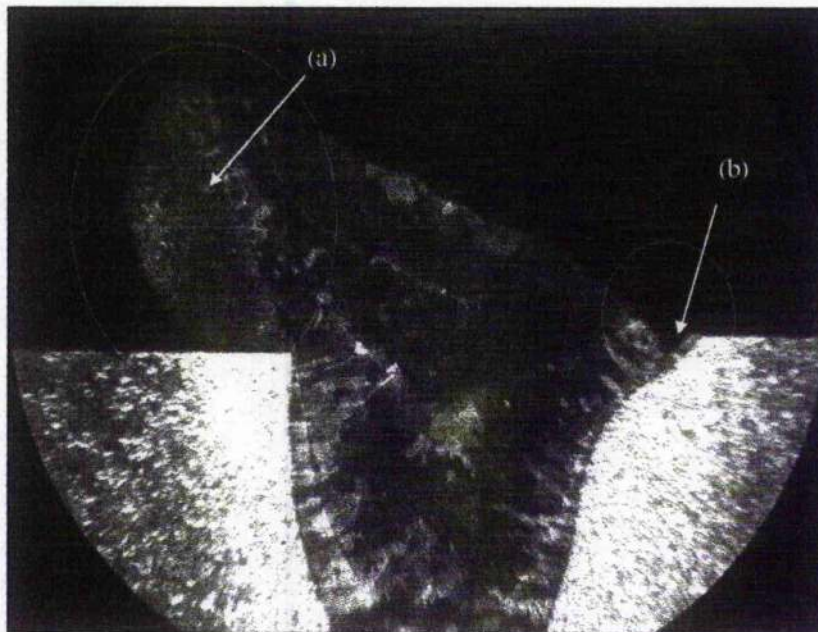


Figure 5.6. Welding defaults from Misalignment (a) incomplete fusion (b) under cut

Parameters: $E=40J$ / $PRF=8Hz$ / $\tau=7$ msec / $V=2.9mm/sec$

Filler metal: ER4043 (5% Silicon, Round Surface)

Appendix 2. Image Libraries

**i.1. Fusion size alterations from welding variables.
(A-1-1 to -10 , B-1 to -5)**

i.2. Microstructures (Optical microscope / SEM)

1. A-1 , B-1

2. A-2 , B-2

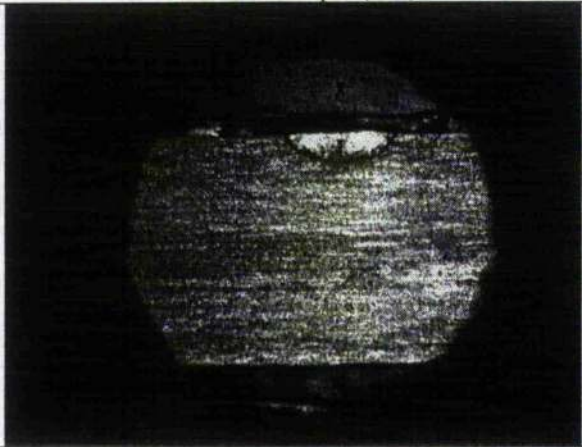
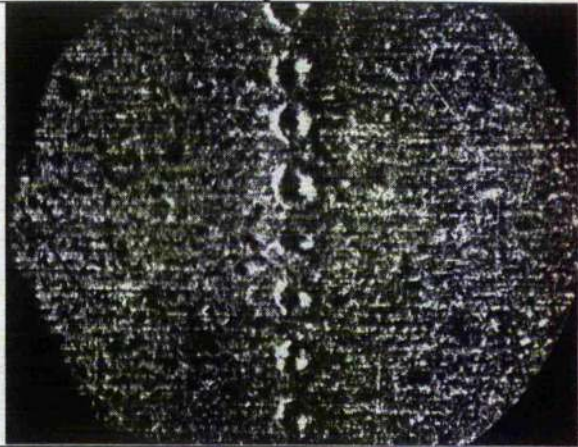
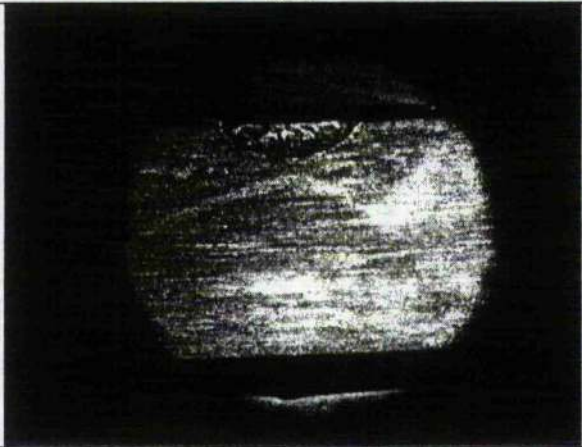
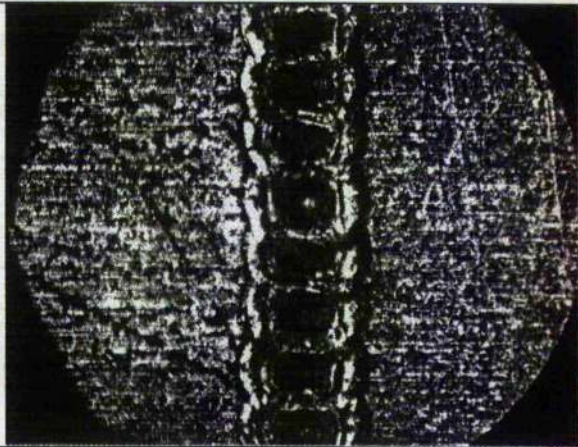
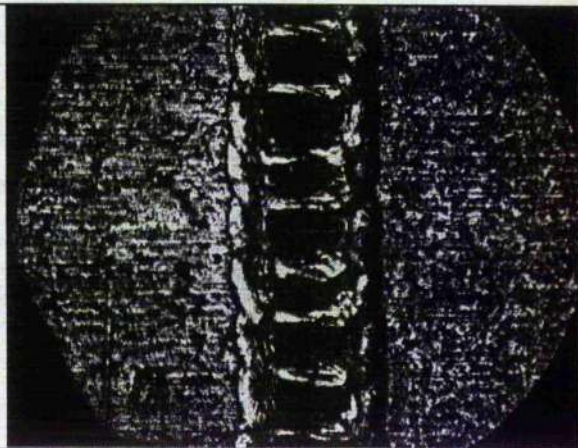
3. A-3 , B-3

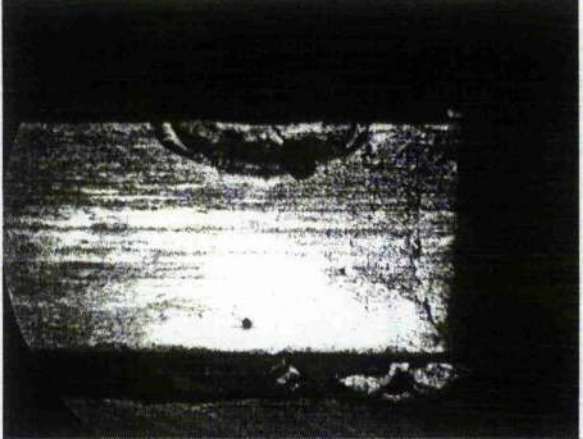
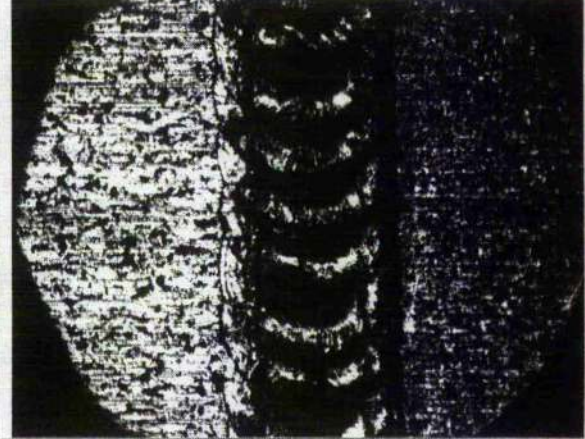
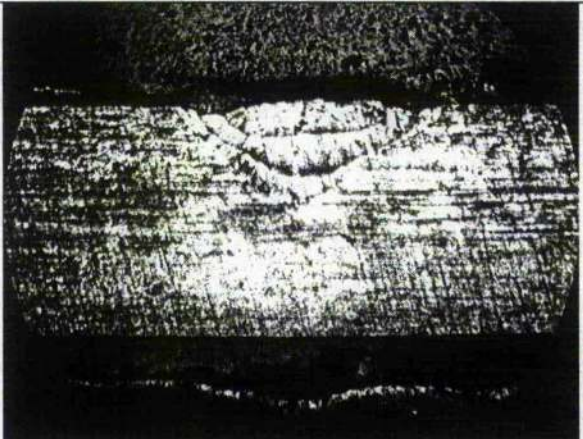
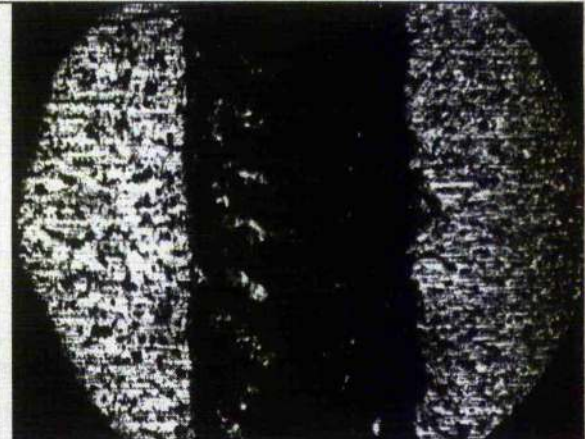
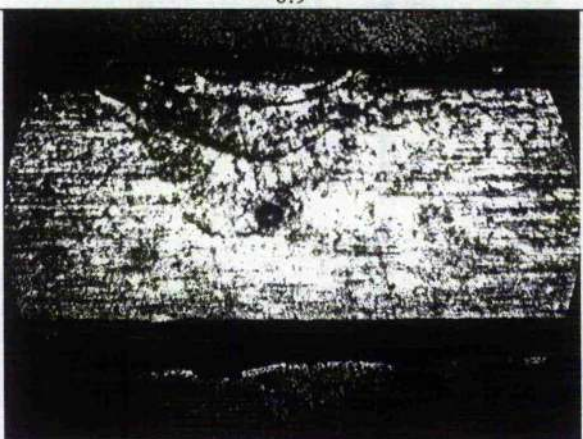
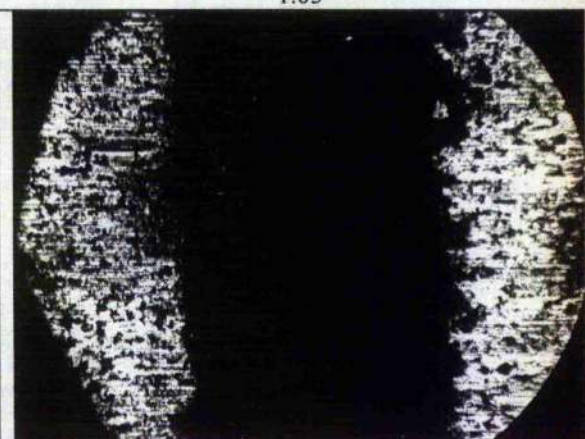
4. Single pulse irradiated on the Aluminum Alloys

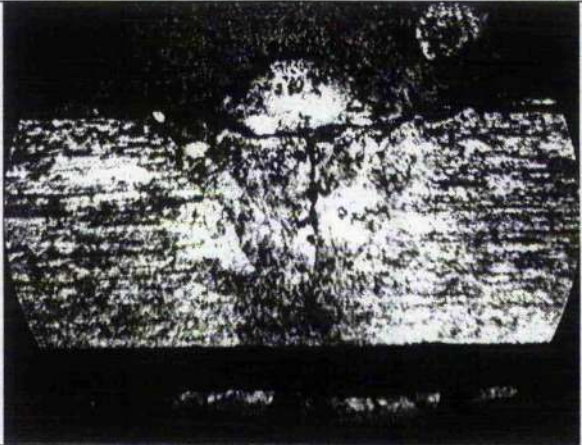
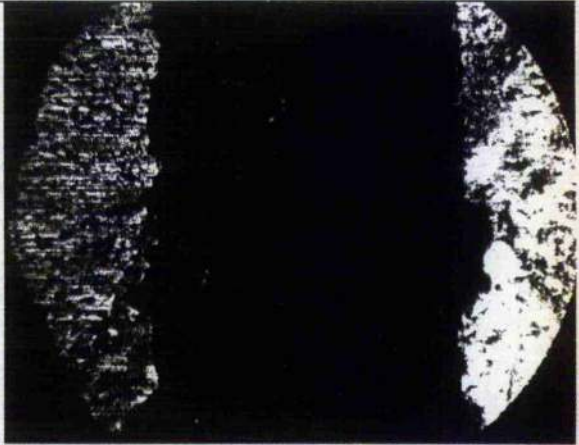
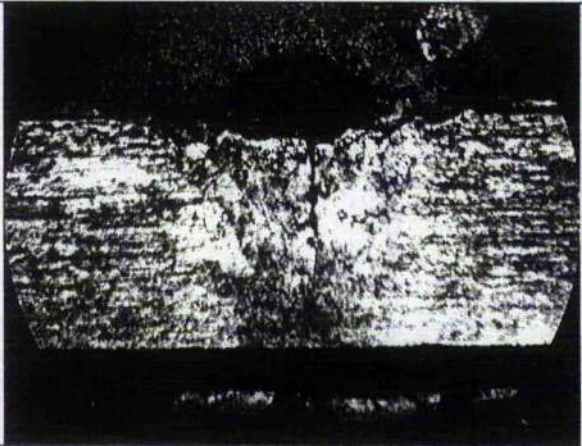
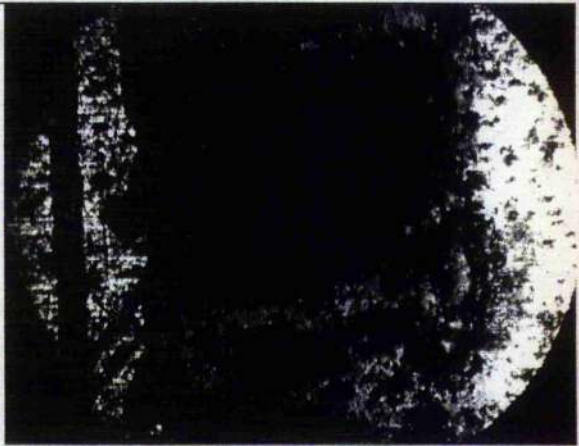
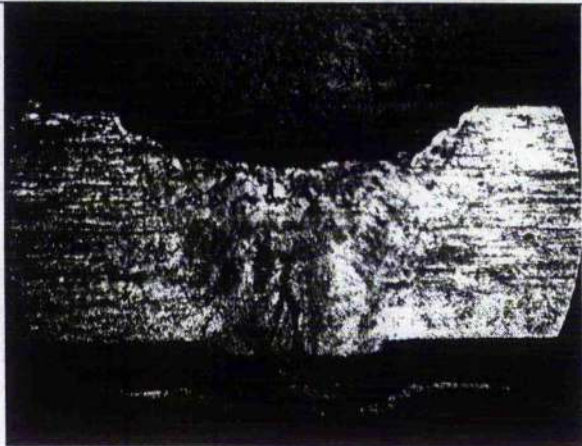
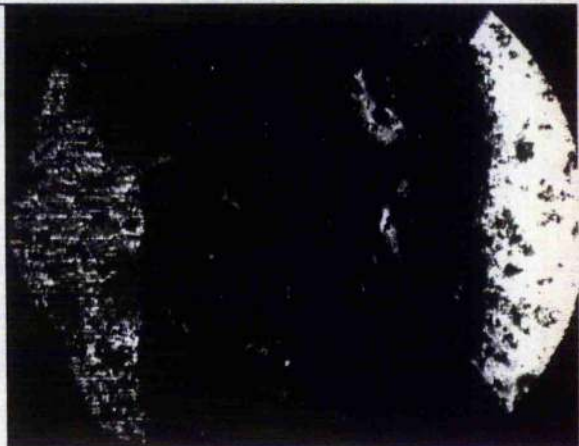
i.3. Specimens After the Tensile Strength Test

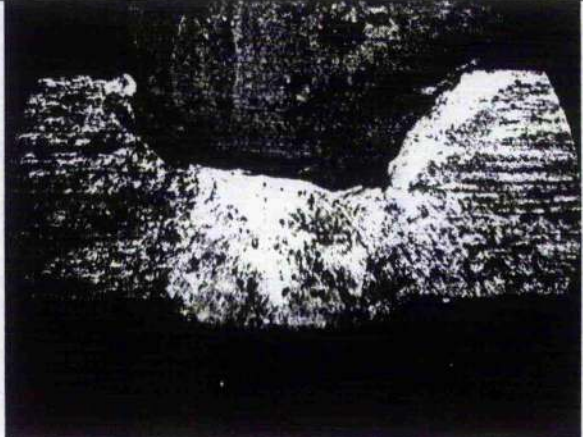
A-1-1

Pulse energy alteration to the fusion size on 6082-T6 O / X : weld crack formation

	Penetration depth (mm)	Welding width (mm)
1 5J 8Hz 7 msec 2.9 mm/s ec		
X	0.18	0.15
2 10J 8Hz 7 msec 2.9 mm/s ec		
X	0.225	0.6
3 15J 8Hz 7 msec 2.9 mm/s ec		
X	0.3	0.675

<p>4</p> <p>20J 8Hz</p> <p>7 msec</p> <p>2.9 mm/s ec</p>		
O	0.345	0.75
<p>5</p> <p>25J 8Hz</p> <p>7 msec</p> <p>2.9 mm/s ec</p>		
X	0.9	1.05
<p>6</p> <p>30J 8Hz</p> <p>7 msec</p> <p>2.9 mm/s ec</p>		
X	0.975	1.35

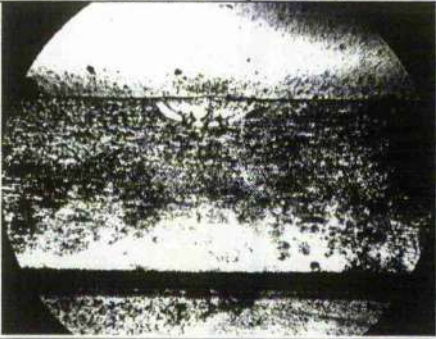
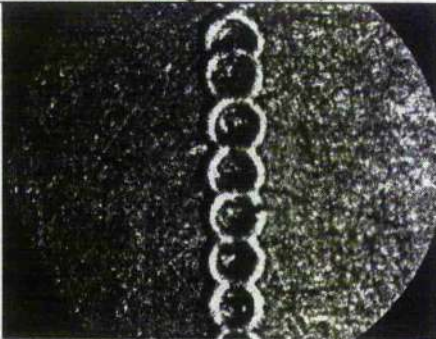
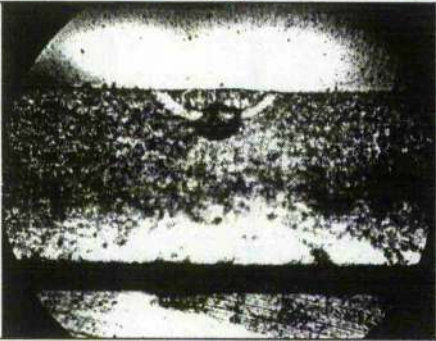
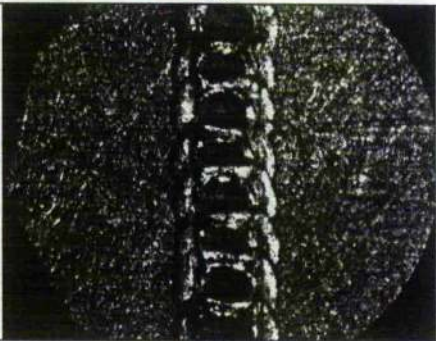
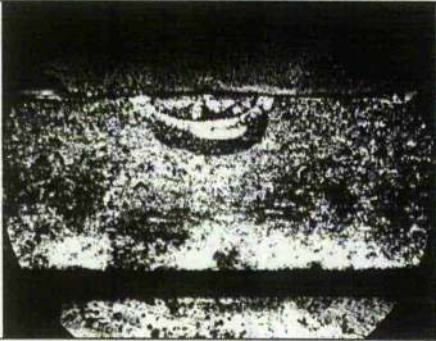
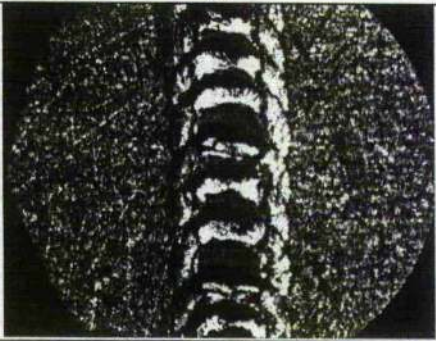
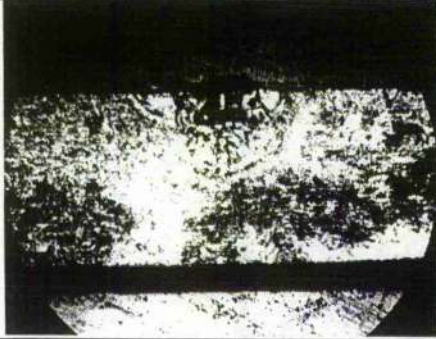
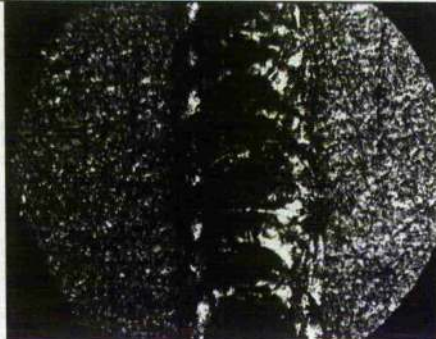
<p>7 35J 8Hz 7 msec 2.9 mm/s ec</p>		
O	1.2	1.5
<p>8 40J 8Hz 7 msec 2.9 mm/se c</p>		
O	1.35	1.68
<p>9 45J 8Hz 7 msec 2.9 mm/se c</p>		
O	1.5	1.725

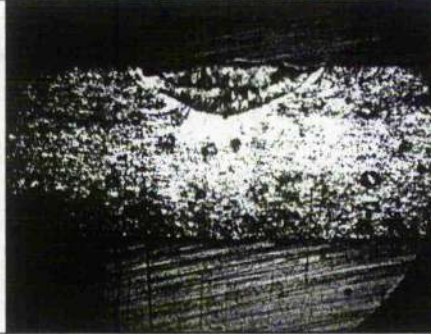
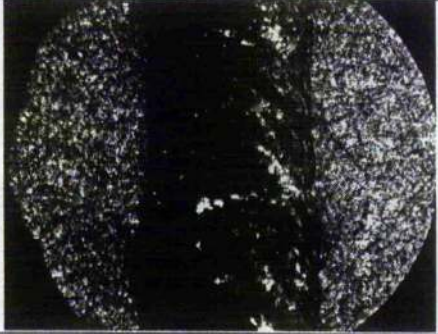
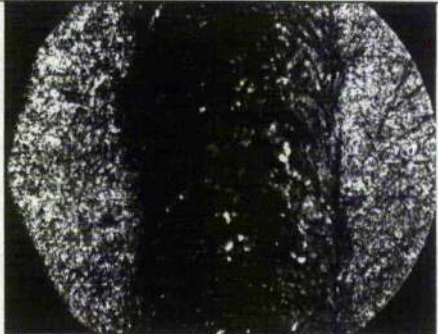
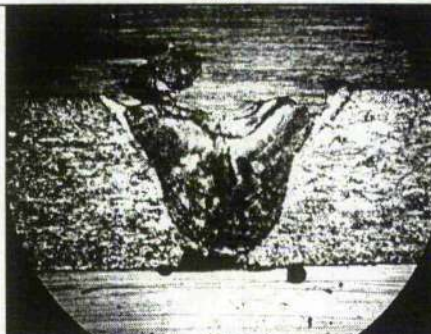
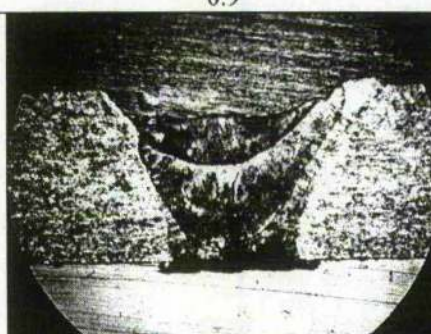
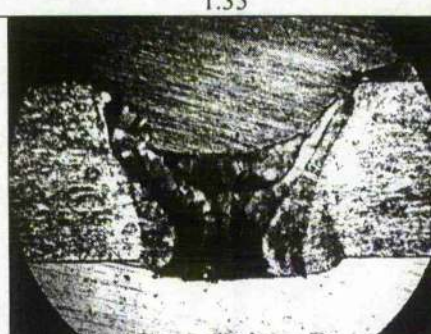
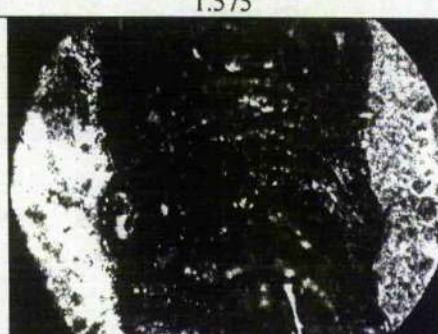
<p>10</p> <p>50J</p> <p>8Hz</p> <p>7 msec</p> <p>2.9 mm/sec</p> <p>c</p>		
<p>O</p>	<p>1.5</p>	<p>1.8</p>

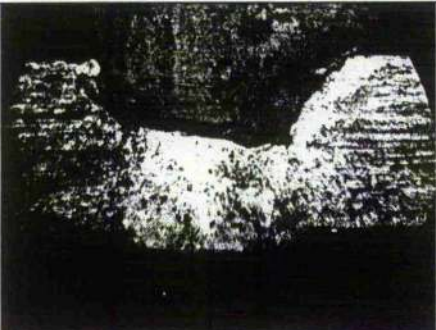
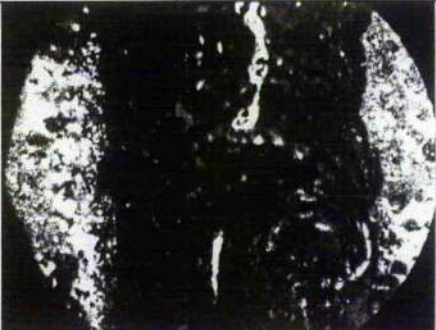
A-1-2

Pulse energy alteration to the fusion size on 6082-T6(SURFACE ROUGHNESS EFFECT)

O / X : weld crack formation

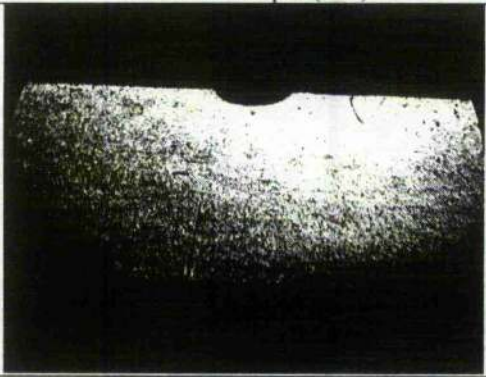
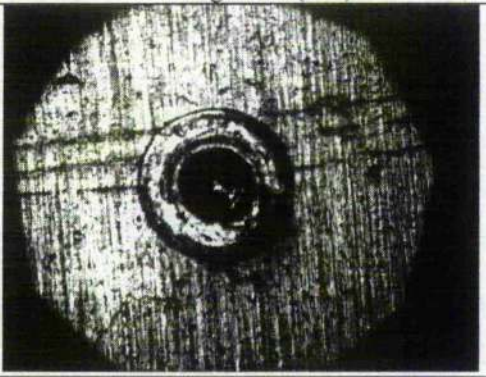
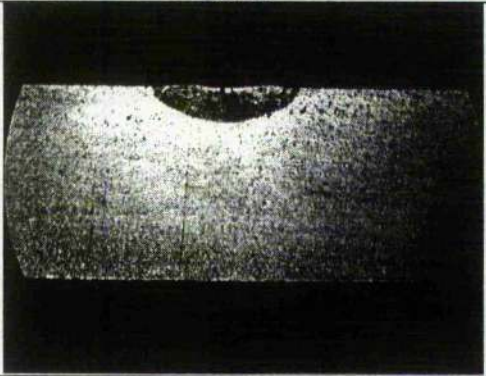
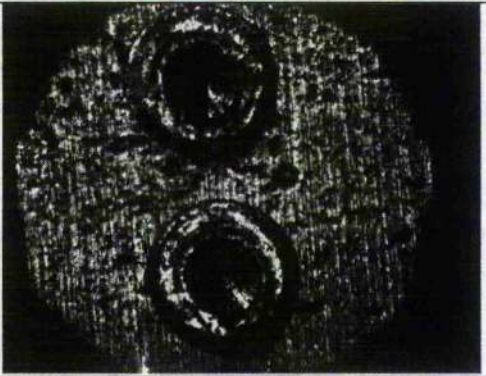
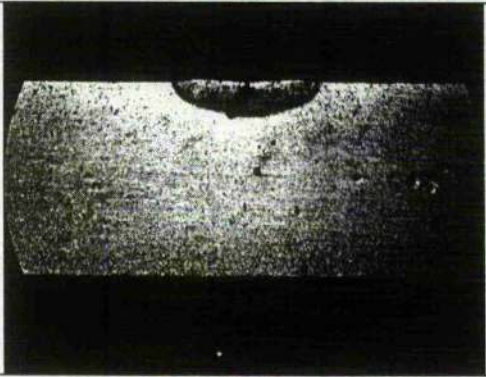
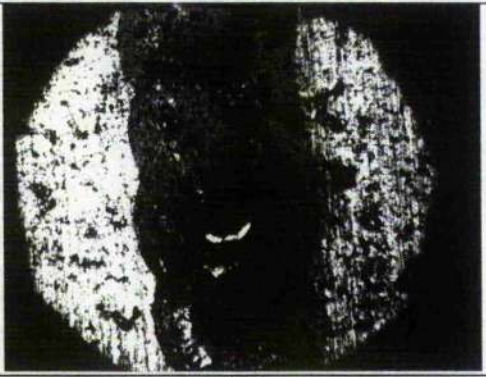
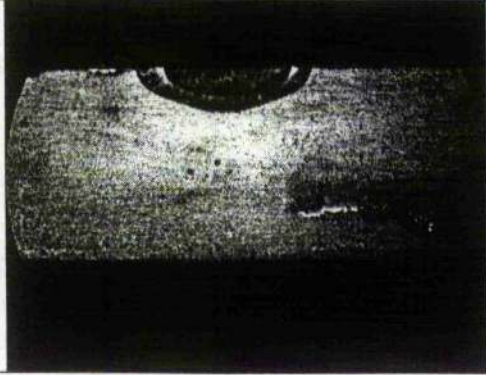
	Penetration depth (mm)	Welding width (mm)
1 5J 8Hz 7msec 2.9m m/sec		
X	0.18	0.3
2 10J 8Hz 7msec 2.9m m/sec		
X	0.2	0.6
3 15J 8Hz 7msec 2.9m m/sec		
X	0.3	0.675
4 20J 8Hz 7msec 2.9m m/sec		
O	0.345	0.9

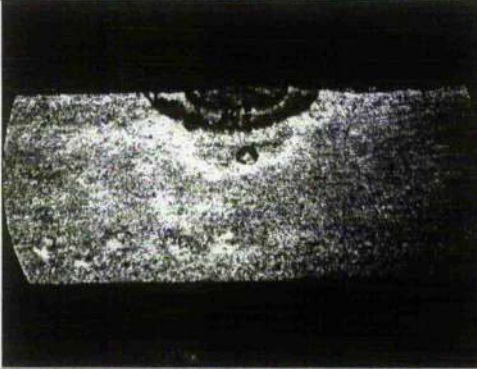
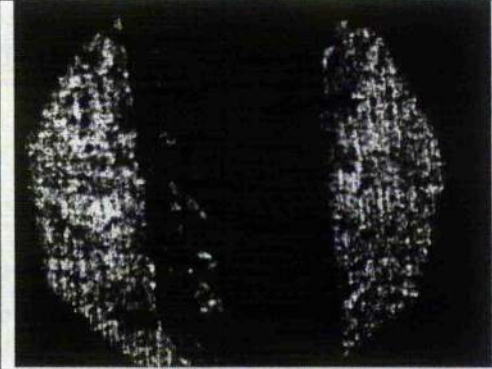
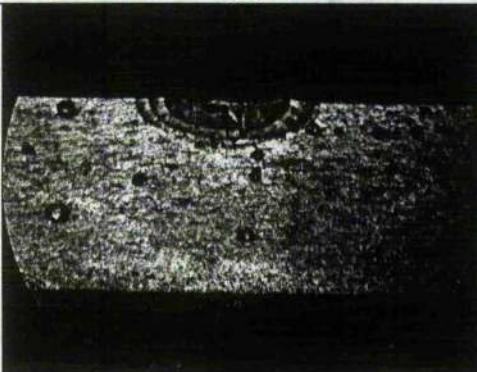
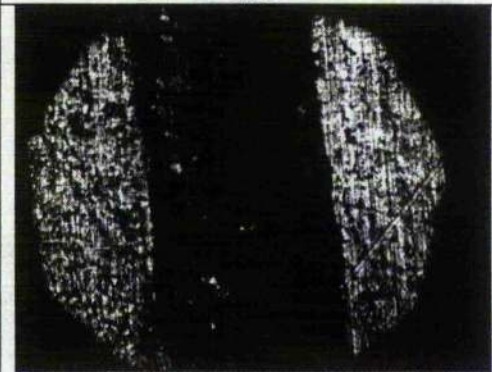
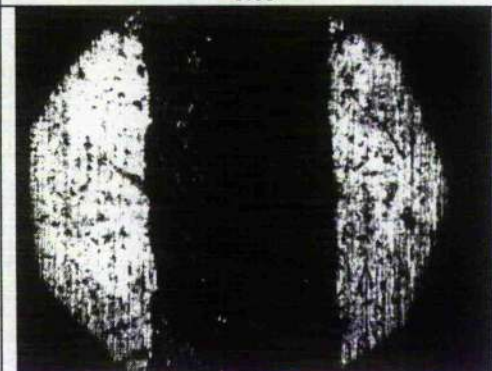
<p>5</p> <p>25J 8Hz 7msec 2.9m m/sec</p>		
<p>X</p>	<p>0.48</p>	<p>1.125</p>
<p>6</p> <p>30J 8Hz 7msec 2.9m m/sec</p>		
<p>O</p>	<p>0.75</p>	<p>1.35</p>
<p>7</p> <p>35J 8Hz 7msec 2.9m m/sec</p>		
<p>O</p>	<p>0.9</p>	<p>1.5</p>
<p>8</p> <p>40J 8Hz 7msec 2.9m m/sec</p>		
<p>O</p>	<p>1.35</p>	<p>1.575</p>
<p>9</p> <p>45J 8Hz 7msec 2.9m m/sec</p>		
<p>O</p>	<p>1.5</p>	<p>1.68</p>

<p>10</p> <p>50J 8Hz 7msec 2.9m m/sec</p>		
<p>O</p>	<p>1.5</p>	<p>1.725</p>

A-1-3

Frequency alteration to the fusion size (6082-T6) O / X : Welding crack formation

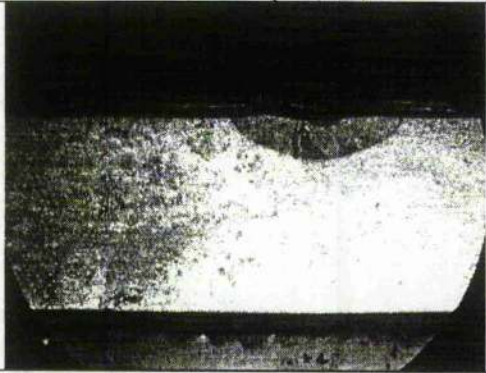
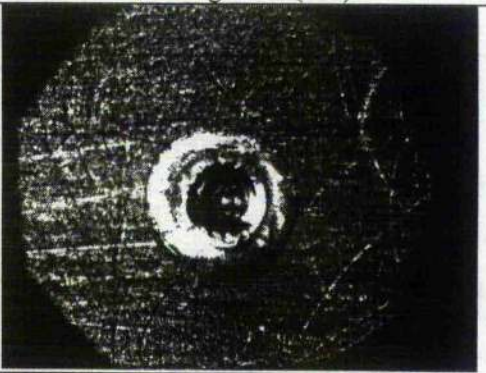
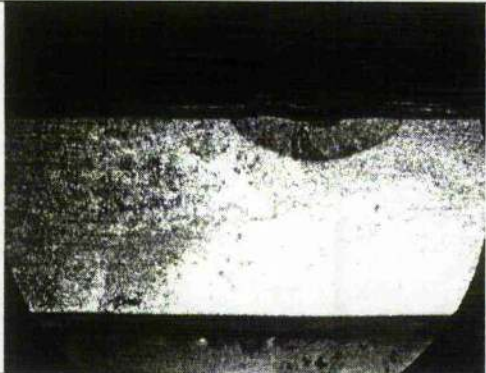
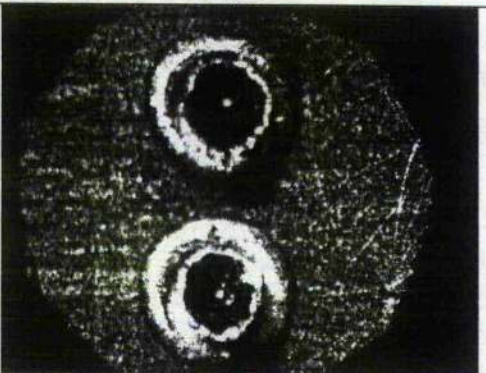
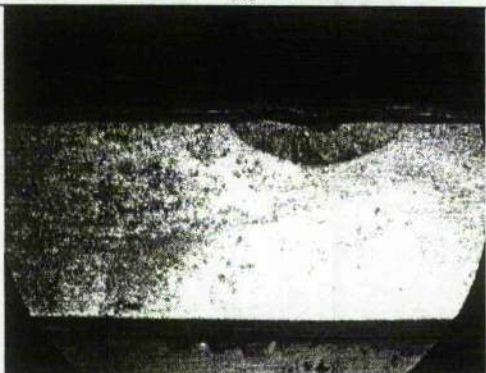
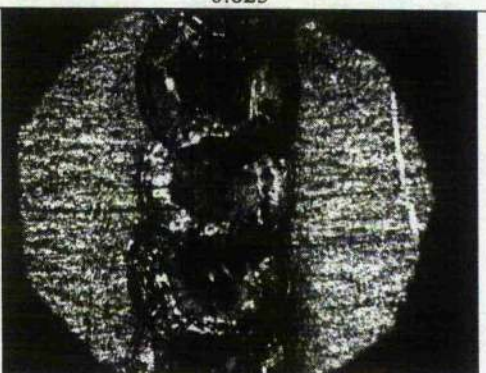
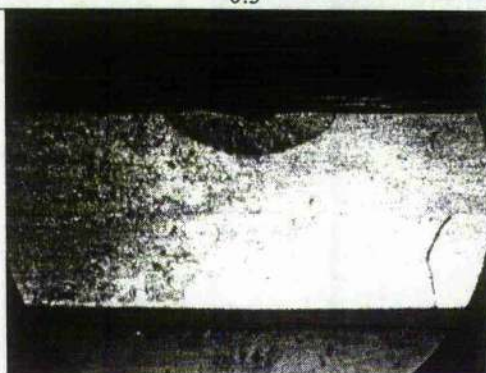
	Penetration depth (mm)	Welding width (mm)
1 25J 1Hz 7msec 2.9mm /sec		
X	0.225	0.9
2 25J 2Hz 7msec 2.9mm /sec		
X	0.245	0.9
3 25J 4Hz 7msec 2.9mm /sec		
X	0.3	0.9
4 25J 6Hz 7msec 2.9mm /sec		
X	0.33	0.975

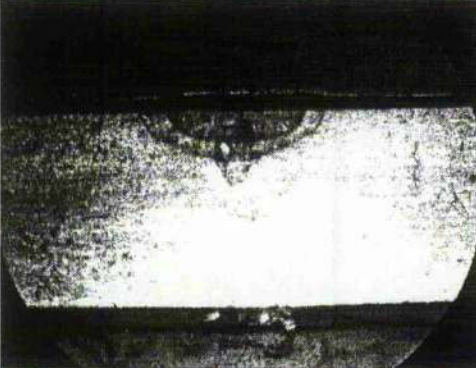
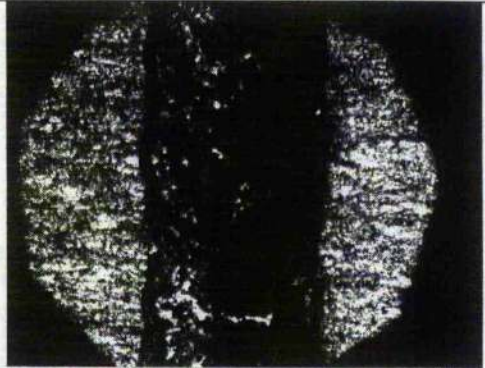
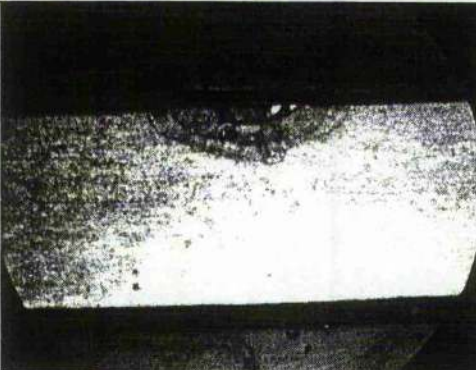
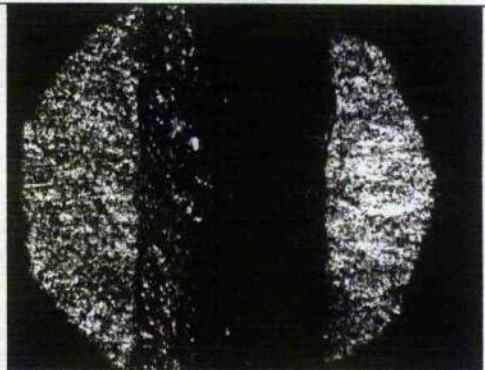
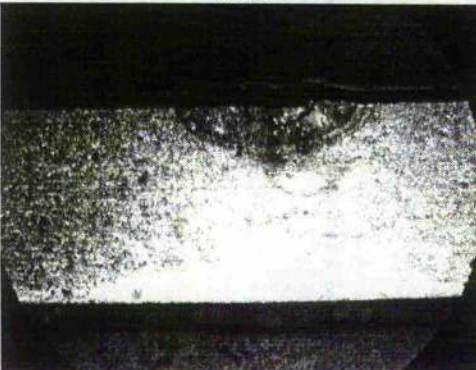
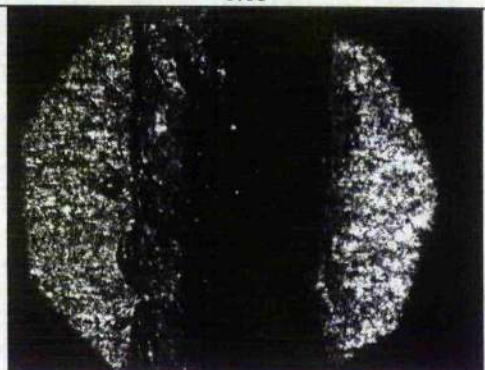
<p>5</p> <p>25J</p> <p>8Hz 7msec 2.9mm /sec</p>		
<p>X</p>	<p>0.36</p>	<p>1.05</p>
<p>6</p> <p>25J</p> <p>12Hz 7msec 2.9mm /sec</p>		
<p>O</p>	<p>0.375</p>	<p>1.05</p>
<p>7</p> <p>25J</p> <p>16Hz 7msec 2.9mm /sec</p>		
<p>O</p>	<p>0.45</p>	<p>1.05</p>

A-1-4

Frequency alteration to the fusion size (6082-T6)

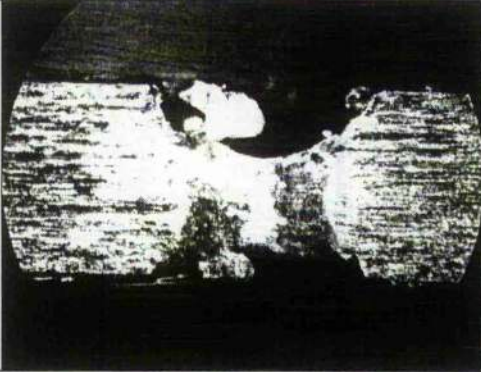
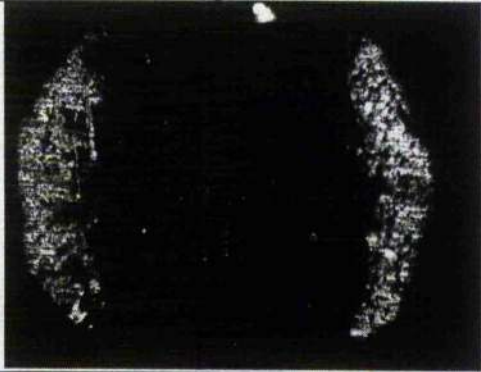
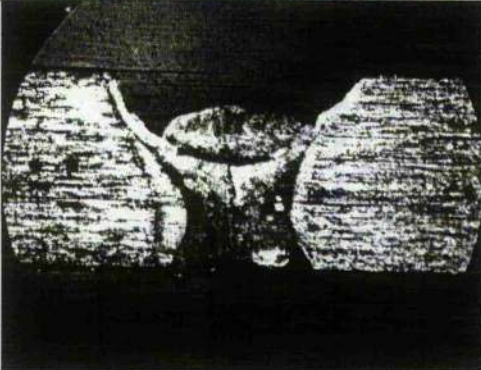
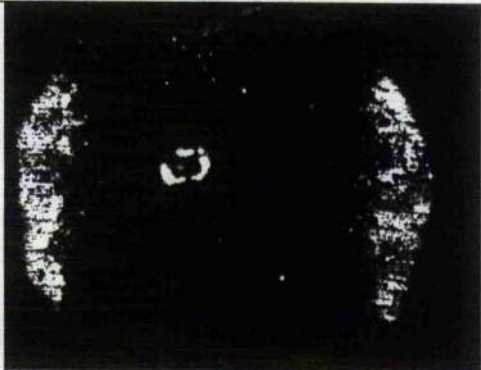
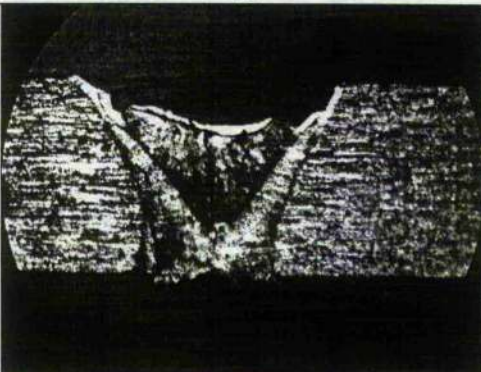
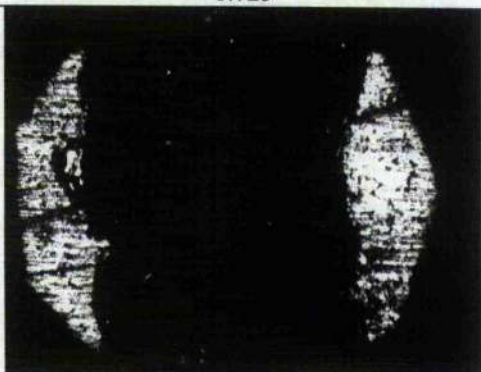
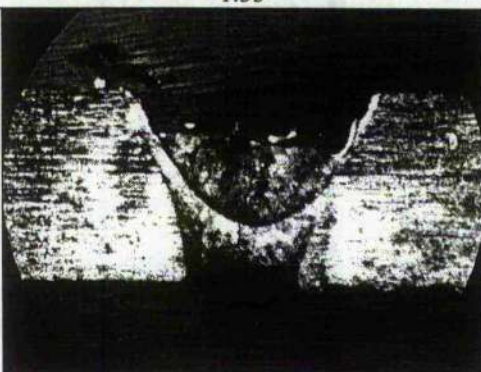
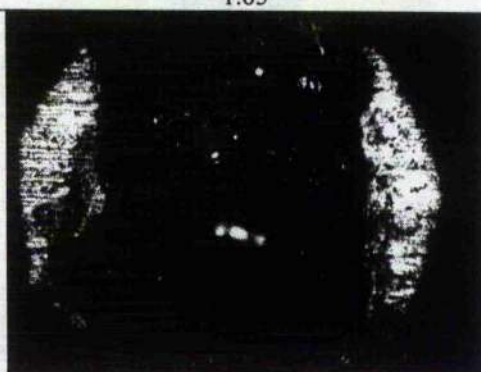
O / X : crack formation

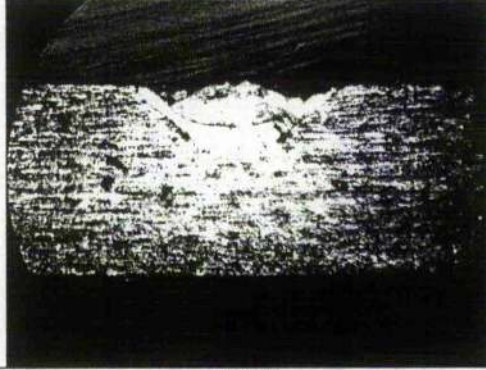
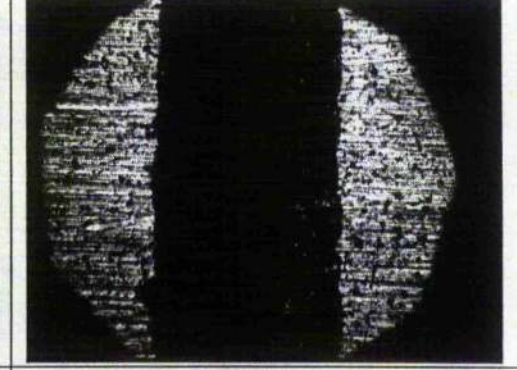
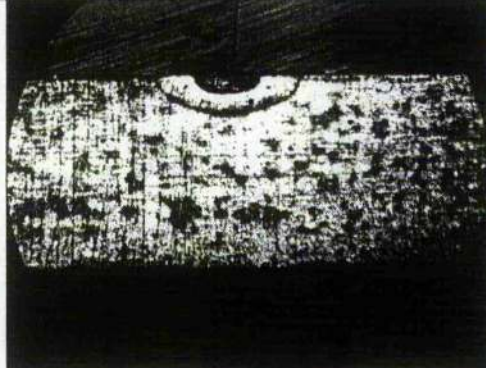
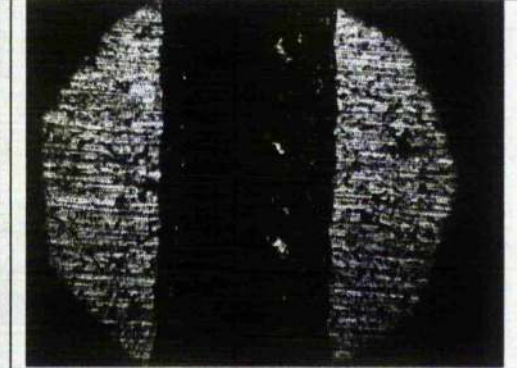
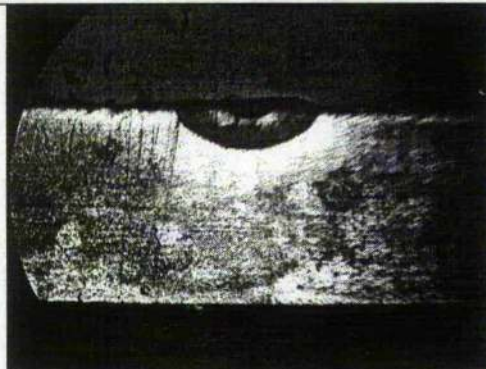
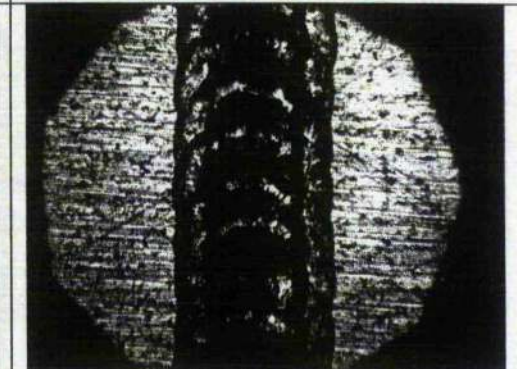
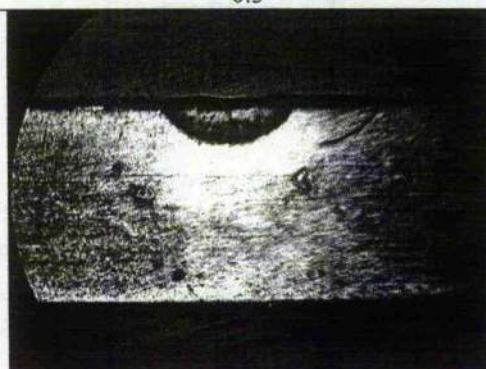
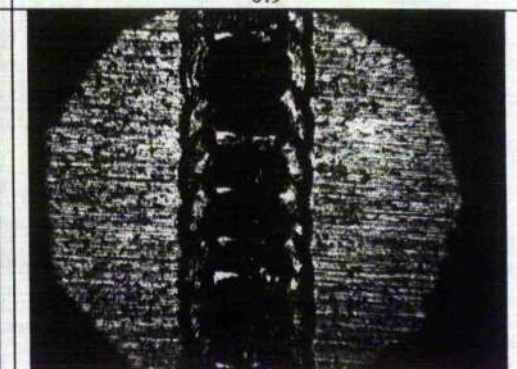
	Penetration depth (mm)	Welding width (mm)
1		
25J 1Hz 7msec 2.9mm/sec		
X	0.3	0.825
2		
25J 2Hz 7msec 2.9mm/sec		
X	0.3	0.825
3		
25J 4Hz 7msec 2.9mm/sec		
X	0.3	0.9
4		
25J 6Hz 7msec 2.9mm/sec		
X	0.345	1.01

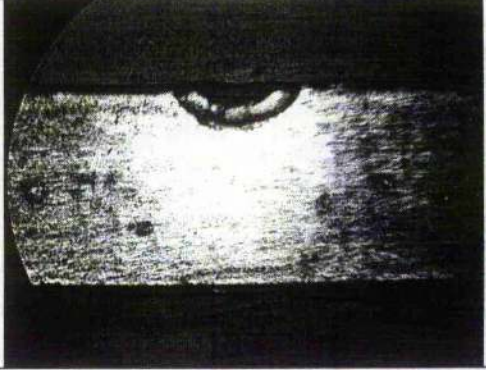
<p>5</p> <p>25J</p> <p>8Hz 7msec 2.9mm /sec</p>		
<p>O</p>	<p>0.345</p>	<p>1.05</p>
<p>6</p> <p>25J</p> <p>12Hz 7msec 2.9mm /sec</p>		
<p>O</p>	<p>0.375</p>	<p>1.05</p>
<p>7</p> <p>25J</p> <p>16Hz 7msec 2.9mm /sec</p>		
<p>O</p>	<p>0.42</p>	<p>1.08</p>

Pulse duration to the fusion size (6082-T6)

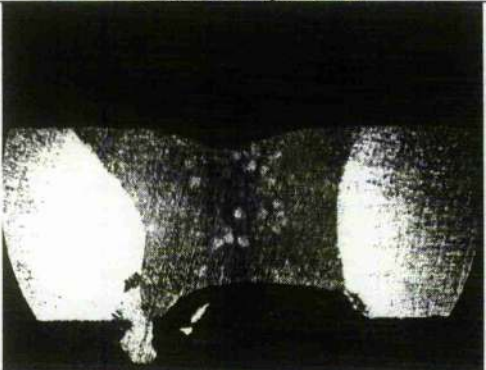
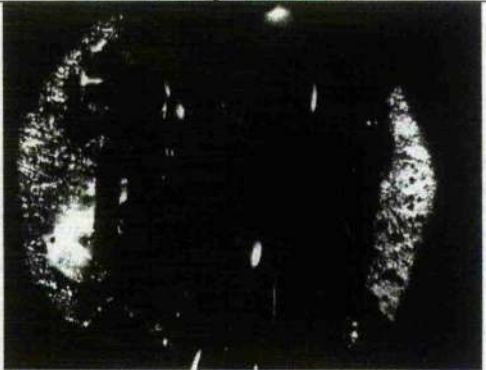
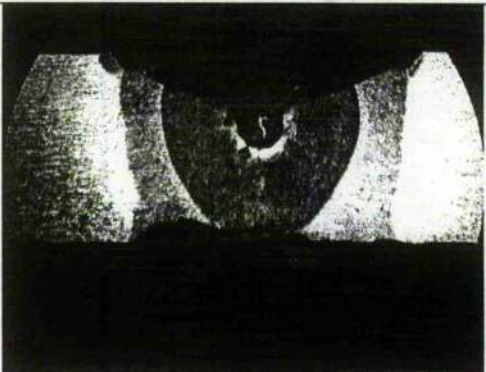
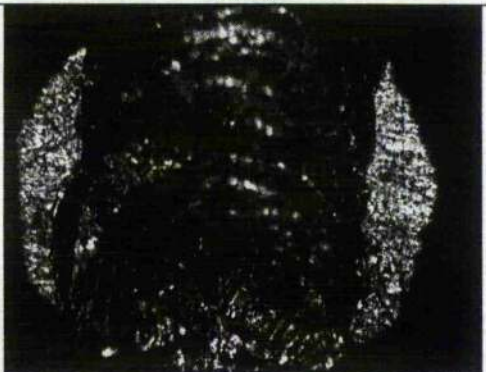
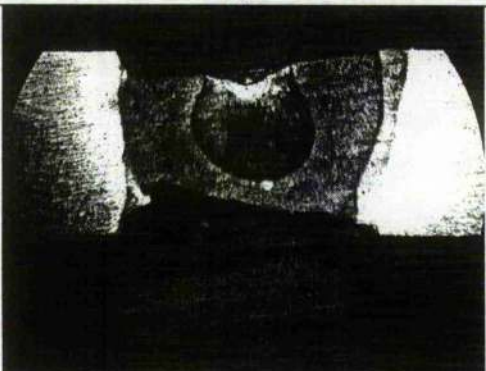
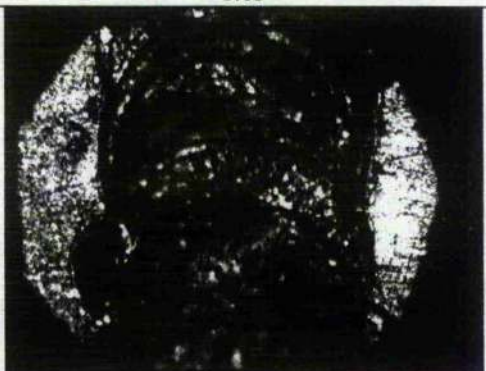
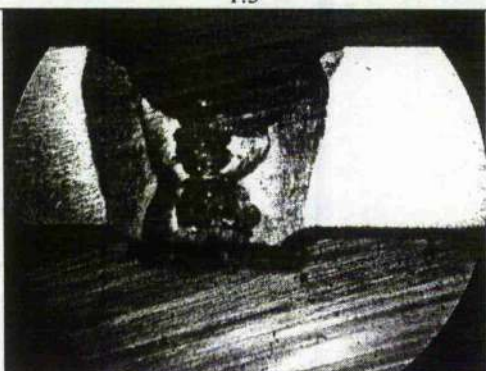
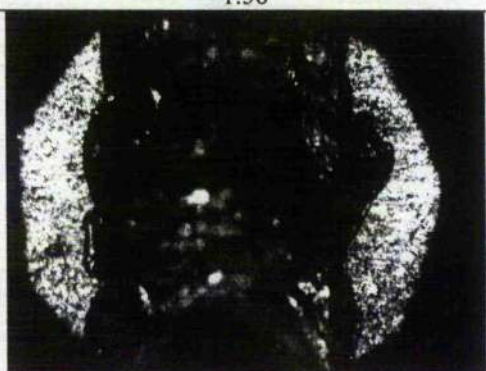
O / X : crack formation

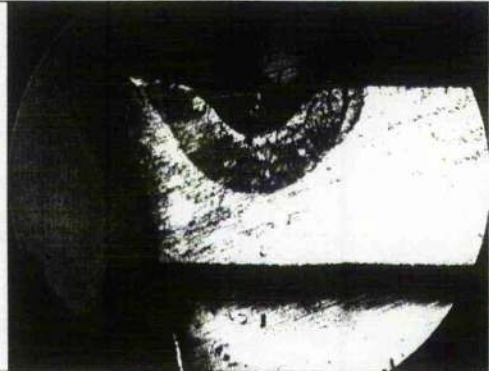
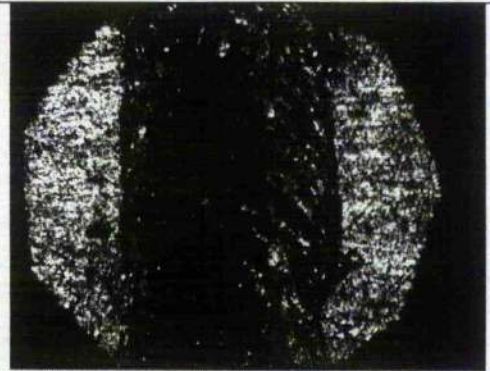
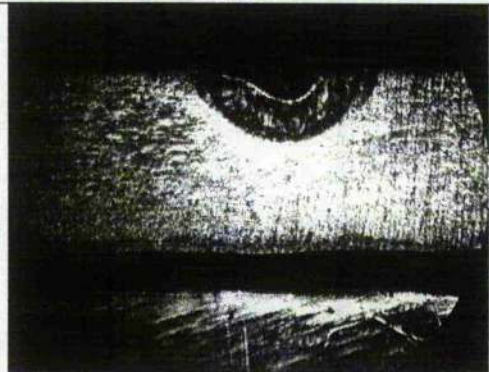
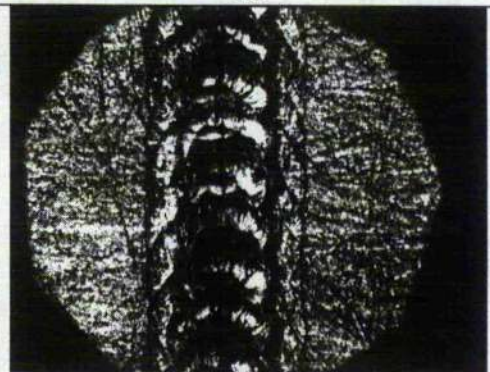
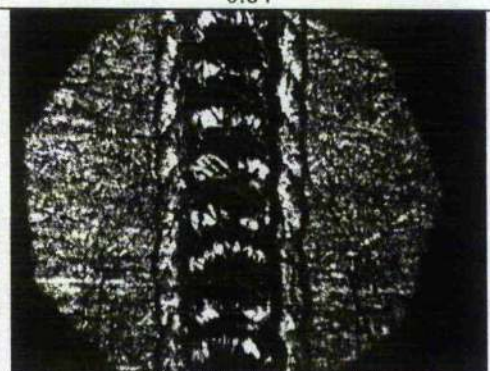
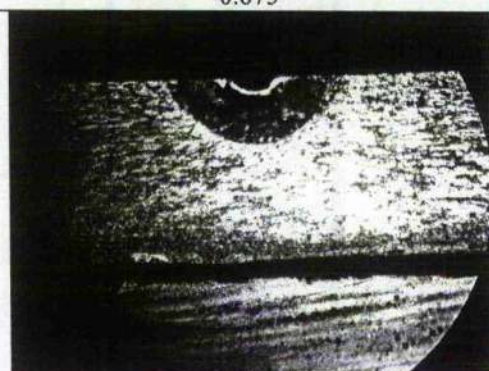
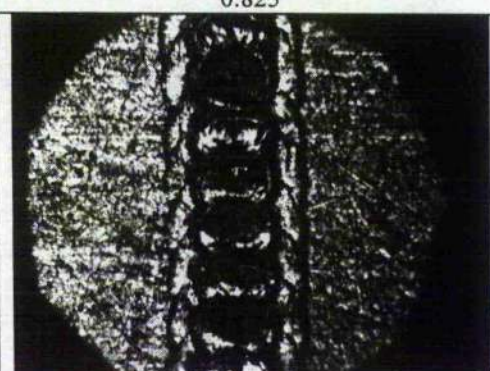
	Penetration depth (mm)	Welding width (mm)
<p>1</p> <p>35J 8Hz 5msec 2.9mm /sec</p>		
O	1.5	1.725
<p>2</p> <p>35J 8Hz 6.2 msec 2.9mm /sec</p>		
O	1.5	1.725
<p>3</p> <p>35J 8Hz 7.5 msec 2.9mm /sec</p>		
O	1.35	1.65
<p>4</p> <p>35J 8Hz 8.8 msec 2.9mm /sec</p>		
O	1.05	1.575

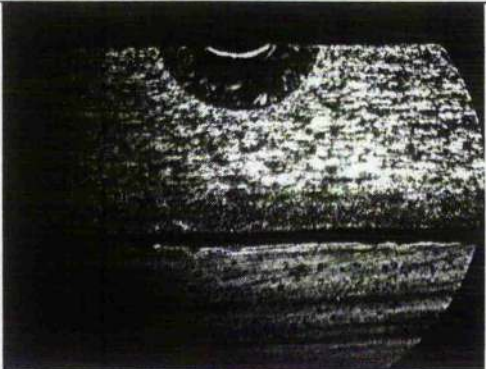
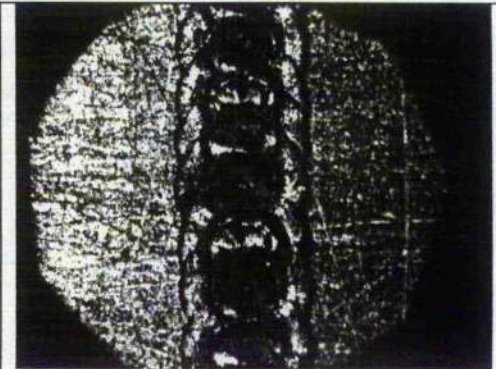
<p>5</p> <p>35J 8Hz 10 msec</p> <p>2.9mm /sec</p>		
X	0.675	1.05
<p>6</p> <p>35J 8Hz 12.5 msec</p> <p>2.9mm /sec</p>		
X	0.315	0.93
<p>7</p> <p>35J 8Hz 15 msec</p> <p>2.9mm /sec</p>		
X	0.3	0.9
<p>8</p> <p>35J 8Hz 17.5 msec</p> <p>2.9mm /sec</p>		
X	0.3	0.75

9 35J 8Hz 19.9 msec 2.9mm /sec		
X	0.285	0.675

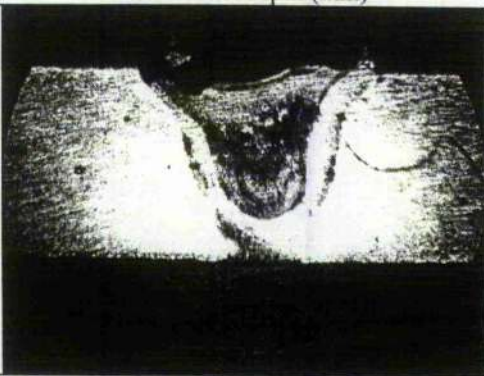
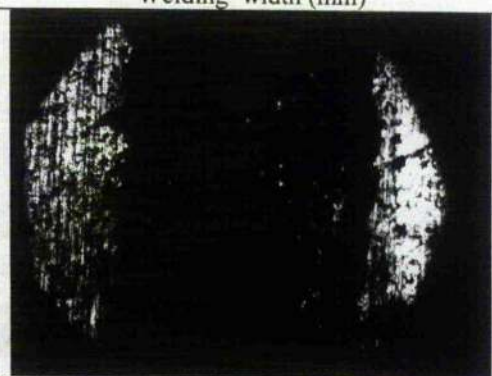
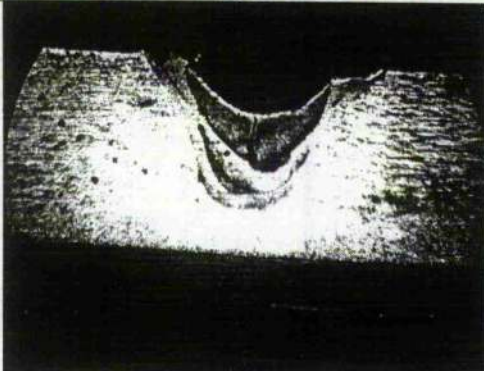
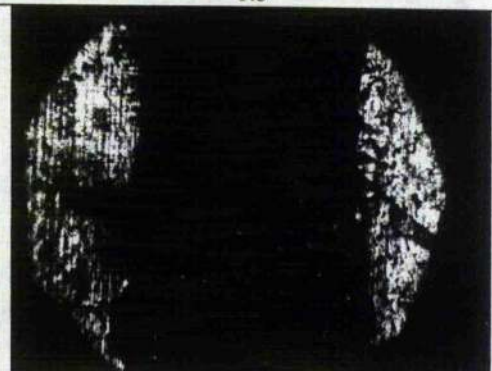
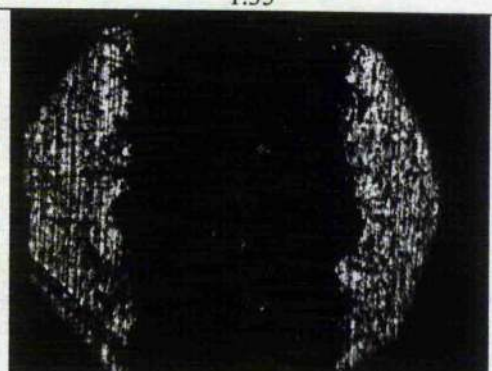
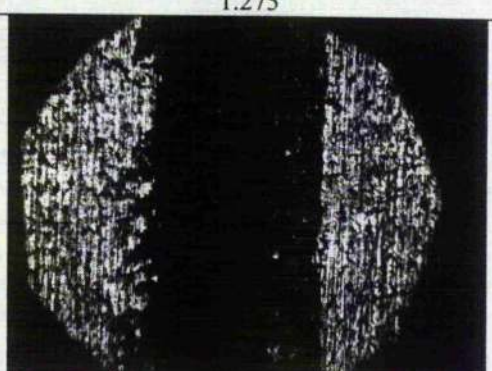
Pulse duration alteration to the fusion size in 35J of pulse energy (6082-T6) O/X : crack formation

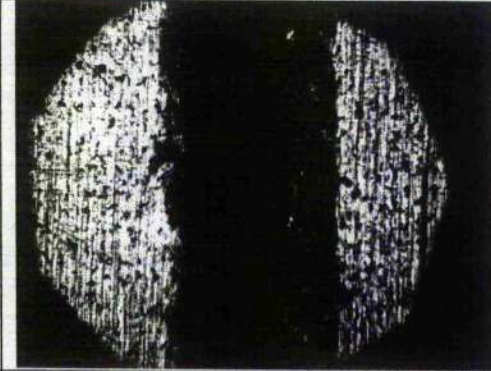
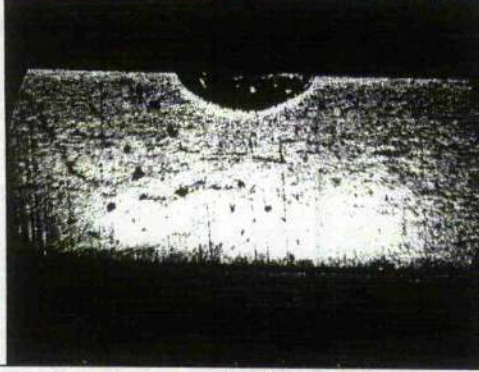
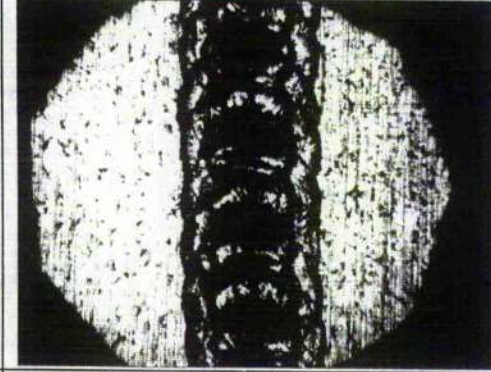
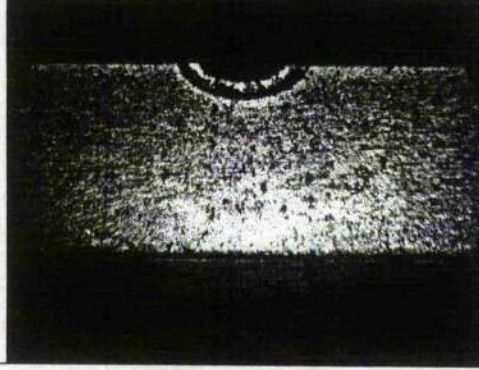
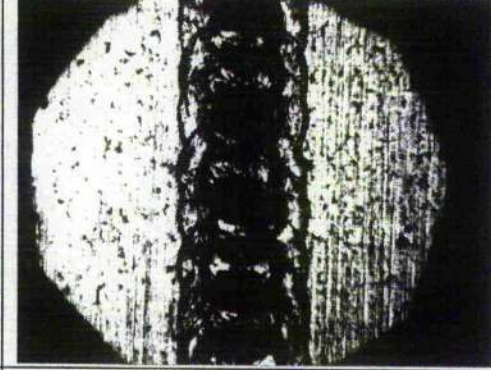
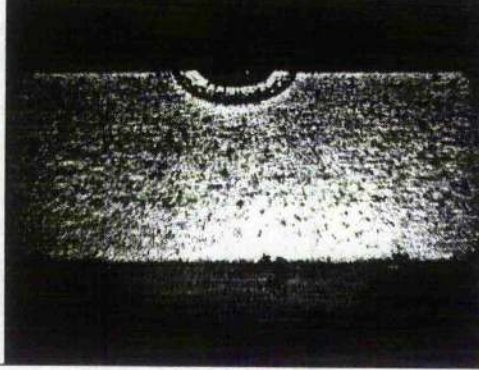
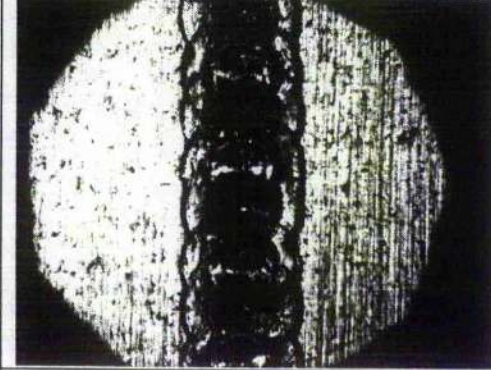
	Penetration depth (mm)	Welding width (mm)
<p>1</p> <p>35J 8Hz</p> <p>5msec 2.9mm /sec</p>  		
	1.5	1.725
<p>2</p> <p>35J 8Hz</p> <p>6.2 msec 2.9mm /sec</p>  		
	1.5	1.65
<p>3</p> <p>35J 8Hz</p> <p>7.5 msec 2.9mm /sec</p>  		
	1.5	1.56
<p>4</p> <p>35J 8Hz</p> <p>8.8 msec 2.9mm /sec</p>  		
	1.5	1.5

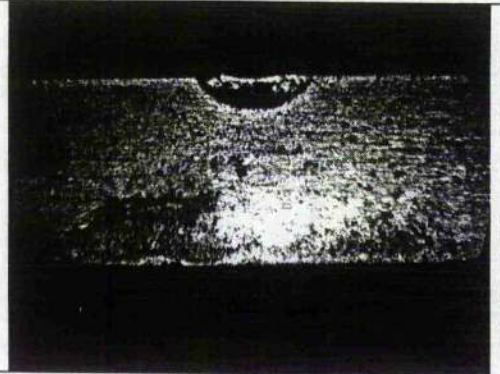
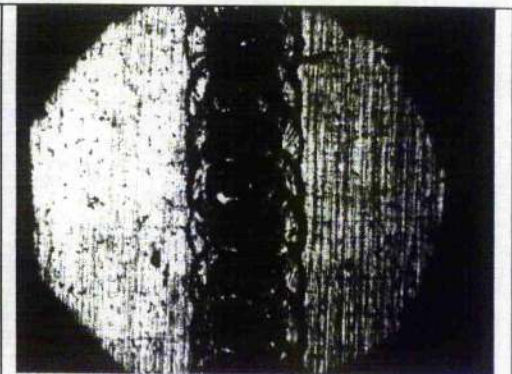
<p>5</p> <p>35J 8Hz</p> <p>10 msec 2.9mm /sec</p>		
O	0.9	1.2
<p>6</p> <p>35J 8Hz</p> <p>12.5 msec 2.9mm /sec</p>		
O	0.72	0.84
<p>7</p> <p>35J 8Hz</p> <p>15 msec 2.9mm /sec</p>		
O	0.675	0.825
<p>8</p> <p>35J 8Hz</p> <p>17.5 msec 2.9mm /sec</p>		
X	0.66	0.75

9 35J 8Hz 19.9 msec 2.9mm /sec		
X	0.45	0.675

Pulse duration alteration to the fusion size in 30J of pulse energy(6082-T6) O/X : crack formation

	Penetration depth (mm)	Welding width (mm)
<p>1</p> <p>30J 8Hz 5msec</p> <p>2.9mm /sec</p>		
X	1.2	1.5
<p>2</p> <p>30J 8Hz 6.2 msec</p> <p>2.9mm /sec</p>		
O	1.17	1.35
<p>3</p> <p>30J 8Hz 7.5 msec</p> <p>2.9mm /sec</p>		
X	0.75	1.275
<p>4</p> <p>30J 8Hz 8.8 msec</p> <p>2.9mm /sec</p>		
O	0.675	1.05

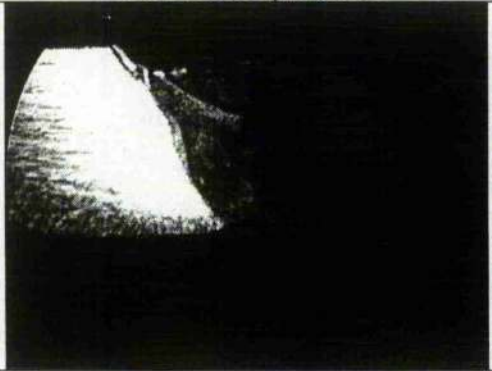
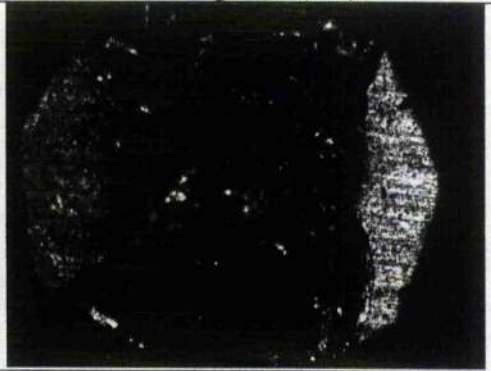
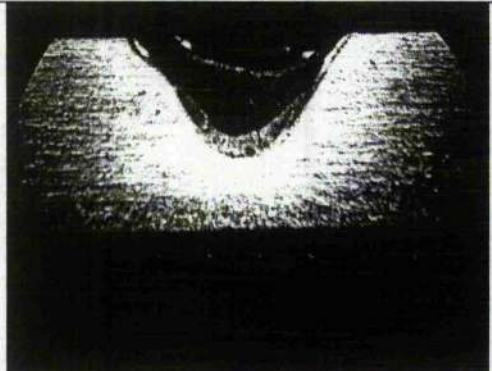
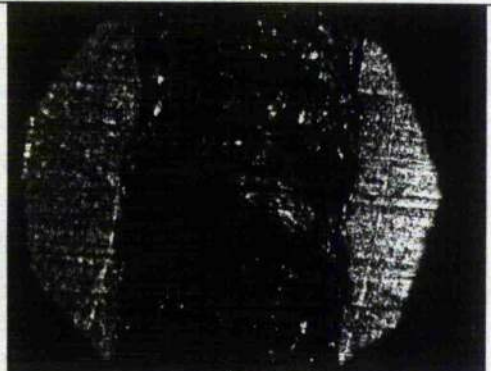
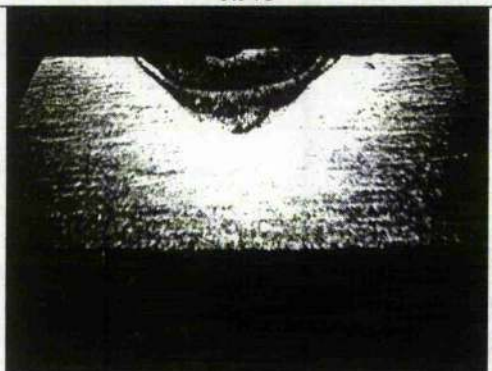
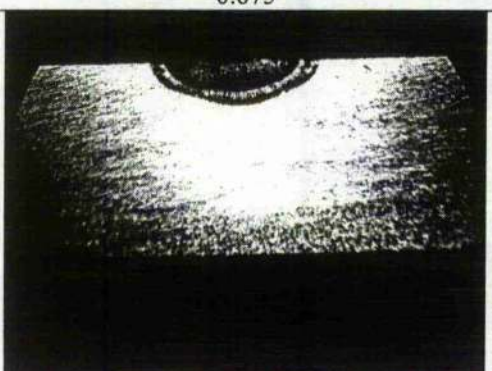
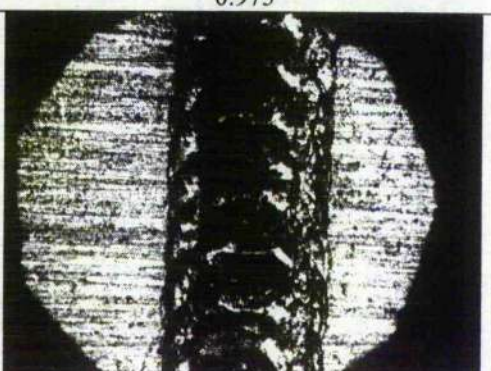
<p>5</p> <p>30J 8Hz 10 msec</p> <p>2.9mm /sec</p>		
<p>X</p>	<p>0.45</p>	<p>0.975</p>
<p>6</p> <p>30J 8Hz 12.5 msec</p> <p>2.9mm /sec</p>		
<p>O</p>	<p>0.375</p>	<p>0.78</p>
<p>7</p> <p>30J 8Hz 15 msec</p> <p>2.9mm /sec</p>		
<p>O</p>	<p>0.3</p>	<p>0.75</p>
<p>8</p> <p>30J 8Hz 17.5 msec</p> <p>2.9mm /sec</p>		
<p>O</p>	<p>0.27</p>	<p>0.705</p>

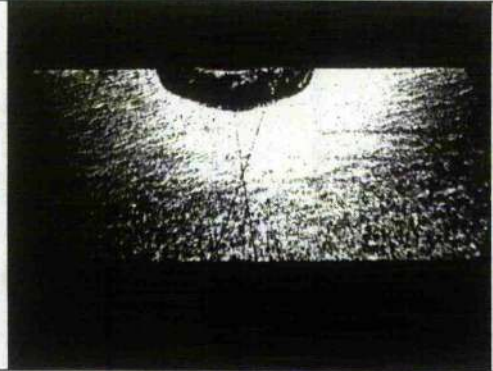
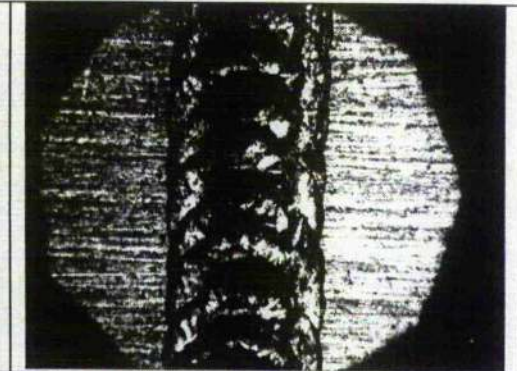
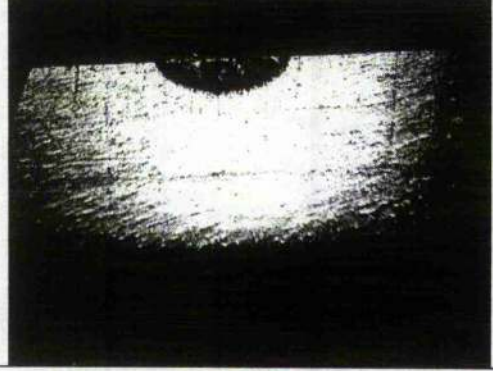
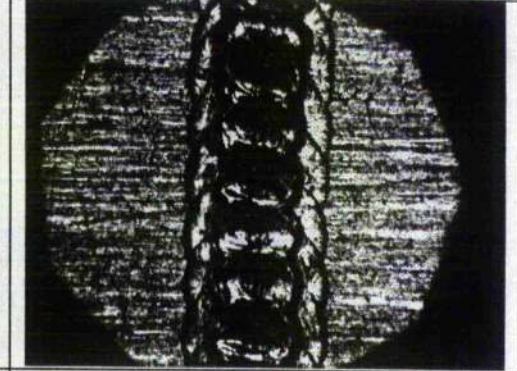
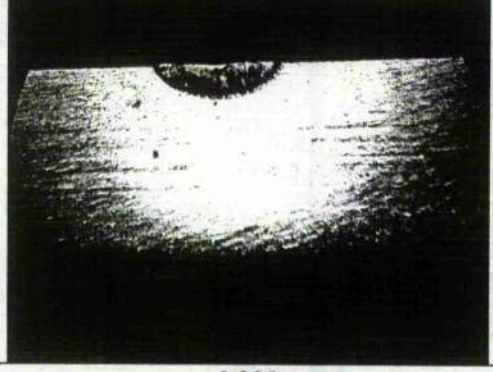
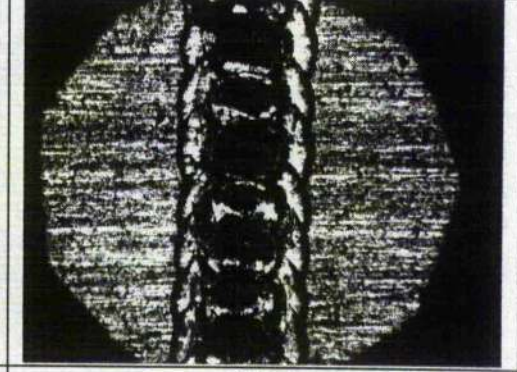
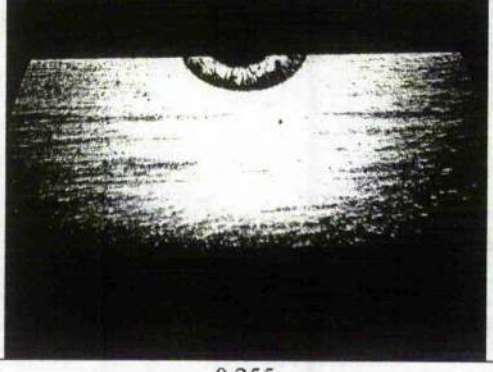
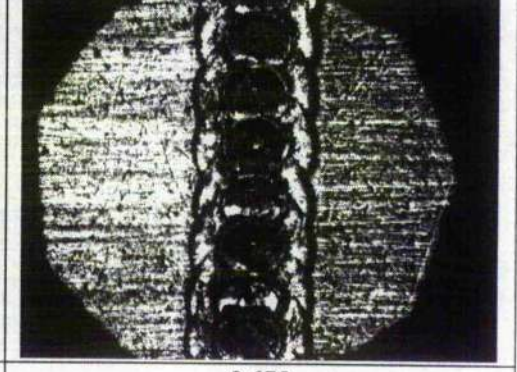
9 30J 8Hz 19.9 msec 2.9mm /sec		
X	0.24	0.675

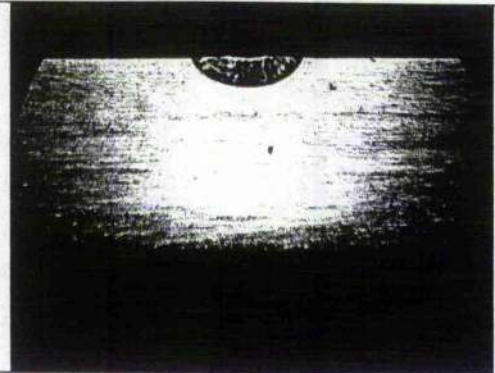
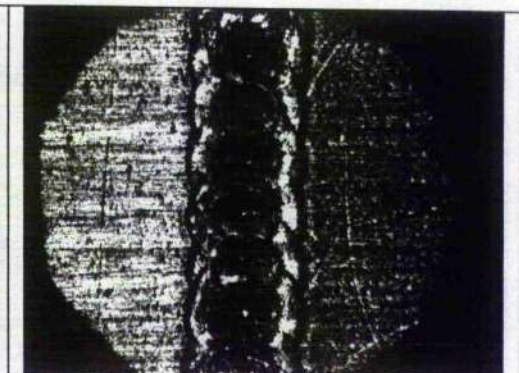
A-1-8

Pulse duration to the fusion size in 30J of pulse energy (6082-T6)

O/X : crack formation

	Penetration depth (mm)	Welding width (mm)
<p>1</p> <p>30J 8Hz</p> <p>5msec 2.6mm /sec</p>		
	1.5	1.5
<p>2</p> <p>30J 8Hz</p> <p>6.2 msec 2.6mm /sec</p>		
	0.975	1.2
<p>3</p> <p>30J 8Hz</p> <p>7.5 msec 2.6mm /sec</p>		
	0.675	0.975
<p>4</p> <p>30J 8Hz</p> <p>8.8 msec 2.6mm /sec</p>		
X	0.45	0.915

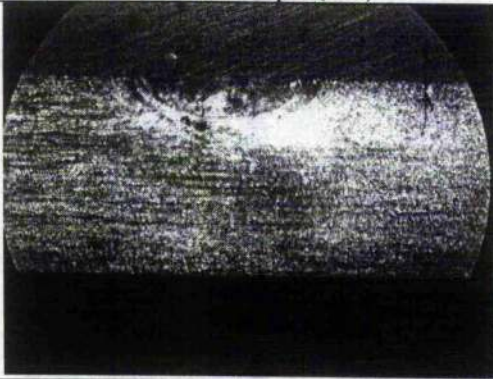
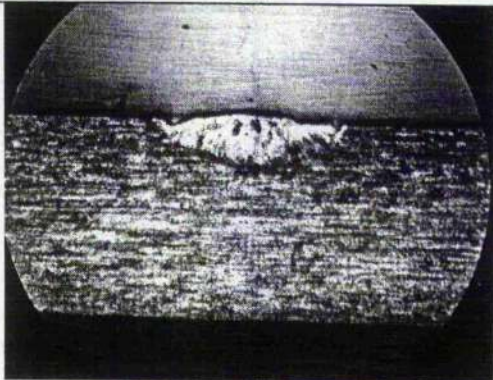
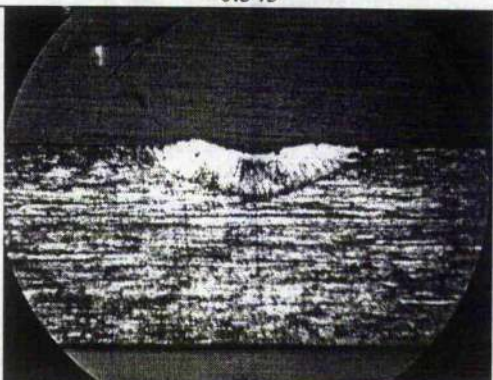
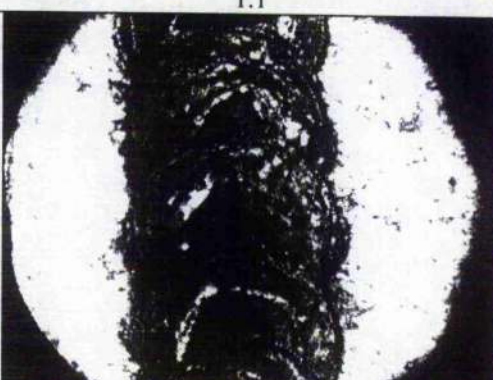
<p>5</p> <p>30J 8Hz</p> <p>10 msec 2.6mm /sec</p>		
<p>X</p>	<p>0.42</p>	<p>0.9</p>
<p>6</p> <p>30J 8Hz</p> <p>12.5 msec 2.6mm /sec</p>		
<p>O</p>	<p>0.315</p>	<p>0.75</p>
<p>7</p> <p>30J 8Hz</p> <p>15 msec 2.6mm /sec</p>		
<p>O</p>	<p>0.285</p>	<p>0.705</p>
<p>8</p> <p>30J 8Hz</p> <p>17.5 msec 2.6mm /sec</p>		
<p>O</p>	<p>0.255</p>	<p>0.675</p>

9 30J 8Hz 19.9 msec 2.6mm /sec		
O	0.225	0.675

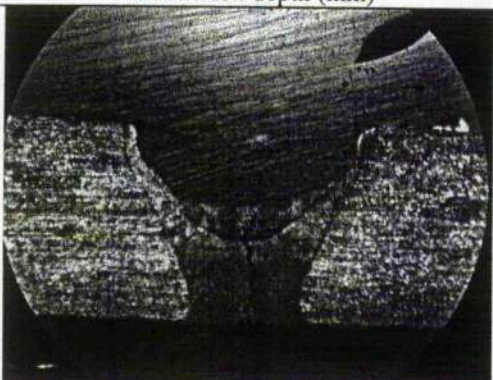
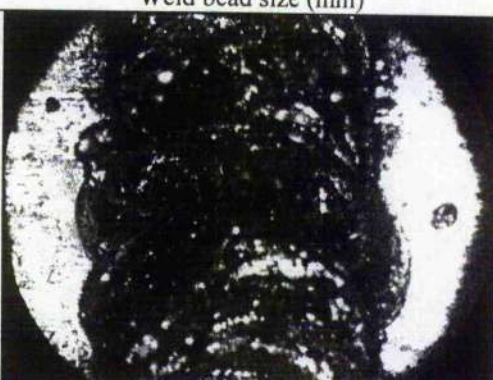
Different welding speed to the fusion size (6082-T6)

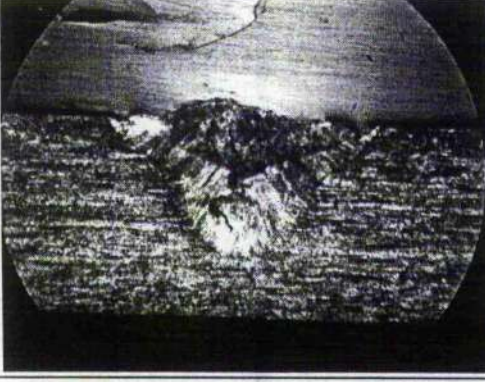
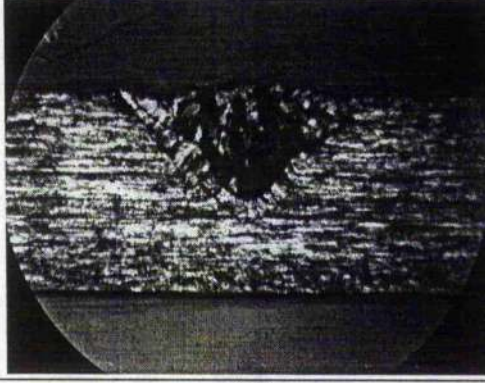
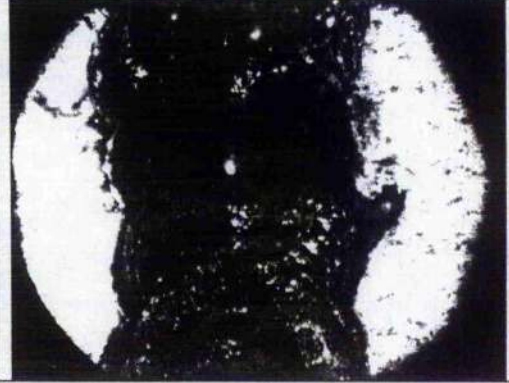
O/X : crack formation

A-1-9-1 30J

	Penetration depth (mm)	Welding width (mm)
1 30J 8Hz 7msec 2.9m m/sec		
X	0.48	1.1
2 30J 8Hz 7msec 4.0m m/sec		
X	0.345	1.1
3 30J 8Hz 7msec 5.8m m/sec		
X	0.315	1.1

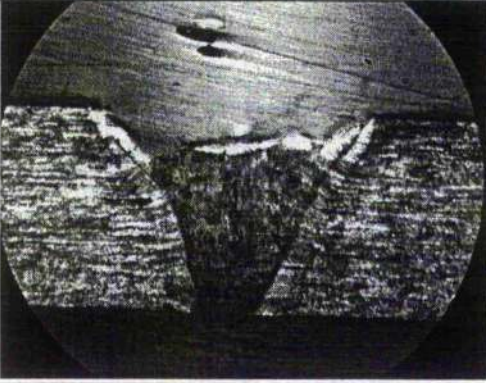
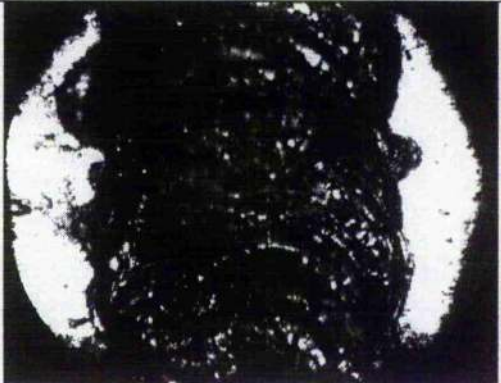
A-1-9-2 40J

	Penetration depth (mm)	Weld bead size (mm)
4 40J 8Hz 7msec 2.9m m/sec		
O	1.5	1.6

5		
40J 8Hz 7msec 4.0m m/sec		
O	1.05	1.4
6		
40J 8Hz 7msec 5.8m m/sec		
O	0.75	1.4

A-1-9-3

50J

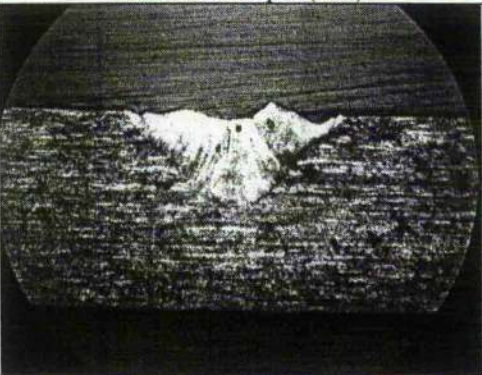
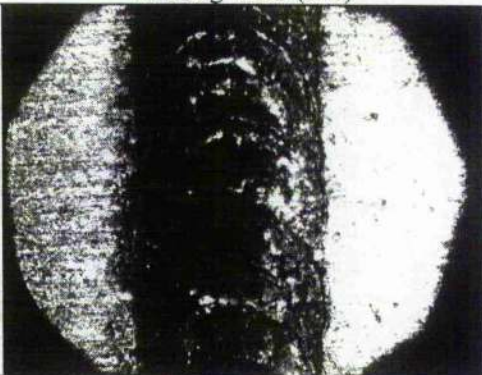
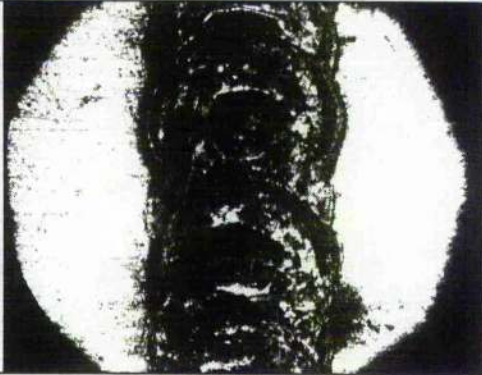
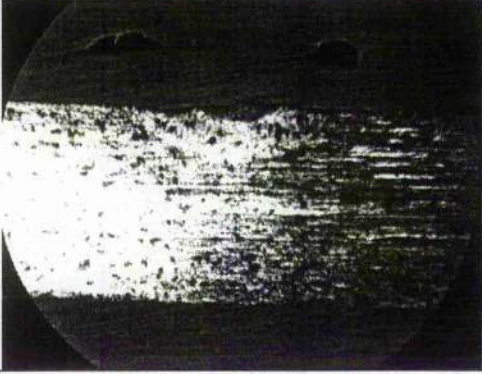
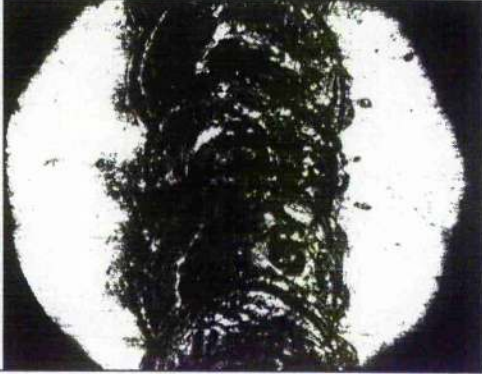
	Penetration depth (mm)	Weld bead size (mm)
7		
50J 8Hz 7msec 2.9m m/sec		
O	1.5	1.7
8		
50J 8Hz 7msec 4.0m m/sec		
O	1.5	1.6

9 50J 8Hz 7msec 5.8m m/sec		
O	1.5	1.6

Different Welding speed to the penetration depth (6082-T6) O/X : crack formation

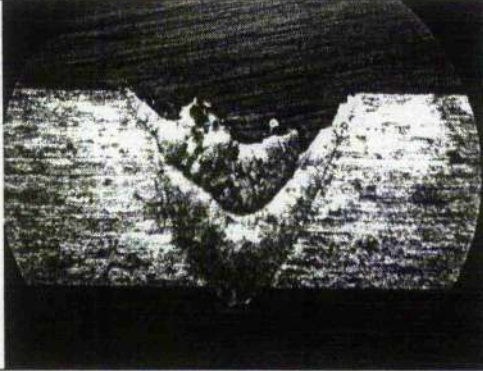
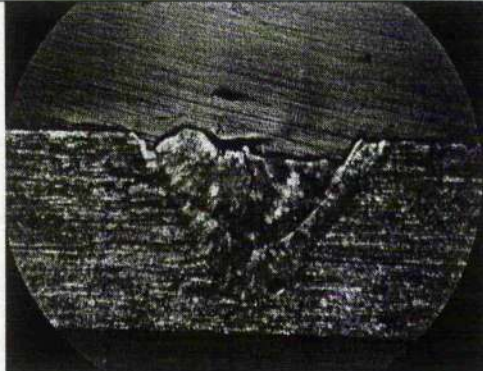
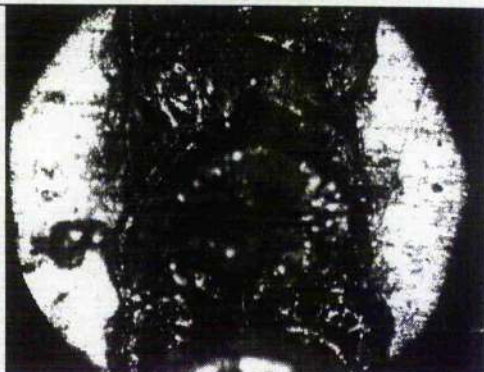
A-1-10-1

30J

	Penetration depth (mm)	Welding width (mm)
<p>1</p> <p>30J 8Hz 7msec</p> <p>2.9mm /sec</p>		
O	0.705	1.1
<p>2</p> <p>30J 8Hz 7msec</p> <p>4.0mm /sec</p>		
O	0.675	1.1
<p>3</p> <p>30J 8Hz 7msec</p> <p>5.8mm /sec</p>		
X	0.6	1.1

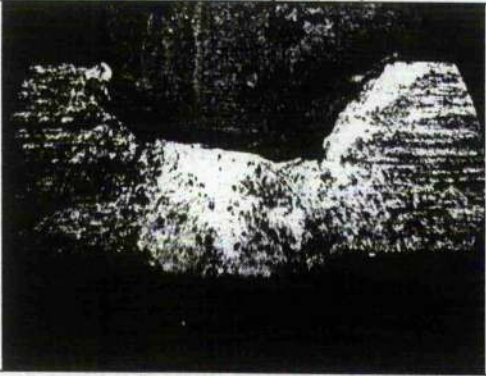
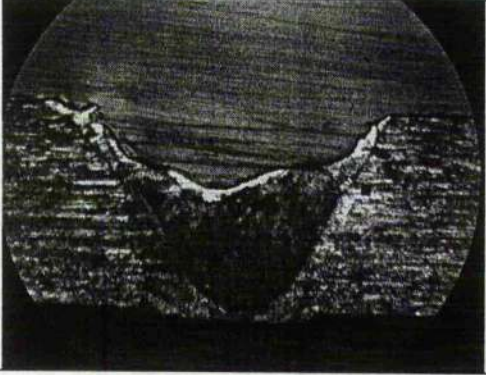
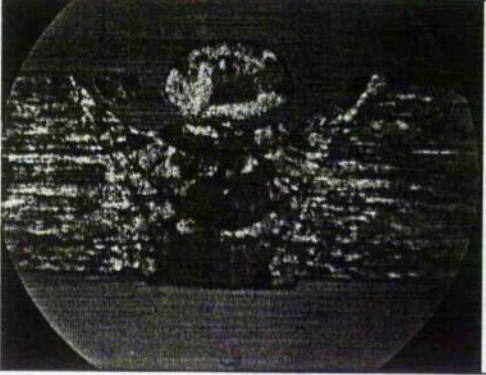
A-1-10-2

40J

	Penetration depth (mm)	Weld bead size (mm)
4 40J 8Hz 7msec 2.9mm /sec		
O	1.35	1.4
5 40J 8Hz 7msec 4.0mm /sec		
O	1.125	1.4
6 40J 8Hz 7msec 5.6mm /sec		
O	0.9	1.4

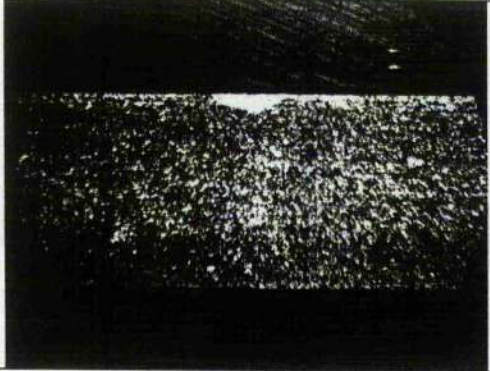
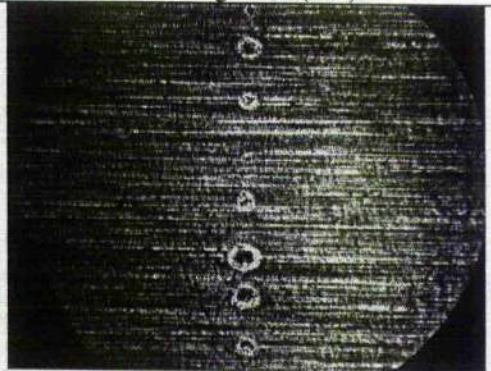
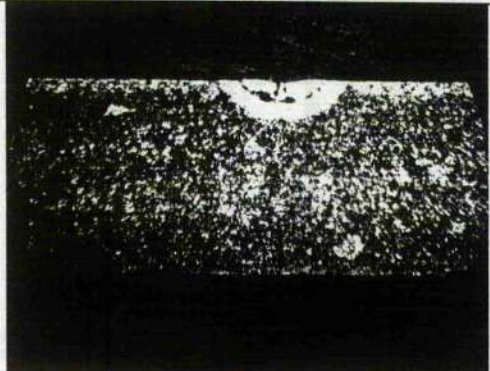
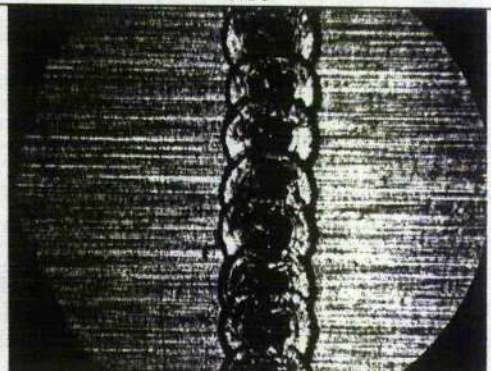
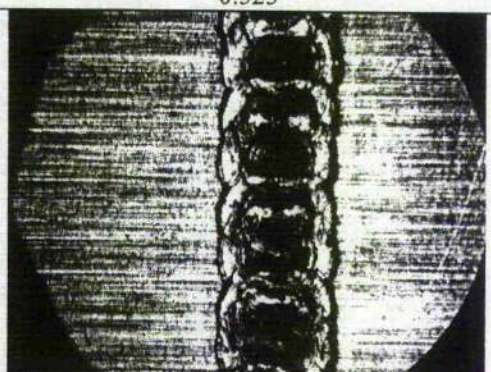
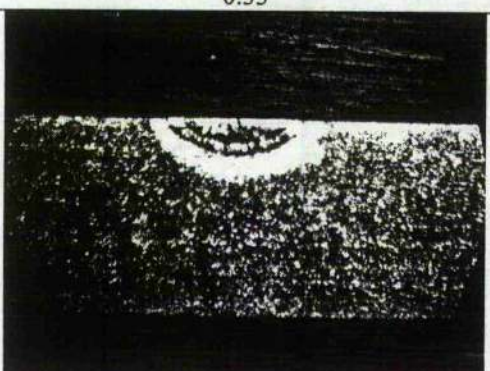
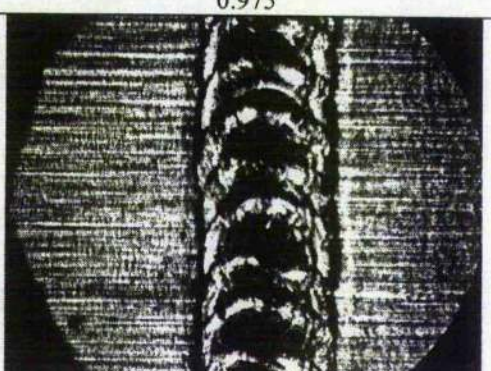
A-1-10-3

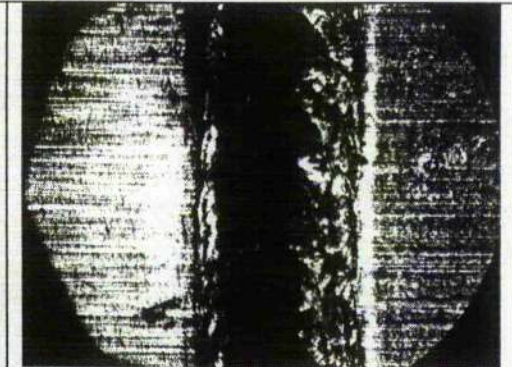
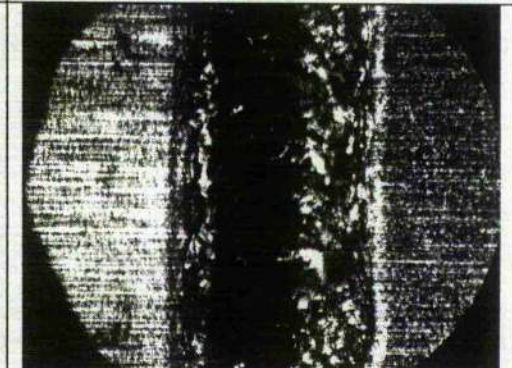
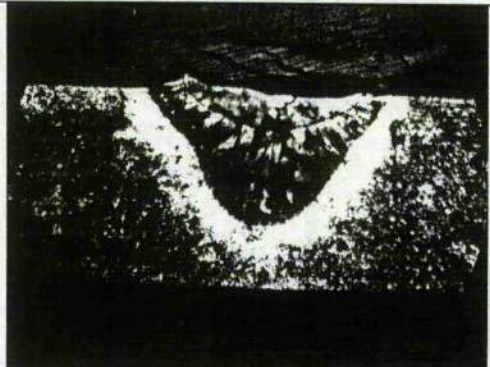
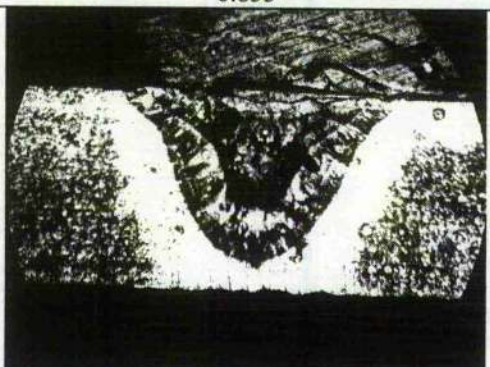
50J

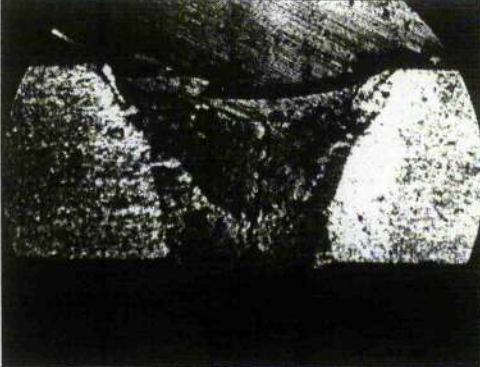
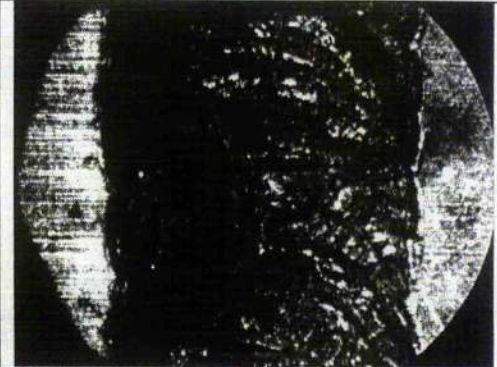
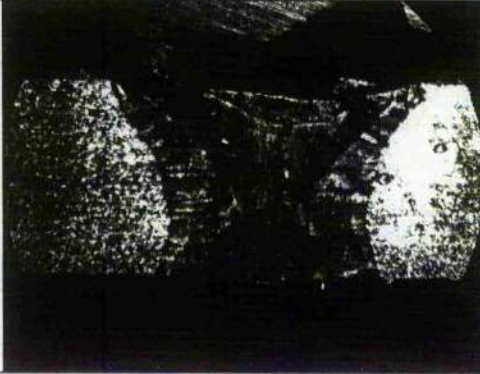
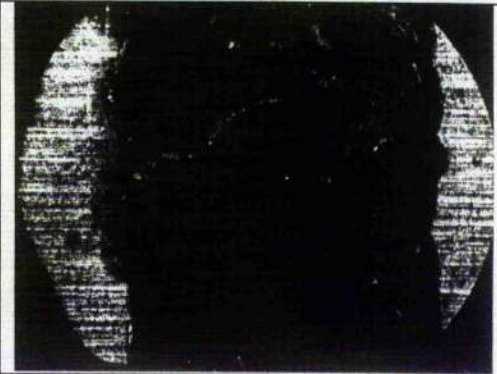
	Penetration depth (mm)	Weld bead size (mm)
<p>7</p> <p>50J 8Hz 7msec</p> <p>2.9mm /sec</p>		
	1.5	1.7
<p>8</p> <p>50J 8Hz 7msec</p> <p>4.0mm /sec</p>		
	1.6	
<p>9</p> <p>50J 8Hz 7msec</p> <p>5.8mm /sec</p>		
	1.5	1.6

B-1-1

Pulse energy alteration to the fusion size (5251-H24) O/X : crack formation

	Penetration depth (mm)	Welding width (mm)
<p>1</p> <p>5J 8Hz 7msec 2.9mm /sec</p> 	0.15	
X		0.18
<p>2</p> <p>10J 8Hz 7msec 2.9mm /sec</p> 	0.24	
O		0.525
<p>3</p> <p>15J 8Hz 7msec 2.9mm /sec</p> 	0.33	
X		0.975
<p>4</p> <p>20J 8Hz 7msec 2.9mm /sec</p> 	0.42	
O		0.825

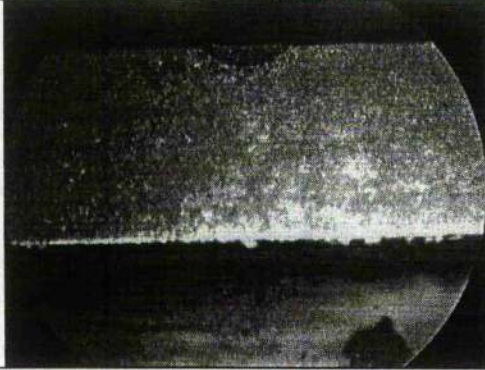
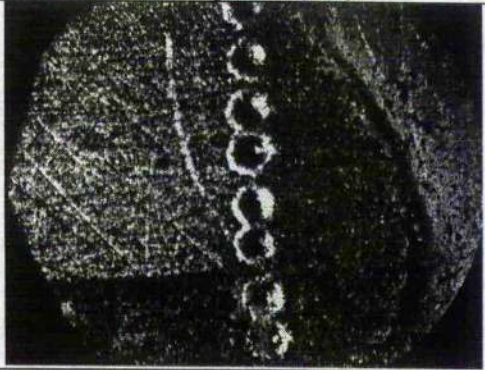
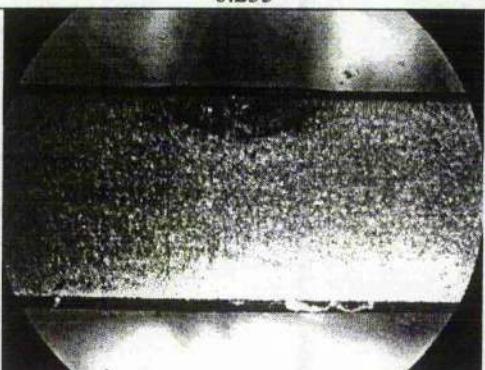
<p>5</p> <p>25J 8Hz 7msec 2.9mm /sec</p>		
O	0.45	0.975
<p>6</p> <p>30J 8Hz 7msec 2.9mm /sec</p>		
O	0.525	1.2
<p>7</p> <p>35J 8Hz 7msec 2.9mm /sec</p>		
O	0.855	1.35
<p>8</p> <p>40J 8Hz 7msec 2.9mm /sec</p>		
X	1.125	1.5

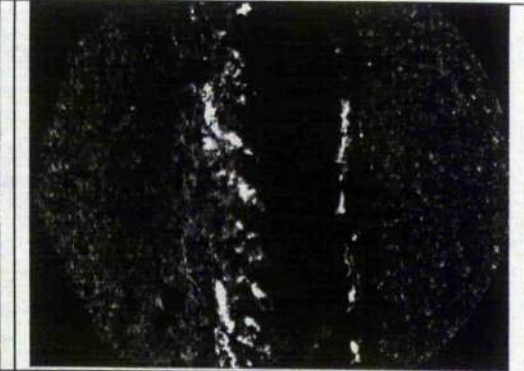
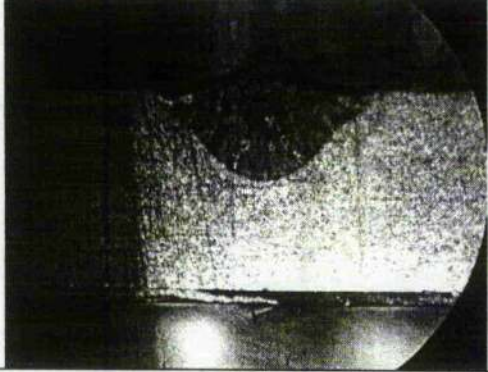
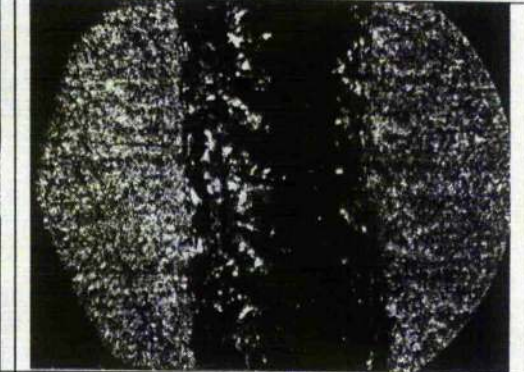
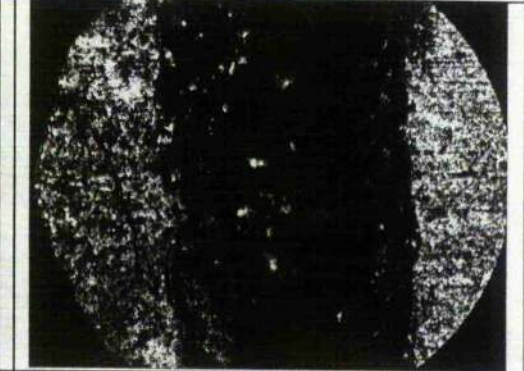
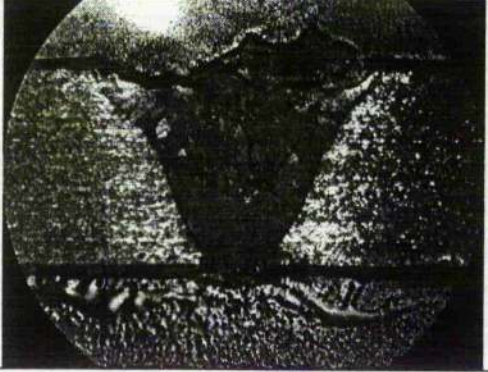
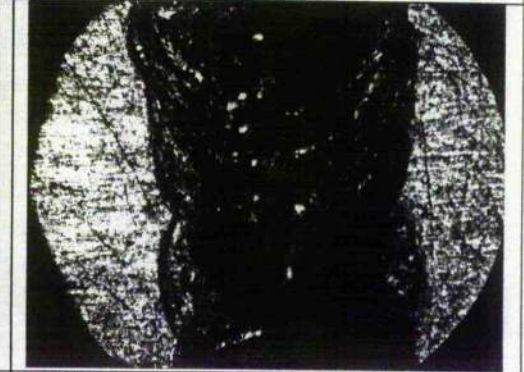
<p>9</p> <p>45J 8Hz 7msec 2.9mm /sec</p>		
O	1.5	1.65
<p>10</p> <p>50J 8Hz 7msec 2.9mm /sec</p>		
O	1.5	1.8

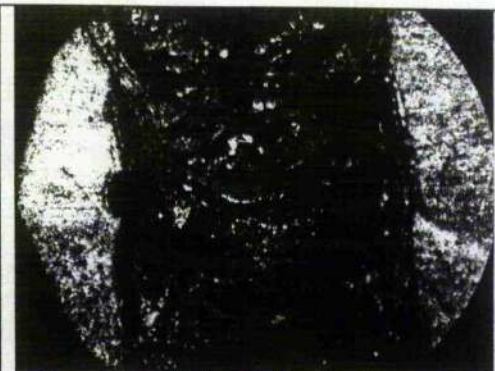
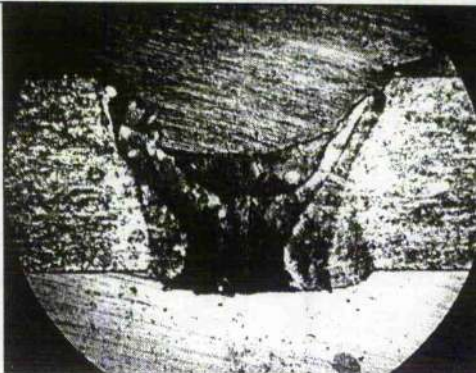
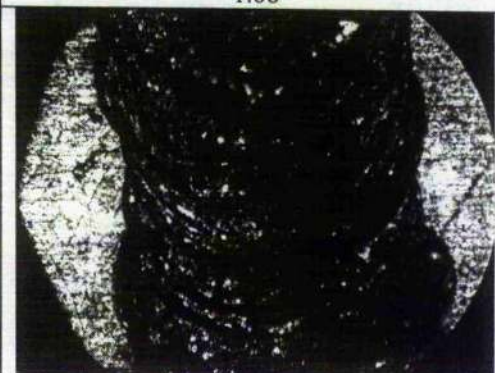
B-1-2

Pulse energy alteration to the fusion size on 5251-H24(SURFACE ROUGHNESS EFFECT)

O / X : Weld crack formation

	Penetration depth (mm)	Welding width (mm)
1 5J 8Hz 7msec 2.9mm /sec		
X	0.15	0.225
2 10J 8Hz 7msec 2.9mm /sec		
O	0.225	0.6
3 15J 8Hz 7msec 2.9mm /sec		
X	0.255	0.645
4 20J 8Hz 7msec 2.9mm /sec		
X	0.3	0.75

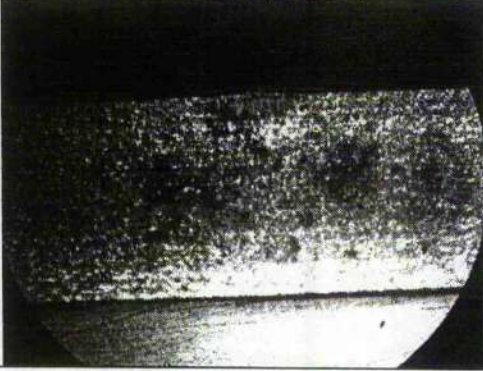
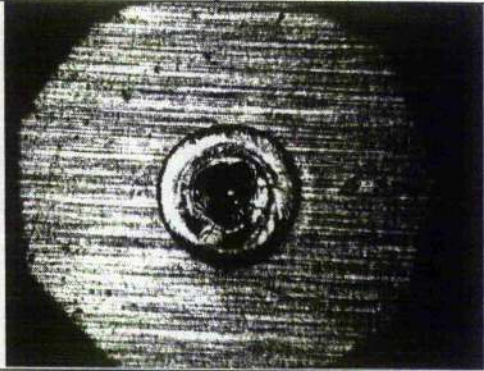
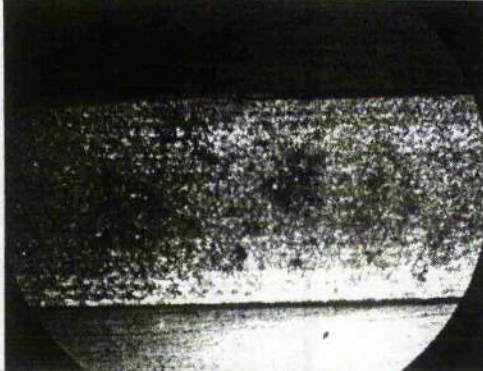
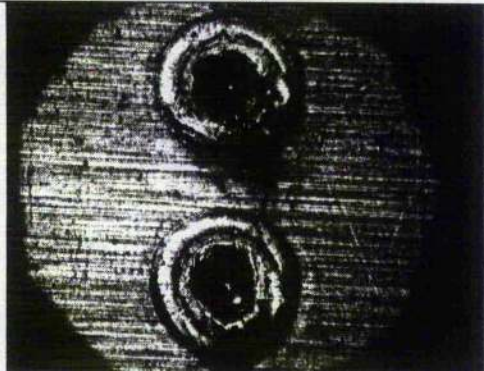
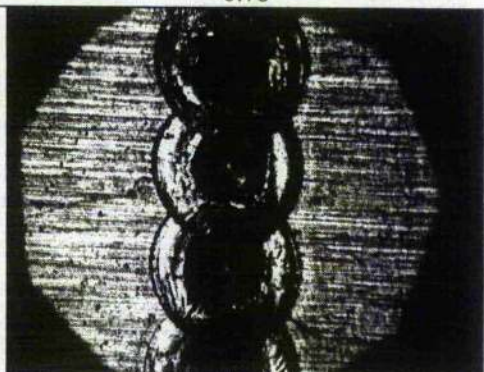
<p>5</p> <p>25J 8Hz 7msec 2.9mm /sec</p>		
O	0.36	0.9
<p>6</p> <p>30J 8Hz 7msec 2.9mm /sec</p>		
X	0.75	1.35
<p>7</p> <p>35J 8Hz 7msec 2.9mm /sec</p>		
O	0.9	1.5
<p>8</p> <p>40J 8Hz 7msec 2.9mm /sec</p>		
O	1.35	1.575

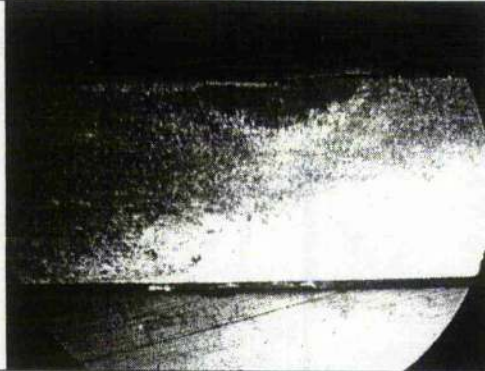
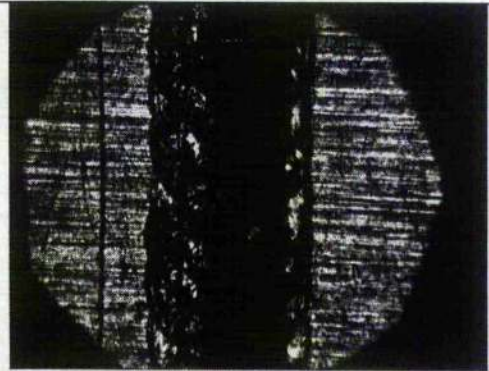
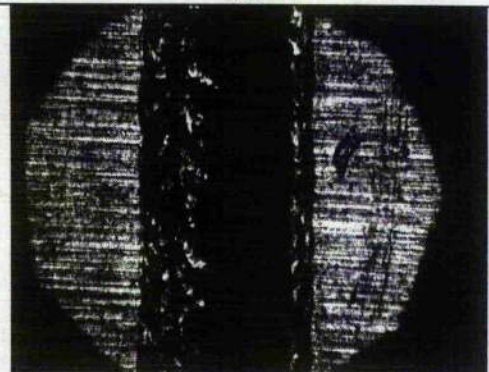
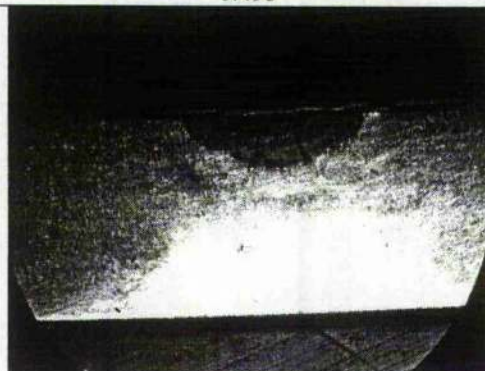
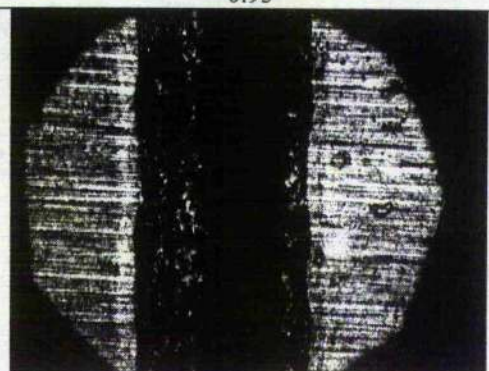
<p>9</p> <p>45J 8Hz 7msec 2.9mm /sec</p>		
<p>O</p>	<p>1.5</p>	<p>1.68</p>
<p>10</p> <p>50J 8Hz 7msec 2.9mm /sec</p>		
<p>O</p>	<p>1.5</p>	<p>1.725</p>

B-1-3

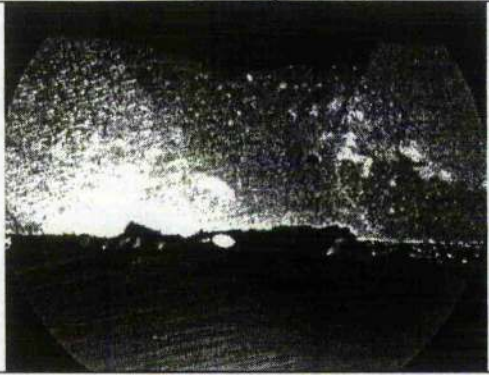
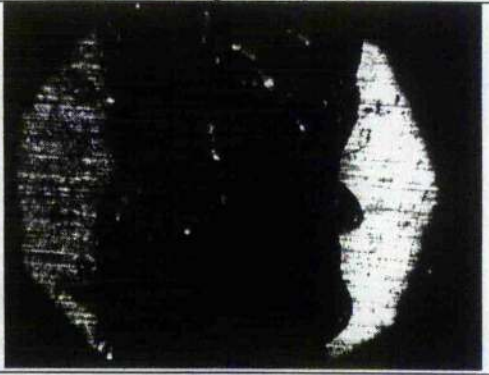
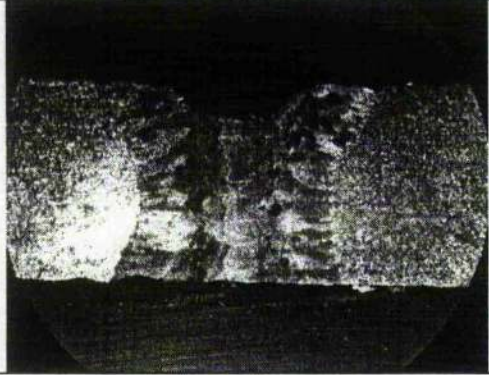
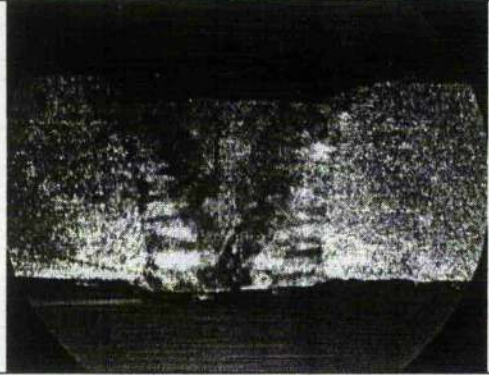
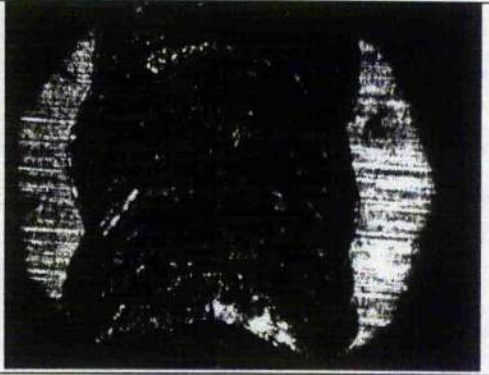
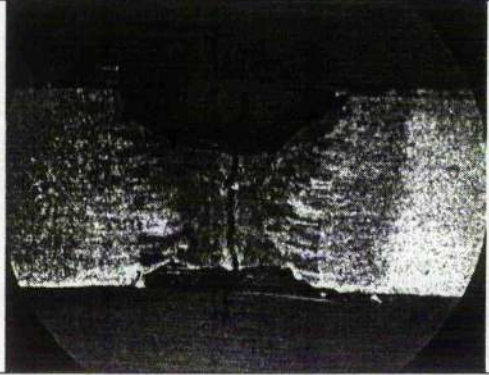
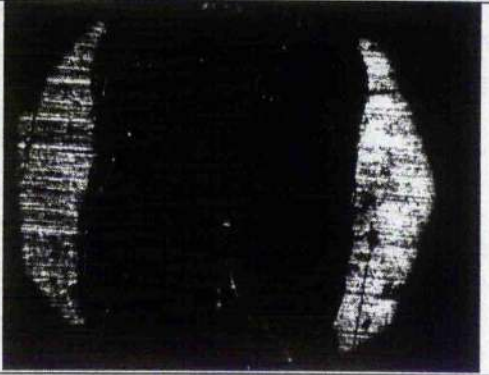
Frequency alteration to the fusion size (5251-H24)

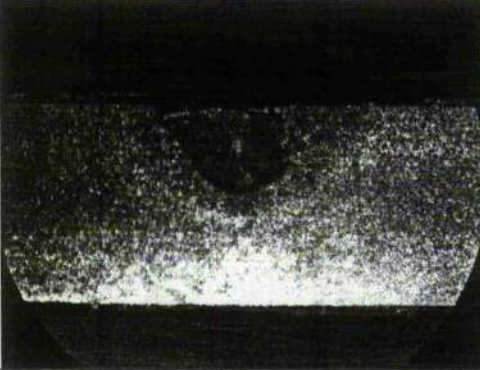
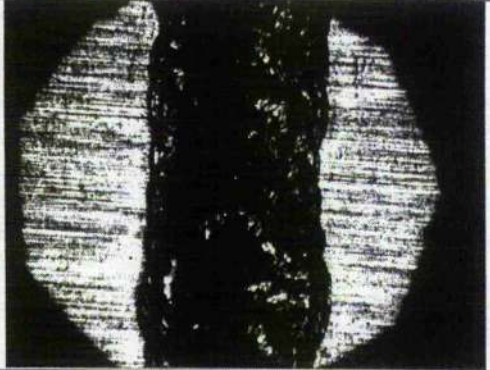
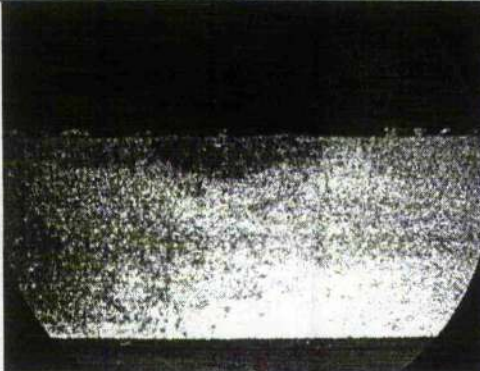
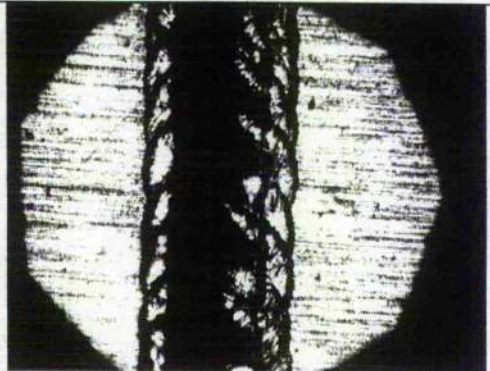
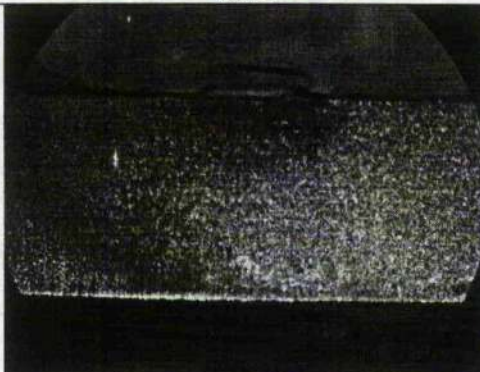
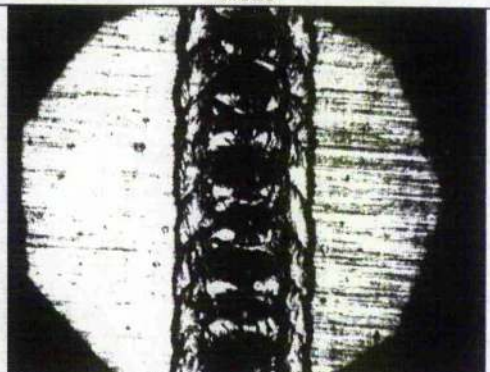
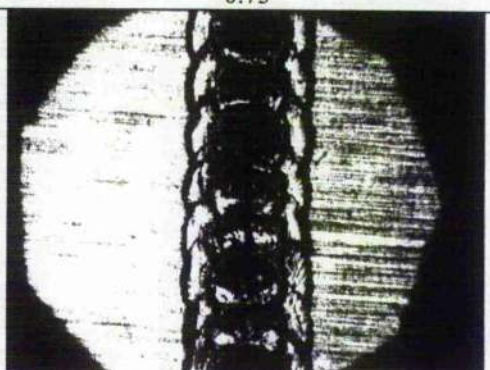
O / X : crack formation

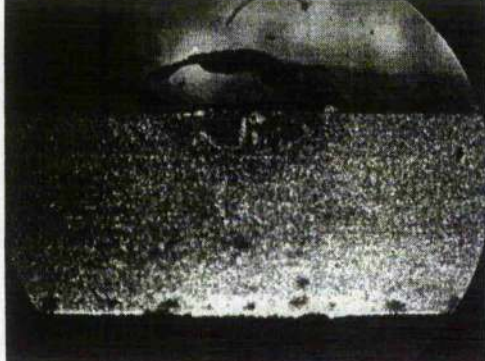
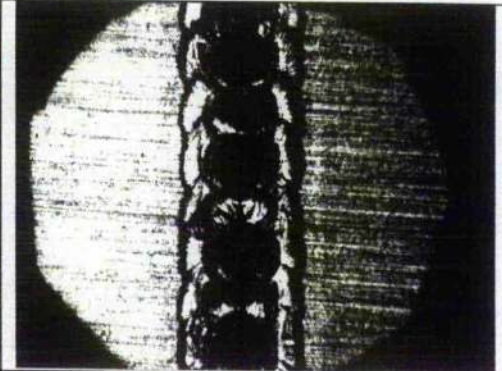
	Penetration depth (mm)	Welding width (mm)
<p>1</p> <p>25J 1Hz 7msec 2.9mm /sec</p> 		
X	0.225	0.6
<p>2</p> <p>25J 2Hz 7msec 2.9mm /sec</p> 		
X	0.225	0.78
<p>3</p> <p>25J 4Hz 7msec 2.9mm /sec</p> 		
X	0.3	0.795
<p>4</p> <p>25J 6Hz 7msec 2.9mm /sec</p> 		
X	0.3	0.9

<p>5</p> <p>25J 8Hz 7msec 2.9mm /sec</p>		
O	0.375	0.9
<p>6</p> <p>25J 12Hz 7msec 2.9mm /sec</p>		
O	0.495	0.93
<p>7</p> <p>25J 16Hz 7msec 2.9mm /sec</p>		
O	0.525	0.975

Pulse duration alteration to the fusion size (5251-H24) O/X : crack formation

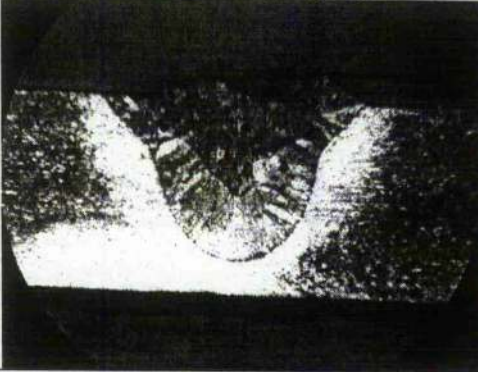
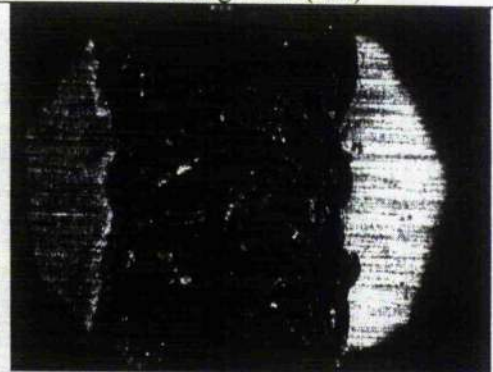
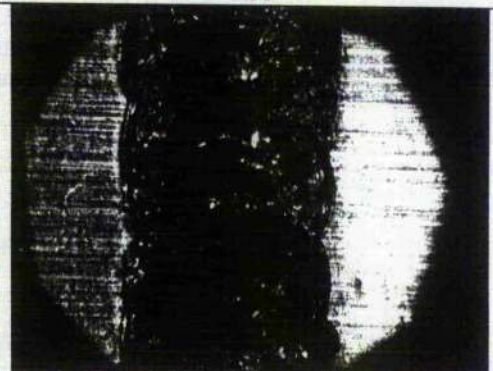
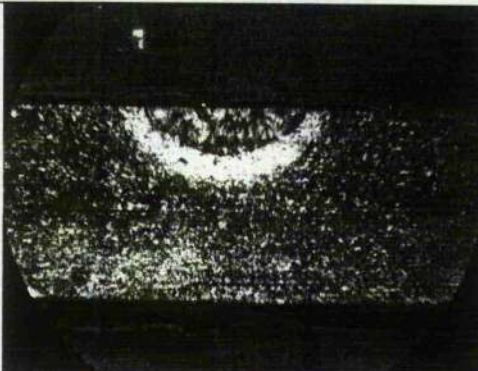
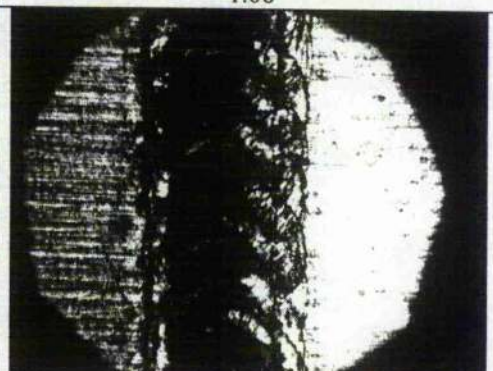
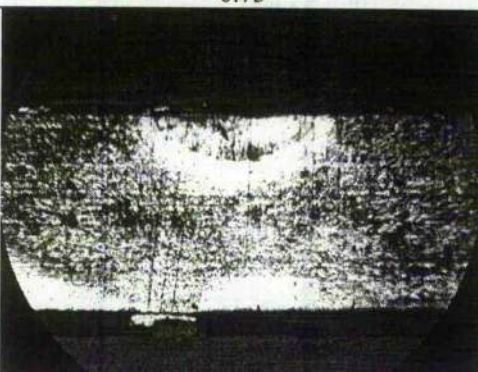
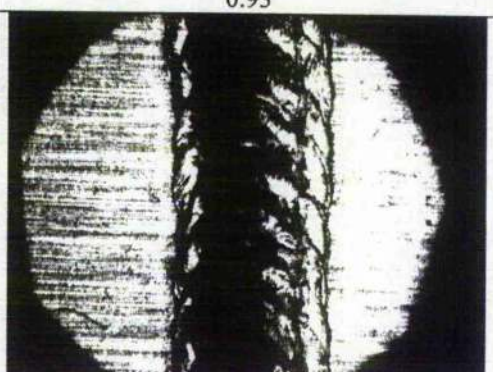
	Penetration depth (mm)	Welding width (mm)
<p>1</p> <p>35J 8Hz 5msec</p> <p>2.9mm /sec</p>		
X	1.5	1.725
<p>2</p> <p>35J 8Hz 6.2 msec</p> <p>2.9mm /sec</p>		
O	1.5	1.68
<p>3</p> <p>35J 8Hz 7.5 msec</p> <p>2.9mm /sec</p>		
O	1.5	1.65
<p>4</p> <p>35J 8Hz 8.8 msec</p> <p>2.9mm /sec</p>		
O	1.5	1.5

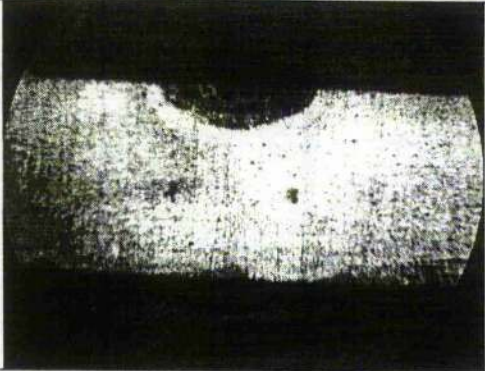
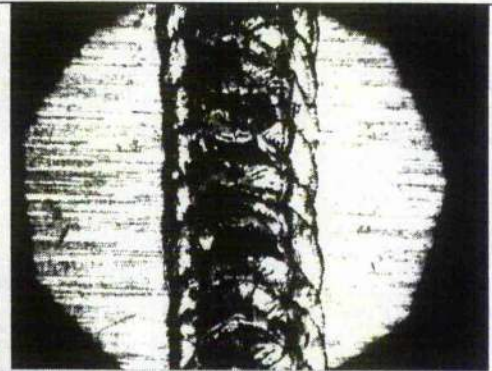
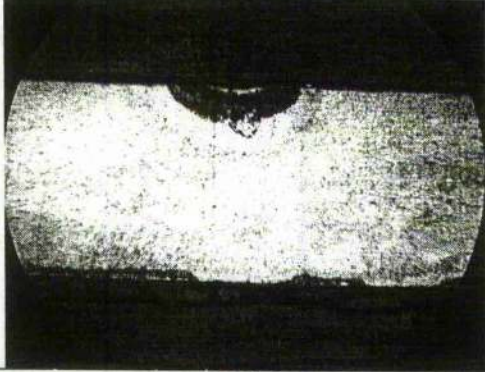
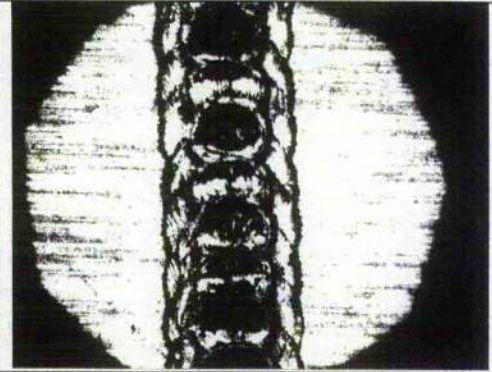
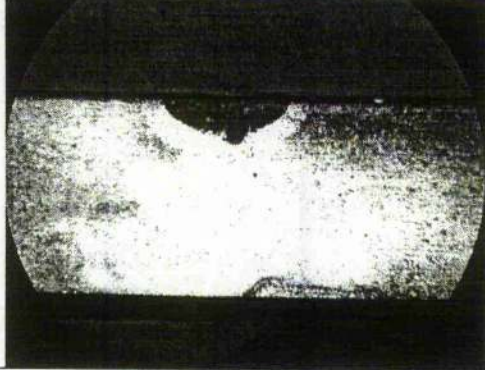
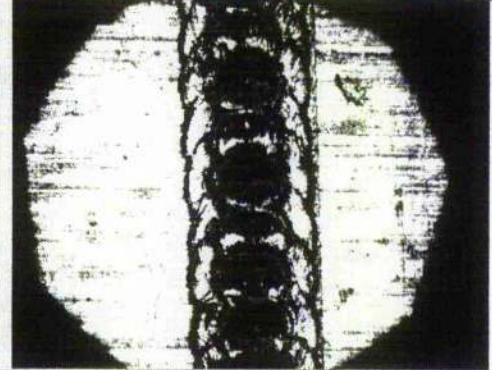
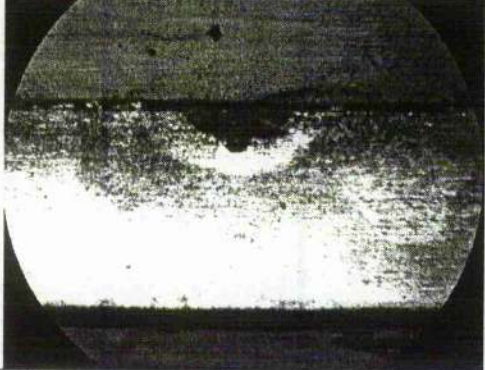
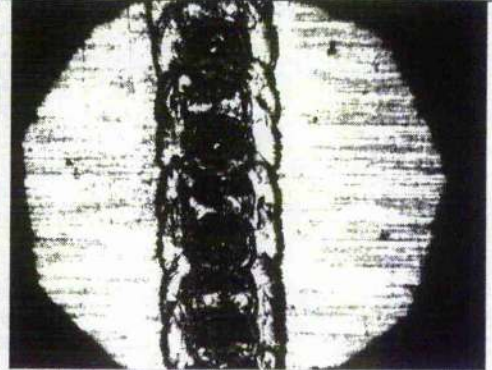
<p>5</p> <p>35J 8Hz 10 msec</p> <p>2.9mm /sec</p>		
O	0.9	1.05
<p>6</p> <p>35J 8Hz 12.5 msec</p> <p>2.9mm /sec</p>		
X	0.675	0.825
<p>7</p> <p>35J 8Hz 15 msec</p> <p>2.9mm /sec</p>		
O	0.6	0.75
<p>8</p> <p>35J 8Hz 17.5 msec</p> <p>2.9mm /sec</p>		
O	0.6	0.675

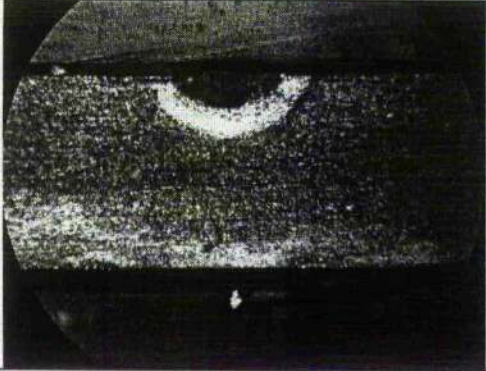
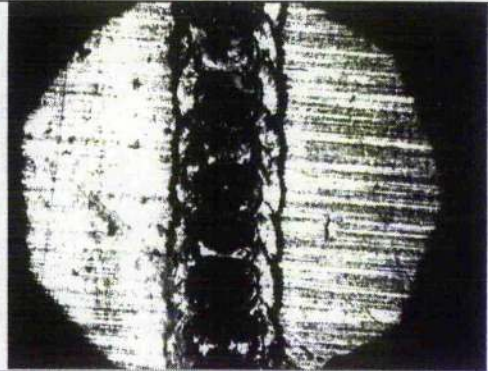
9 35J 8Hz 19.9 msec 2.9mm /sec		
O	0.525	0.675

B-1-5

Pulse duration alteration to the fusion size in 30J of pulse energy (5251-H24) O/X : crack formation

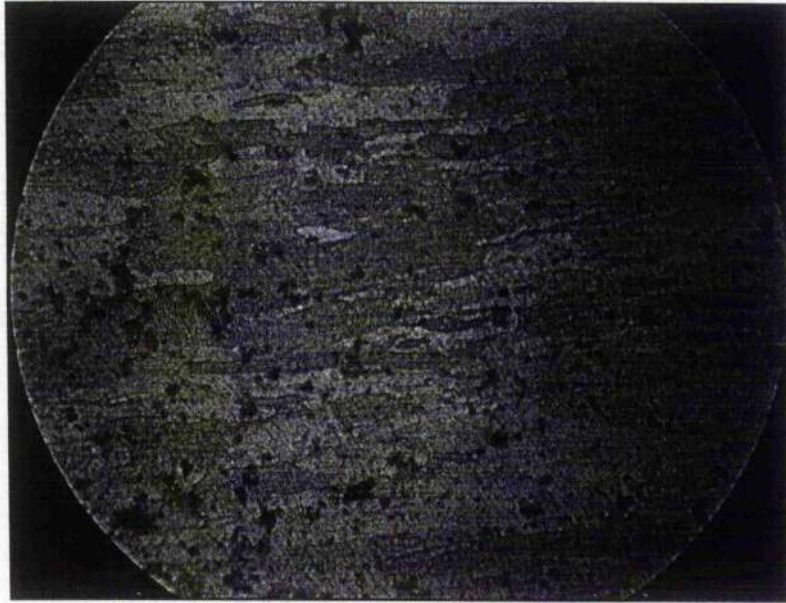
	Penetration depth (mm)	Welding width (mm)
1 30J 8Hz 5msc 2.9mm /sec		
O	1.275	1.35
2 30J 8Hz 6.2msc 2.9mm /sec		
O	1.095	1.08
3 30J 8Hz 7.5msc 2.9mm /sec		
X	0.75	0.93
4 30J 8Hz 8.8 msc 2.9mm /sec		
X	0.675	0.9

<p>5</p> <p>30J 8Hz 10msc</p> <p>2.9mm /sec</p>		
<p>O</p>	<p>0.645</p>	<p>0.87</p>
<p>6</p> <p>30J 8Hz 12.5 msc</p> <p>2.9mm /sec</p>		
<p>O</p>	<p>0.615</p>	<p>0.78</p>
<p>7</p> <p>30J 8Hz 15msc</p> <p>2.9mm /sec</p>		
<p>O</p>	<p>0.6</p>	<p>0.75</p>
<p>8</p> <p>30J 8Hz 17.5 msc</p> <p>2.9mm /sec</p>		
<p>X</p>	<p>0.6</p>	<p>0.675</p>

9 30J 8Hz 19.9 msc 2.9mm /sec		
X	0.525	0.6

Microstructures

1. A-1 , B-1¹⁾

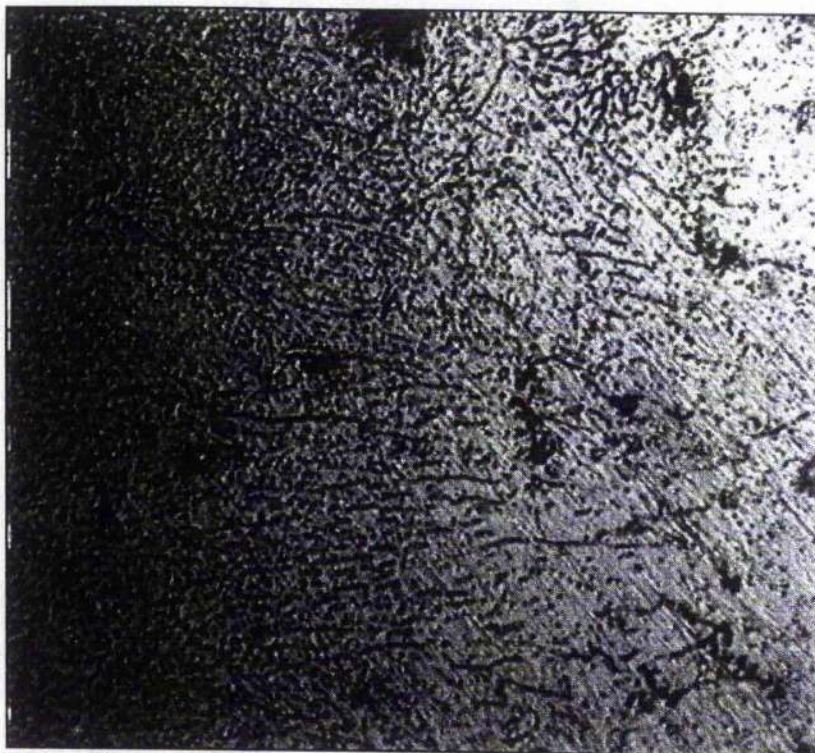


(1) Micro structure of 5251-H24 Base metal
Optical microscope $\times 50$
Etchant : 10ml HF, 15ml HCl, 25ml HNO₃, 50ml H₂O (2min)

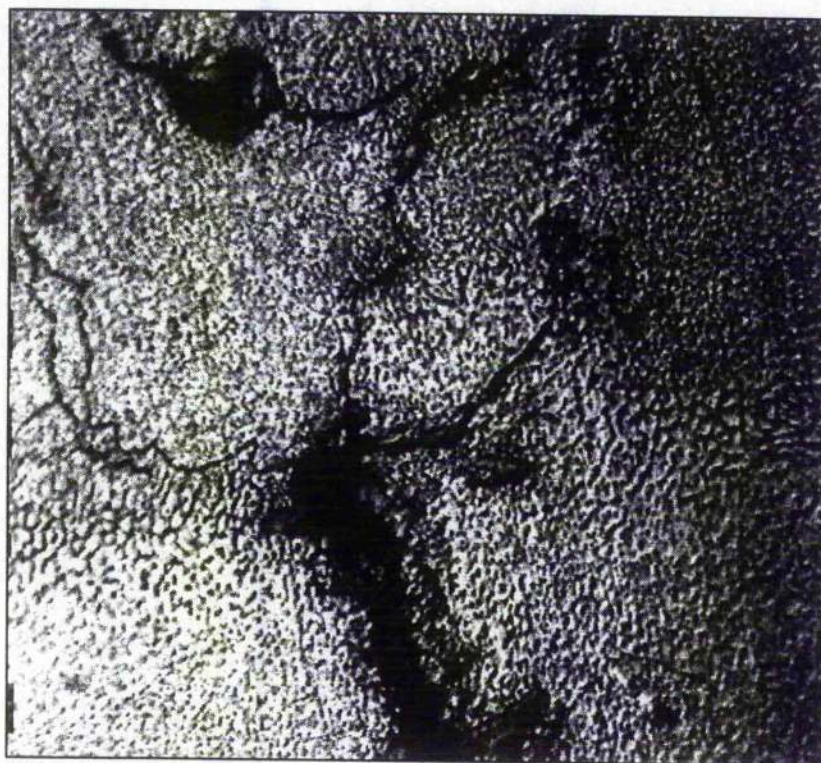


(2) Micro picture of fusion / base metal boundary (A-1). Optical microscope $\times 50$
Etchant : Keller's etch for 5 min.

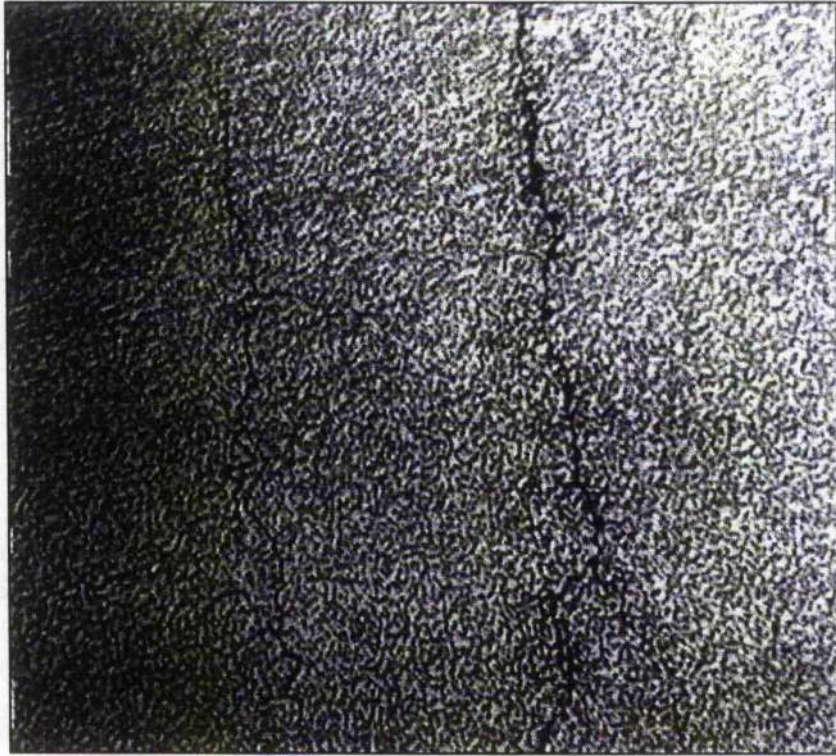
¹⁾ A-1 , B-1 : specimen preparations (refer to chapter 3.4.1. Preparing the specimens, table 3.2.)



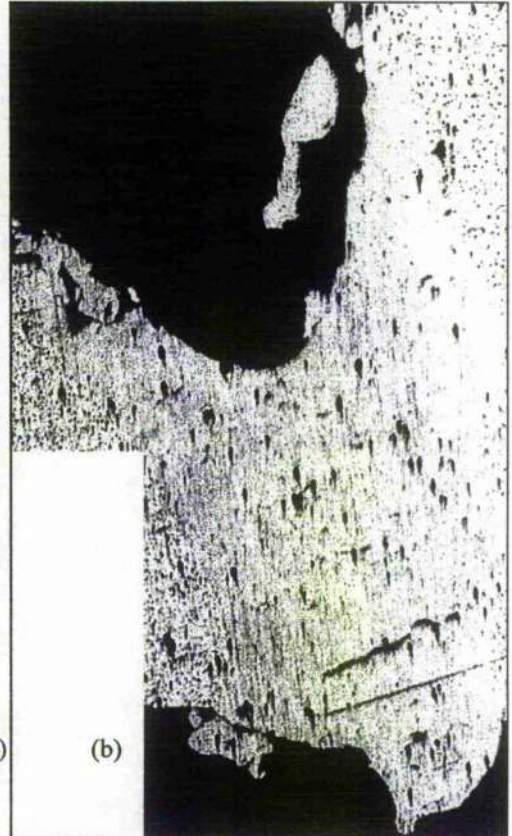
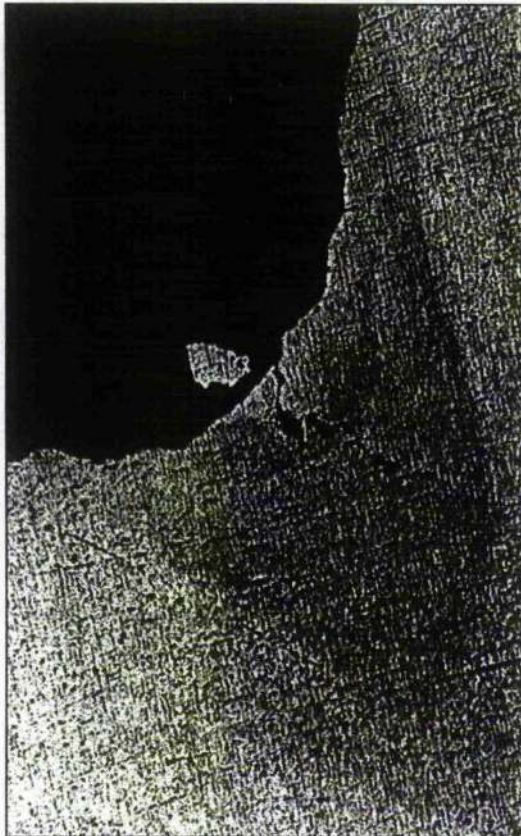
(3) Micro picture of fusion / base metal boundary (B-1). Optical microscope $\times 100$
Typical columnar dendrite structure Etchant: Keller's etch (5 min).



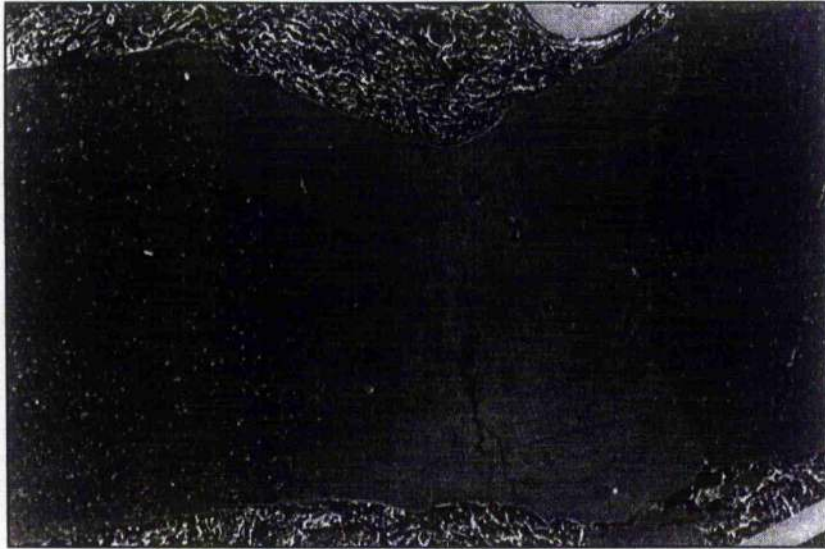
(4) Solidification crack on the centre of fusion (B-1). Optical microscope $\times 100$
Etchant : Keller's etch (5 min)



(5) Solidification crack on the centre (A-1)
Optical microscope $\times 100$, Etchant : Keller's etch (5 min).



(6) Macro pictures of lap joint welding of (a) 5251-H24 and (b) 6082-T6 without filler metal. Laser angle: 45° Laser parameters : $E=40\text{J}$ / $\text{PRF}=10\text{Hz}$ / $\tau=5.8\text{msec}$ / $V=4.0\text{mm/sec}$. (a) welding crack found on the centre (b) welding shrinkage and poor welding geometry caused by evaporation or spatter production. Etchant : Keller's etch.

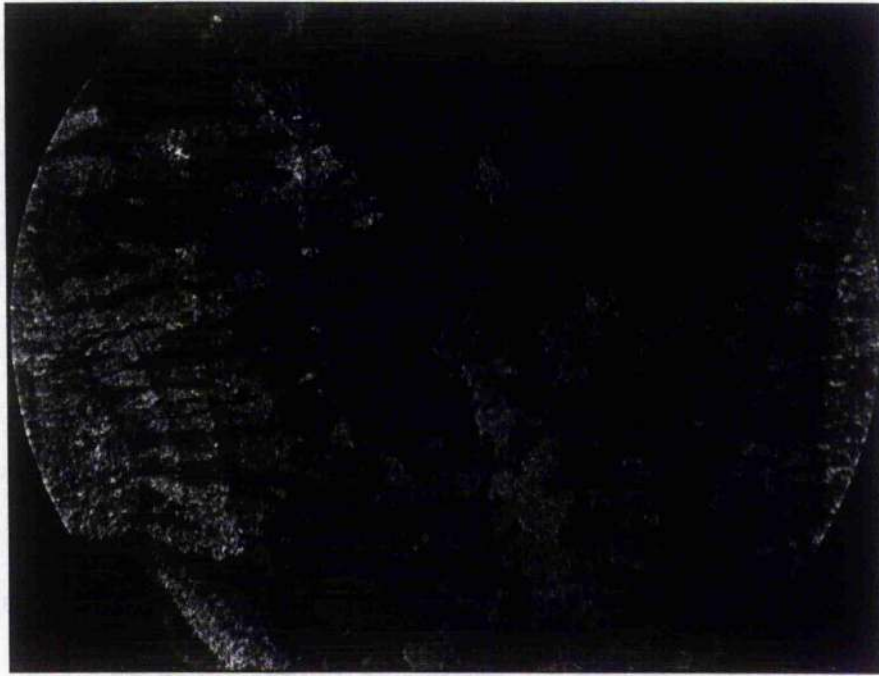


(7) Micro picture of 6082-T6 alloy butt joint welding without filler metal (A-1).
Solidification cracking formed on the fusion centre. Welding parameters : $E=45\text{J}$ / $\text{PRF}=8\text{Hz}$ / $\tau=6.5$
msec / $V=2.9$ mm/sec. SEM



(8) Typical micro porosity on the fusion and centre line welding crack
Base metal : 5251-H24 , filler metal : none (B-1)
Welding parameter : $E=40\text{J}$ / $\text{PRF}=10\text{Hz}$ / $\tau=6.5\text{msec}$ / $V=2.9\text{mm/sec}$
Power Intensity(I) = $2.07 \times 10^9 \text{W/m}^2$. SEM

2. A-2 , B-2²⁾



(9) Macro picture of 6082-T6 alloy with 5% Si filler metal (A-2). Left and right end : HAZ , Centre : Equiaxed structure / Between HAZ and Equiaxed : Columnar
Optical microscope $\times 10$, Etchant : same as (1)

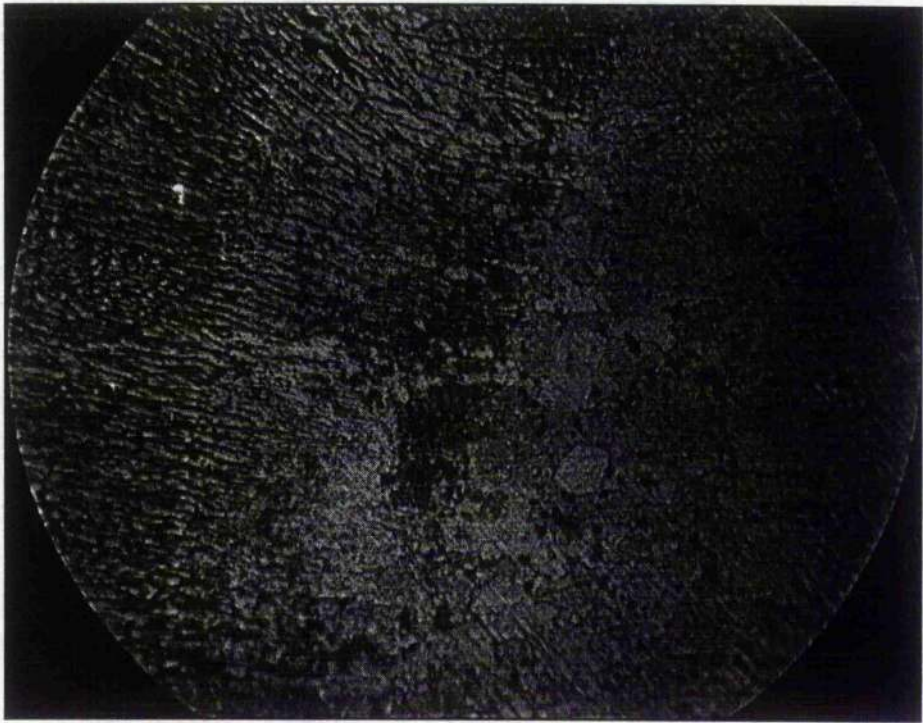


(10) Micro structure of HAZ. Coarser than Base metal.
Optical microscope $\times 50$

²⁾ A-2 , B-2 : specimen preparations (refer to chapter 3.4.1. Preparing the specimens, table 3.2.)



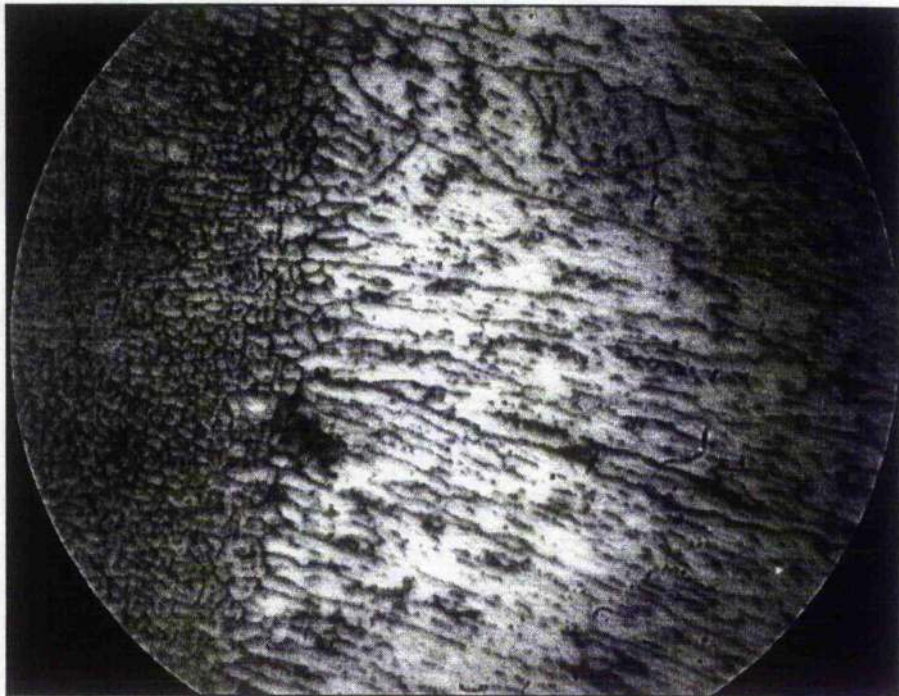
(11) Columnar structure near fusion boundary. Micro structure of base metal centre (B-2).
Optical microstructure $\times 50$



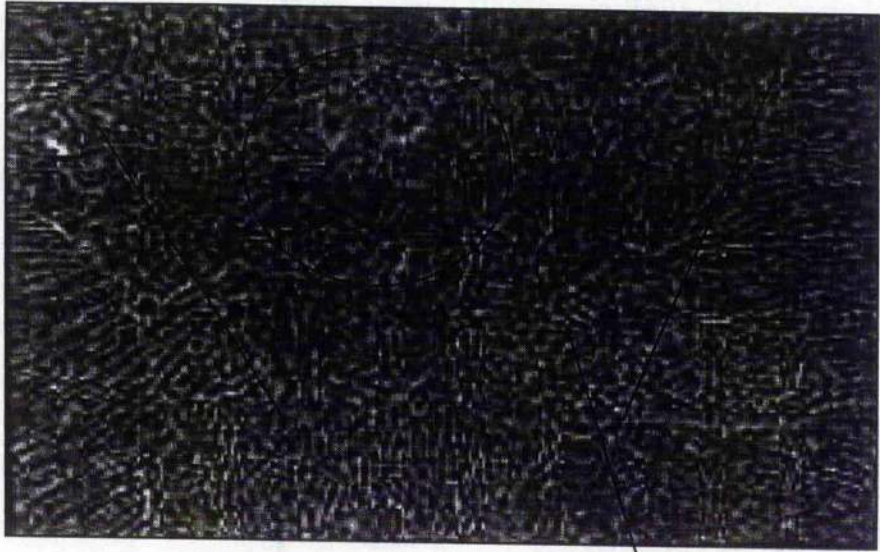
(12) Fusion line boundary between HAZ and Columnar structure (A-2).
Optical micro scope $\times 100$



(13) Grain Boundary between Columnar / Equiaxed structure (A-2).
Optical microscope $\times 50$
Etchant : same as micro structure (1)

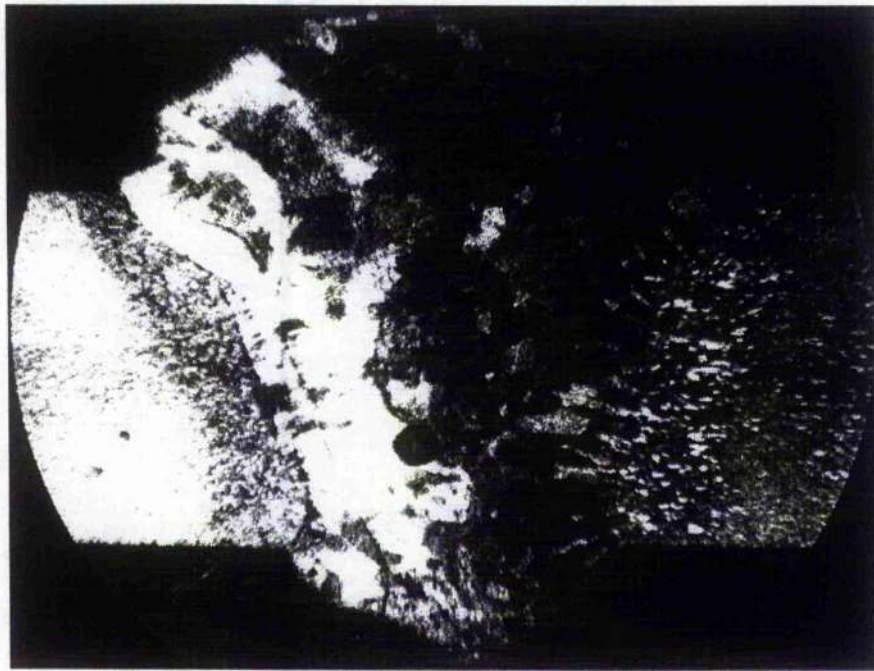


(14) Grain Boundary between Columnar / Equiaxed structure (B-2).
Optical microscope $\times 100$
Etchant : same as micro structure (1)



(15) Micro structure of near fusion centre region. Centre of picture (A-2) : Equiaxed structure. Small micro porosity found (in the circle).
SEM

3. A-3 , B-3³⁾



(16) Macro srtructure of 6082-T6 with 12% Si filler metal (A-3).
Weld fusion, HAZ, Base metal. Optical microscope $\times 5$
Etchant : same as (1)



(17) Micro structure of Base metal 6082-T6
Optical microscope $\times 100$, Etchant : same as (1)

³⁾ A-3 , B-3 : specimen preparations (refer to chapter 3.4.1.Preparing the specimens, table3.2.)



(18) Micro structure of HAZ Optical microscope $\times 100$
Etchant : same as (1)



(19) Micro structure of fusion boundary (B-3). Base metal, Columnar structure and Equiaxed structures.
Optical microscope $\times 100$, Etchant : same as (1)

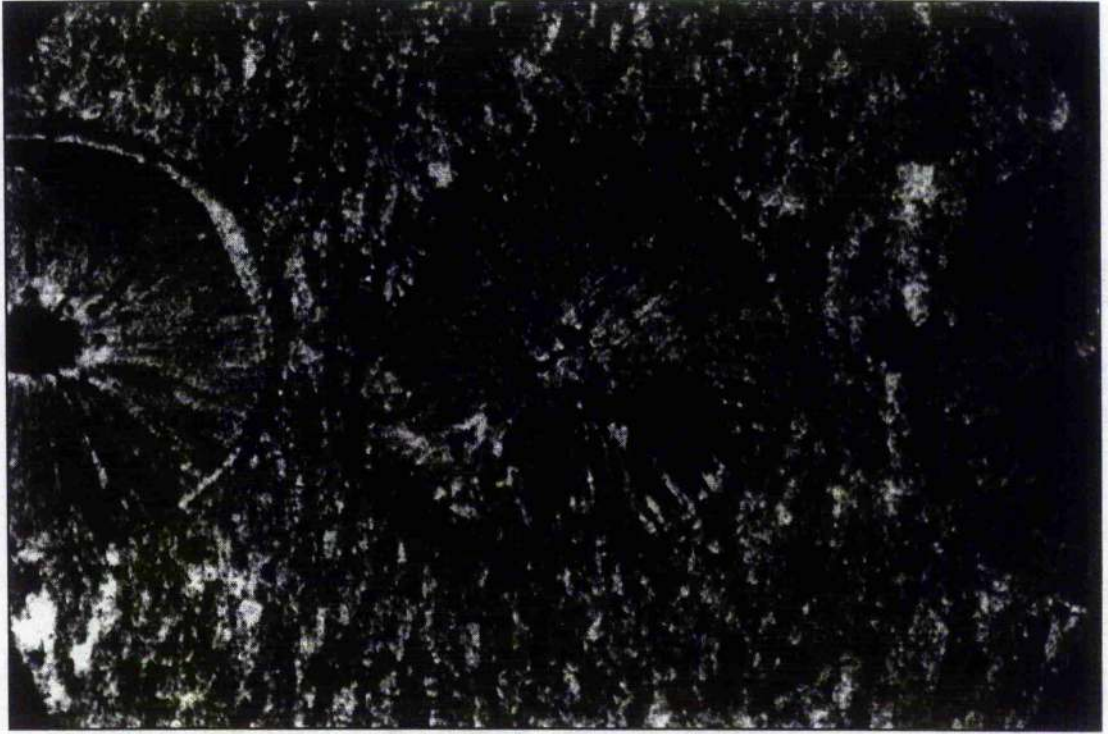


(20) Micro structure of fusion centre (B-3).
Optical microscope $\times 50$, Etchant : same as (1)

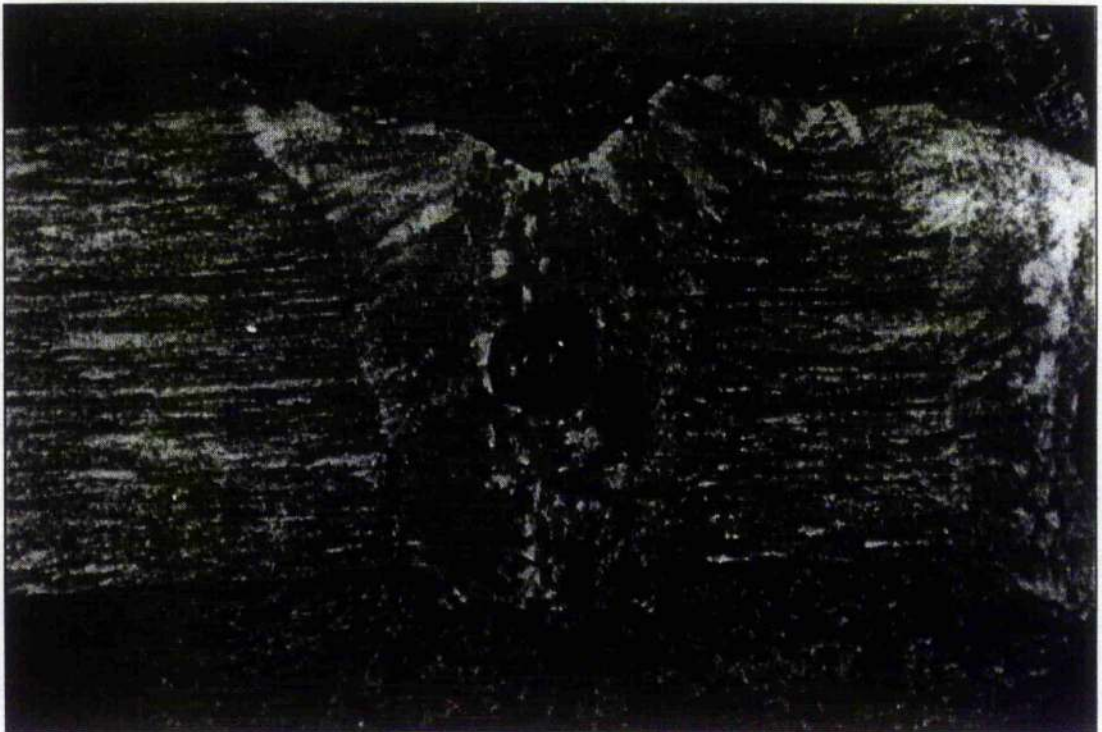


(21) Micro structure of fusion centre (B-3).
Optical microscope $\times 100$, etchant : same as (1)

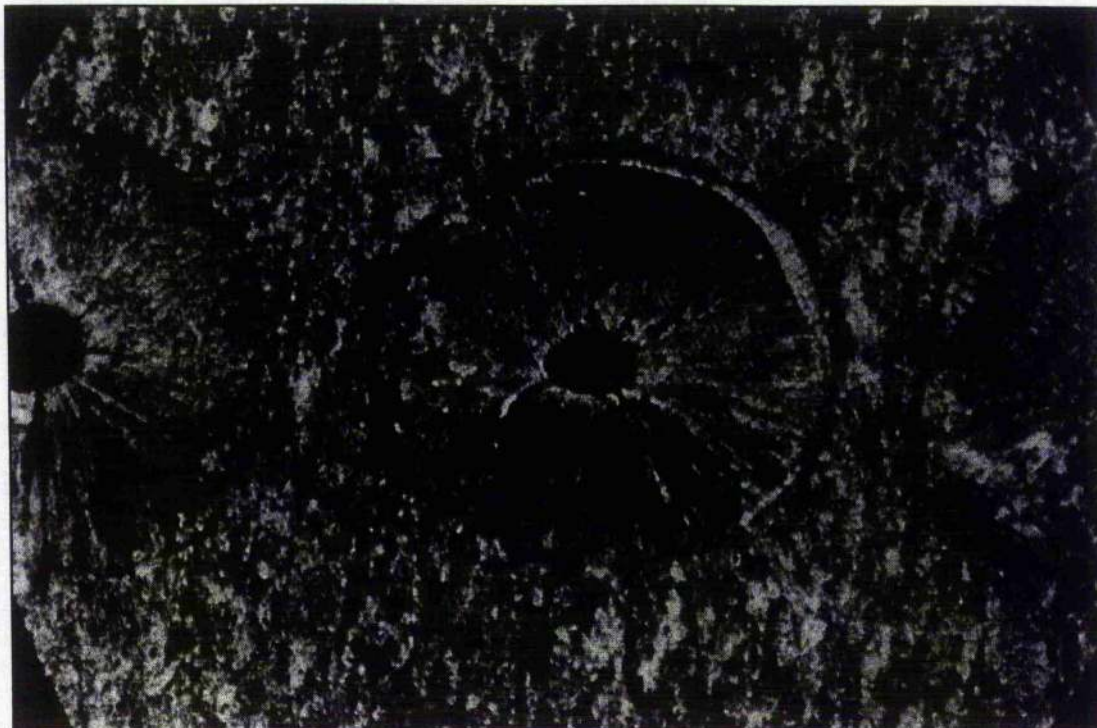
Single pulse Irradiated on the Aluminum Alloys



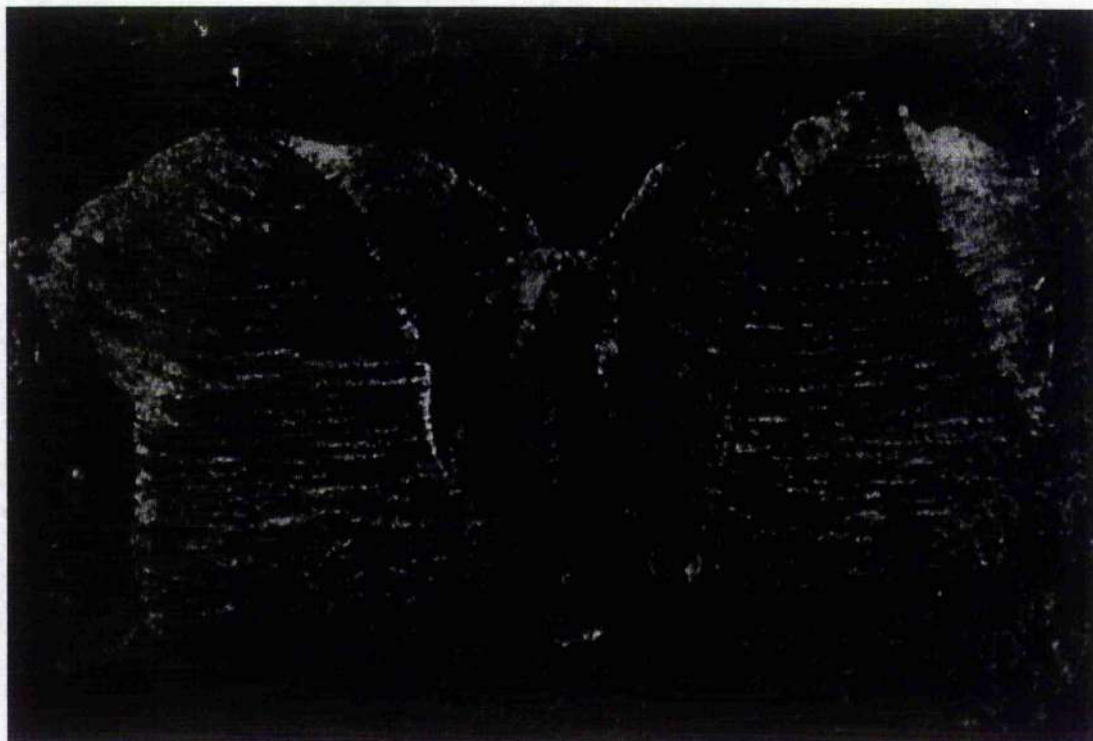
(22) A single pulse irradiated on 5251-H24 alloy (top view). Solidification cracking occurs on the centre region. Laser parameter : $E=40\text{J}$ / $\text{PRF}=2\text{Hz}$ / $\tau=6.8\text{msec}$ / $V=4.0\text{mm/sec}$



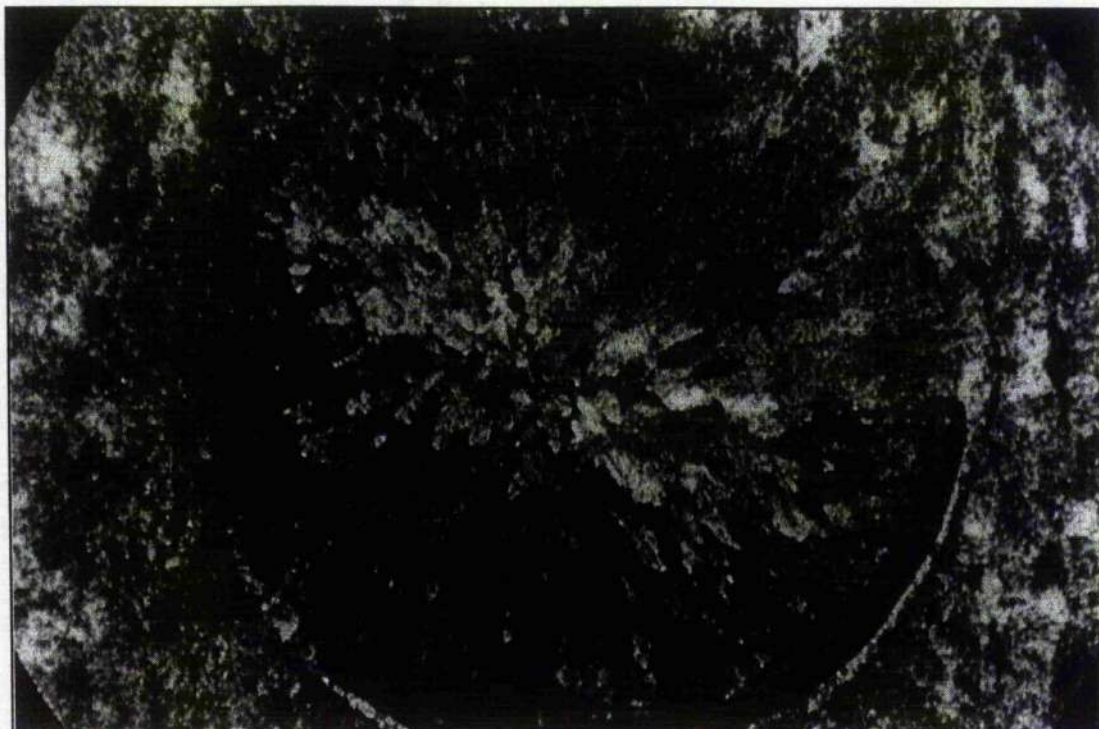
(23) A single pulse irradiated on 5251-H24 alloy (welding cross section). Solidification cracking occurs on the centre region and macro porosity observed. Laser parameter : $E=40\text{J}$ / $\text{PRF}=2\text{Hz}$ / $\tau=6.8\text{msec}$ / $V=4.0\text{mm/sec}$



(24) A single pulse irradiated on 6082-T6 alloy (top view). Key hole produced and small hole formed on the surface. Solidification cracking occurs on the centre region. Laser parameter : $E=40\text{J}$ / $\text{PRF}=2\text{Hz}$ / $\tau=6.8\text{msec}$ / $V=4.0\text{mm/sec}$



(25) A single pulse irradiated on 6082-T6 alloy (welding cross section). Solidification cracking occurs on the centre region. Equiaxed dendrite structure formed almost all the fusion zone. Laser parameter : $E=40\text{J}$ / $\text{PRF}=2\text{Hz}$ / $\tau=6.8\text{msec}$ / $V=4.0\text{mm/sec}$



(26) A single pulse irradiated on 5251-H24 alloy (top view $\times 10$). Solidification cracking occurs on the centre region. Laser parameter: $E=45\text{J}$ / $\text{PRF}=1\text{Hz}$ / $\tau=7\text{msec}$ / $V=2.9\text{mm/sec}$.
Etchant : same as (1)

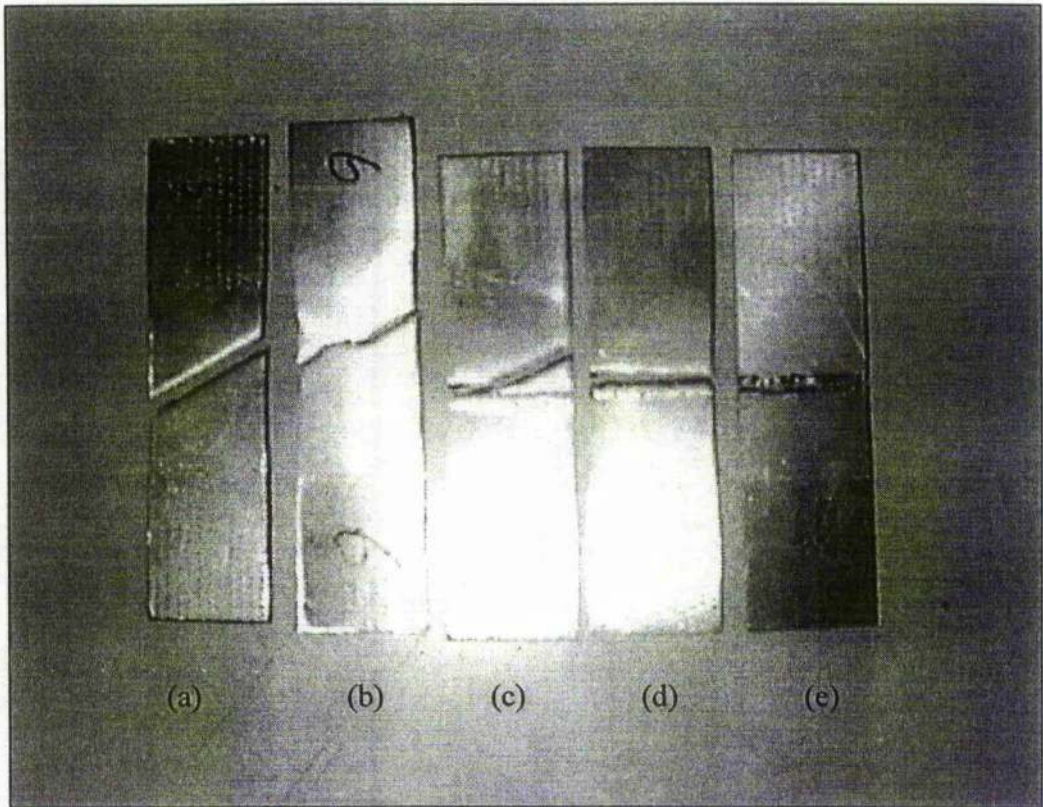


(27) A higher magnification picture (26) of single pulse irradiated on 5251-H24 alloy (top view $\times 50$). Solidification cracking occurs on the centre region. Laser parameter: $E=45\text{J}$ / $\text{PRF}=1\text{Hz}$ / $\tau=7\text{msec}$ / $V=2.9\text{mm/sec}$. Etchant : same as (1)



(28) A higher magnification of single pulse irradiated on 5251-H24 alloy (cross section of fusion top $\times 50$). Solidification cracking occurs on the centre region. Laser parameter: $E=45\text{J}$ / $\text{PRF}=1\text{Hz}$ / $\tau=7\text{msec}$ / $V=2.9\text{mm/sec}$. Etchant : same as (1)

i.3. Specimens after Tensile strength test

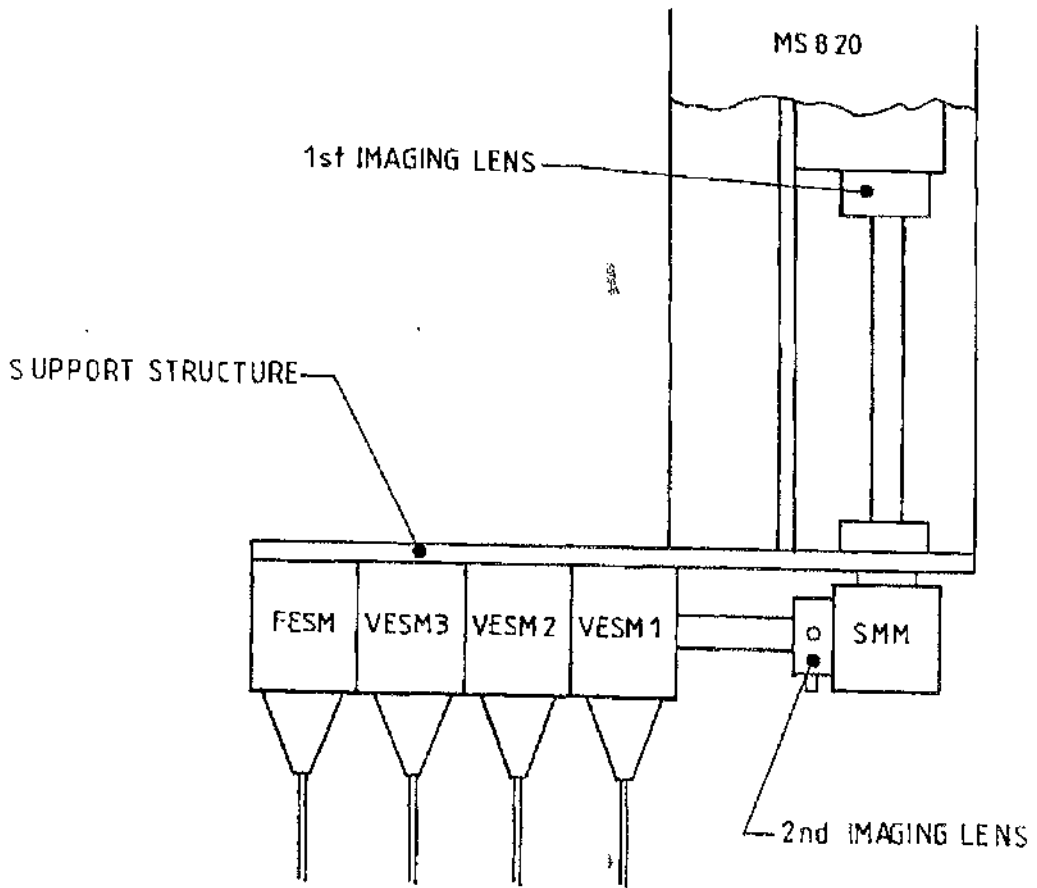


(29) Fracture area after the tensile strength test.

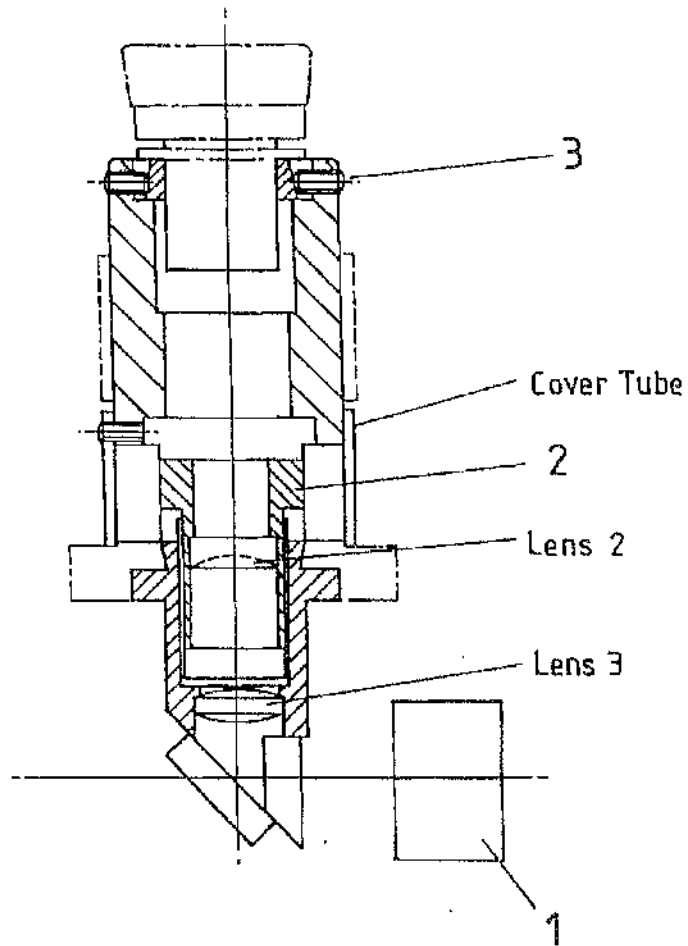
- (a) Base metal of 5251-H24 alloy, (b) Base metal of 6082-T6 alloy, (c) 6082 alloy with 12%Si filler metal (A,B-3). Fracture point : base metal, (d) 6082-T6 alloy with 5% Si filler metal (A,B-2) fracture point : HAZ, (e) 6082-T6 without filler metal (A,B-1) fracture point : fusion centre.

Appendix 3. Laser Head Assembly and Sharing System Drawings

(Lumonics)

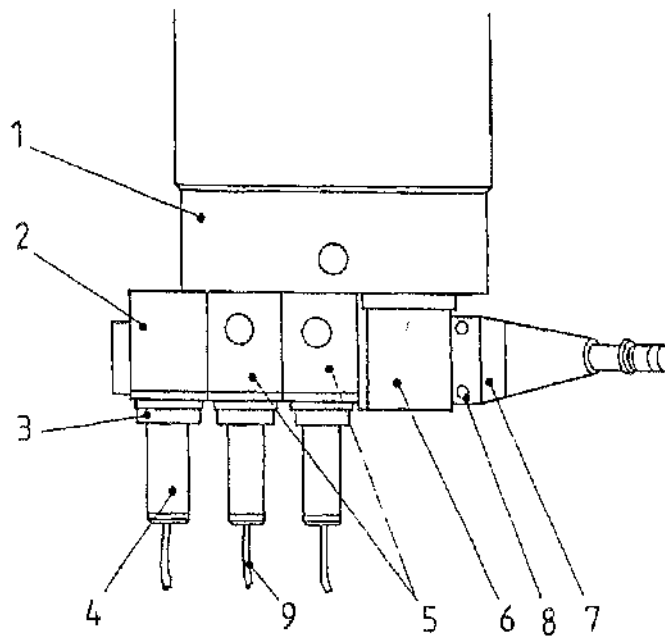


(30) Special fiber optic beam delivery construction



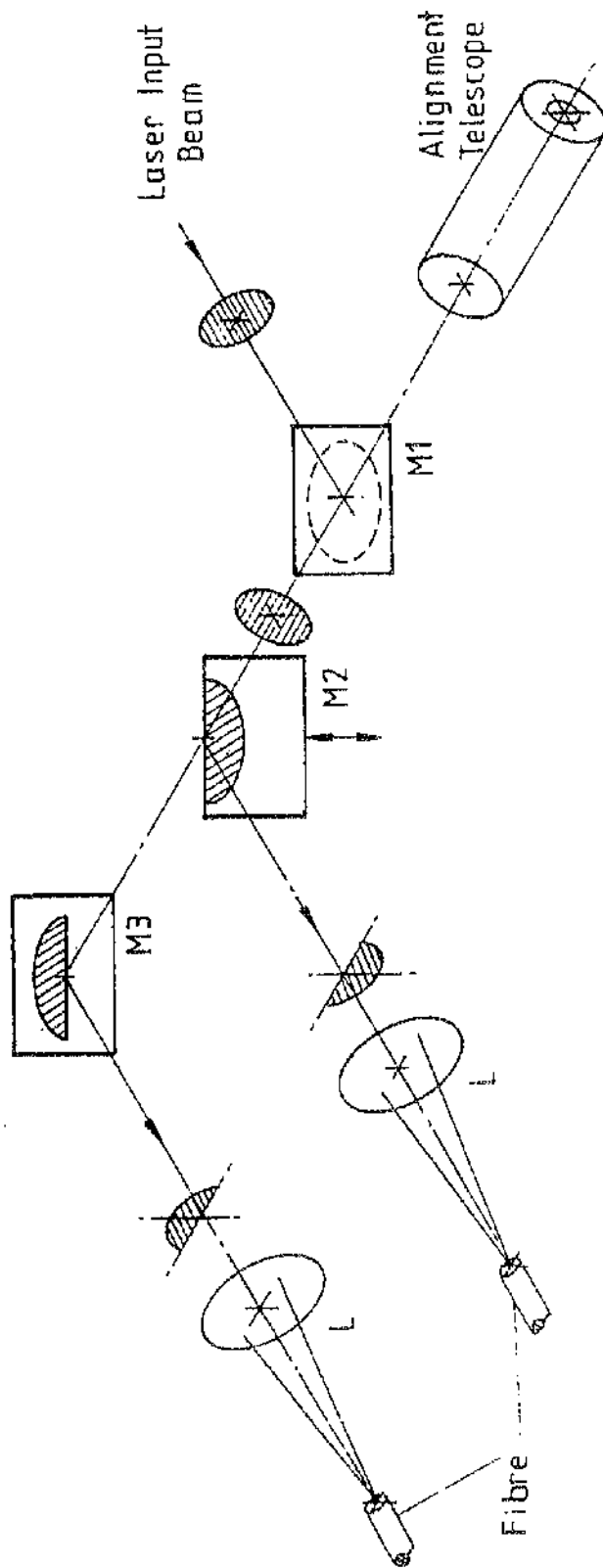
1. Input Lens (Fibre)
2. Knurled Ring
3. Graticule Alignment screws

(31) Fiber optic alignment viewer

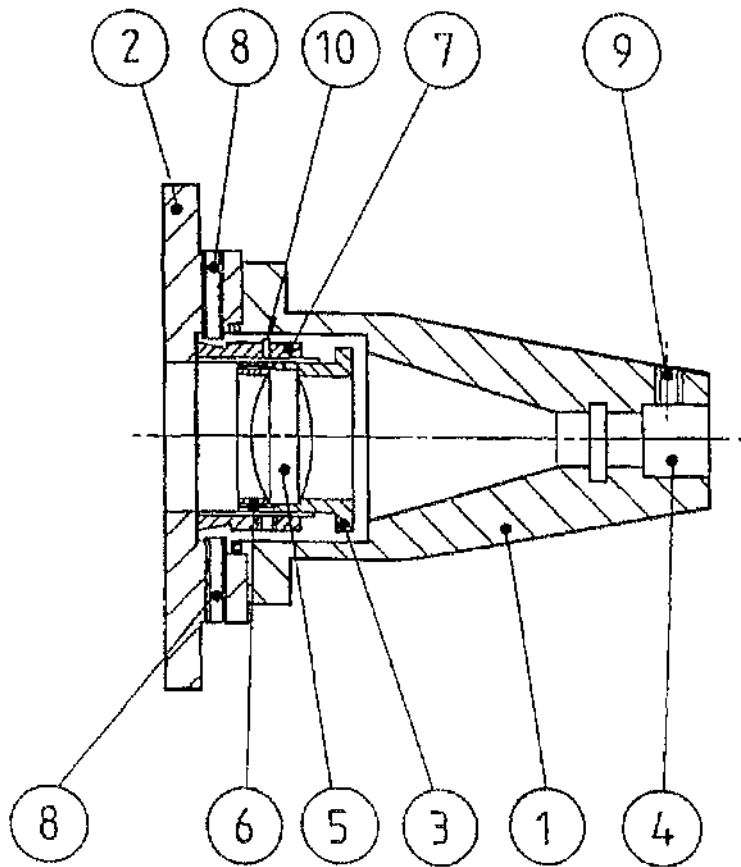


- | | |
|---------------------------------|------------------------------------|
| 1. Laser | 6. Steering Mirror Module |
| 2. Fixed Energy Share Module | 7. Alignment Telescope |
| 3. Front Input Module | 8. Telescope Lens Centering Screws |
| 4. Rear Input Module | 9. Fibres |
| 5. Variable Energy Share Module | |

(32) Diagram of energy sharing unit

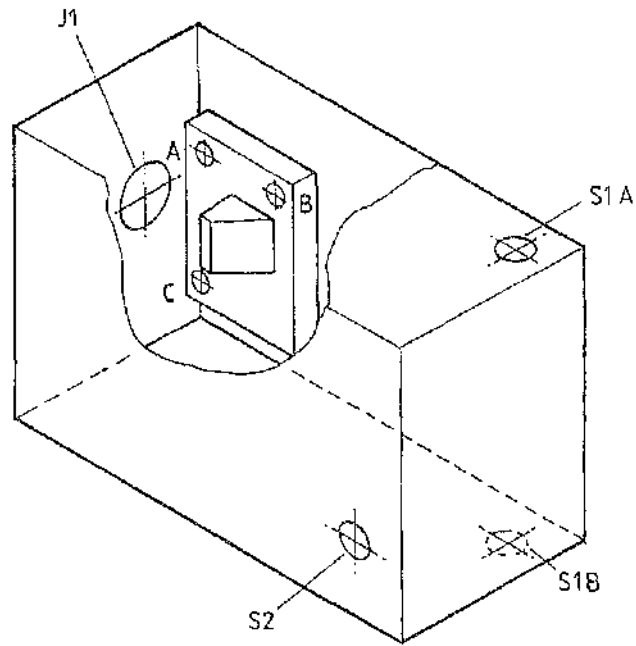


(33) A schematic of 2-way energy share unit



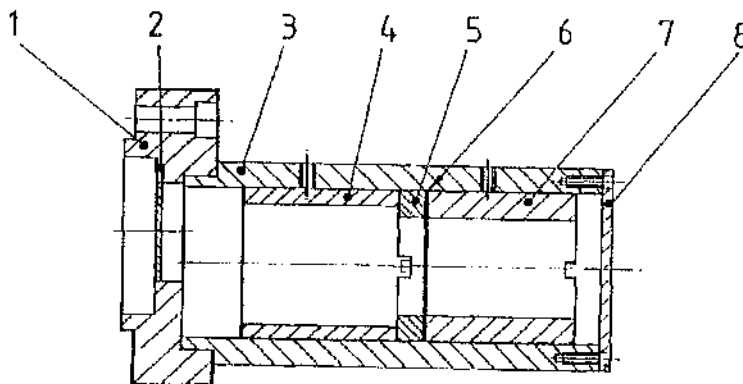
1. Module Body (rear)
2. Module Body (front)
3. Input Lens Mount
4. Fibre Input Ferrule location
5. Input Lens
6. Lens Retaining Ring
7. Lens Centering Mount
8. Adjusting Screws
9. Fibre Locating Set - Screw
10. Locking Screw

(34) A schematic of input module



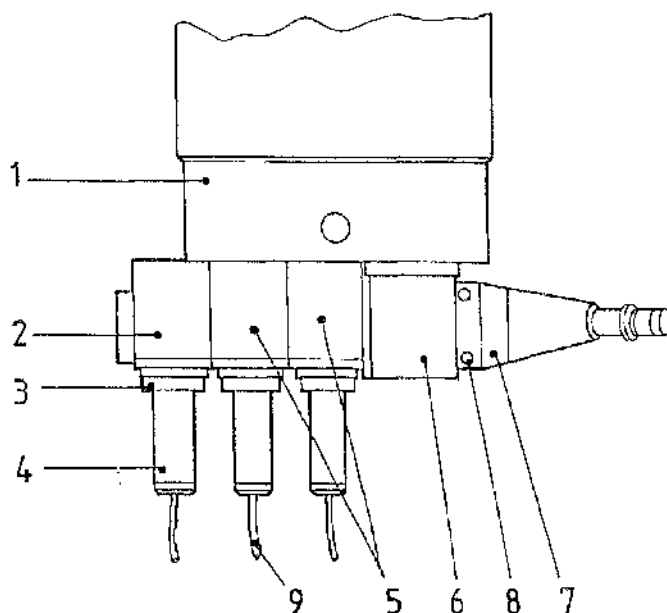
- S1A, S1B, S2 - Adjustment Screws (SMM)
 A, B, C - Fixing Screws (Energy Share Modules)
 J1 - Alignment Jig Port (FESM)

(35) A schematic of energy share unit



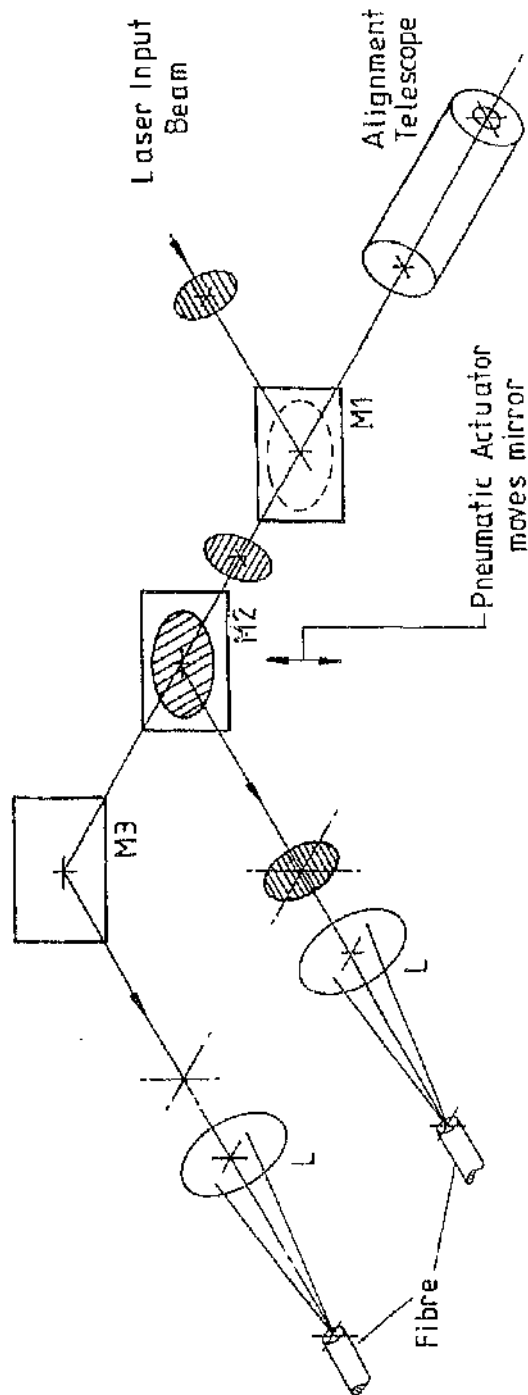
1. Mounting Flange
2. Cover Slide
3. Tube
4. Setting Ring
5. Film Clamp
6. Kapton Film
7. Film Holder
8. Protective Cap

(36) Kapton film module

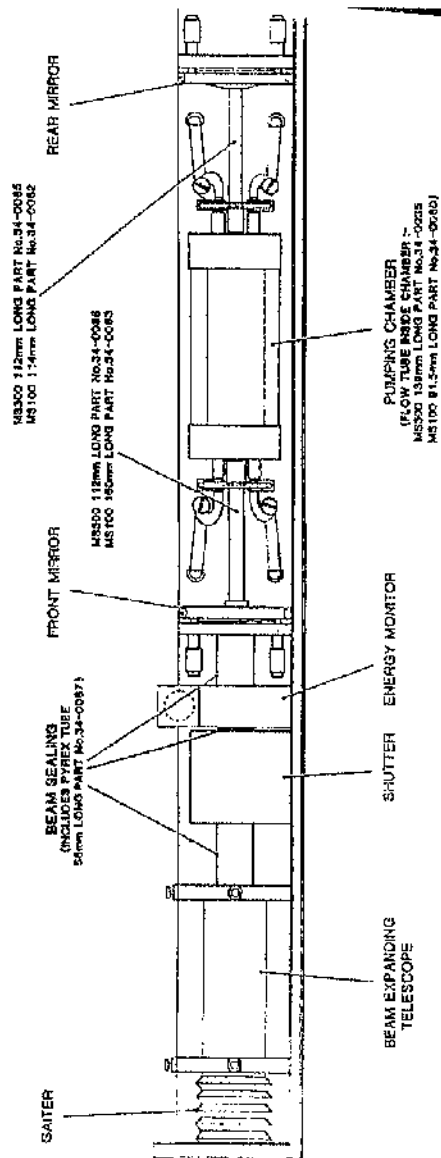


- | | |
|-------------------------------|-------------------------------------|
| 1. Laser. | 6. Steering Mirror Module. |
| 2. Fixed Energy Share Module. | 7. Alignment Telescope. |
| 3. Front Input Module. | 8. Telescope Lens Centering Screws. |
| 4. Rear Input Module. | 9. Fibres. |
| 5. Time Share Module. | |

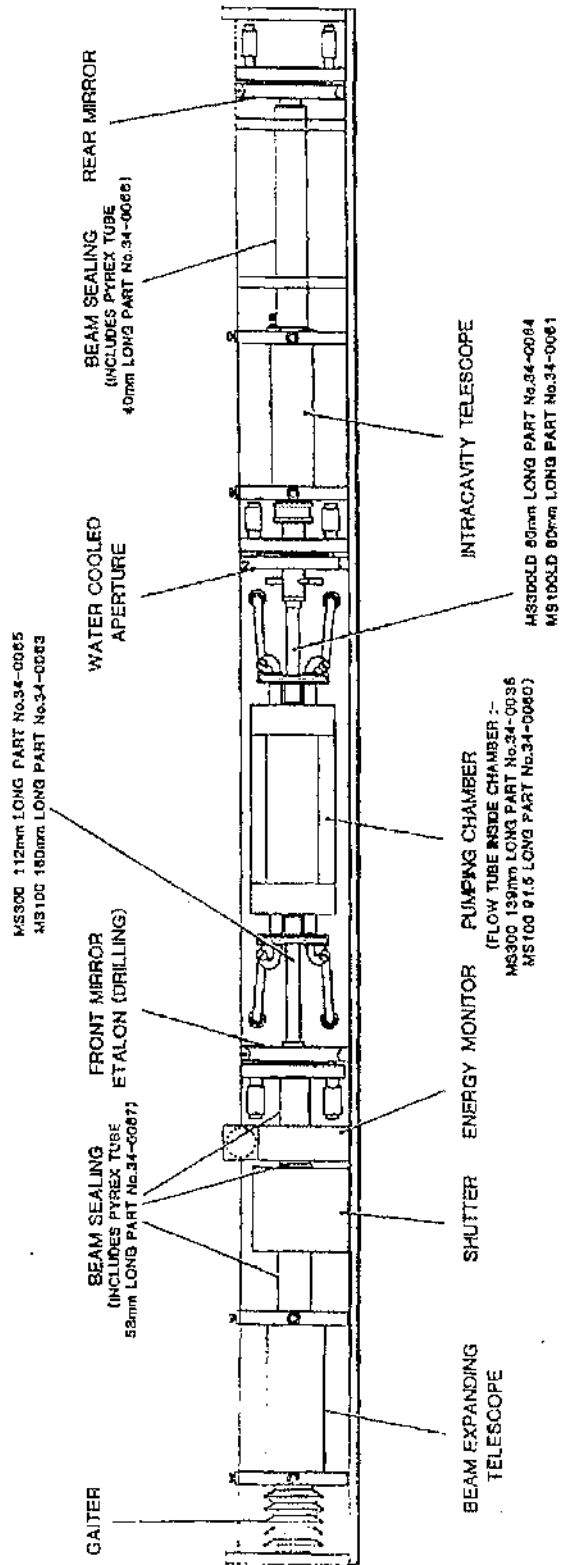
(37) A diagram of time share unit



(38) A schematic of 2-way time share unit



(39) Laser head configuration -Conventional resonator



(40) Laser head configuration - L.D. resonator

**Appendix 4. Physical & Mechanical Properties / Chemical
Compositions of Aluminum Alloys**

4.1. 6082-T6, 5251-H24 AALCO Ltd.

4.2. ER4043 , ER4047 MUREX Ltd.

Appendix 4.1. 6082-T6 , 5251-H24 alloys

Chemical composition											
Material Destination	Si	Fe	Cu	Mn	Mg	Cr	Zn	special	Ti	Others(total)	Aluminum
6082-T6	0.7-1.3	0.5	0.1	0.4-1.0	0.6-1.2	0.25	0.2	—	0.1	0.15	Rem
5251-H24	0.4	0.5	0.15	0.1-0.5	1.7-2.4	0.15	0.15	—	0.15	0.15	Rem

Physical and Mechanical properties

Material Destination	Density	Melting range	Coefficient of Linear Expansion (20-100°C)	Thermal Conductivity (0-100°C)	Electrical Conductivity (20°C)	0.2% Proof stress	Tensile Strength	Elongation percent On 50mm	Shear strength	Fatigue Strength 50*10 ⁶ H _z	Hardness Vickers	Modulus of Elasticity
unit	g/cm ³	°C	10 ⁻⁶ /°C	W/°C	%IACS	Mpa	Mpa	mm	Mpa	Mpa	kg/mm ³	Gpa
6082-T4	2.7	570-660	23	172	42.1	130	225	15	178	106	64-74	69
6082-T6	2.7	570-660	23	184	46.4	270	310	8	218	124	95-105	69
5251-O	2.69	595-650	24	155	36.7	87	180	18	125	92	47	70
5251-H22	2.69	595-650	24	155	36.7	150	220	6	—	124	65	70
5251-H24	2.69	595-650	24	155	36.7	190	250	5	139	—	74	70

Comparison of Alloy Destinations

BS AND INTERNATIONAL DESTINATION	OLD BS DESTINATION	ISO DESTINATION
1081A	1A	Al 99.8
1050A	1B	Al 99.5
1200	1C	Al 99.0
1350	1E	Al 99.5
2011	FC1	Al Cu 5.5 Pb Bi
2014A	H15	Al Cu 4 Si Mg
2031	H12	Al Cu 2 Ni 1 Mg Fe Si
2618A	H16	Al Cu 2 Mg 1.5 Fe 1 Ni 1
3103	N3	Al Mn 1
3105	N31	Al Mn Mg
4043A	N21	Al Si 5
4047A	N2	Al Si 12
5005	N41	Al Mg 1
5056A	N6	Al Mg 5
5083	N8	Al Mg 4.5 Mn
5154A	N5	Al Mg 3.5
5251	N4	Al Mg 2
5454	N51	Al Mg 3 Mn
5554	N52	Al Mg 3 Mn
5556A	N61	Al Mg 5.2 Mn Cr
6061	H20	Al Mg 1 Si Cu
6063	H9	Al Mg Si
6082	H30	Al Si 1 Mg Mn
6101A	91E	Al Mg Si
6463	BTR E6	Al Mg Si
7020	H17	Al Zn 4.5 Mg 1

Appendix 4.2. ER 4043 , ER4047 MUREX Ltd.

Bostland 281

BS 2901 : Part 4: 1990 : 4043A
 AWS A/SFA 5.10-93 : ER4043
 DIN 1732 (1988) : SG AISi 5

Applications

Parent Alloy	6061 (H20) 6063 (H9) 6082 (H30)	3103 (N3)	1050A (1B)
1050A (1B)	YES	YES	YES
3103 (N3)	YES	YES	
6061 (H9) 6063 (H9) 6082 (H30)	YES		

Wire and all-weld metal properties

Wire Analysis (Wt%)	Mechanical	As - welded	unit
Si : 4.5-5.5	0.2% PS	50 min	N/mm ²
Mn : 0.05 max	UTS	150 min	N/mm ²
Cr : 0.05 max	Elongation	15 min	%
Cu : 0.05 max			
Ti : 0.15 max	Tensile strength of wire	180 min	N/mm ²
Al : balance			

Saffire Aluminum 10% Silicon

BS 2901 : Part 4: 1990 : 4047A (TIG rods)
 BS 1453 : 1972 (1987) : 4047A (GAS rods)
 AWS A/SFA 5.10-93 : ER4047
 DIN 1732 (1988) : SG-AISI 12

Composition

Wire Analysis	Wt %	Wire Analysis	Wt %
Si	11.0-13.0	Zn	0.1 max
Mn	0.15 max	Fe	0.50 max
Mg	0.05 max	Be	0.0008 max
Cu	0.05 max	Other	0.15 max
Ti	0.15 max	Al	balance

